

# **Thiophene and Pyrazole based Fluorescent Boron Compounds: Synthesis and Study of Bidentate Mercury and Tin Compounds**

*By*  
**SHREENIBASA SA**  
**CHEM11201604011**

**National Institute of Science Education and Research,  
Bhubaneswar, Odisha**

*A thesis submitted to the  
Board of Studies in Chemical Sciences  
In partial fulfillment of requirements  
for the Degree of*

**DOCTOR OF PHILOSOPHY**  
*of*  
**HOMI BHABHA NATIONAL INSTITUTE**



**October, 2021**

# Homi Bhabha National Institute<sup>1</sup>

## Recommendations of the Viva Voce Committee


As members of the Viva Voce Committee, we certify that we have read the dissertation prepared by **Shreenibasa Sa** entitled "**Thiophene and Pyrazole based Fluorescent Boron Compounds: Synthesis and Study of Bidentate Mercury and Tin Compounds**" and recommend that it may be accepted as fulfilling the thesis requirement for the award of Degree of Doctor of Philosophy.

Chairman - Prof. A. Srinivasan



Date: 14.01.22

Guide / Convener - Dr. V. Krishnan



Date: 14/1/2022

Examiner - Prof. R. Boomi Shankar



Date: 14/01/2022

Member 1- Dr. S. Peruncheralathan



Date: 14.01.2022

Member 2- Dr. S. Nembenna



Date: 14/01/2022

Member 3- Dr. P. Singru



Date: 14.01.2022

Final approval and acceptance of this thesis is contingent upon the candidate's submission of the final copies of the thesis to HBNI.

I/~~We~~ hereby certify that I/~~we~~ have read this thesis prepared under my/our direction and recommend that it may be accepted as fulfilling the thesis requirement.

Date: 14.01.2022



Signature

Place: NISER, Bhubaneswar

Guide

<sup>1</sup> This page is to be included only for final submission after successful completion of viva voce.

---

## STATEMENT BY AUTHOR

This dissertation has been submitted in partial fulfillment of requirements for an advanced degree at Homi Bhabha National Institute (HBNI) and is deposited in the Library to be made available to borrowers under rules of the HBNI.

Brief quotations from this dissertation are allowable without special permission, provided that accurate acknowledgement of source is made. Requests for permission for extended quotation from or reproduction of this manuscript in whole or in part may be granted by the Competent Authority of HBNI when in his or her judgment the proposed use of the material is in the interests of scholarship. In all other instances, however, permission must be obtained from the author.

Shreenibasa Sa  
Shreenibasa Sa

---

## DECLARATION

I, hereby declare that the investigation presented in the thesis has been carried out by me. The work is original and has not been submitted earlier as a whole or in part for a degree / diploma at this or any other Institution / University.

Shreenibasa Sa  
Shreenibasa Sa



---

## List of Publications

### a. Published

\*1) **Sa, S.**; Murali, A. C.; Nayak, P.; Venkatasubbaiah, K. Thiophene-fused boracycles as photoactive analogues of diboraanthracenes. *Chem. Commun.*, **2021**, 57, 10170.

\*2) <sup>†</sup>**Sa, S.**; <sup>†</sup>Mukundam, V.; Kumari, A.; Das, R.; Venkatasubbaiah, K. Synthesis of pyrazole anchored three-coordinated organoboranes and their application in the detection of picric acid. *Dalton Trans.*, **2021**, 50, 6204-6212.

(<sup>†</sup> equal contribution)

\*3) **Sa, S.**; Sathesh, V.; Murali, A. C.; Nayak, P.; Venkatasubbaiah, K. Synthesis and complexation behavior of 3,4-bis(chloromercurio)2,5-dimethylthiophene. *J. Organomet. Chem.*, **2021**, 121977.

4) Dhanunjayarao, K.; **Sa, S.**; Aradhyula, B. P. R.; Venkatasubbaiah, K.; Synthesis of phenanthroimidazole-based four coordinate organoboron compounds. *Tetrahedron*, **2018**, 74, 5819.

5) Dhanunjayarao, K.; **Sa, S.**; Nayak, P.; Ponniah, S J.; Venkatasubbaiah, K.; Tetrahydrodibenzophenanthridine-based boron-bridged polycyclic aromatic hydrocarbons: Synthesis, structural diversity, and optical properties. *Organometallics*, **2019**, 38, 870.

6) Mukundam, V.; **Sa, S.**; Kumari, A.; Das, R.; Venkatasubbaiah, K.; B–N coordinated triaryl pyrazole: effect of dimerization, and optical and NLO properties. *J. Mater. Chem. C*, **2019**, 7, 12725.

7) Mukundam, V.; **Sa, S.**; Kumari, A.; Murali, A. C.; Nayak, P.; Das, R.; Venkatasubbaiah, K.; Synthesis of  $\pi$ -extended B  $\leftarrow$  N coordinated

---

phenanthroimidazole dimers and their linear and nonlinear optical properties.

*Dalton Trans.*, **2020**, 49, 7737.

(\* pertaining to thesis)

**b. Manuscript Under Preparation**

1. \***Sa, S.**; Venkatasubbaiah, K. Synthesis and characterisation of thiophene fused organotin (iv) complexes and its application to hydroboration of carbonyl compounds.
2. \***Sa, S.**; Venkatasubbaiah, K. Tetraaryl pyrazole based four coordinated boron compounds: Synthesis, characterisation and AIEE phenomenon.
3. \***Sa, S.**; Venkatasubbaiah, K. Boron doped tetraarylpyrazole AIEgens: Synthesis, characterisation and optical properties.

**Conferences**

1. Synthesis, characterization and photophysical studies of tetracoordinate dinuclear pyrazole boron complexes. **Sa, S.**; Mukundam, V.; Dhanunjayarao, K.; Venkatasubbaiah, K. in 17<sup>th</sup> biennial symposium, 'Modern Trends in Inorganic Chemistry' (MTIC-XVII) held at CSIR-NCL, Pune and IISER, Pune during 11<sup>th</sup> to 14<sup>th</sup> December 2017. (**Poster presentation**)
2. Synthesis, characterisation and photophysical studies of tri-aryl pyrazole based mononuclear boron complexes. Mukundam, V.; **Sa, S.**; Dhanunjayarao, K.; Venkatasubbaiah, K. in 'Inter IISER & NISER Chemistry Meet (IINCM-2017)' held at NISER, Bhubaneswar during 22<sup>nd</sup> to 24<sup>th</sup> December 2017. (**Poster presentation**)

- 
3. Synthesis, characterization and photophysical studies of phenanthroimidazole based diboron complexes. Sa, S.; Mukundam, V.; Dhanunjayarao, K.; Venkatasubbaiah, K. in 1<sup>st</sup> International Symposium on 'Main group Molecules to Materials (MMM)' held at the Department of Inorganic and Physical Chemistry, IISc-Bangalore during 28<sup>th</sup> to 31<sup>st</sup> October 2018. (**Poster presentation**)

Shreenibasa Sa  
Shreenibasa Sa

---

***Dedicated to My Family***

---

## ACKNOWLEDGEMENTS

I would like to express my sincere gratitude to my thesis supervisor **Dr. Venkatasubbaih Krishnan** for his insightful advice, constant encouragement and patient guidance during my PhD studies.

I take this opportunity to thank my doctoral committee members, Prof. A. Srinivasan, Dr. S. Peruncheralathan, Dr. S. Nembenna and Dr. P. Singru for their useful suggestions. I am grateful to all the faculties of school of chemical sciences, NISER.

I would like to acknowledge Prof. Sudhakar Panda, Director, NISER and Prof. V. Chandrasekhar, Former Director, NISER for giving the laboratory facilities and DAE for financial support. I am thankful to Dr. Ritwick Das and Anupa Kumari of school of physical science, NISER for their help in the measurement of nonlinear optical properties. I am also thankful to Dr. Arun Kumar, Dr. Priyanka Pandey and all the technicians of school of chemical sciences. My sincere thanks go to all my teachers starting from my school days.

I am grateful to my past labmate Dr. Mukundam, Dr. Dhanunjaya, Dr. Ramesh, Dr. Ramu, Dr. Sathesh, Dr. Joseph, Dr. Basava, Asutosh, Preeta, Sanket, Pratiksha, Anjali, Bastab, Arihant, Omkar and present labmate Samser, Priyabrata, Prakash, Murali, Sushanta, Dhairya, Saran, Riya and Adya for the help and useful discussions in the lab.

I am also grateful to my friends Dr. Mainak, Pragati, Jiban, Bibhuti, Nabin and all other friends at NISER. Many thanks to my friends Subhashree, Biswajit, Subash, Dibyananda, Sudam, Sourav, Hemananda and all other friends starting from my childhood days.

I deeply thank my parents (Jibardhan and Jogeshwari) and my sisters (Santoshini, Sarojini and Sukesini) for the love, patience, blessings and support.

Shreenibasa Sa  
Shreenibasa Sa

---

# CONTENTS

	<b>Page No.</b>
<b>Thesis title</b>	i
<b>Recommendations of the viva-voce committee</b>	ii
<b>Statement by author</b>	iii
<b>Declaration</b>	iv
<b>List of publications</b>	v
<b>Dedications</b>	viii
<b>Acknowledgements</b>	ix
<b>Contents</b>	x
<b>Synopsis</b>	xi
<b>List of Tables</b>	xvi
<b>List of Schemes</b>	xviii
<b>List of Figures</b>	xix
<b>List of Abbreviations</b>	xxx
<b>Chapter 1</b>	1
<b>Chapter 2</b>	61
<b>Chapter 3</b>	83
<b>Chapter 4</b>	111
<b>Chapter 5A</b>	135
<b>Chapter 5B</b>	177
<b>Chapter 6</b>	207
<b>Summary</b>	243

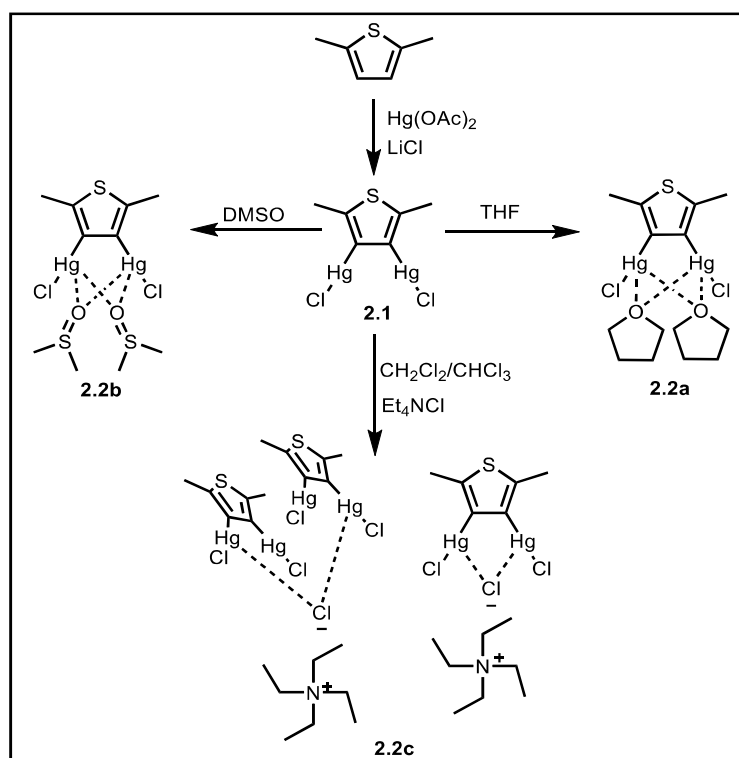


---

## SYNOPSIS

This thesis has been organized into six chapters. Chapter 1 represents a brief review on (a) tri-coordinated boron compounds, (b) tetra-coordinated boron compounds and (c) main group bidentate Lewis acids.

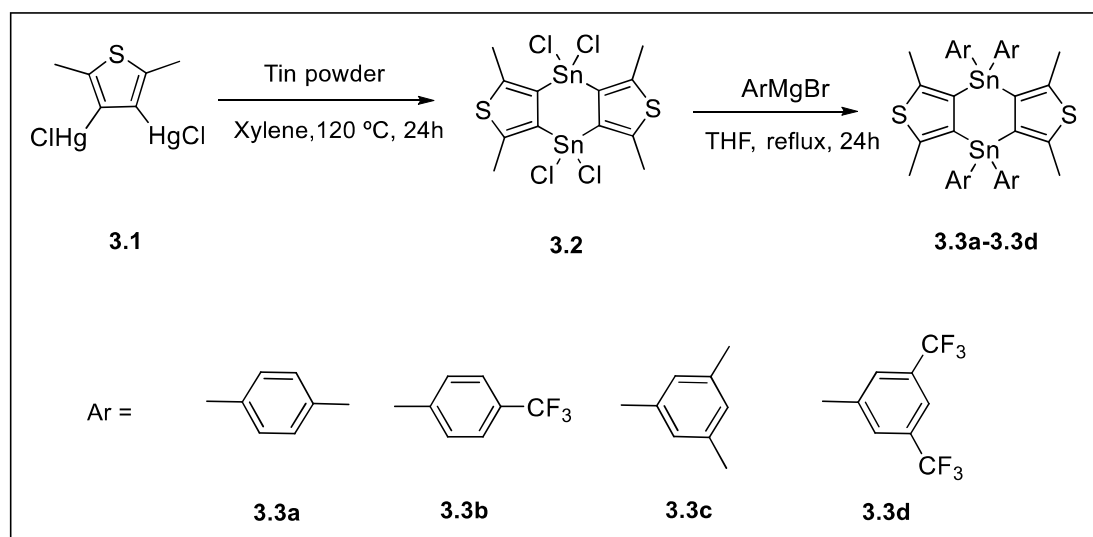
Chapter 2 deals with the synthesis of bidentate Lewis acid 3,4-bis(chloromercurio)2,5-dimethylthiophene and its complexation with THF, DMSO and Et<sub>4</sub>NCl. Compound **2.1** was synthesized by treating 2,5-dimethylthiophene with mercuric acetate in methanol followed by addition of lithium chloride in methanol (Scheme 1). The formation of compound **2.1** was characterized by <sup>1</sup>H, <sup>13</sup>C and HRMS analysis. Slow evaporation of a THF and DMSO solution of compound **2.1** yield complex **2.2a** and **2.2b** respectively. Complex **2.2c** was prepared by treatment of compound **2.1** with Et<sub>4</sub>NCl. All the complexes were characterized without any



**Scheme 1:** Synthesis of bidentate lewis acid **2.1** and its complexes **2.2a- 2.2c**.

ambiguity using different analytical techniques. Compounds **2.1** and **2.2a-2.2c** have been found to form supramolecular assemblies in the solid state.

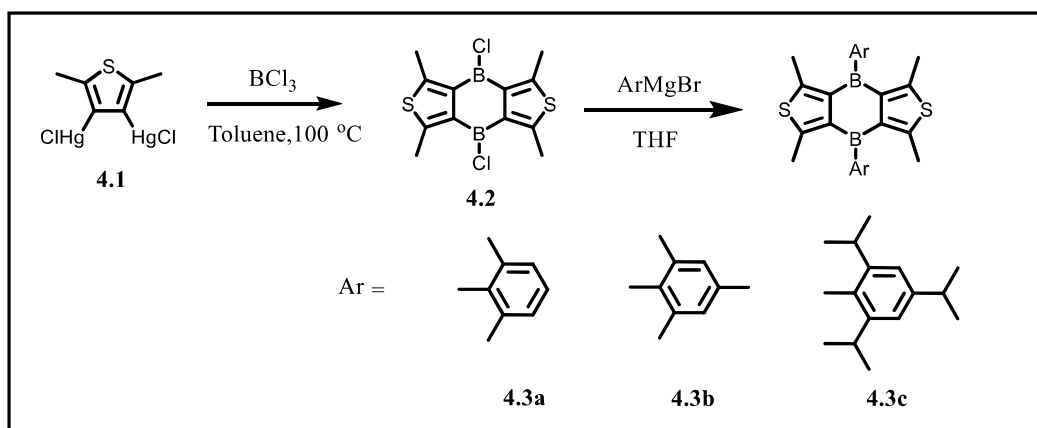
Chapter **3** deals with the synthesis of distannadithiophenes analogue of 9,10-distannaanthracenes (Scheme 2). All the newly synthesized distannadithiophenes were characterized by  $^1\text{H}$ ,  $^{13}\text{C}$ ,  $^{119}\text{Sn}$  NMR and HRMS analysis. Compounds **3.3a**, **3.3b** and **3.3d** were also characterized using X-ray crystallography. These compounds were employed for the hydroboration of carbonyl compounds. Out of all compounds studied, **3.3a** showed excellent catalytic activity over other three compounds. Using **3.3a** as a catalyst, a wide range of aldehydes and ketones were reduced to produce the corresponding products.



**Scheme 2:** Synthesis of organotin(IV) complexes **3.3a-3.3d**.

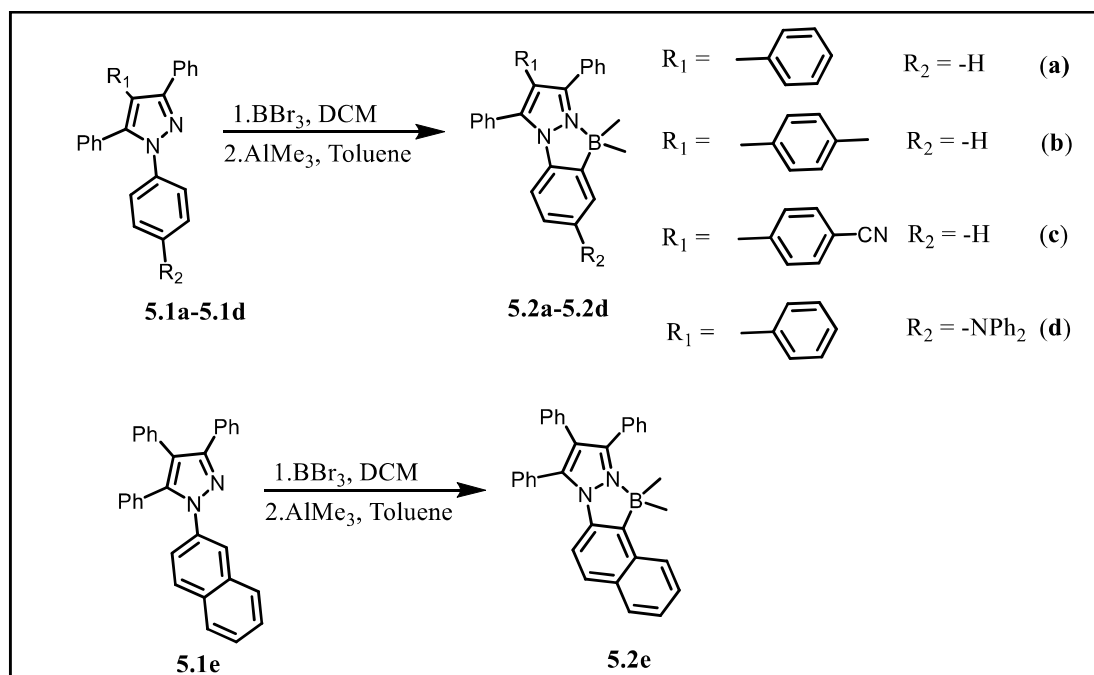
Chapter **4** describes the synthesis of thiophene analogue of diboraanthracenes *i.e.* diboradithiophenes (Scheme 3). Three new aryl substituted diboradithiophenes have been synthesized starting from **4.2**. All the diboradithiophenes have been characterized using multinuclear NMR, elemental analysis and X-ray crystallography. Photophysical properties of these compounds showed quantum yield of ~5 % in the solution states and

~2 % in the thin film state. Upon exposure to UV light, the absorption and emission intensity of compounds **4.3a-4.3c** decreases which was exploited for the detection of UV radiation.



**Scheme 3:** Synthesis of diboradithiophene derivatives **4.3a-4.3c**.

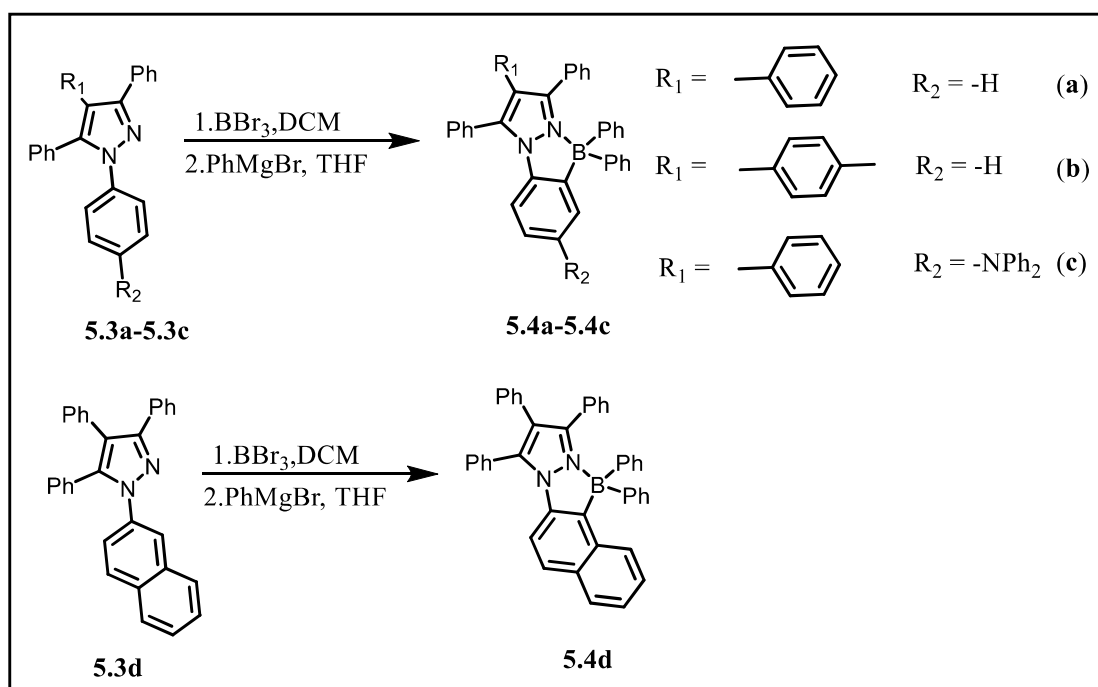
Chapter **5** is divided into two parts. The first part describes the synthesis of dimethyl substituted tetra-coordinated boron compounds supported on tetraaryl pyrazoles and the second part describes the preparation of diphenyl substituted tetra-coordinated boron



**Scheme 4:** Synthesis of pyrazole based four coordinate boron compounds **5.2a-5.2e**.

compounds. Part A of this chapter describes the synthesis and characterization of tetraaryl pyrazoles based four coordinate boron compounds **5.2a-5.2e** (Scheme 4). These compounds were characterized by  $^1\text{H}$  NMR,  $^{13}\text{C}$  NMR,  $^{11}\text{B}$  NMR and HRMS analysis. Compounds **5.2a-5.2d** were also characterized using X-ray crystallography. Photophysical studies of **5.2a-5.2e** were studied in five different solvents and in the solid state. Electrochemical studies of **5.2a-5.2e** displayed an irreversible reduction wave at  $\sim -2.85\text{V}$ . All these boron compounds showed AIEE properties. Complex **5.2e** was used as a probe for the detection of picric acid.

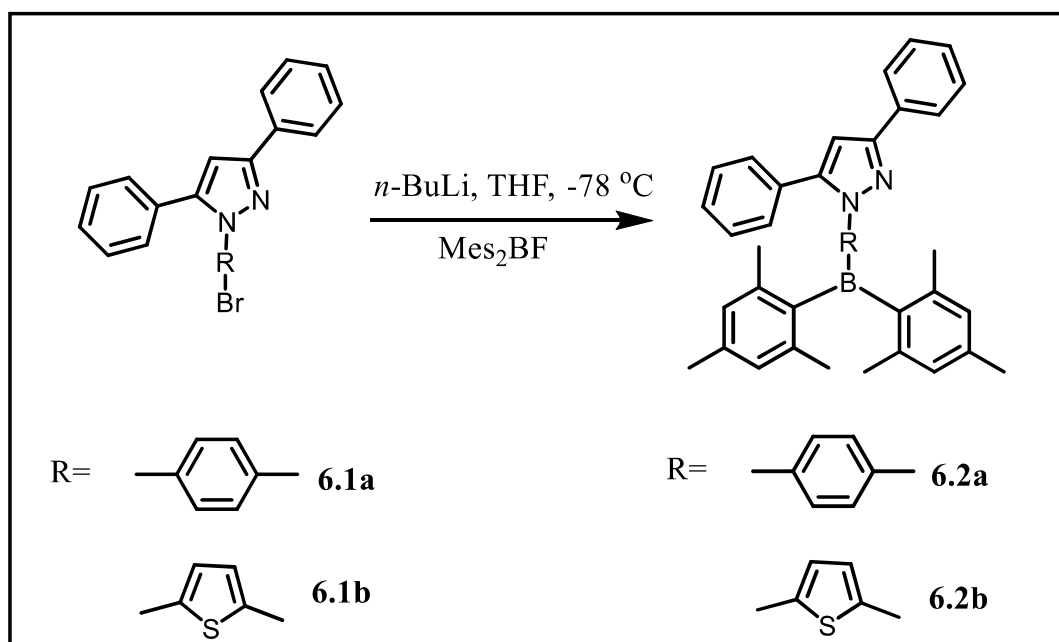
Part B of this chapter describes the synthesis and characterization of boron doped tetraarylpyrazole AIEgens **5.4a-5.4d** (Scheme 5). All the boron compounds **5.4a-5.4d** were characterized by  $^1\text{H}$  NMR,  $^{13}\text{C}$  NMR,  $^{11}\text{B}$  NMR, HRMS analysis and X-ray crystallography. Thermogravimetric analysis showed that these compounds are thermally stable upto  $330\text{ }^\circ\text{C}$ . Electrochemical studies of the compounds **5.4a-5.4d**



**Scheme 5:** Synthesis of pyrazole based four coordinate boron compounds **5.4a-5.4d**.

displayed an irreversible reduction wave at  $\sim -2.8\text{V}$ . Photophysical properties of compounds **5.4a-5.4d** were investigated in solution and solid states.

Chapter 6 deals with the synthesis and characterization of two triaryl boron compounds **6.2a** and **6.2b** (Scheme 6). These two complexes were characterized by  $^1\text{H}$  NMR,  $^{13}\text{C}$  NMR,  $^{11}\text{B}$  NMR, HRMS analysis and X-ray crystallography. Compound **6.2a** and **6.2b** were used as probe for detection of picric acid. NLO properties (namely  $n_2$  and  $\beta$ ) for compounds **6.2a** and **6.2b** reveal a direct dependence on addition of concentration of PA to the solution.



**Scheme 6:** Synthetic routes to compound **6.2a** and **6.2b**.

---

## List of tables

1	<b>Table 2.1</b>	Crystal data and structure refinement parameters for compound <b>1</b> and <b>2</b>	74
2	<b>Table 2.2</b>	Crystal data and structure refinement parameters for compound <b>3</b> and <b>4</b>	75
6	<b>Table 3.1</b>	Comparison of distance between the two tin atoms (Å) and interplanar angles ( °) for complexes <b>3</b> , <b>4</b> and <b>6</b>	90
7	<b>Table 3.2</b>	Crystal data and structure refinement parameters for complexes <b>3</b> , <b>4</b> & <b>6</b>	90
8	<b>Table 3.3</b>	Optimization reaction condition for hydroboration	93
9	<b>Table 3.4</b>	Scope of hydroboration of aldehydes catalysed by complex <b>3</b>	95
10	<b>Table 3.5</b>	Scope of hydroboration of ketones catalysed by complex <b>3</b>	96
3	<b>Table 4.1</b>	Crystal data and structure refinement parameters for compounds <b>3</b> and <b>4</b>	118
4	<b>Table 4.2</b>	Photophysical properties of compounds <b>3-5</b>	120
5	<b>Table 4.3</b>	Electrochemical data and frontier orbital energies [eV] derived from UV/Vis onset absorption and electrochemical data.	122
11	<b>Table 5A.1</b>	Comparison of deviation of boron from C <sub>2</sub> N <sub>2</sub> B plane (Å) and interplanar angles ( °) for compounds <b>6-8</b> and <b>12</b>	143
12	<b>Table 5A.2</b>	Crystal data and structure refinement parameters for compound <b>6</b> and <b>7</b>	144
13	<b>Table 5A.3</b>	Crystal data and structure refinement parameters for compound <b>8</b> and <b>12</b>	145
14	<b>Table 5A.4</b>	Photophysical data of compounds <b>6-8</b> , <b>12</b> and <b>18</b>	146
15	<b>Table 5A.5</b>	Refractive index ( <sup>n</sup> ), dielectric constant (ε), orientation polarizability (Δ <i>f</i> ) and Stokes shift (Δ <i>ν</i> (cm <sup>-1</sup> )) of	149



---

		compound <b>18</b> as a function of different solvents are shown.	
16	<b>Table 5B.1</b>	Comparison of deviation of boron from C <sub>2</sub> N <sub>2</sub> B plane (Å) and interplanar angles (degree) for compound <b>6-8</b> and <b>12</b>	183
17	<b>Table 5B.2</b>	Crystal data and structure refinement parameters for compounds <b>1</b> and <b>2</b>	186
18	<b>Table 5B.3</b>	Crystal data and structure refinement parameters for compounds <b>3</b> and <b>4</b>	186
19	<b>Table 5B.4</b>	Photophysical data of compounds <b>1-4</b>	188
20	<b>Table 6.1</b>	Crystal data and structure refinement parameters for compound <b>2</b> and <b>5</b>	212
21	<b>Table 6.2</b>	Photophysical data of compound <b>2</b> and <b>5</b>	214
22	<b>Table 6.3</b>	Calculated electronic transitions for compound <b>2</b> & <b>5</b> from TD-DFT (B3LYP/631g(d,p))– PCM solvation (THF))) calculations	217
23	<b>Table 6.4</b>	Limit of detection (LOD) data for compound <b>2</b> and <b>5</b>	224
24	<b>Table 6.5</b>	Limit of detection (LOD) data for recently reported probes for picric acid	224
25	<b>Table 6.6</b>	Optical nonlinear coefficients of <b>2</b> and <b>5</b> at 1kHz repetition rates	228
26	<b>Table 6.7</b>	Comparison of optical nonlinearity coefficients of similar molecules	231

---

## List of schemes

1	<b>Scheme 2.1</b>	Synthesis of thiophene based bidentate Lewis acid and its complexes.	65
2	<b>Scheme 3.1</b>	Synthesis of compounds <b>Sn3-Sn6</b>	86
3	<b>Scheme 3.2</b>	Selectivity study for intermolecular hydroboration of aldehydes and ketones.	97
4	<b>Scheme 3.3</b>	Plausible catalytic cycles for hydroboration of carbonyl compounds catalysed by complex <b>3</b>	98
5	<b>Scheme 4.1</b>	Synthesis of diboradithiophene derivatives.	115
6	<b>Scheme 5A.1</b>	Synthesis of compounds <b>6-8</b>	138
7	<b>Scheme 5A.2</b>	Synthesis of compound <b>12</b>	139
8	<b>Scheme 5A.3</b>	Synthesis of compound <b>18</b>	139
9	<b>Scheme 5B.1</b>	Synthetic route to boron compounds <b>1-4</b>	181
10	<b>Scheme 6.1</b>	Synthetic route to compound <b>2</b> and <b>5</b>	211

---

## List of figures

1	<b>Figure 1.1</b>	Schematic representation of trivalent boron compounds	4
2	<b>Figure 1.2</b>	Tricoordinate boron as anion sensors <b>1-7</b>	5
3	<b>Figure 1.3</b>	Tricoordinate boron as anion sensors <b>8-10</b>	5
4	<b>Figure 1.4</b>	Tricoordinate boron as anion sensors <b>11-13</b>	6
5	<b>Figure 1.5</b>	Tricoordinate boron as anion sensors <b>14-16</b>	7
6	<b>Figure 1.6</b>	Tricoordinate boron as anion sensors <b>17-20</b>	7
7	<b>Figure 1.7</b>	Tricoordinate boron as anion sensors <b>21-22</b>	8
8	<b>Figure 1.8</b>	Tricoordinate boron as anion sensors <b>23-26</b>	9
9	<b>Figure 1.9</b>	Tricoordinate boron as NLO materials <b>27-33</b>	10
10	<b>Figure 1.10</b>	Tricoordinate boron as NLO materials <b>34-45</b>	11
11	<b>Figure 1.11</b>	Tricoordinate boron as NLO materials <b>46-52</b>	12
12	<b>Figure 1.12</b>	Tricoordinate boron as NLO materials <b>53-56</b>	13
13	<b>Figure 1.13</b>	Tricoordinate boron as NLO materials <b>57-63</b>	14
14	<b>Figure 1.14</b>	Tricoordinate boron as photochromic materials <b>64-70</b>	15
15	<b>Figure 1.15</b>	Tricoordinate boron as photochromic materials <b>71-74</b>	16
16	<b>Figure 1.16</b>	Schematic representation of tetracoordinate boron compound	17
17	<b>Figure 1.17</b>	N,C-chelate four coordinate boron compounds <b>75-78</b>	17
18	<b>Figure 1.18</b>	N,C-chelate four coordinate boron compounds <b>79-94</b>	18
19	<b>Figure 1.19</b>	N,C-chelate four coordinate boron compounds <b>95-103</b>	20
20	<b>Figure 1.20</b>	N,C-chelate four coordinate boron compounds <b>104-109</b>	21
21	<b>Figure 1.21</b>	N,C-chelate four coordinate boron compounds <b>110-118</b>	22
22	<b>Figure 1.22</b>	N,C-chelate four coordinate boron compounds <b>119-133</b>	23
23	<b>Figure 1.23</b>	N,C-chelate four coordinate boron compounds <b>134-140</b>	24
24	<b>Figure 1.24</b>	N,C-chelate four coordinate boron compounds <b>141-146</b>	25
25	<b>Figure 1.25</b>	N,C-chelate four coordinate boron compounds <b>147-159</b>	26
26	<b>Figure 1.26</b>	N,C-chelate four coordinate boron compounds <b>160-175</b>	28
27	<b>Figure 1.27</b>	N,C-chelate four coordinate boron compounds <b>176-189</b>	28
28	<b>Figure 1.28</b>	Schematic representation of BODIPY	30
29	<b>Figure 1.29</b>	N,N-chelate four coordinate boron compounds <b>190-210</b>	30

30	<b>Figure 1.30</b>	N,N-chelate four coordinate boron compounds <b>211-219</b>	32
31	<b>Figure 1.31</b>	N,N-chelate four coordinate boron compounds <b>220-224</b>	33
32	<b>Figure 1.32</b>	N,N-chelate four coordinate boron compounds <b>225-228</b>	34
33	<b>Figure 1.33</b>	N,O-chelate four coordinate boron compounds <b>229-238</b>	35
34	<b>Figure 1.34</b>	N,O-chelate four coordinate boron compounds <b>239-248</b>	36
35	<b>Figure 1.35</b>	N,O-chelate four coordinate boron compounds <b>249-260</b>	37
36	<b>Figure 1.36</b>	Bidentate mercury Lewis acid <b>261</b> and its adduct <b>262-263</b>	38
37	<b>Figure 1.37</b>	Bidentate mercury Lewis acid <b>265</b> and its adduct <b>266</b>	39
38	<b>Figure 1.38</b>	Bidentate mercury Lewis acid <b>267</b> and its adduct <b>268-269</b>	39
39	<b>Figure 1.39</b>	Bidentate mercury Lewis acid <b>270</b> and its adduct <b>271-274</b>	40
40	<b>Figure 1.40</b>	Bidentate mercury Lewis acid <b>270</b> and its adduct <b>278-286</b>	41
41	<b>Figure 1.41</b>	Bidentate mercury Lewis acid <b>287</b> and its adduct <b>288-290</b>	42
42	<b>Figure 1.42</b>	Bidentate tin Lewis acid and its adduct <b>291-312</b>	43
43	<b>Figure 1.43</b>	Bidentate tin Lewis acid <b>313-319</b>	44
44	<b>Figure 1.44</b>	Bidentate boron Lewis acid <b>320-324</b>	45
45	<b>Figure 1.45</b>	Bidentate boron Lewis acid <b>325-333</b>	45
46	<b>Figure 1.46</b>	Bidentate boron Lewis acid <b>334-340</b>	46
47	<b>Figure 1.47</b>	Bidentate boron Lewis acid <b>341</b>	47
48	<b>Figure 1.48</b>	Bidentate boron Lewis acid <b>342</b>	47
49	<b>Figure 1.49</b>	Bidentate boron Lewis acid and its adduct <b>343-363</b>	48
50	<b>Figure 1.50</b>	Bidentate boron Lewis acid and its adduct <b>364-369</b>	49
51	<b>Figure 2.1</b>	1,2-Phenylenedimercury dichloride (A), 1,2-bis(chloromercurio)tetrafluorobenzene (B), 1,8-bis(chloromercurio)naphthalene (C), 1,2-bis(chloromercury)ferrocene (D).	64
52	<b>Figure 2.2</b>	<sup>1</sup> H NMR spectrum of compound <b>1</b> in DMSO- <i>d</i> <sub>6</sub>	66
53	<b>Figure 2.3</b>	HRMS spectrum of compound <b>1</b>	66
54	<b>Figure 2.4</b>	<sup>1</sup> H NMR spectrum of compound <b>4</b> in DMSO- <i>d</i> <sub>6</sub>	67
55	<b>Figure 2.5</b>	TGA curves for compound <b>2</b> (left) and <b>3</b> (Right) under N <sub>2</sub> at a heating rate of 10 °C min <sup>-1</sup>	67

56	<b>Figure 2.6</b>	Molecular structure of compound <b>1</b> (left) and its 1D polymeric network <i>via</i> Hg $\cdots$ Cl interactions (right, all hydrogen atoms are omitted for clarity).	68
57	<b>Figure 2.7</b>	Portion of a chain like structure of compound <b>1</b> through C-H $\cdots$ Cl hydrogen bonding (top); 3D network of compound <b>1</b> (bottom) through C-H $\cdots$ Cl hydrogen bonding and Hg $\cdots$ Cl interactions.	69
58	<b>Figure 2.8</b>	Molecular structure of compound <b>2</b> (left) and its 1D polymeric network <i>via</i> Hg $\cdots$ Cl interactions (right, all hydrogen atoms are omitted for clarity).	70
59	<b>Figure 2.9</b>	Molecular structure of compound <b>3</b> (left) and its 1D polymeric network <i>via</i> Hg $\cdots$ Cl interactions (right, all hydrogen atoms are omitted for clarity).	71
60	<b>Figure 2.10</b>	Portion of chain like structure of compound <b>2</b> (left) and its 3D polymeric network <i>via</i> C-H $\cdots$ Cl interactions	72
61	<b>Figure 2.11</b>	View of sheet like network in compound <b>3</b>	72
62	<b>Figure 2.12</b>	Molecular structure of compound <b>4</b> (left) and its ball and stick model showing 3:2 complex with four Hg $\cdots$ Cl contacts (right, all hydrogen atoms are omitted for clarity).	73
63	<b>Figure 2.13</b>	View of extended structure in compound <b>4</b> <i>via</i> Hg $\cdots$ Cl & C-H $\cdots$ Cl interactions (top) and its 3D-polymeric network (bottom).	74
64	<b>Figure 3.1</b>	$^1\text{H}$ NMR spectrum of <b>Sn3</b> in $\text{CDCl}_3$ .	87
65	<b>Figure 3.1</b>	$^{119}\text{Sn}$ NMR spectrum of <b>Sn3</b> in $\text{CDCl}_3$ .	87
66	<b>Figure 3.3</b>	Molecular structure of <b>Sn3</b>	88
67	<b>Figure 3.4</b>	Molecular structure of <b>Sn4</b>	89
68	<b>Figure 3.5</b>	Molecular structure of <b>Sn6</b>	89
69	<b>Figure 3.6</b>	Packing diagram in <b>Sn4</b>	92
70	<b>Figure 3.7</b>	(Left) Reaction progress of 4-methoxybenzaldehyde monitored by $^1\text{H}$ NMR spectroscopy. (Right)	94

		Comparison of conversion percentage with <b>Sn3</b> (2eq) and <b>Sn(Tol)<sub>4</sub></b> (4eq).	
71	<b>Figure 4.1</b>	Examples of diboracycles (A) diboraanthracene, (B) diboradiferrocene, (C) diboradithiophene	114
72	<b>Figure 4.2</b>	<sup>1</sup> H NMR spectrum of compound <b>4</b> in CDCl <sub>3</sub> .	116
73	<b>Figure 4.3</b>	<sup>11</sup> B NMR spectrum of compound <b>4</b> in CDCl <sub>3</sub> .	116
74	<b>Figure 4.4</b>	Molecular structure of compound <b>3</b> (Left) and <b>4</b> (Right).	118
75	<b>Figure 4.5</b>	Side view of <b>3</b> and <b>4</b> .	118
76	<b>Figure 4.6</b>	(left) Absorption spectra of compounds <b>3-5</b> in 10 <sup>-5</sup> M THF, (right) Normalized emission spectra of compounds <b>3-5</b> in 10 <sup>-5</sup> M THF.	120
77	<b>Figure 4.7</b>	Photograph of compounds <b>3-5</b> in 2% PMMA film under handheld UV lamp irradiated at 365 nm.	121
78	<b>Figure 4.8</b>	Cyclic voltammogram of compounds <b>3-5</b> (vs. Ferrocene/Ferrocenium) with 0.1 M Bu <sub>4</sub> NPF <sub>6</sub> as the supporting electrolyte (scan rate 100 mV/s) in DME.	121
79	<b>Figure 4.9</b>	Absorption (left) and emission spectra (right) of compound <b>4</b> in THF (10 <sup>-5</sup> M) after passing of UV light (365 nm).	123
80	<b>Figure 4.10</b>	Absorption (left) and emission spectra (right) of compound <b>3</b> in THF (10 <sup>-5</sup> M) after passing of UV light (365 nm).	123
81	<b>Figure 4.11</b>	Absorption (left) and emission spectra (right) of compound <b>5</b> in THF (10 <sup>-5</sup> M) after passing of UV light (365 nm).	124
82	<b>Figure 4.12</b>	Plausible product formation after photoirradiation of compound <b>4</b> .	124
83	<b>Figure 4.13</b>	<sup>1</sup> H NMR spectrum of compound <b>4</b> in C <sub>6</sub> D <sub>6</sub> after irradiation of UV light for 5h.	125
84	<b>Figure 4.14</b>	<sup>13</sup> C DEPT-135 NMR spectrum of compound <b>4</b> in C <sub>6</sub> D <sub>6</sub> after irradiation of UV light for 5h.	125



85	<b>Figure 4.15</b>	$^1\text{H}$ NMR of compound <b>4</b> in $\text{C}_6\text{D}_6$ after irradiation of UV light for 24h.	126
86	<b>Figure 4.16</b>	$^{13}\text{C}$ DEPT-135 NMR spectrum of compound <b>4</b> in $\text{C}_6\text{D}_6$ after irradiation of UV light for 24h.	126
87	<b>Figure 5A.1</b>	$^1\text{H}$ NMR spectrum of compound <b>6</b> in $\text{CDCl}_3$ .	140
88	<b>Figure 5A.2</b>	$^{11}\text{B}$ NMR spectrum of compound <b>6</b> in $\text{CDCl}_3$ .	141
89	<b>Figure 5A.3</b>	HRMS spectrum of compound <b>6</b> .	141
90	<b>Figure 5A.4</b>	Molecular structure of compound <b>6</b> (Left) and compound <b>7</b> (Right)	142
91	<b>Figure 5A.5</b>	Molecular structure of compound <b>8</b> (Left) and compound <b>12</b> (Right)	143
92	<b>Figure 5A.6</b>	Intermolecular interaction in compound <b>6</b> ( $\text{C-H}\cdots\pi$ : 2.81 Å) and <b>7</b> ( $\text{C-H}\cdots\pi$ : 2.81 Å).	144
93	<b>Figure 5A.7</b>	(Left) Absorption spectra of compounds <b>6-8</b> , <b>12</b> and <b>18</b> in $10^{-5}$ M THF. (Right) Normalised emission spectra of compounds <b>6-8</b> , <b>12</b> and <b>18</b> in $10^{-5}$ M THF.	148
94	<b>Figure 5A.8</b>	(Left) Solvatochromic emission spectra of compound <b>18</b> . (Right) Photograph of compound <b>18</b> in toluene, dichloromethane (DCM), tetrahydrofuran (THF), dimethylformamide (DMF) and acetonitrile (ACN) under handheld UV lamp irradiated at 365 nm.	148
95	<b>Figure 5A.9</b>	Lippert-Mataga plot of compound <b>18</b> depicting Stokes shift ( $\Delta\nu$ ) versus the solvent orientation polarizability ( $\Delta f$ ).	150
96	<b>Figure 5A.10</b>	(Left) Solid state emission spectra of compounds <b>6-8</b> , <b>12</b> and <b>18</b> . (Right) Photograph of thin film of compounds <b>6-8</b> , <b>12</b> and <b>18</b> (4% PMMA) under handheld UV lamp irradiated at 365 nm.	150
97	<b>Figure 5A.11</b>	(Left) Fluorescence spectra of compound <b>6</b> ( $10^{-5}$ M, excited at 300 nm) in THF: $\text{H}_2\text{O}$ mixture. (Right) Variation of quantum yield of compound <b>6</b> in THF: $\text{H}_2\text{O}$ mixture.	151

---

98	<b>Figure 5A.12</b>	Particle size distribution graph of compound <b>6</b> in THF:H <sub>2</sub> O (10:90) mixture.	151
99	<b>Figure 5A.13</b>	(Left) Fluorescence spectra of compound <b>7</b> ( $10^{-5}$ M, excited at 300 nm) in THF:H <sub>2</sub> O mixture. (Right) Variation of quantum yield of compound <b>7</b> in THF: H <sub>2</sub> O mixture.	152
100	<b>Figure 5A.14</b>	(Left) Fluorescence spectra of compound <b>8</b> ( $10^{-5}$ M, excited at 302 nm) in THF:H <sub>2</sub> O mixture. (Right) Variation of quantum yield of compound <b>8</b> in THF:H <sub>2</sub> O mixture.	152
101	<b>Figure 5A.15</b>	(Left) Fluorescence spectra of compound <b>12</b> ( $10^{-5}$ M, excited at 319 nm) in THF:H <sub>2</sub> O mixture. (Right) Variation of quantum yield of compound <b>12</b> in THF:H <sub>2</sub> O mixture.	153
102	<b>Figure 5A.16</b>	Photograph of compound <b>12</b> in THF/H <sub>2</sub> O mixture under a handheld UV lamp irradiated at 365 nm.	153
103	<b>Figure 5A.17</b>	(Left) Fluorescence spectra of compound <b>18</b> ( $10^{-5}$ M, excited at 353 nm) in THF:H <sub>2</sub> O mixture. (Right) Variation of quantum yield of compound <b>18</b> in THF:H <sub>2</sub> O mixture.	154
104	<b>Figure 5A.18</b>	Photograph of compound <b>18</b> in THF/H <sub>2</sub> O mixture under a handheld UV lamp irradiated at 365 nm.	155
105	<b>Figure 5A.19</b>	Emission spectra of compound <b>6</b> (Left) and compound <b>7</b> (Right) in $10^{-5}$ M THF at different temperatures.	155
106	<b>Figure 5A.20</b>	Emission spectra of compound <b>8</b> (Left) and compound <b>12</b> (Right) in $10^{-5}$ M THF at different temperatures.	155
107	<b>Figure 5A.21</b>	Emission spectra of compound <b>18</b> in $10^{-5}$ M THF at different temperatures.	156
108	<b>Figure 5A.22</b>	Emission spectra of complex <b>6</b> (Left) and <b>7</b> (Right) in methanol/glycerol mixture with increasing glycerol fraction (0 to 95%).	156

---

109	<b>Figure 5A.23</b>	Emission spectra of compound <b>8</b> (Left) and <b>12</b> (Right) in methanol/glycerol mixture with increasing glycerol fraction (0 to 95%).	157
110	<b>Figure 5A.24</b>	Emission spectra of compound <b>18</b> in methanol/glycerol mixture with increasing glycerol fraction (0 to 95%).	157
111	<b>Figure 5A.25</b>	(Left) Fluorescence quenching of compound <b>18</b> ( $10^{-5}$ M, excited at 352 nm) in a mixed solvent of THF: H <sub>2</sub> O (10 : 90) with different concentrations of PA (0, 1.0, 2.0, 3.0, 4.0, 5.0, 6.0, 7.0, 8.0, 9.0, 10.0, 11.0 and 12.0 equiv. of PA). (Right) Stern-Volmer plot of compound <b>18</b> in THF: H <sub>2</sub> O (10 : 90) with different concentrations of PA.	158
112	<b>Figure 5A.26</b>	(Left) Fluorescence lifetime decay of compound <b>18</b> after the addition of 0, 2, 4, 6, 8 and 12 equiv. of PA in THF:H <sub>2</sub> O (10:90) mixture.(Right) Fluorescence quenching efficiencies of compound <b>18</b> in THF : H <sub>2</sub> O (10:90) mixture towards of different nitroaromatics (8 equiv).	159
113	<b>Figure 5A.27</b>	Cyclic voltammograms of compounds <b>6-8</b> , <b>12</b> and <b>18</b> (vs. ferrocene/ferrocenium) with 0.1 M Bu <sub>4</sub> NPF <sub>6</sub> in DME as the supporting electrolyte (scan rate 100 mV s <sup>-1</sup> ).	159
114	<b>Figure 5B.1</b>	<sup>11</sup> B NMR spectrum of compound <b>4</b> .	180
115	<b>Figure 5B.2</b>	Molecular structure of compound <b>1</b> (Left) and compound <b>2</b> (right)	182
116	<b>Figure 5B.3</b>	Molecular structure of compound <b>3</b> (Left) and compound <b>4</b> (right)	182
117	<b>Figure 5B.4</b>	Intermolecular interaction in compound <b>1</b> (C-H... $\pi$ : 2.842 Å to 2.907 Å).	184
118	<b>Figure 5B.5</b>	Intermolecular interaction in compound <b>2</b> (C-H... $\pi$ : 2.857 Å to 2.947 Å).	185
119	<b>Figure 5B.6</b>	Intermolecular interaction in compound <b>3</b> (C-H... $\pi$ : 2.933 Å).	185

120	<b>Figure 5B.7</b>	Intermolecular interaction in compound <b>4</b> (C-H $\cdots\pi$ : 2.778 Å to 2.864 Å)	185
121	<b>Figure 5B.8</b>	(Left) Absorption spectra of compounds <b>1-4</b> in 10 <sup>-5</sup> M THF. (Right) Normalised emission spectra of compounds <b>1-4</b> in 10 <sup>-5</sup> M THF.	188
122	<b>Figure 5B.9</b>	(Left) Solvatochromic studies of compound <b>4</b> . (Right) Photograph of compound <b>4</b> in different solvents under handheld UV lamp irradiated at 365 nm.	189
123	<b>Figure 5B.10</b>	Normalised emission spectra of compounds <b>1-4</b> in solid state.	190
124	<b>Figure 5B.11</b>	(Left) Emission spectra of compound <b>1</b> (excited at 305nm) in THF:H <sub>2</sub> O mixture. (Right) Relative intensity vs. water fraction of compound <b>1</b> in THF:H <sub>2</sub> O mixture.	191
125	<b>Figure 5B.12</b>	(Left) Emission spectra of compound <b>2</b> (excited at 305nm) in THF:H <sub>2</sub> O mixture. (Right) Relative intensity vs. water fraction of compound <b>2</b> in THF:H <sub>2</sub> O mixture..	192
126	<b>Figure 5B.13</b>	(Left) Emission spectra of compound <b>3</b> (excited at 328 nm) in THF:H <sub>2</sub> O mixture. (Right) Relative intensity vs. water fraction of compound <b>3</b> in THF:H <sub>2</sub> O mixture.	192
127	<b>Figure 5B.14</b>	(Left) Photograph of compound <b>3</b> in THF:H <sub>2</sub> O mixture under a handheld UV lamp at 365 nm. (Right) Particle size distribution graph of compound <b>3</b> at H <sub>2</sub> O:THF (85:15).	192
128	<b>Figure 5B.15</b>	(Left) Emission spectra of compound <b>4</b> (excited at 362 nm) in THF:H <sub>2</sub> O mixture. (Right) Relative intensity vs. water fraction of compound <b>4</b> in THF:H <sub>2</sub> O mixture.	193
129	<b>Figure 5B.16</b>	(Left) Photograph of compound <b>4</b> in THF:H <sub>2</sub> O mixture under a hand held UV lamp. (Right) Particle size distribution graph of compound <b>4</b> at H <sub>2</sub> O: THF (95:5).	193
130	<b>Figure 5B.17</b>	Temperature dependent emission spectra of compound <b>1</b> (Left) and <b>2</b> (Right) in THF(10 <sup>-5</sup> M).	193

131	<b>Figure 5B.18</b>	Temperature dependent emission spectra of compound <b>3</b> (Left) and <b>4</b> (Right) in THF( $10^{-5}$ M).	194
132	<b>Figure 5B.19</b>	Emission spectra of compound <b>1</b> (Left) and <b>2</b> (Right) in methanol/glycerol mixture with increasing glycerol fraction (0 to 95%).	194
133	<b>Figure 5B.20</b>	Emission spectra of compound <b>3</b> (Left) and <b>4</b> (Right) in methanol/glycerol mixture with increasing glycerol fraction (0 to 95%).	195
134	<b>Figure 5B.21</b>	TGA curves of compounds <b>1-4</b> under nitrogen at a heating rate of $10\text{ }^{\circ}\text{C min}^{-1}$ .	195
135	<b>Figure 5B.22</b>	(Left) Cyclic voltammograms of compounds <b>1-4</b> (vs. ferrocene/ferrocenium) with 0.1 M $\text{Bu}_4\text{NPF}_6$ in DME as the supporting electrolyte (scan rate $100\text{ mV s}^{-1}$ ). (Right) Plot depicting oxidation in compound <b>4</b> .	196
136	<b>Figure 6.1</b>	Molecular structure of compound <b>2</b> (Left) and <b>5</b> (Right).	212
137	<b>Figure 6.2</b>	Normalised emission spectra of compound <b>2</b> with increasing solvent polarity.	215
138	<b>Figure 6.3</b>	Normalized UV-Vis absorption and fluorescence spectra of compounds <b>2</b> (left) and <b>5</b> (right) in $10^{-5}$ M acetonitrile.	215
139	<b>Figure 6.4</b>	Cyclic voltammograms of compound <b>2</b> & <b>5</b> (vs. Ferrocene/Ferrocenium) with 0.1 M $\text{Bu}_4\text{NPF}_6$ in DMF as the supporting electrolyte (scan rate $100\text{ mV/s}$ ).	216
140	<b>Figure 6.5</b>	Computed orbitals for compound <b>2</b> and <b>5</b> .	217
141	<b>Figure 6.6</b>	(a) Fluorescence quenching of compound <b>2</b> with the addition of different concentrations of PA (0, 0.25, 0.5, 0.75, 1.0, 1.5, 2.0, 3.0, 4.0, 5.0, 6.0, 7.0, 8.0, 9.0, 10.0, 12.0, 14.0, 16.0, 18.0, 23.0, and 27.0 equiv. of PA) in THF ( $10^{-5}$ M; excited at 333 nm). (b) Color change under a UV lamp before (left) and after (right) the addition of PA.	219

142	<b>Figure 6.7</b>	Fluorescence quenching of compound <b>5</b> with the addition of different concentrations of PA (0, 2, 4, 6, 8, 10, 12, 14, 16, 18, 20, 23, 26, 29, 33, 37, 41, 45, 50, 55, 60, 65, 70, 75, 80, 90, and 100 equiv of PA) in THF ( $10^{-5}$ M; excited at 366 nm).	219
143	<b>Figure 6.8</b>	(Left) Fluorescence quenching of compound <b>2</b> ( $10^{-5}$ M, excited at 333 nm) in a mixed solvent of THF: H <sub>2</sub> O (70 : 30) with different concentrations of PA (0, 0.25, 0.5, 0.75, 1.0, 1.25, 1.50, 1.75, 2.0, 2.5, 3.0, 3.5, 4.0, 4.5, 5.0, 6.0, 7.0, 10.0, 12.0, and 14.0 equiv. of PA). (Right) Fluorescence quenching of compound <b>5</b> ( $10^{-5}$ M, excited at 366 nm) in a mixed solvent of THF: H <sub>2</sub> O (70 :30) with different concentrations of PA (0, 0.2, 0.4, 0.6, 0.8, 1.0, 1.2, 1.4, 1.6, 1.8, 2.0, 2.2, 2.4, 2.6, 2.8, 3.0, 3.3, 3.6, 4.0, 4.4, 5.0, 5.5, 6.0, 7.0 and 8.0 equiv. of PA).	220
144	<b>Figure 6.9</b>	Stern-Volmer plot of compound <b>2</b> (left) and <b>5</b> (Right) in $10^{-5}$ M with addition of different concentration of PA in THF.	221
145	<b>Figure 6.10</b>	Stern-Volmer plot of compound <b>2</b> (left) and <b>5</b> (Right) in $10^{-5}$ M with addition of different concentration of PA in THF: H <sub>2</sub> O (70:30) mixture.	221
146	<b>Figure 6.11</b>	(Left) Fluorescence lifetime decay of compound <b>2</b> after the addition of 0, 1, 2, 3, 4 and 5 equiv. of PA in $10^{-5}$ M THF. (Right) Fluorescence lifetime decay of compound <b>5</b> after the addition of 0, 1, 2, 3, 4 and 5 equiv. of PA in $10^{-5}$ M THF.	222
147	<b>Figure 6.12</b>	Fluorescence quenching efficiencies of compounds <b>2</b> and <b>5</b> in THF : H <sub>2</sub> O (70 : 30) ( $10^{-5}$ M; excited at 333 nm) toward different nitroaromatics and other analytes (6 equiv.) like picric acid (PA), 1,3-dinitrobenzene (1,3-DNB), 1,4-dinitrobenzene (1,4-DNB), 2,4-dinitrotoluene (2,4-DNT), 2,6-dinitrotoluene (2,6-	223



---

	DNT), 4-nitrotoluene (4-NT), nitrobenzene (NB), DDQ, nitromethane (NM), benzoic acid (BA), phenol and trifluoroacetic acid (TFA).	
148	<b>Figure 6.13</b> Proposed quenching mechanism	223
149	<b>Figure 6.14</b> $^1\text{H}$ NMR titration of compound <b>2</b> upon the addition of 0, 2.5, 5.0, 7.5, 10.0, 12.5, 15.0, 17.5 and 20.0 equiv. of PA in DMSO- <i>d</i> <sub>6</sub> .	225
150	<b>Figure 6.15</b> Normalized Z-scan (a and b) CA transmittance. (c and d) OA transmittance of <b>2</b> and <b>5</b> respectively in dichloromethane.	227
151	<b>Figure 6.16</b> Normalized Z-scan (a and b) CA transmittance. (c and d) OA transmittance after adding 7.0 equiv. and 14.0 equiv. PA in compounds <b>2</b> and <b>5</b> respectively. Solvent: dichloromethane.	230

---

## List of Abbreviations

THF	Tetrahydrofuran
DMSO	Dimethyl sulfoxide
Et <sub>4</sub> NCl	Tetraethyl ammonium chloride
<sup>1</sup> H NMR	Proton nuclear magnetic resonance
<sup>13</sup> C NMR	Carbon nuclear magnetic resonance
IR	Infrared
CH <sub>2</sub> Cl <sub>2</sub>	Dichloromethane
CHCl <sub>3</sub>	Chloroform
HRMS	High resolution mass spectrometry
TGA	Thermogravimetric Analysis
DMF	Dimethylformamide
3D	Three dimensional
Hg(OAc) <sub>2</sub>	Mercuric acetate
LiCl	Lithium chloride
CaH <sub>2</sub>	Calcium hydride
<sup>119</sup> Sn NMR.	Tin nuclear magnetic resonance
MW	Molecular weight
HBpin	Pinacol borane
Me <sub>2</sub> SnCl <sub>2</sub>	Dimethyl tin dichloride
EtOAc	Ethyl acetate
CDCl <sub>3</sub>	Chloroform-d
BCl <sub>3</sub>	Boron trichloride
UV-Vis	Ultraviolet visible
PMMA	Poly(methyl methacrylate)
DME	Dimethoxyethane
HOMO	Highest occupied molecular orbital
LUMO	Lowest occupied molecular orbital
C <sub>6</sub> D <sub>6</sub>	Benzene-d <sub>6</sub>
DEPT-135	Distortionless enhancement by polarization transfer
ESI	Electrospray ionisation

---

Bu <sub>4</sub> NPF <sub>6</sub>	Tetrabutyl ammonium hexafluorophosphate
AIEE	Aggregation induced emission enhancement
ACQ	Aggregation caused quenching
BODIPY	Boron dipyromethene
NBS	N-Bromosuccinimide
Pd(PPh <sub>3</sub> ) <sub>4</sub>	Tetrakis(triphenylphosphine)palladium(0)
KOtBu	Potassium tert-butoxide
AlMe <sub>3</sub>	Trimethyl aluminium
DIPEA	N, N-Diisopropylethylamine
CH <sub>3</sub> CN	Acetonitrile
LE	Locally excited
TICT	Twisted intramolecular charge transfer
ICT	Intramolecular charge transfer
RIR	Restriction of intramolecular rotation
PA	Picric acid
OLED	Organic light emitting diode
K <sub>2</sub> CO <sub>3</sub>	Potassium carbonate
Na <sub>2</sub> SO <sub>4</sub>	Sodium sulphate
AIE	Aggregation induced emission
DLS	Dynamic light scattering
PL	Photoluminescence
TNT	Trinitrotoluene
AcOH	Acetic acid
<i>n</i> -BuLi	<i>n</i> -Butyllithium
TD-DFT	Time dependent density functional theory
MO	Molecular orbital
1,3-DNB	1,3-dinitrobenzene
1,4-DNB	1,4-dinitrobenzene
2,4-DNT	2,4-dinitrotoluene
2,6-DNT	2,6-dinitrotoluene
4-NT	4-nitrotoluene
NB	Nitrobenzene

---

---

DDQ	2,3-Dichloro-5,6-dicyano-1,4-benzoquinone
NM	Nitromethane
BA	Benzoic acid
TFA	Trifluoroacetic acid
LOD	Limit of detection
CA	Close aperture
OA	Open aperture
NLA	Nonlinear absorption
TPA	Two photon absorption
MPA	Multiphoton absorption
NLO	Nonlinear optics
CW	Continuous wave
TPAC	Two photon absorption count
GM	Goppert Meyer

# **CHAPTER 1**

## **Introduction**

<b>1.1 Tricoordinate boron compounds</b>	<b>03</b>
<b>1.1.1</b> Tricoordinate boron as anion sensors	<b>04</b>
<b>1.1.2</b> Tricoordinate boron as NLO materials	<b>10</b>
<b>1.1.3</b> Tricoordinate boron as photochromic materials	<b>14</b>
<b>1.2 Tetracoordinate boron compounds</b>	<b>16</b>
<b>1.2.1</b> N,C-chelate tetracoordinate boron compounds	<b>17</b>
<b>1.2.2</b> N,N-chelate tetracoordinate boron compounds	<b>29</b>
<b>1.2.3</b> N,O-chelate tetracoordinate boron compounds	<b>35</b>
<b>1.3 Main group bidentate Lewis acids</b>	<b>38</b>
<b>1.3.1</b> Bidentate mercury Lewis acid	<b>38</b>
<b>1.3.2</b> Bidentate tin Lewis acid	<b>42</b>
<b>1.3.3</b> Bidentate boron Lewis acid	<b>44</b>
<b>1.4 References</b>	<b>49</b>



---

## 1.1 Tricoordinate boron compounds

Fluorescent organic  $\pi$ -conjugated materials have drawn remarkable progress in the field of organic light emitting diodes (OLEDs),<sup>1,2</sup> nonlinear optics,<sup>3,4</sup> dye sensitized solar cells,<sup>5,6</sup> bioimaging,<sup>7,8</sup> thermally activated delayed fluorescence (TADF) material,<sup>9</sup> Aggregation-induced emission enhancement (AIEE) responsive dyes<sup>10</sup> and so on. Introduction of a heteroatom such as B, Al, Si, P, Sn etc into the backbone of  $\pi$ -conjugated material has proven to be a powerful approach to tune the electronic properties of  $\pi$ -conjugated materials.<sup>11,12</sup> In particular boron-based materials have gained recent research attention due to their advantages over organic  $\pi$ -conjugated material. Boron based fluorophores are broadly divided into two types.

1. Tricoordinate boron compounds and 2. Tetracoordinate boron compounds

### Tricoordinate boron compounds:

Fluorescent tri-coordinate organoboron compounds gained attention owing to their potential application in various fields. Boron centre adopts a  $sp^2$  hybridised mode in the tricoordinated boron compounds. Trivalent boron having an empty  $2p_z$  orbital possess a trigonal planar geometry. Due to this the tricoordinate boron compounds behave as lewis acids and have high tendency to coordinate with lewis bases. Tricoordinate boron compounds with organic  $\pi$ -system show significant delocalisation *via* the empty p-orbital of the boron centre. The interaction between the empty p-orbital of the boron and the organic  $\pi$ -system lead to the formation of interesting linear and nonlinear optical (NLO) properties and electroluminescence.<sup>13-16</sup> As the tricoordinate boron compounds are air and moisture sensitive, bulky substituents like mesityl are frequently used to improve the stability (**Figure 1.1**). Bulky aryl substitution on boron centre allows only attack of small anions, which makes this as a sensor for fluoride and cyanide sensing.

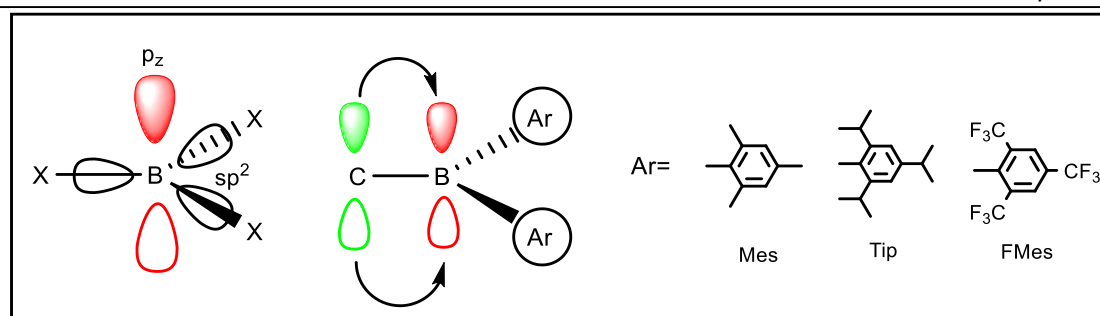


**Figure 1.1:** Schematic representation of trivalent boron compounds.

### 1.1.1 Tricoordinate boron as anion sensors

Anion sensing is a prime focus in the supramolecular chemistry since many decades. Especially fluoride sensing has drawn remarkable research attention due to its relevance for biological and industrial applications.<sup>17,18</sup> The strong affinity of fluoride towards boron atom has led to develop enormous sensory materials based on boron atom. In triaryl boron compound, the coordination of fluoride anion to the  $\pi$ -conjugated boron centre disturbs the extended conjugation. Taking advantage of this, Yamaguchi and coworkers<sup>19</sup> reported a series of  $\pi$ -conjugated triaryl boron systems **1-4** (**Figure 1.2**). Compounds **1-4** showed significant color change upon complexation with fluoride ion. The binding constant determined were  $(2.8 \pm 0.3) \times 10^5 \text{ M}^{-1}$  for compound **1**,  $(2.1 \pm 0.4) \times 10^2 \text{ M}^{-1}$  for compound **2**,  $(2.6 \pm 0.2) \times 10^5 \text{ M}^{-1}$  for compound **3**,  $(2.9 \pm 0.3) \times 10^5 \text{ M}^{-1}$  for compound **4**. Yamaguchi and coworkers<sup>20</sup> also reported a series of dibenzoborrole derivatives (**5-7**), which showed the absorption at 480-504 nm in THF (**Figure 1.2**). Upon excitation at the absorption maxima these compounds showed emission band at 550-576 nm with low fluorescence quantum yield. The emission intensity of the compounds decreases gradually with incremental addition of fluoride ions. The binding constant determined were  $(3.5 \pm 0.4) \times 10^5 \text{ M}^{-1}$  for **5**,  $(1.1 \pm 0.5) \times 10^6 \text{ M}^{-1}$  for **6** and  $(1.4 \pm 0.3) \times 10^6 \text{ M}^{-1}$  for **7**.



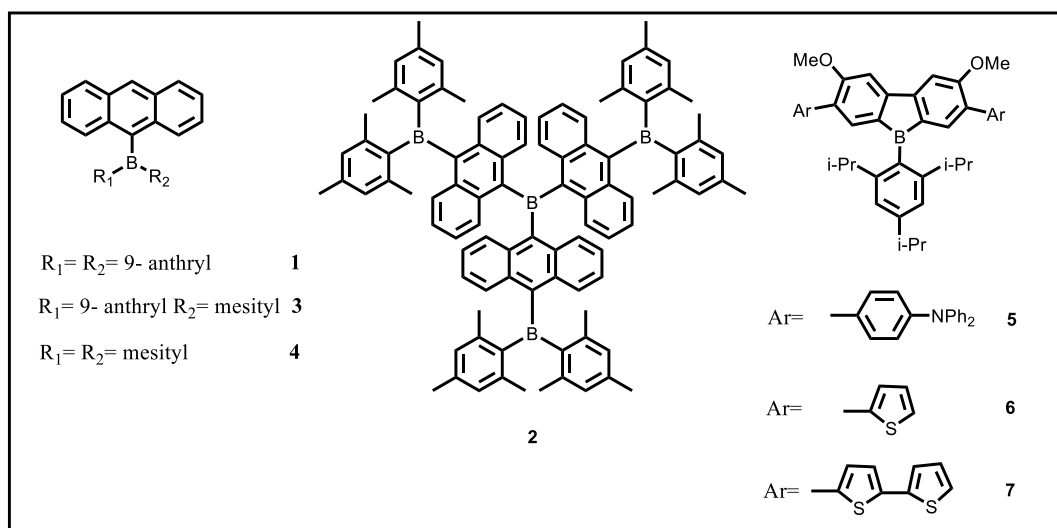


**Figure 1.2:** Tricoordinate boron as anion sensors (**1-7**).

Huang and coworkers<sup>21</sup> have synthesized a series of organoboranes (**8-10**), which showed absorption maxima at 402-435 nm (**Figure 1.3**). Complexation of fluoride ions to these boranes results in alteration of absorption and emission properties. THF solution of compound **8** upon complexation with tetrabutyl ammonium fluoride (TBAF) change the colour from yellow green to colorless in ambient light. Disappearance of absorbance band at 400 nm and rise of band at 370 nm, shows the formation of fluoroborate. From the absorption titration experiments the binding constants were found to be  $(2.3 \pm 0.3) \times 10^5 \text{ M}^{-1}$  for compound **8** and  $3.2 (\pm 0.3) \times 10^5 \text{ M}^{-1}$  for compound **10**.

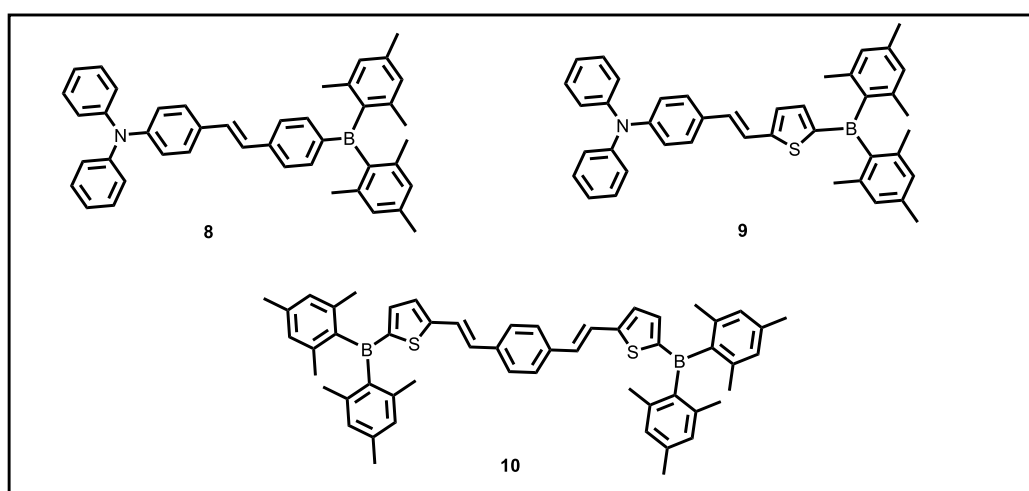


**Figure 1.3:** Tricoordinate boron as anion sensors (**8-10**).

Gabbai and coworkers<sup>22</sup> have reported two cationic boranes **11** and **12** (**Figure 1.4**). DFT calculations showed that HOMO is localized on mesityl rings whereas LUMO is having contribution from the empty p-orbital of boron. Complex **11** act as a receptor for cyanide ion in aqueous solution with a binding constant of  $3.9 (\pm 0.1) \times 10^8 \text{ M}^{-1}$ , whereas complex **12** forms fluoroborate complex with fluoride ion with a binding constant of  $910 (\pm 50) \text{ M}^{-1}$ .

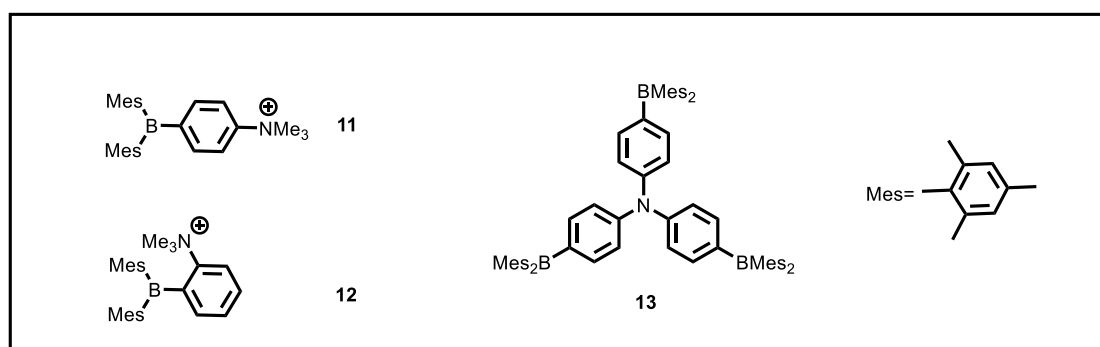


**Figure 1.4:** Tricoordinate boron as anion sensors (**11-13**).

Wenger and coworkers<sup>23</sup> have reported tris(4-(dimesitylboryl)phenyl)amine (**13**), having three dimesitylboryl groups (**Figure 1.4**). On addition of TBAF to the dichloromethane solutions of compound **13**, the absorption peak at 400 nm decreases gradually. Using SPECFIT program they led to the conclusion that, fluoride addition forms the 1:1, 1:2 and 1:3 adduct of compound **13** and fluoride ion. The association constant obtained are  $K_{a1} = 4 \times 10^7 \text{ M}^{-1}$  for 1:1 adduct,  $K_{a2} = 2.5 \times 10^6 \text{ M}^{-1}$  for 1:2 adduct and  $K_{a3} = 3.2 \times 10^4 \text{ M}^{-1}$  for 1:3 adduct.

Jäkle and coworkers<sup>24</sup> have reported triaryl boron functionalized luminescent homo and block copolymers (**Figure 1.5**). Upon addition of TBAF solution to the polymer **15** and **16**, the absorption band at 330 nm decreases and an absorption band at 278 nm appeared. The corresponding monomer **14** showed absorption band at 312 nm. The binding constant determined for the monomer and the polymers were  $\log \beta = 7.3$ .

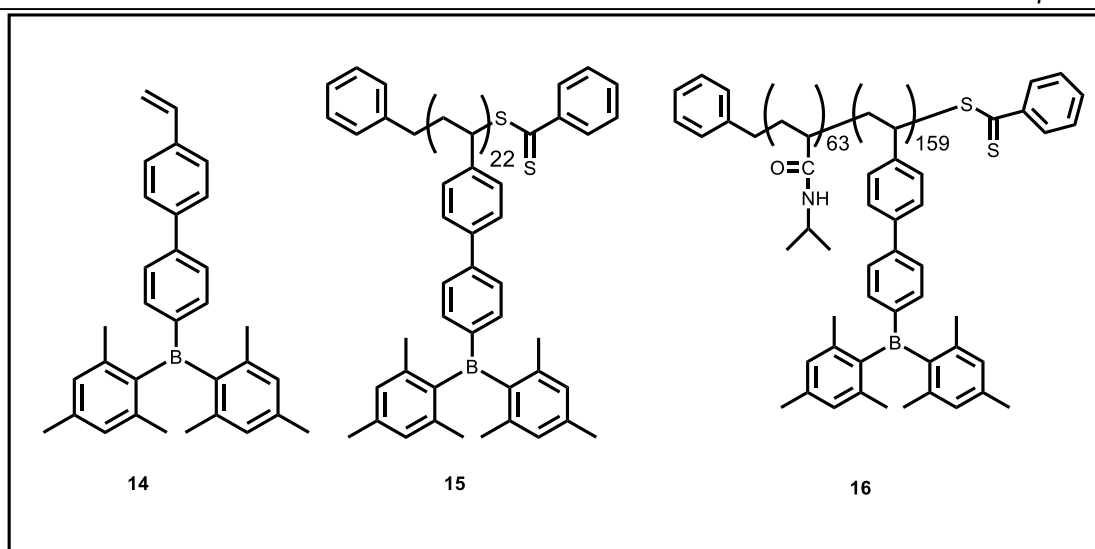


**Figure 1.5:** Tricoordinate boron as anion sensors (**14-16**).

Triaryl boron-phenanthroimidazole complex **17** and **18** were reported by Lee and coworkers<sup>25</sup> (**Figure 1.6**). These complexes are highly fluorescent with a quantum yield of 0.74 for complex **17** and 0.92 for complex **18**. Binding constant was calculated from the changes in fluorescence intensity after the addition of fluoride ion and was found to be  $3.2 \times 10^5 \text{ M}^{-1}$  for complex **17**. The binding constant for complex **18** was estimated to be  $1.6 \times 10^5 \text{ M}^{-1}$  in THF which is lower because of higher LUMO energy in complex **18** compared to complex **17**.

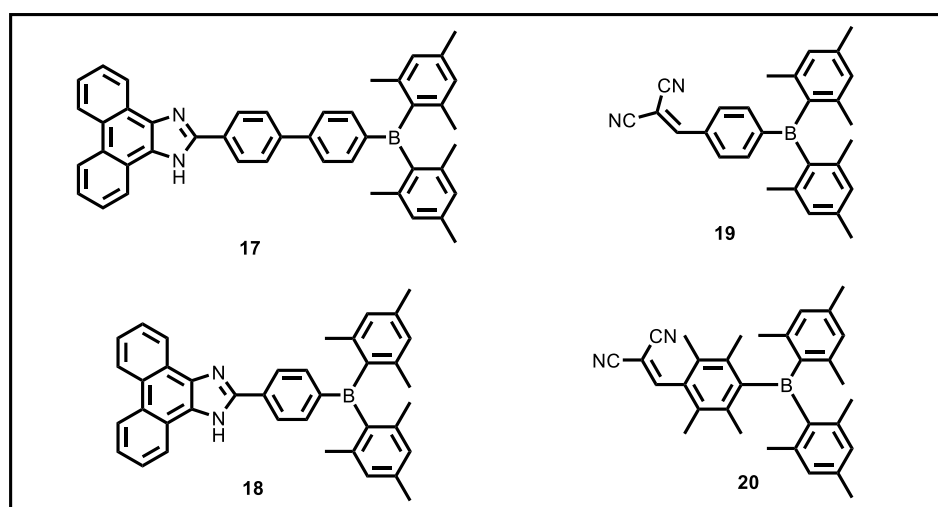


**Figure 1.6:** Tricoordinate boron as anion sensors (**17-20**).

Dicyanovinyl substituted triaryl boranes **19** and **20** were reported by Thilagar and coworkers<sup>26</sup> (**Figure 1.6**). Complex **19** and **20** showed absorption band in the region of 270-400 nm. The emission spectrum of complex **19** showed emission band at 509 nm whereas complex **20** showed dual emission bands at 391 and 493 nm. The binding constant calculated for fluoride ion was found to be  $7.07 \times 10^5 \text{ M}^{-1}$  and  $1.79 \times 10^5 \text{ M}^{-1}$  for complex **19** and **20** respectively. Complex **19** and **20** were also studied for cyanide ion sensing using TBACN. Cyanide ion binds to the boron centre and dicyanovinyl centre in complex **19** whereas in complex **20** it binds selectively to the dicyanovinyl centre. The observed binding constants for cyanide sensing are  $0.96 \times 10^5 \text{ M}^{-1}$  for complex **19** and  $1.70 \times 10^5 \text{ M}^{-1}$  for complex **20**.

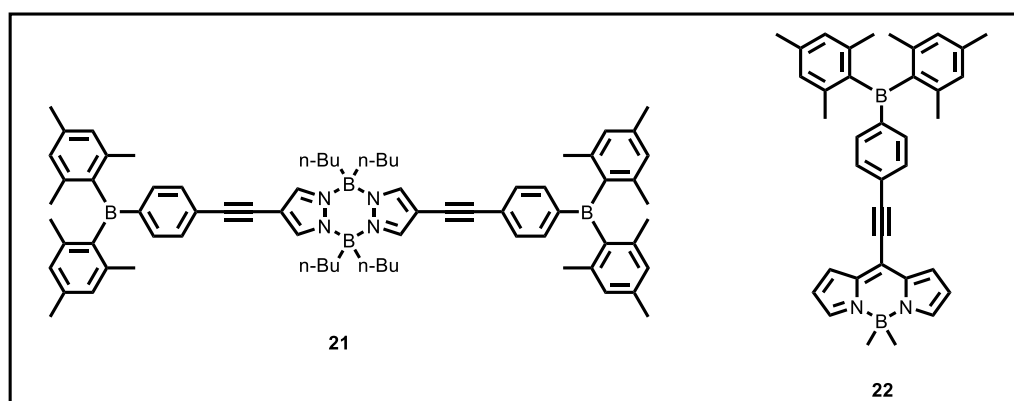


**Figure 1.7:** Tricoordinate boron as anion sensors (**21-22**).

Misra and coworkers<sup>27</sup> have reported tri and tetracoordinated boron molecules namely pyrazabole **21** and BODIPY **22** (**Figure 1.7**). Pyrazabole showed absorption band at 340 nm while BODIPY **22** exhibited absorption band at 420 nm and 540 nm. Pyrazabole **21** showed emission band at 402 nm with a quantum yield of 9% while BODIPY **22** emitted at 540 nm with a quantum yield of 35%. The binding constant for fluoride sensing calculated were found to be  $5.96 \times 10^9 \text{ M}^{-2}$  and  $2.41 \times 10^4 \text{ M}^{-1}$  for **21** and **22** respectively. Pyrazabole **21** and BODIPY **22** also utilized for sensing of cyanide

ion and the corresponding binding constant was calculated to be  $8.17 \times 10^8 \text{ M}^{-2}$  for pyrazabole **21** and  $1.07 \times 10^3 \text{ M}^{-1}$  for BODIPY **22**.

Wang and coworkers<sup>28</sup> have reported the synthesis of triarylboron functionalized bisbenzimidazole **23** and its dicationic bisbenzimidazolium salt **24** (**Figure 1.8**). Anion sensing of both complex **23** and **24** were monitored using absorption and emission spectroscopy. The calculated binding constant for complex **23** was found to be  $6.3 \times 10^4 \text{ M}^{-1}$  to  $8.3 \times 10^4 \text{ M}^{-1}$  for sensing of fluoride ion and  $4.6 \times 10^4 \text{ M}^{-1}$  to  $2.7 \times 10^5 \text{ M}^{-1}$  for sensing of cyanide ion. Similarly complex **24** was also tested for sensing of fluoride and cyanide ion. The binding constant were found to be  $2.9 \times 10^4 \text{ M}^{-1}$  to  $5 \times 10^5 \text{ M}^{-1}$  for fluoride anions and  $7.5 \times 10^4 \text{ M}^{-1}$  to  $3.3 \times 10^5 \text{ M}^{-1}$  for cyanide anions.

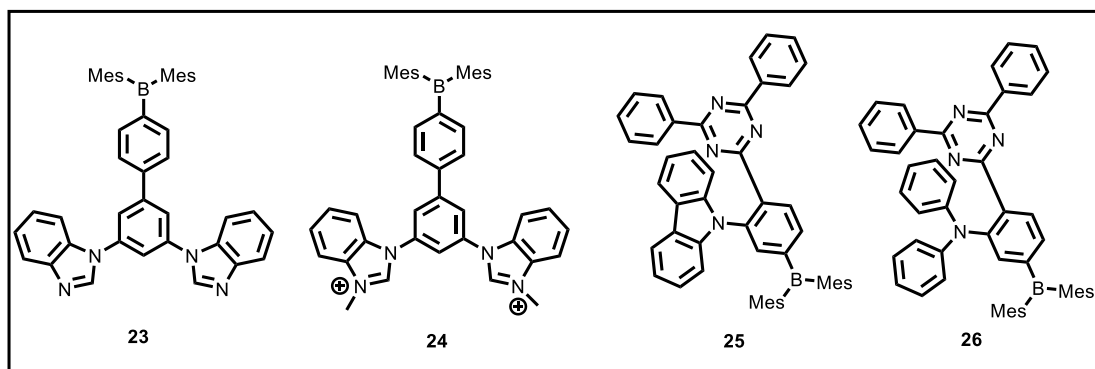


**Figure 1.8:** Tricoordinate boron as anion sensors (**23-26**).

Recently Lee and coworkers<sup>29</sup> have reported two triarylboron complexes. In complex **25** carbazole donor is linked as a donor group and in complex **26** diphenylamine group is linked as a donor group along with triazine acceptor (**Figure 1.8**). Both complexes were used for sensing fluoride ion in THF using TBAF as a fluoride source. The calculated binding constant was found to be  $8.5 \times 10^6 \text{ M}^{-1}$  for complex **25** and  $9.5 \times 10^6 \text{ M}^{-1}$  for complex **26**.

### 1.1.2 Tricoordinate boron as NLO materials

Nonlinear optical properties (NLO) of an organic molecule mainly depends on the position of the donor-acceptor groups and conjugation length of the  $\pi$ -system.<sup>30</sup> For a molecule to show second order NLO properties, molecule must be non-centrosymmetric so that the first order hyperpolarizability ( $\beta$ ) is non zero. On the otherhand, centrosymmetric molecules are better candidate for third order NLO properties. As the tricoordinate boron is lewis acidic character, due to intramolecular charge transfer in a  $\pi$ -conjugated system, tricoordinate boron shows NLO properties. In 1990 Marder and coworkers<sup>31</sup> have reported a series of air stable triaryl borane (**27-31**) by hydroboration of substituted alkyne with dimesitylborane and obtained a  $\beta$  value of  $5.1 \times 10^{-30}$  esu for **27**,  $9.3 \times 10^{-30}$  esu for **28**,  $8.6 \times 10^{-30}$  esu for **29**,  $18 \times 10^{-30}$  esu for **30** and  $11 \times 10^{-30}$  esu for **31** (Figure 1.9).

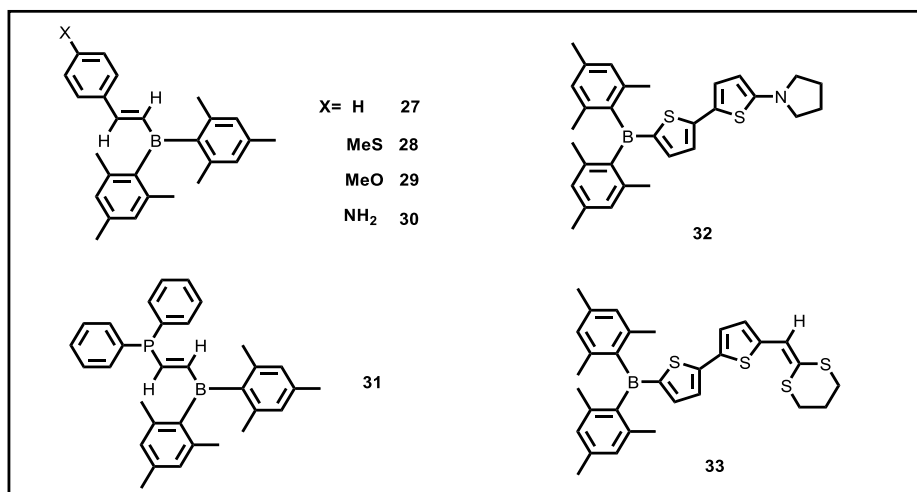


**Figure 1.9:** Tricoordinate boron as NLO materials(**27-33**).

In 1996, Branger and coworkers<sup>32</sup> have reported two tricoordinate boron chromophores (**32** and **33**), where pyrrolidin-1-yl, dithianylidene and thienyl used as the donor group and dimesitylborane as the acceptor group (Figure 1.9). The  $\beta$  values were

measured using electric field induced second harmonic (EFISH) techniques and found to be  $37 \times 10^{-30}$  esu for **32** and  $31 \times 10^{-30}$  esu for **33**.

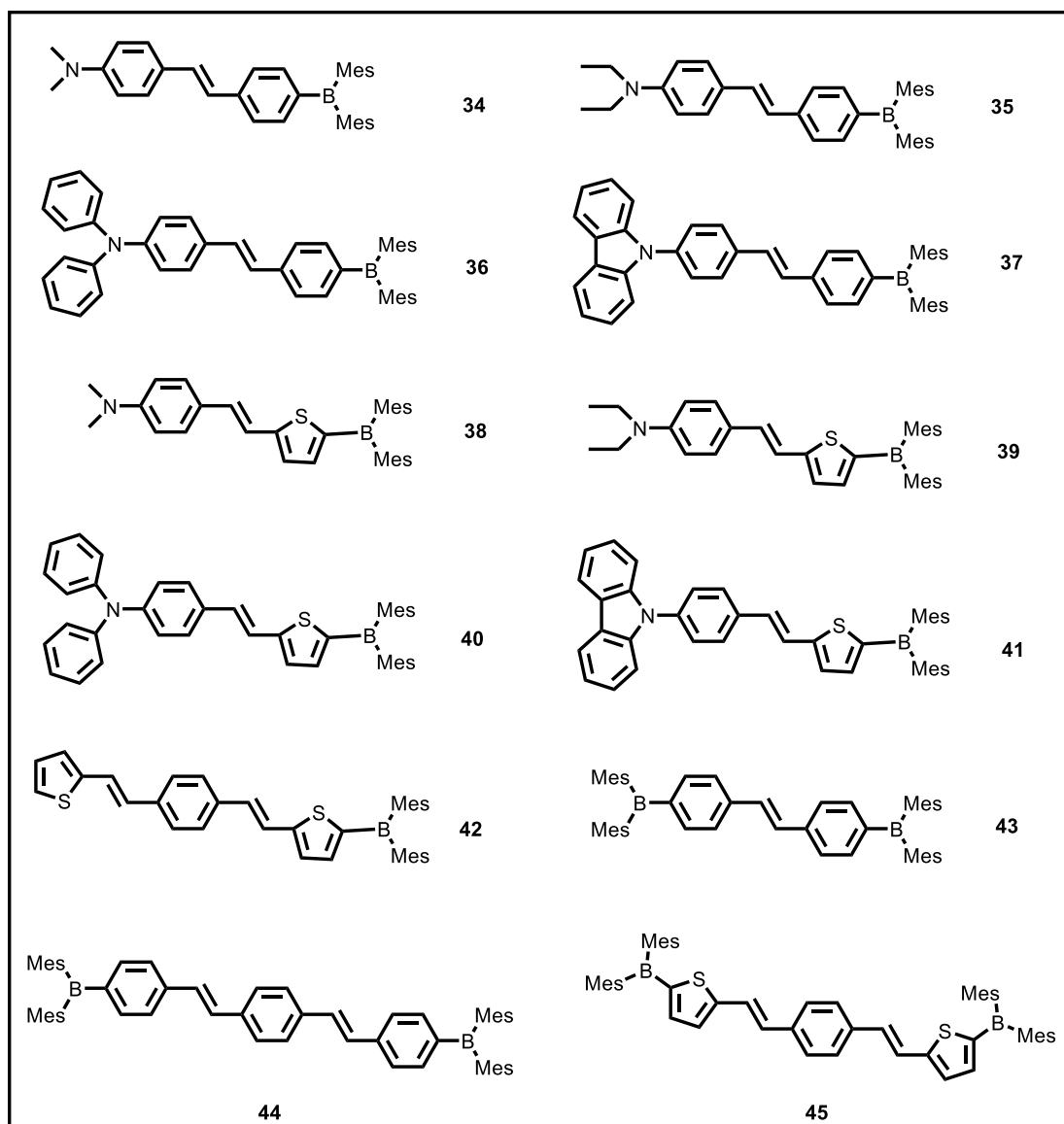


**Figure 1.10:** Tricoordinate boron as NLO materials (**34-45**).

Liu and coworkers<sup>33</sup> have reported a series of triaryl boron based donor- $\pi$ -acceptor chromophores (**34-42**) and studied the NLO properties. The two photon absorption (TPA) cross section ( $\sigma$ ) values were found to be 188, 194, 300, 212, 74, 93, 119, 123 and 239 GM respectively (**Figure 1.10**). Two photon emission cross section (TPEF) were also calculated for these molecules and were found to be 3.2, 3.6, 8.3, 5.1, 0.8,

1.0, 3.0, 3.2 and 4.8 GM for **34-42** respectively. In 2004, Liu and coworkers<sup>34</sup> reported acceptor- $\pi$ -acceptor type of compounds, conjugated with triaryl borane (**43-45**) (**Figure 1.10**). The TPA cross section values were found to be 34, 593 and 817 GM and TPEF cross section were calculated to be 41, 835 and 1340 GM for **43-45** respectively. (1 GM =  $10^{-50}$  cm<sup>4</sup> s photon<sup>-1</sup>)

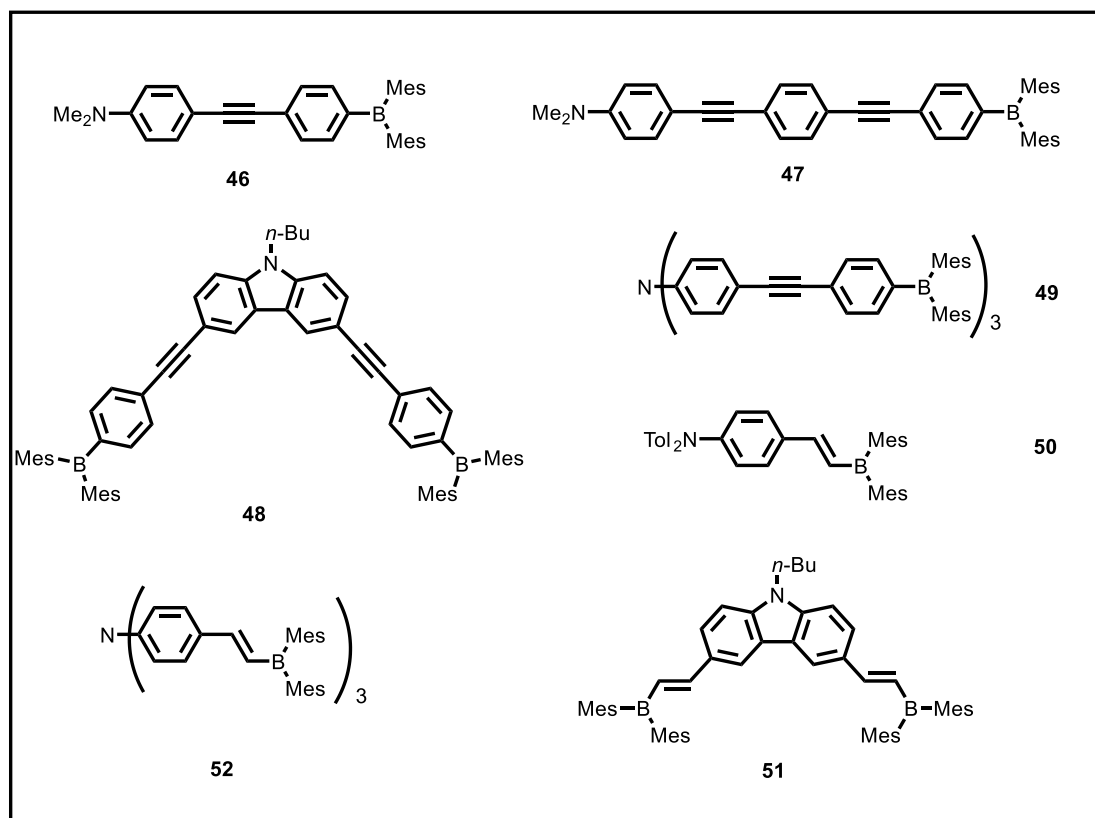


**Figure 1.11:** Tricoordinate boron as NLO materials (**46-52**).

In 2009, Marder and coworkers<sup>35</sup> have synthesized a series of dipolar, quadrupolar and octupolar donor- $\pi$ -acceptor molecule and studied the one and two photo absorption properties (**Figure 1.11**). The two photon absorption cross section ( $\sigma_2$ ) values of complexes **46-52** were found to be ~200, ~375, ~350, ~250, ~200, ~50 and ~1000 GM respectively. Complex **52** having the large TPA cross section and high quantum yield (0.94) makes it as a good candidate for application in TPEF.



Jäkle and coworkers<sup>36</sup> have synthesized a set of fluorescent quadrupolar borazine oligomers (**53-56**). They also studied the two photon absorption cross section maximum ( $\delta_{\max}$ ) which are found to be 280, 700, 1000 and 1410 GM respectively (**Figure 1.12**).

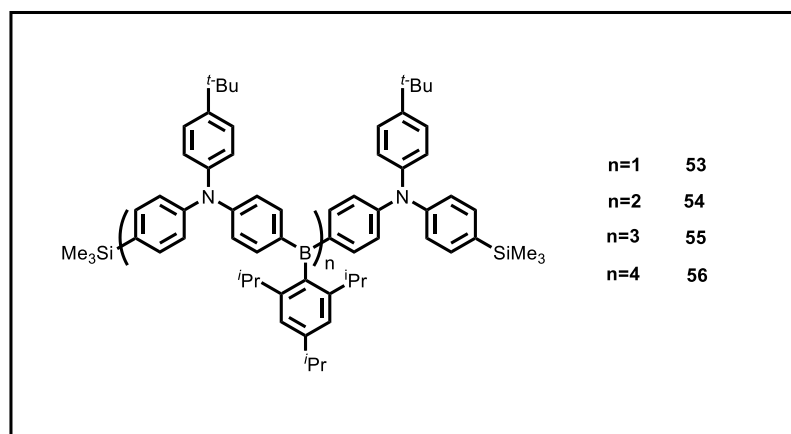


**Figure 1.12:** Tricoordinate boron as NLO materials (**53-56**).

In 2019, Marder and coworkers<sup>37</sup> have reported two cationic triaryl borane chromophores (**57** and **58**), a dipolar system and an octupolar system for cell imaging (**Figure 1.13**). In these chromophore triphenyl amine act as the donor and triaryl borane act as the acceptor. The dipolar **57** shows the TPA brightness of 17 GM whereas octupolar **58** shows about 5 to 87 GM. These two chromophores are applied in TPEF cell imaging. Marder and coworkers<sup>38</sup> have synthesized a set of quadrupolar chromophores by tuning the  $\pi$ -bridge (**59-63**) and obtained two photon absorption cross section ( $\sigma_2$ ) values of 72, 79, 162, 134 and 4560 GM for **59-63** respectively (**Figure 1.13**). Compound **63** showed two photon brightness upto 2545 GM in acetonitrile because of diketopyrrole unit, which makes the system elongated. All these dyes were tested for live cell imaging. Compound **63** with highest TPA value did not show any cell toxicity upon staining the concentration 20 times.

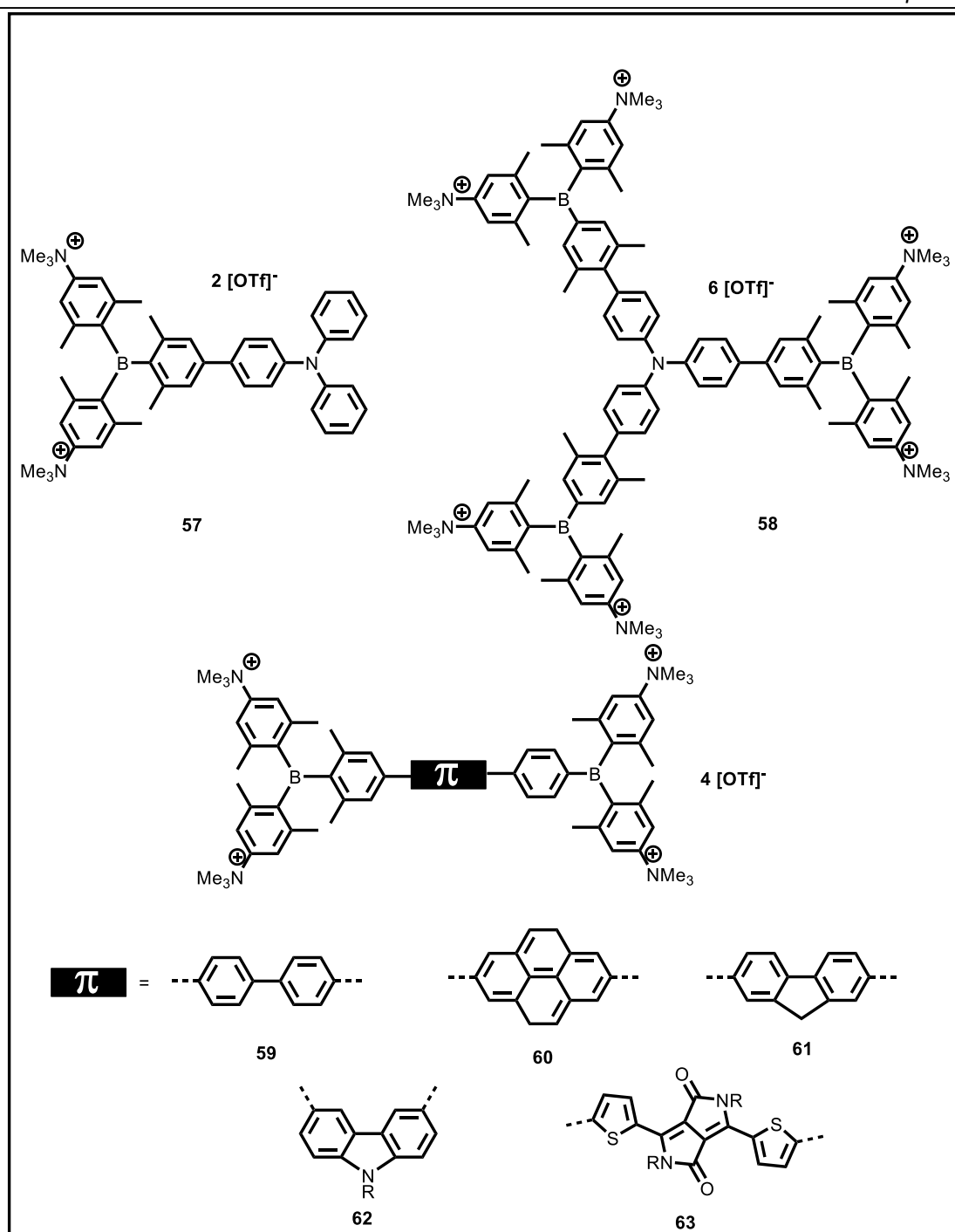


**Figure 1.13:** Tricoordinate boron as NLO materials (57-63).

### 1.1.3 Tricoordinate boron as photochromic materials

Photochemistry of boron compounds have seen large development since past several decades.<sup>39</sup> The photochemistry of four coordinate boron compounds conjugated with  $\pi$ -systems have been explored by Wang and coworkers.<sup>40-43</sup> However the reactivity of

triaryl borane are explored rarely. In 2013, Yamaguchi and coworkers<sup>44</sup> have synthesized a borylated dibenzoborepin (**64**) through a skeletal rearrangement (**Figure 1.14**). This dibenzoborepin shows photochromic properties, which proceed *via* bora-Nazarov cyclisation reactions to give the photoproduct.

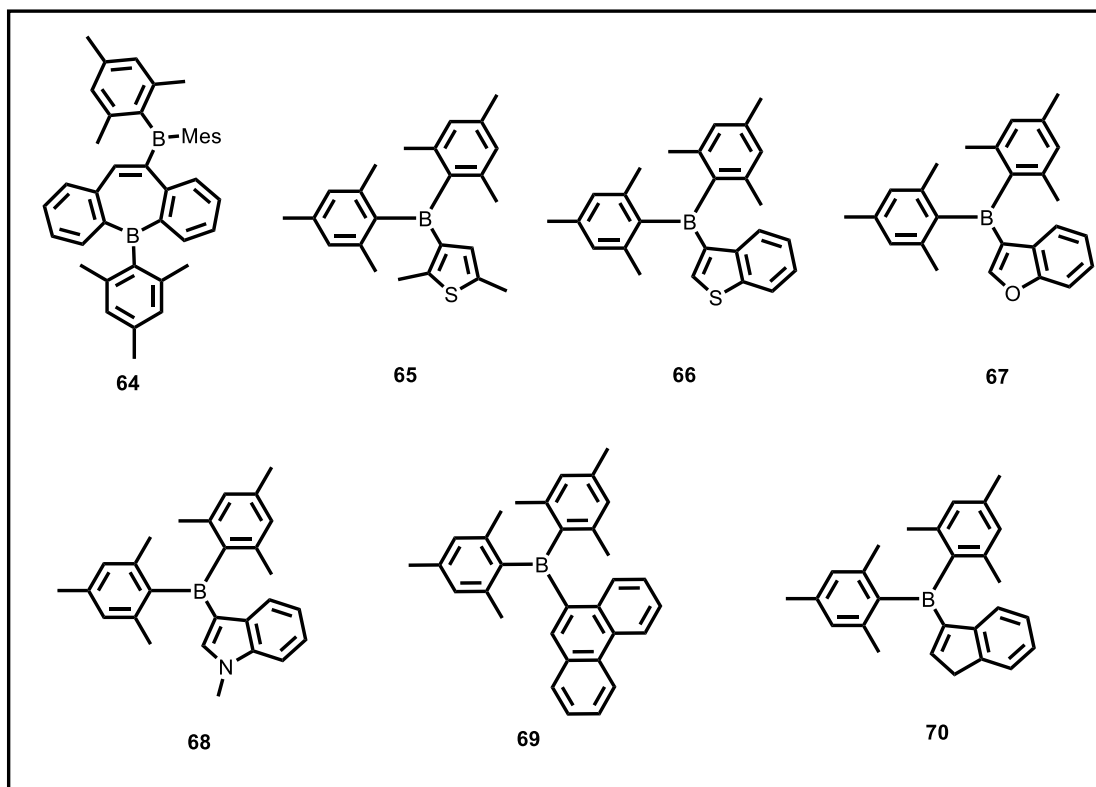


**Figure 1.14:** Tricoordinate boron as photochromic materials (**64-70**).

Yamaguchi and coworkers<sup>45</sup> in 2017, reported a series of dimesityl(heteroaryl)boranes (**65-70**) (**Figure 1.14**). Upon photoirradiation to these dimesityl(heteroaryl)boranes spirocyclic boraindanes are formed. However the bora-Nazarov cyclisation products are not observed. The experimental and theoretical study confirms that the reaction proceeded through [1,6]-sigmatropic rearrangement. Wang and coworkers<sup>46</sup> have synthesized a series of dimesitylborane functionalized stilbene (**71-74**), which undergo multistep photoisomerisation with dearomatisation of one mesityl ring to give a three fused five membered ring.

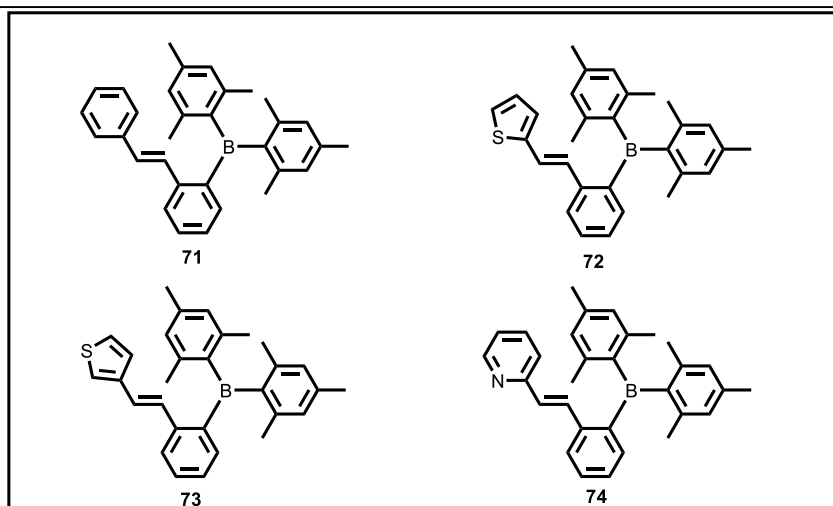


**Figure 1.15:** Tricoordinate boron as photochromic materials (**71-74**).

## 1.2 Tetracoordinate boron compounds

The chemistry of tetracoordinate boron compounds have been developed extensively over past few decades due to their wide applications in organic field effect transistors (OFETs), organic light emitting diodes (OLEDs), thermally activated delayed fluorescence materials (TADF), bioimaging materials, sensing and so on.<sup>47-52</sup>

Tetracoordinate boron compounds are derived by formation of covalent bond with monoanionic ligands. The incorporation of boron atom to a conjugated  $\pi$ -system in a tetracoordinate fashion increases the planarity of the conjugated molecule. The coordination saturation of boron atom increases the thermal stability and rigidity of the  $\pi$ -conjugated framework in tetracoordinate boron compounds, which also helps to get better fluorescent quantum yield. In tetracoordinate boron compounds highest occupied molecular orbital (HOMO) is located on the conjugated chelating ligand or on the R group where as LUMO is located on the chelating ligand (**Figure 1.16**). The variation of chelating ligand or R group greatly influences the HOMO-LUMO level and are responsible for emissions in these types of complex. The tetracoordinate boron compounds generally classified into four types. (i) N,C-chelate boron compounds, (ii)

N,O-chelate boron compounds ,(iii) N,N-chelate boron compounds and other types of boron compounds.

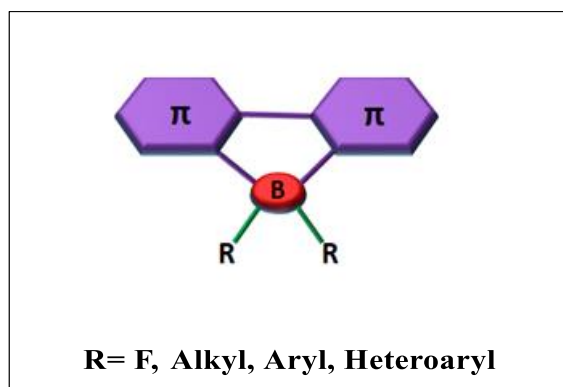


**Figure 1.16:** Schematic representation of tetracoordinate boron compound.

### 1.2.1 N,C-chelate boron compounds

Wakamiya *et al.*<sup>53</sup> in 2006 reported thienyl thiazole based N,C-chelate boron compound (**75**) and corresponding three diboron compounds **76-78** (**Figure 1.17**). Compound **75** shows absorption band at 333 nm while compounds **76-78** show absorption band around 414-443 nm. These compounds are weakly emissive in nature, show emission band in the range of 452-492 nm.

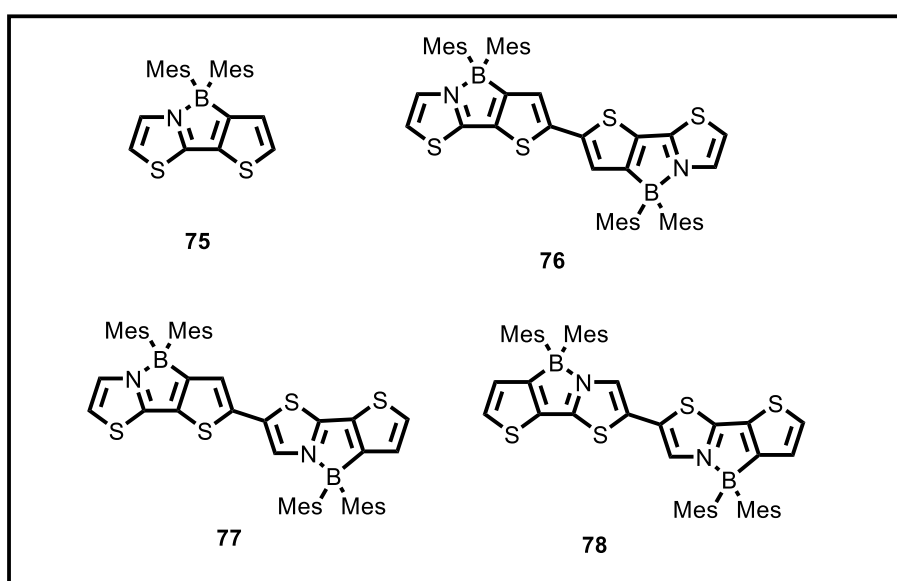


**Figure 1.17:** N,C-chelate four coordinate boron compounds **75-78**.

Wang and coworkers<sup>54</sup> synthesized a series of N,C-chelate boron compounds **79-88** based on phenyl pyridine ligand (**Figure 1.18**). For all these molecules HOMO is located on one of the aryl group while LUMO is located on the  $\pi^*$  orbital of the chelating unit. Compounds **79-88** show photochromic response upon irradiation of UV light. Zhang and coworkers<sup>55</sup> synthesized a set of ladder type  $\pi$ -conjugated diboron molecules **89-92** based on diphenyl thienothiazole system (**Figure 1.18**).

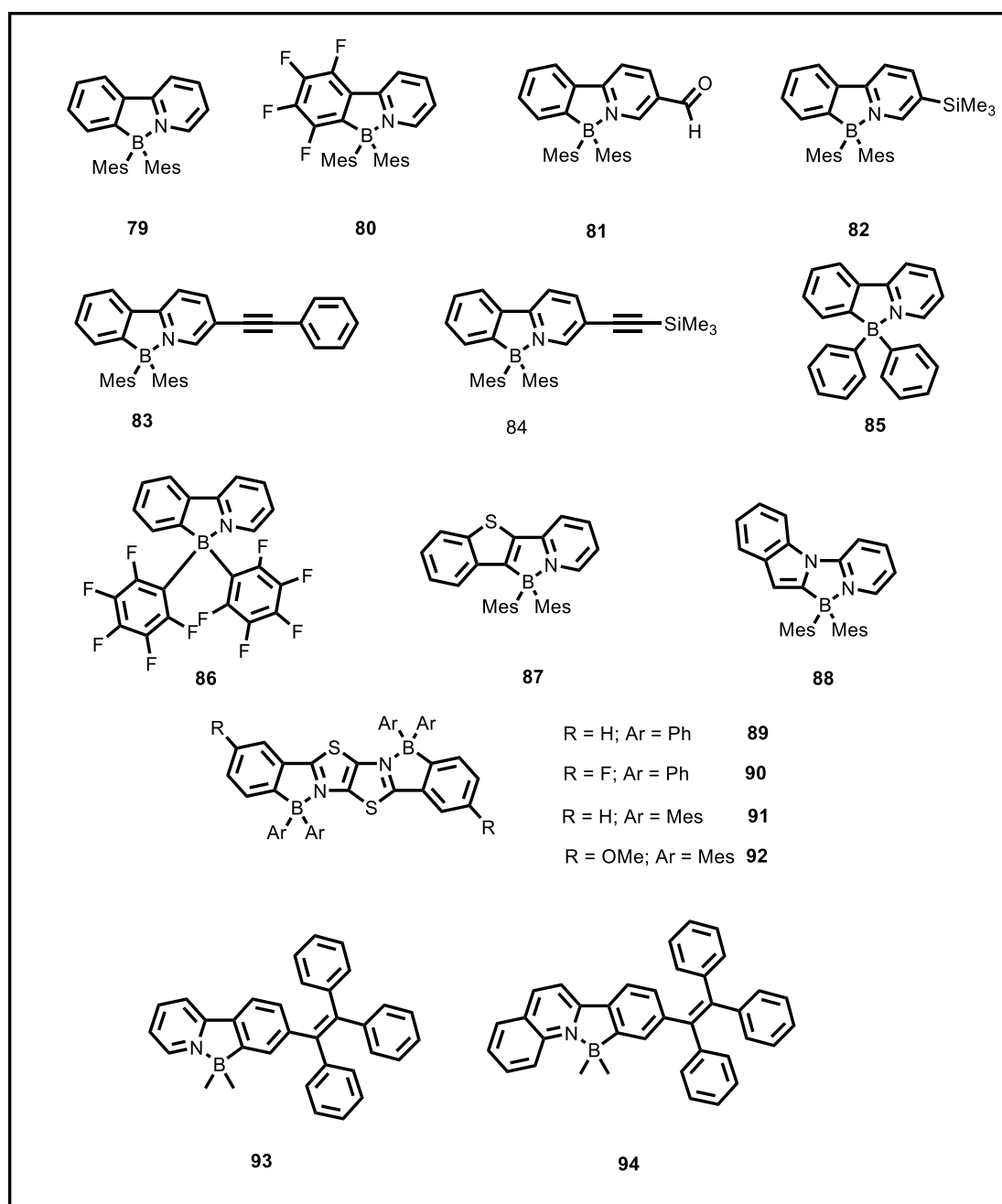


**Figure 1.18:** N,C-chelate four coordinate boron compounds **79-94**.

Electrochemical analysis reveal that compounds **89-92** show a reversible reduction wave in the range of -1.72 V to -1.92 V. Compounds **89-92** exhibit absorption maxima in the range of 402-450 nm and emission band in the range of 439-520 nm. Tang and coworkers<sup>56</sup> reported pyridine and quinoline substituted tetraphenylethylene based four coordinate boron compounds **93** and **94** (**Figure 1.18**). Electrochemical analysis showed two reversible oxidation state at 1.34 V and 1.54 V. Compound **93** showed absorption band at 351 nm while compound **94** showed absorption band at 388 nm. These two compounds exhibit AIE property in THF/water mixture upto 99.5% water fraction. Jäkle and coworkers<sup>57</sup> reported pyridyl ferrocene based four coordinate chiral organoboron compounds **95-97** (**Figure 1.19**). Electrochemical studies reveal that, compounds **95** and **97** showed a reversible oxidation peak at +120 mV and +134 mV respectively. Compound **96** showed oxidation peak at -174 mV due to electron rich mesityl ring. Later Jäkle and coworkers<sup>58</sup> synthesized two four coordinate organoborane (**98-99**) *via* electrophilic borylation approach (**Figure 1.19**). Compounds **98** and **99** showed absorbance band in the range of 382-405 nm. Both compounds emit in the range of 413-437 nm with a high quantum yield of 0.42 and 0.68 for compounds **98** and **99** respectively. Cyclic voltammetry data showed that compounds **98** and **99** undergo two reversible reductions. Wang and coworkers<sup>59</sup> synthesized a series of N,C chelate organoboron compounds **100-103** by lithiation using *tert*-butyl lithium (**Figure 1.19**). These compounds showed absorption peak in the range of 300-480 nm. Cyclic voltammetry studies reveal that these compounds exhibit one electron reduction peak at -2.11 V for **100**, -2.18 V for **101**, -2.33 V for **102** and -1.68 V for **103**. Photoreactivity of these complexes are examined upon irradiation of UV-light at 350 nm. Compounds **101** and **102** upon photoirradiation produces a new borazine complex with the

elimination of two mesityl unit. However compounds **100** and **103** under photoirradiation generate unidentified product.

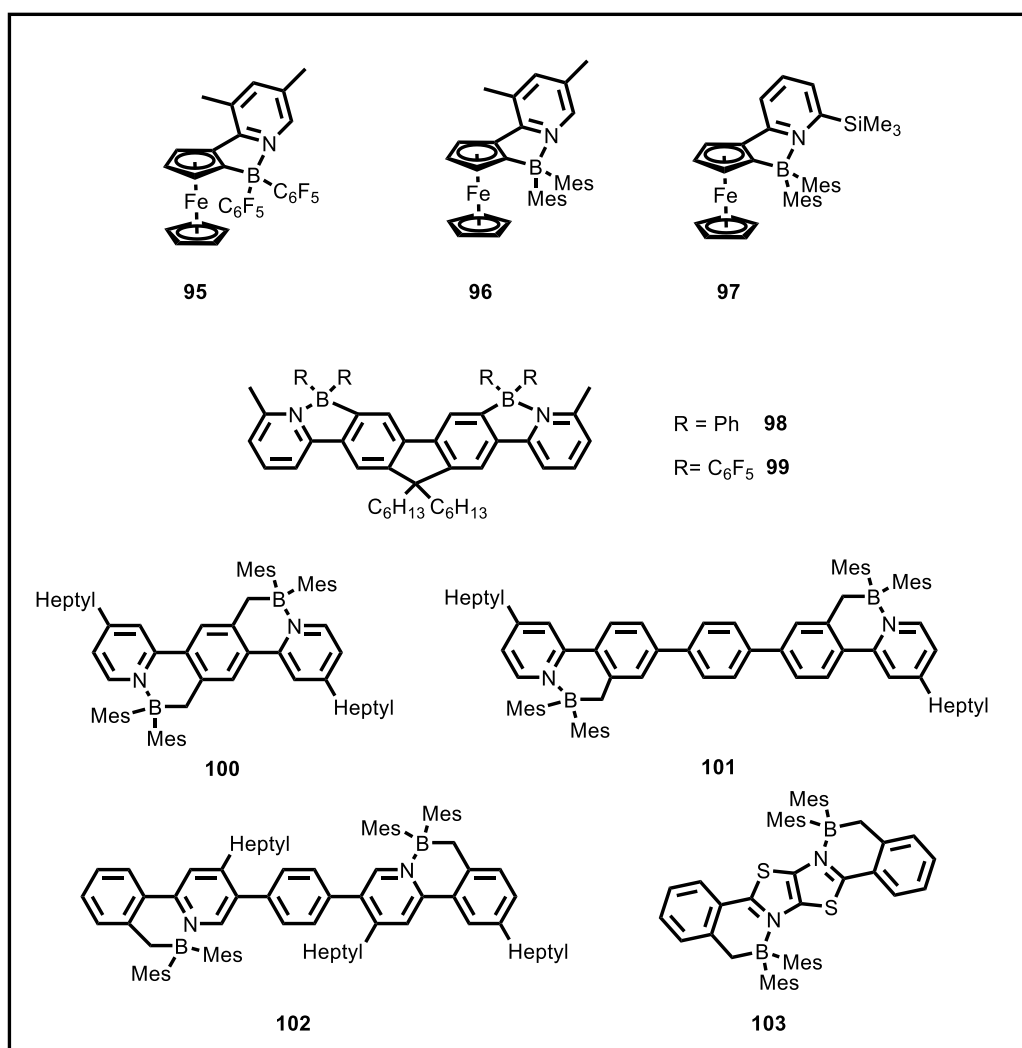


**Figure 1.19:** N,C-chelate four coordinate boron compounds **95-103**.

In 2017, Jäkle and coworkers<sup>60</sup> have reported dipyrrolyl anthracene based N,C-chelate organoboron compounds **104-106** by electrophilic aromatic borylation procedure (**Figure 1.20**). Compound **104** showed absorption band at 453 nm and emits at 538 nm with a quantum yield of 0.22. The diboron compounds **105** and **106** showed enhancement in quantum yield (**105**: 0.56; **106**: 0.53) compared to compound **104**. Compounds **105** and **106** quickly react with oxygen in presence of UV light to form



corresponding endoperoxide product without addition of a photosensitizer. This shows the self sensitizing property of organoboron compound.

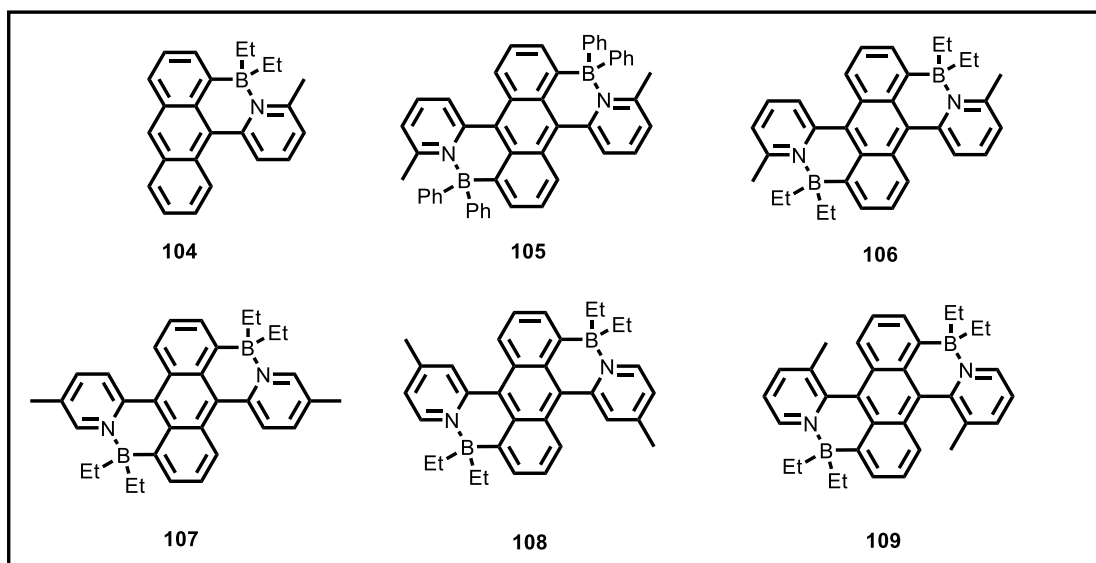


**Figure 1.20:** N,C-chelate four coordinate boron compounds **104-109**.

Recently Jäkle and coworkers<sup>61</sup> reported a series of N,C- chelate boron compounds with dipyrindyl anthracene systems by tuning the position of methyl groups in pyridyl ring **106-109** (**Figure 1.20**). X-ray crystal analysis reveals that compound **106** has longest B-N distance, experiences small distortion and compound **109** having methyl group near to anthracene unit is severely distorted. These compounds show self sensitizing property towards oxygen. Kinetic study shows that the reactivity of **106** is faster compared to **109**. This result suggests the impact of substitution on the steric and electronic property, resulting the change in reactivity.

From our group<sup>62</sup>, we have reported a set of four-coordinate organoboron compounds **110-113** based on phenanthroimidazole unit (**Figure 1.21**). These compounds showed absorption band in the region of 359-393 nm and emission peak in the range of 384-444 nm in THF solution. Compound **113** shows solvatochromic emission. These compounds showed quantum yield in the range of 0.07 to 0.88. Later we also reported

a series of  $\pi$ -extended N,C-chelated phenanthroimidazole boron dimers **114-118** (Figure 1.21).<sup>63</sup> These diboron complexes exhibited high fluorescence emission with an excellent quantum yield upto 99% in solution state and upto 52% in the solid state. The NLO properties ( $n_2$  and  $\beta$ ) of these complexes were examined, which showed the dependence of  $\pi$ -conjugation length on NLO properties.

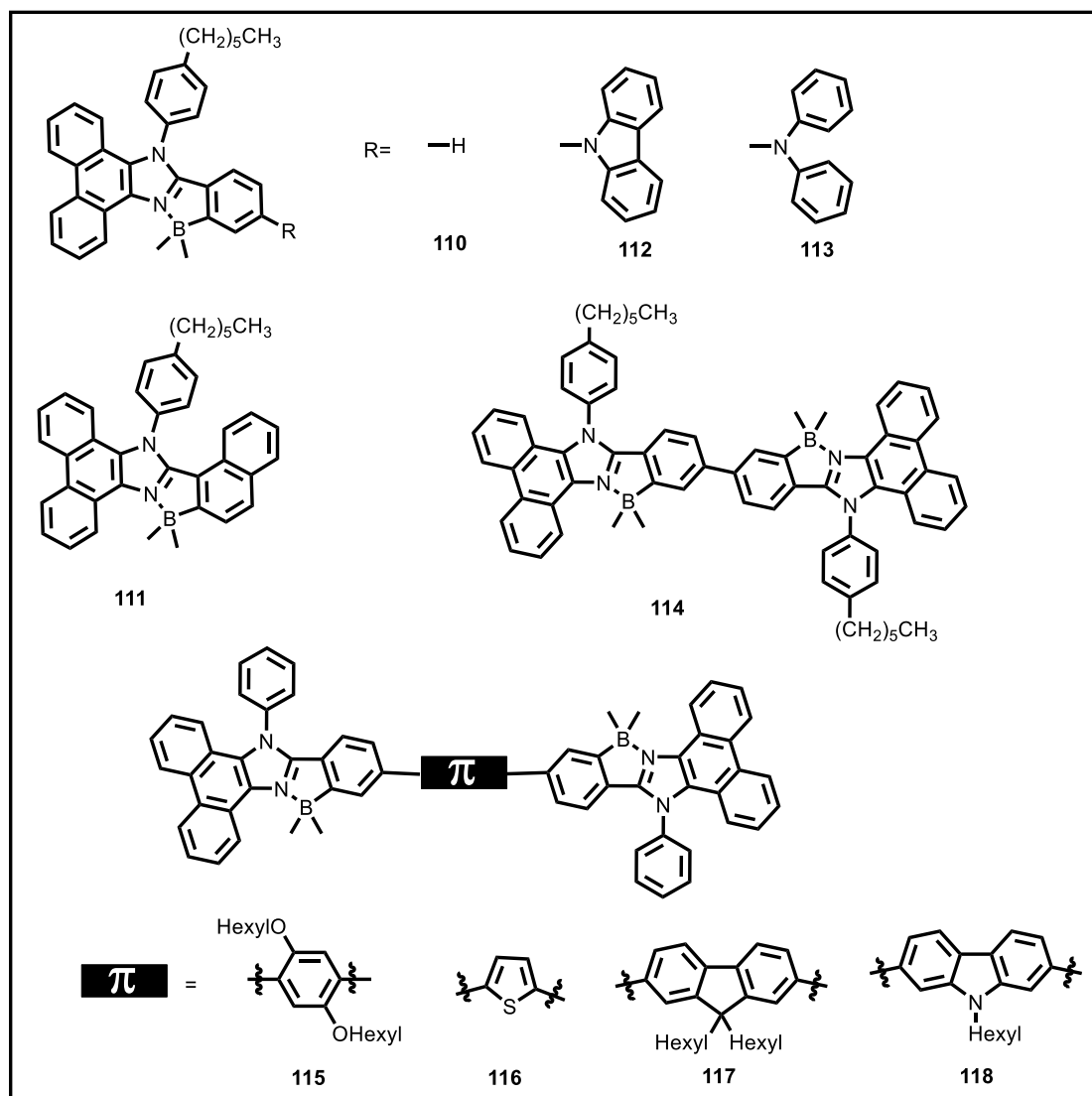


**Figure 1.21:** N,C-chelate four coordinate boron compounds **110-118**.

Wang and coworkers<sup>64</sup> reported a set of pyrazole based four coordinate boron compounds **119-125** (Figure 1.22). These compounds are photoresponsive and upon irradiation with UV light produces azaboratabisnorcaradiene isomers, which further

converted into 14aH-diazaborepins through Walk rearrangement. Later Wang and coworkers<sup>65</sup> synthesized a series of four coordinate chiral organoboron compounds **126-133** (Figure 1.22). The photochromic properties of these complexes were examined upon irradiation with UV light. Compounds **128-130** and **133** undergo photoisomerisation while compounds **131** and **132** were inert to exposure of UV light.

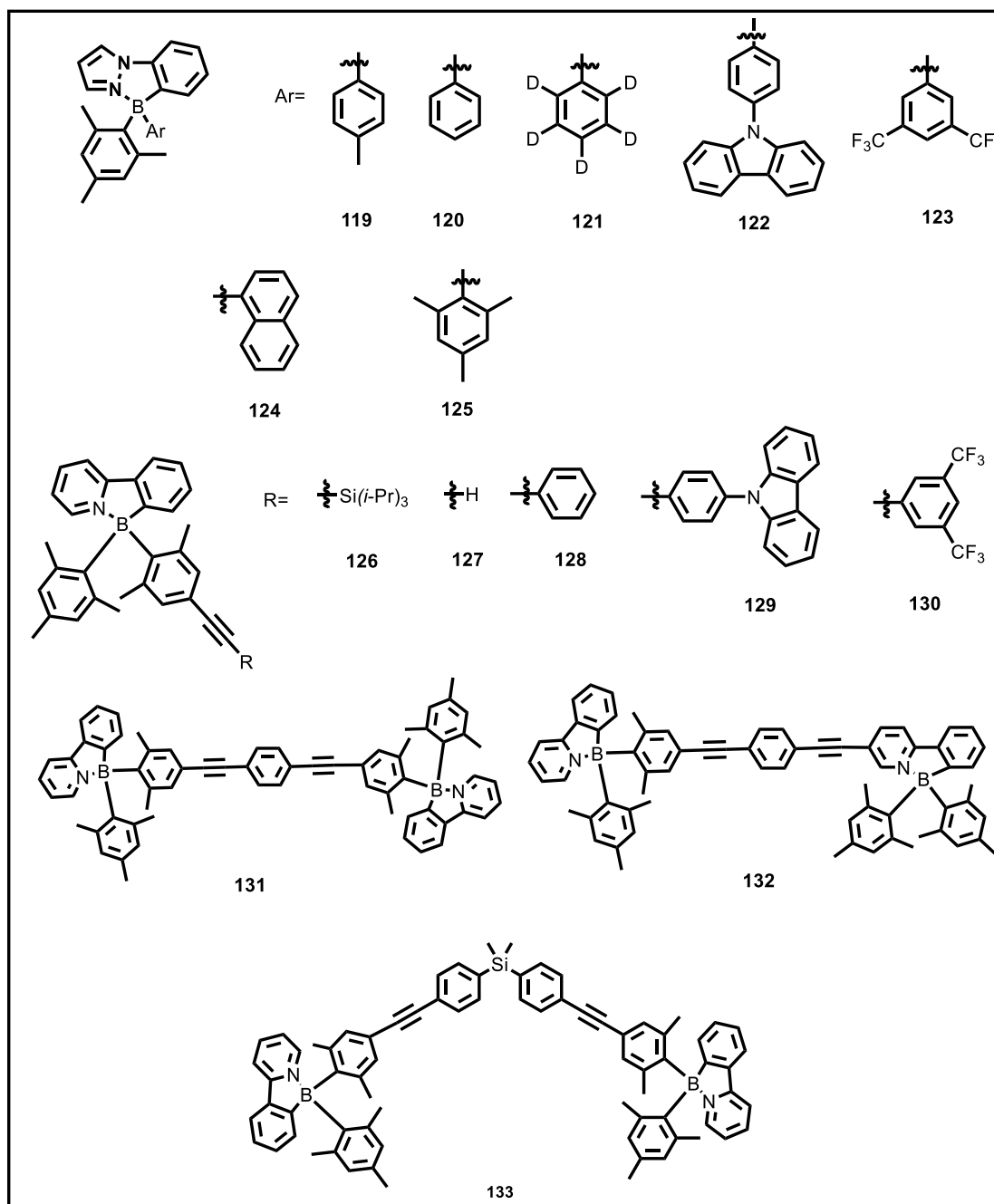


**Figure 1.22:** N,C-chelate four coordinate boron compounds **119-133**.

Indaceneodithiophene based four coordinate boron compounds **134-137** were reported by Zhan and coworkers (**Figure 1.23**).<sup>66</sup> Compounds **134** and **135** showed absorption bands in the range of 400-600 nm while compounds **136** and **137** showed absorption band in the range of 500-750 nm. Compounds **134** and **135** showed emission at 565 ( $\phi=0.46$ ) and 583 nm ( $\phi=0.18$ ) respectively. Compounds **136** and **137** are nonfluorescent due to heavy atom effects caused by bromine atom. Kim and coworkers<sup>67</sup> reported N,C-chelate organoboron compounds **138-140** based on thienyl thiazole and diketopyrrole moiety (**Figure 1.23**). These compounds exhibit absorbance

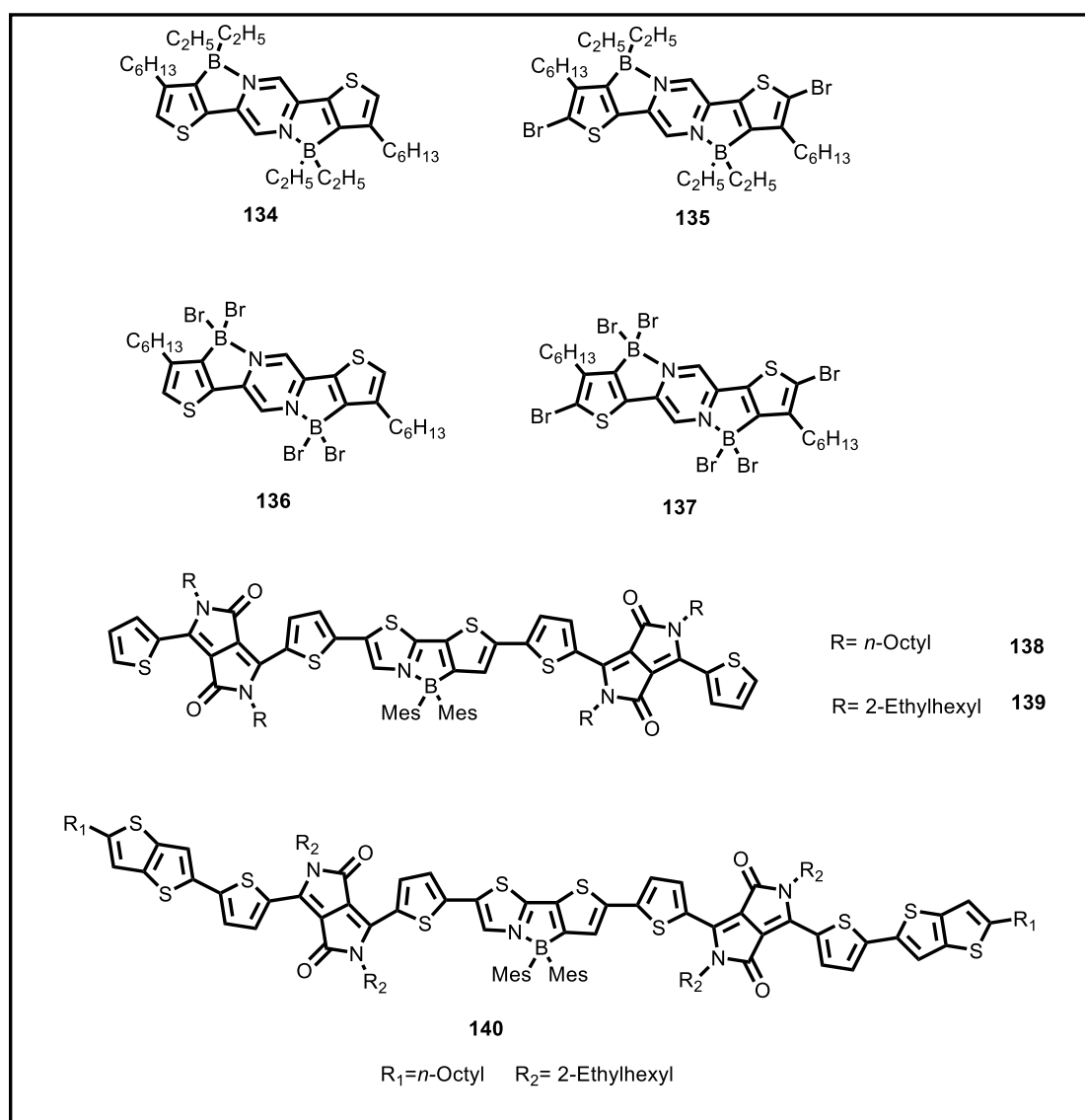


**Figure 1.23:** N,C-chelate four coordinate boron compounds **134-140**.

band at 611(**138**), 611(**139**) and 678(**138**) nm. The photovoltaic properties of these complexes were examined. The maximum external quantum efficiencies (EQE) were found to be 27%, 39% and 29% respectively for compounds **138-140**. A series of N,C-chelate four coordinate boron compounds **141-144** based on benzotriazole and benzoselenadiazole are reported *via* electrophilic borylation approach by Turner and coworkers (**Figure 1.24**).<sup>68</sup> Compounds **141** and **142** showed absorption band at 590 and 612 nm while compounds **143** and **144** showed absorption band 437 and 443 nm. Compounds **141** and **142** showed emission at 728 and 765 nm in the near infrared region. OLED devices were fabricated using these compounds and compounds **141**, **143** and **144** showed external quantum efficiencies (EQE) upto 0.12%, 0.10% and 0.05% respectively.

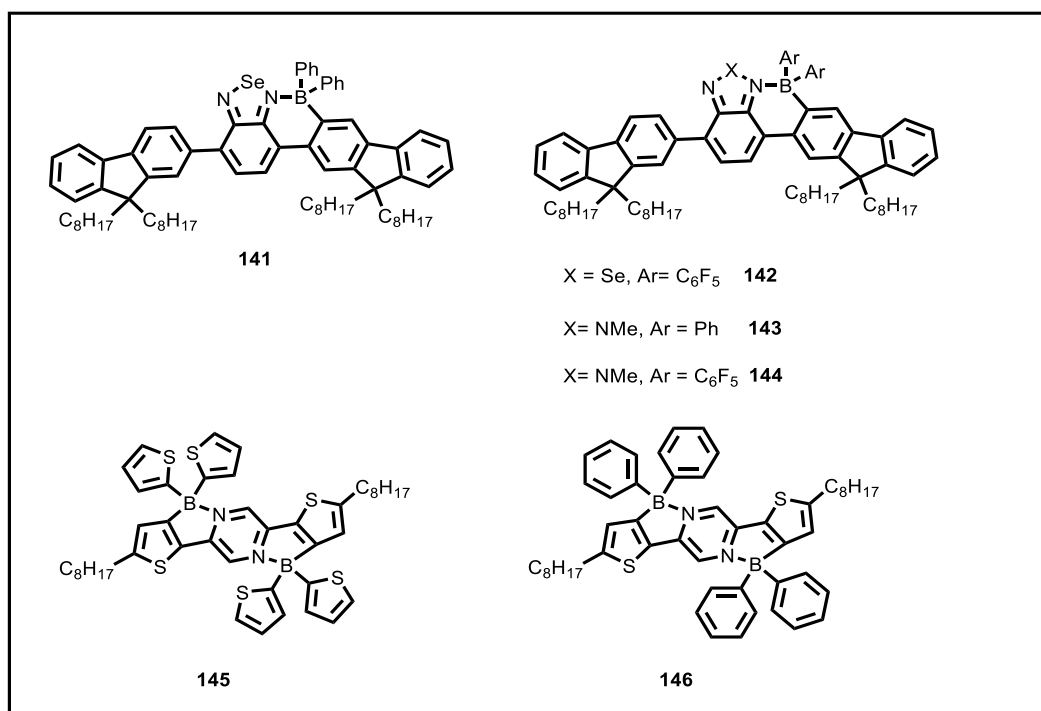


**Figure 1.24:** N,C-chelate four coordinate boron compounds **141-146**.

Huang and coworkers<sup>69</sup> synthesized two indacenodithiophene based N,C-chelated diboron compounds **145-146** (**Figure 1.24**). Compounds **145** and **146** showed

absorption peak at  $\lambda_{\text{max}}$  300-400 nm and  $\lambda_{\text{max}}$  450-600 nm. Both compounds showed emission at 630 nm with a quantum yield of 0.105(**145**) and 0.077(**146**). These two compounds were fabricated for polymer solar cells using a polymer donor and compounds **145** and **146** as an acceptor. Device efficiencies of 0.15% and 0.23% were measured for compounds **145** and **146** respectively.

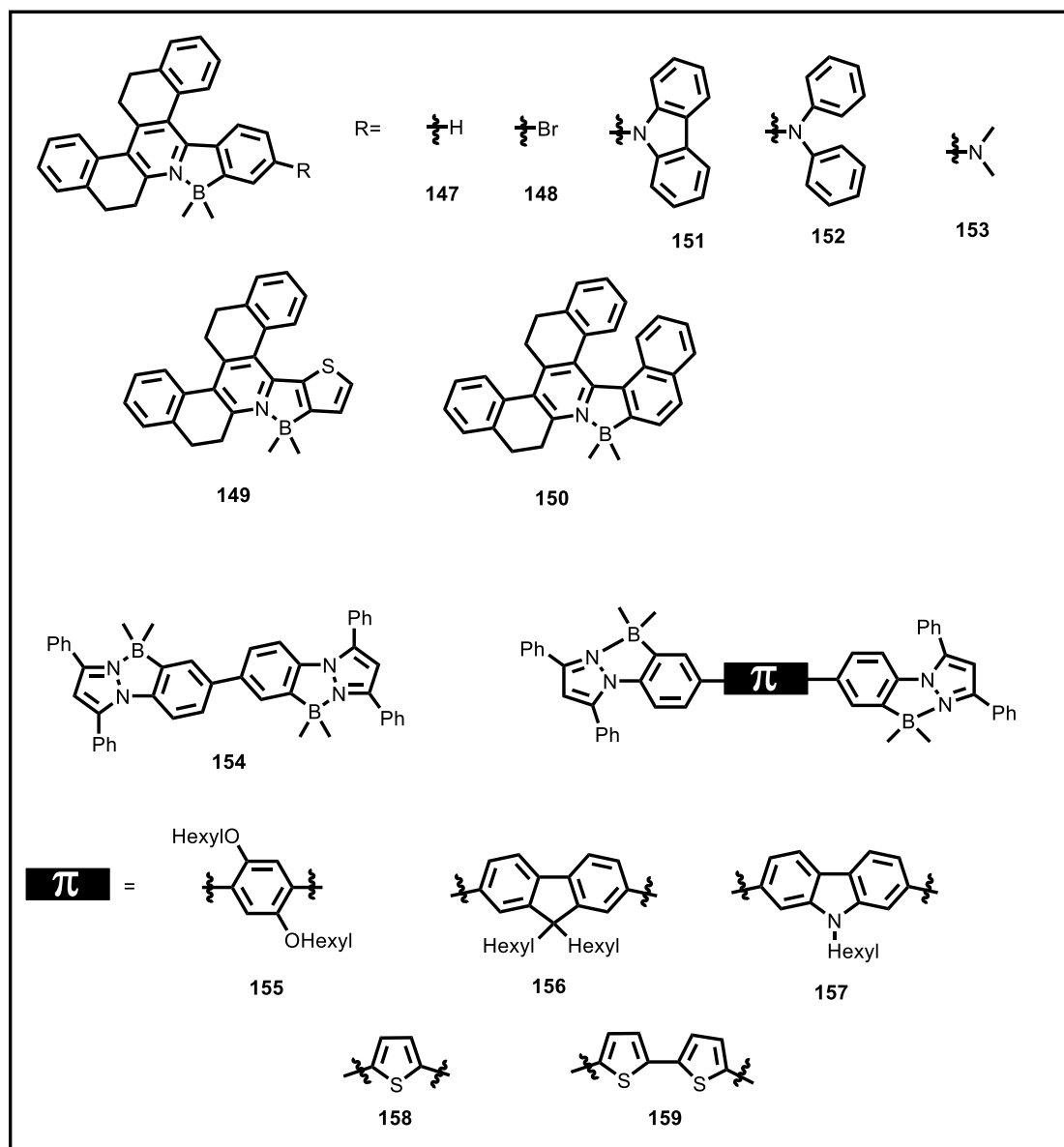


**Figure 1.25:** N,C-chelate four coordinate boron compounds **147-159**.

Tetrahydrodibenzophenanthridine based four coordinate boron compounds **147-153** are reported using electrophilic borylation method by our group (**Figure 1.25**).<sup>70</sup>

Compounds **147-153** showed absorbance in the region of 364-420 nm and emission in the region 403-485 nm. These compounds showed good quantum yield in the solution state (0.90 for **151**, 0.87 for **152**). Later our group<sup>71</sup> also synthesized a series of tri-aryl pyrazole based four coordinate organoboron dimers **154-159** using different  $\pi$ -spacer (**Figure 1.25**). These compounds showed absorption peak in the range of 337-399 nm. Compounds **154-159** are highly emissive with an excellent quantum yield upto 94%. NLO properties of these complexes were examined and non linear absorption ( $\beta$ ) were found to be 4.89, 5.61, 8.93, 49.67, 8.37 and 2.54 for compounds **154-159** respectively. Jäkle and coworkers<sup>72</sup> synthesized 1,6-dipyridylpyrenes based four coordinate boron compounds **160-163** via electrophilic borylation approach (**Figure 1.26**). DFT calculation reveals that HOMOs of these complexes are located on pyrene unit where as LUMOs are spreaded on the pyrene and pyridyl moiety. These compounds showed emission band in the region of 464-564 nm. Compound **160** showed quantum yield upto 74%. Electrochemical analysis reveals that compounds **160-163** undergo two reversible reduction wave. Wang and coworkers<sup>73</sup> synthesized naphthyl-pyridyl and naphthyl-thiazolyl based four coordinate boron compounds **164-175** (**Figure 1.26**). Upon irradiation with UV light these molecules cleanly converted to their corresponding borepin isomers. Further irradiation to the borepin isomers of **170** and **171** resulting the borirane isomer, which can be converted back to the borepin isomers upon irradiation at 450 nm.

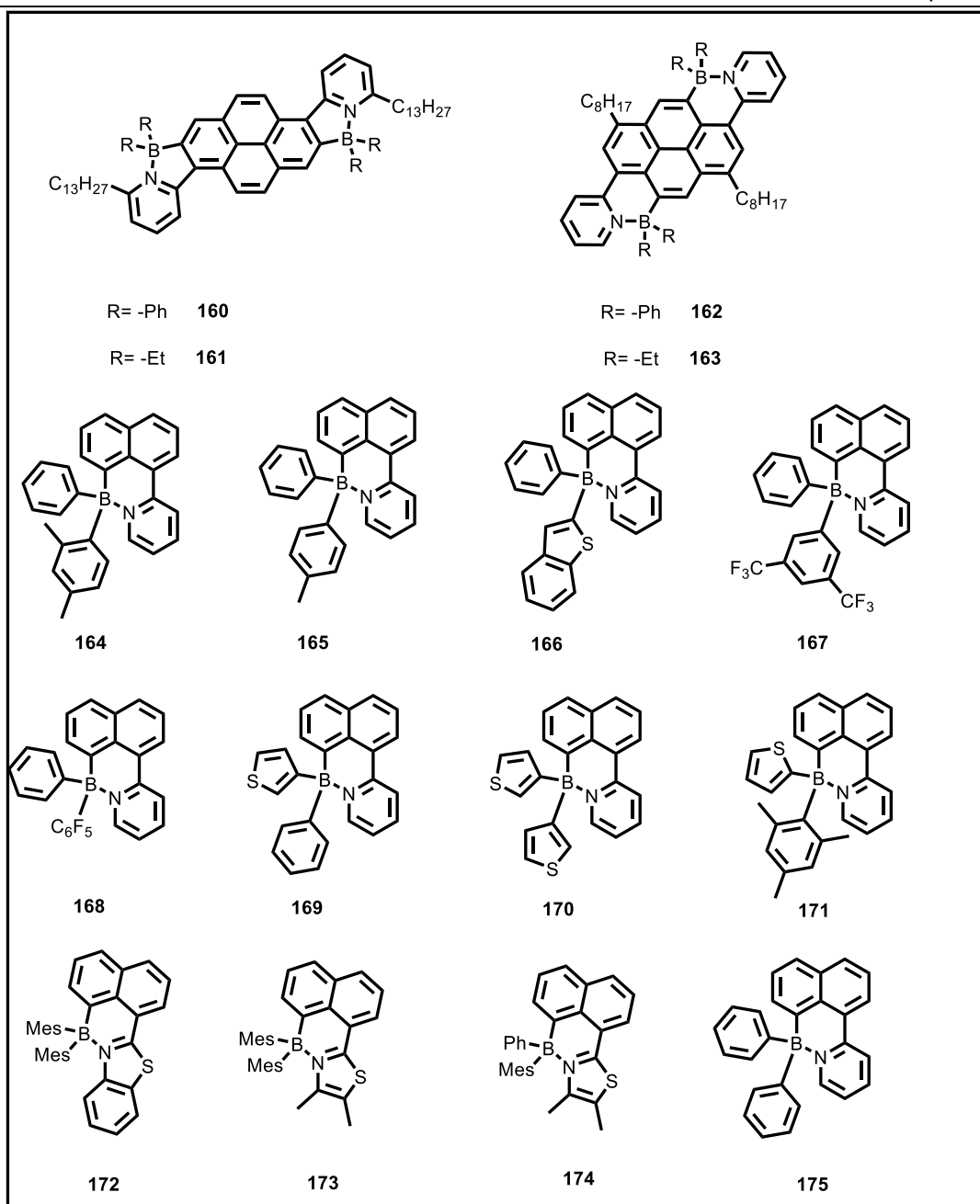


**Figure 1.26:** N,C-chelate four coordinate boron compounds **160-175**.

A set of ten triazole based N,C-chelate boron compounds **176-185** are reported by Pammer and coworkers (**Figure 1.27**).<sup>74</sup> These complexes exhibited absorption band in the range 252-280 nm. Compounds **176-181** and **184** are weakly emissive and other compound are nonfluorescent. Compound **178** showed turn off fluorescent upon addition of cyanide ion and compounds **181-184** showed turn on fluorescence upon addition of TBACN. The binding constant calculated are  $\lg(\text{CN}) = 6.4$  to  $6.5$  for



compounds **181-184** from absorption spectra. Nakamura and coworkers<sup>75</sup> reported *p*-arylenevinylene based tetracoordinate boron compounds **186-189** (Figure 1.27). These compounds showed absorption band in the range of 378-520 nm. Compounds **186-189** are highly emissive and exhibited excellent quantum yield upto 0.98. Electrochemical studies reveal that compounds **186** and **187** showed single irreversible oxidation peak whereas compounds **188** and **189** showed two irreversible oxidation peak.

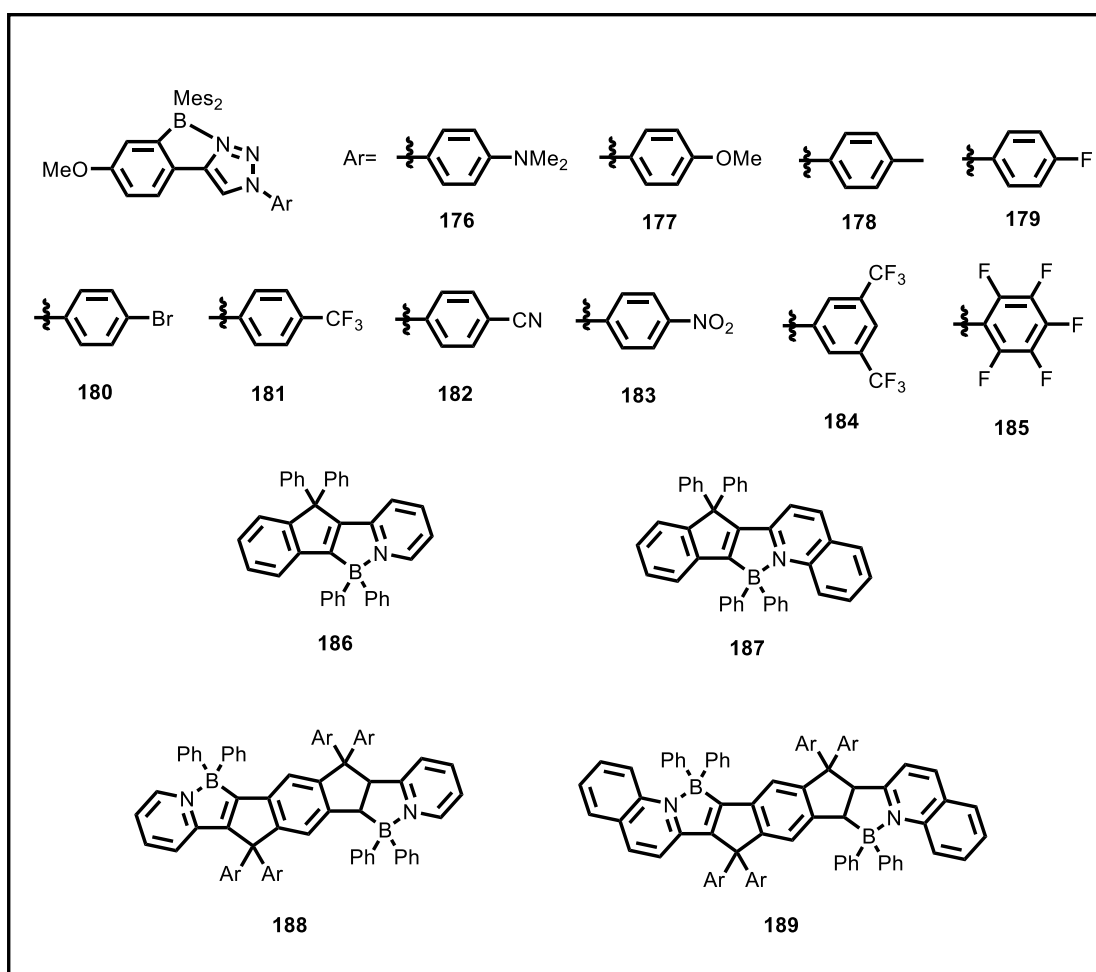


**Figure 1.27:** N,C-chelate four coordinate boron compounds **176-189**.

### 1.2.2 N,N-chelate boron compounds

In N,N-chelate boron compounds, one of the nitrogen atoms form a covalent bond with boron while other nitrogen form coordinate covalent bond by coordinating lone pair of

nitrogen to the vacant  $p_z$  orbital of the boron. BODIPY (boron dipyrromethene) dyes are most studied and well known in literature (**Figure 1.28**).<sup>76-78</sup> BODIPY dyes possess narrow absorption and fluorescence with high quantum yield. They are stable to the pH and polarity of their environment. Being small highly fluorescent molecules, BODIPY dyes have extensively used as sensing materials,<sup>79-83</sup> laser dyes,<sup>84</sup> fluorescent switches<sup>85,86</sup> and labelling reagent.<sup>87-91</sup> However BODIPY dyes are weakly fluorescent in solid state, limiting their application as emitting material in OLEDs. For better electroluminescent properties several groups have reported modified BODIPY by attaching different aryl groups.<sup>92-95</sup>

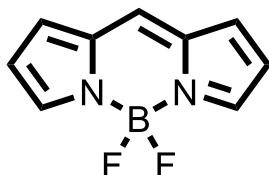


**Figure 1.28:** Schematic representation of BODIPY.

Liu *et al.*<sup>96</sup> investigated a series of N,N-chelate boron compounds based on substituted pyridyl indole systems **190-192** (**Figure 1.29**). These compounds showed emission at 490, 487 and 532 nm respectively in dichloromethane solution. Compound **190** was used as an emitter for fabricating electroluminescence device and showed luminance of 141  $\text{cd/m}^2$  and external efficiency of 0.82  $\text{cd/A}$ .

In 2005, Wang and coworkers<sup>97</sup> reported a series of four coordinate boron compounds **193-202** using different N,N-donor ligands (**Figure 1.29**). These complexes exhibit bright fluorescence with blue to red emission, depending on the chelating ligand. Compounds **199** and **201** were used as an emitter for fabricating electroluminescent devices. Compounds **199** and **201** showed a brightness upto 429  $\text{cd/m}^2$  and 38.5  $\text{cd/m}^2$  respectively.

Piers and coworkers<sup>98</sup> reported a series N,N-chelate anilido-pyridine boron difluoride compounds (**Figure 1.29**). Compounds **203-206** exhibited absorption band in the region 417-419 nm and showed emission in the range 511-531 nm with a quantum yield of 0.27 to 0.33. However compounds **207-210** exhibited high quantum yield compared to other compounds because of presence of rigidified ligand which minimise the non-radiative relaxation pathway.

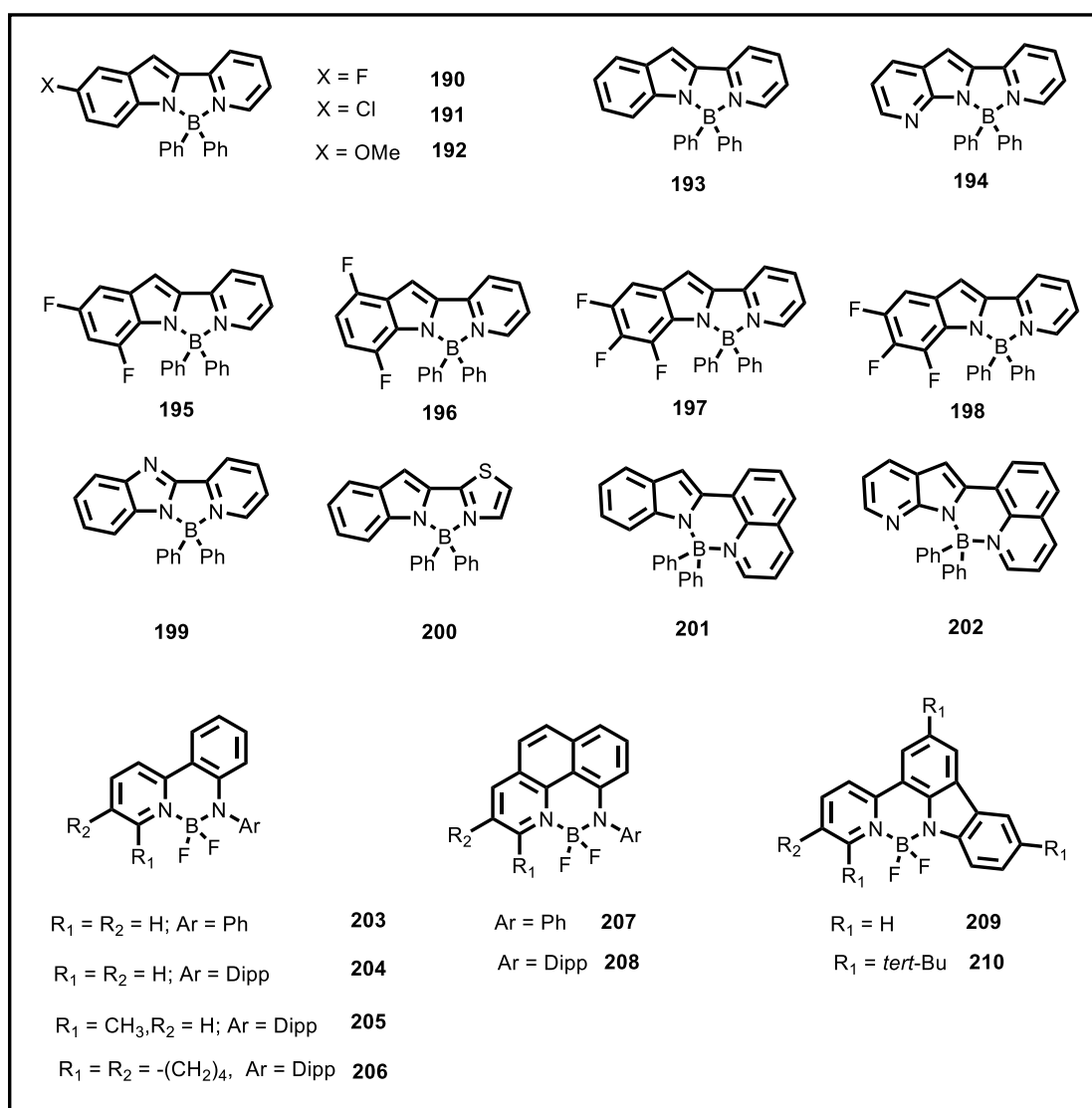


**Figure 1.29:** N,N-chelate four coordinate boron compounds **190-210**.

Photostability of these complexes were examined by irradiating at 420 nm which was monitored through absorption spectra. Compounds **207** and **208** showed high

photostability and absorption spectra remains unchanged even after irradiation of 16 hour. Suresh *et al.*<sup>99</sup> synthesized a set of N,N-chelate four coordinate boron complexes **211-219** based on iminopyrrolyl ligand systems (**Figure 1.30**). These compounds exhibited absorbance band in the region of 353-493 nm. Compounds **214-216** bearing a phenanthrene moiety showed high quantum yield compared to other compounds.

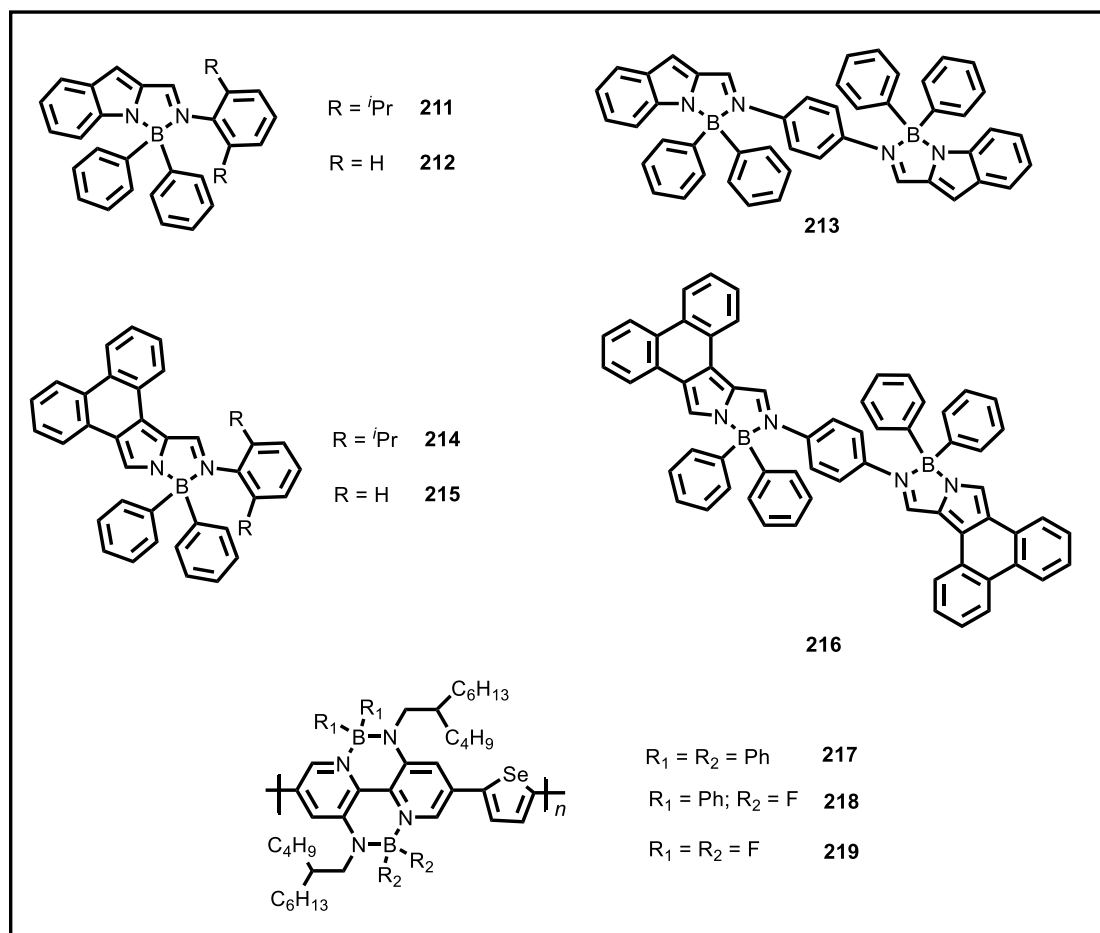


**Figure 1.30:** N,N-chelate four coordinate boron compounds **211-219**.

OLED devices were fabricated for all compounds and compound **215** showed a luminance of 198 cd/m<sup>2</sup>. Wang and coworkers<sup>100</sup> reported three conjugated N,N-chelate organoboron polymers **217-219** (**Figure 1.30**). Polymers **217-219** show absorbance band in the region of 599-651 nm. These polymers were used as electron acceptors in

all-polymer solar cells. Polymers **217-219** exhibited power conversion efficiencies (PCEs) of 0.19, 0.94 and 3.58 % respectively.

Liu and coworkers<sup>101</sup> synthesized two N,N-chelate boron azacenes **220** and **221** with propynyl substituent on boron atom (**Figure 1.31**). These two compounds showed absorption at (706 nm for **220** and 762 nm for **221**) and emission at NIR region (740 nm for **220** and 802 nm for **221**). Min *et al.*<sup>102</sup> reported a disk type N,N-chelate boron compound **222** (**Figure 1.31**). Compound **222** showed absorption at 618 and 569 nm and emission at 630 and 677 nm with a quantum yield of 50%.

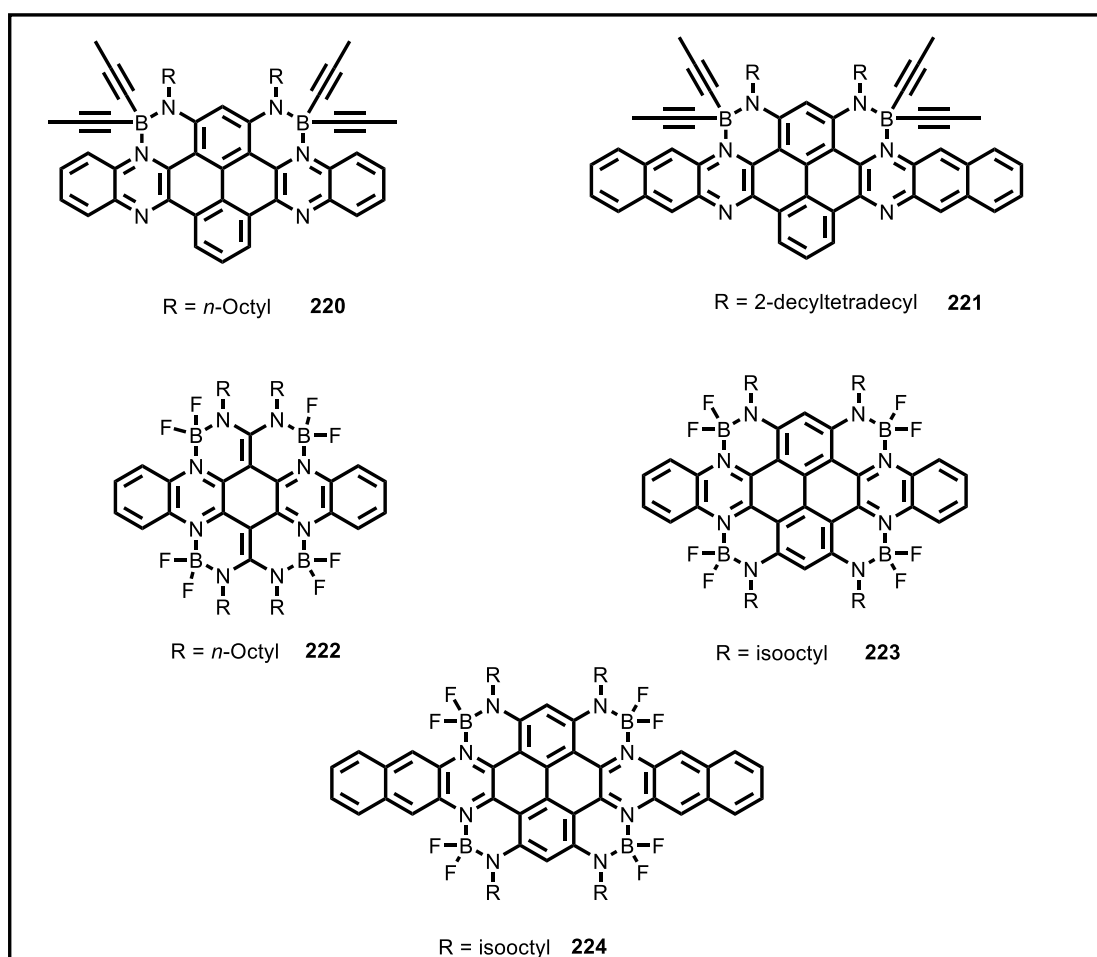


**Figure 1.31:** N,N-chelate four coordinate boron compounds **220-224**.

Dibenzo-azacene based N,N-chelate boron compounds **223** and **224** are reported by Liu and coworkers (**Figure 1.31**).<sup>103</sup> Compounds **223** and **224** exhibited NIR-absorption at

745 and 783 nm respectively. OFET devices are fabricated using compound **224** and showed electron mobility value of  $1.60 \text{ cm}^2 \text{ V}^{-1} \text{ s}^{-1}$ . Recently Fang and coworkers<sup>104</sup> reported a boron embedded 23-fused polycyclic compound **225** (**Figure 1.32**). Compound **225** showed absorption in the range of 600 to 800 nm and emission at 723 nm with a quantum yield of 6.6%. Wang and coworkers<sup>105</sup> synthesized a series of N,N-chelate boron compounds **226-228** based on dibenzo-azacene skeleton. Compounds **226** and **227** showed absorption maxima at 690 nm while compound **228** showed absorption at 808 nm. OFET devices were fabricated using these compounds. Compounds **226-228** showed electron mobilities of 0.12, 0.06 and  $0.07 \text{ cm}^2 \text{ V}^{-1} \text{ s}^{-1}$  respectively.

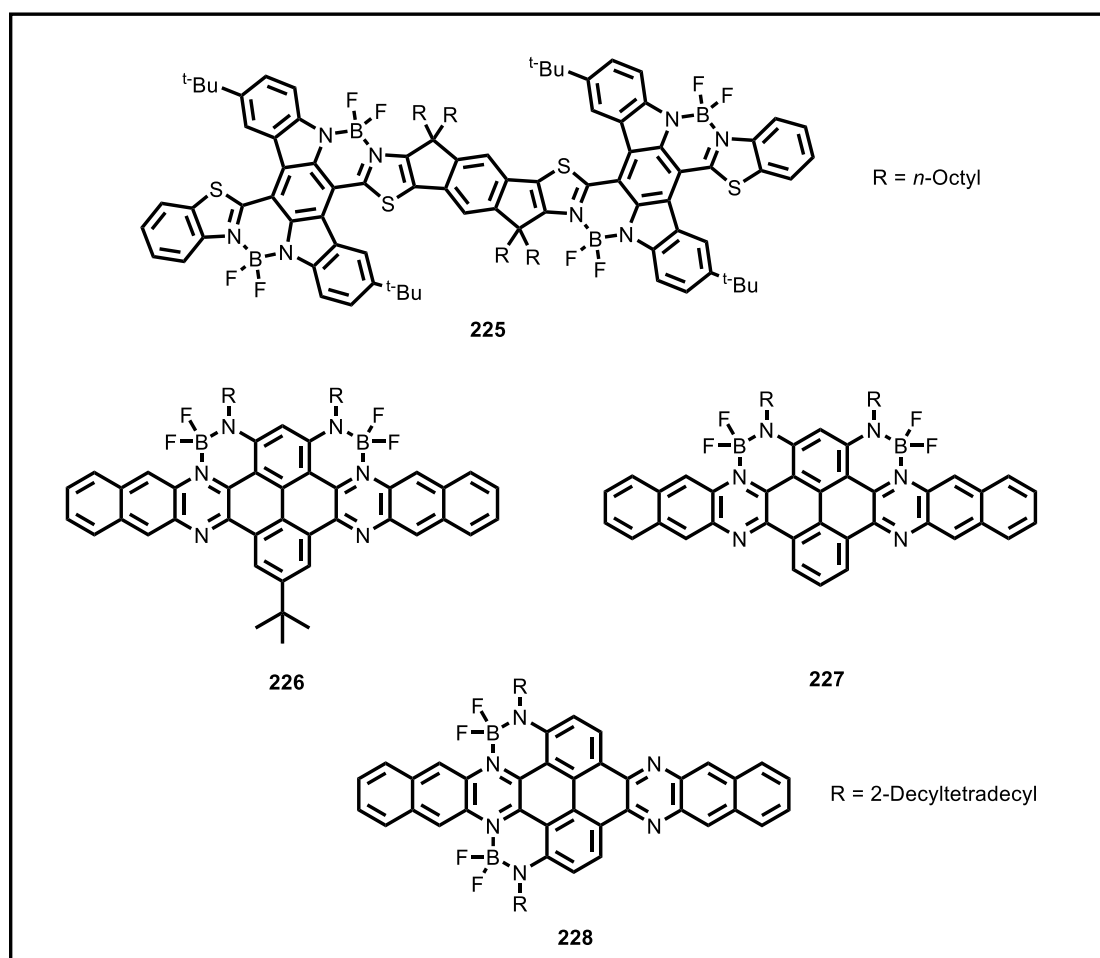


**Figure 1.32:** N,N-chelate four coordinate boron compounds **225-228**.

### 1.2.3 N,O-chelate tetracoordinate boron compounds

Ziessel and coworkers<sup>106</sup> investigated a series of N,O-chelate boron compounds **229-238** based on anil ligands (**Figure 1.33**). Analysis of photophysical properties reveal that intra ligand charge transfer is responsible for emission in these type of complexes. Compound **236** showed a quantum yield of upto 90%.

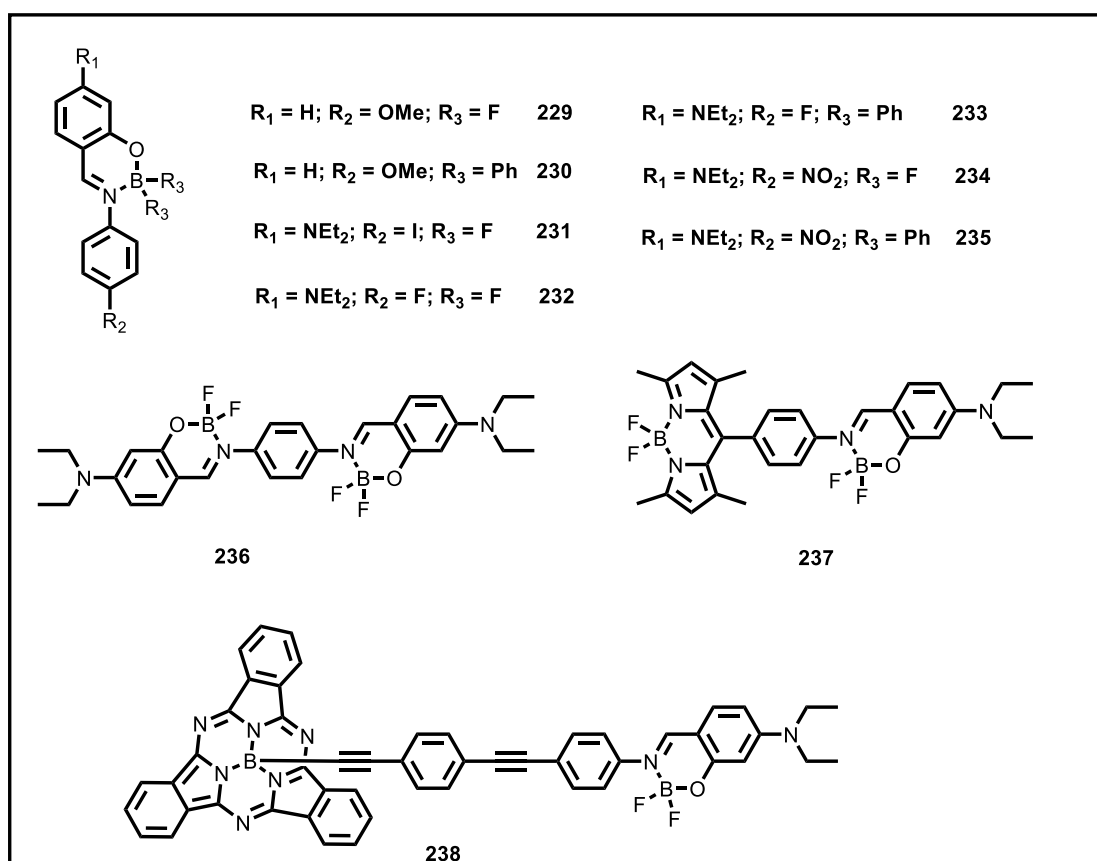


**Figure 1.33:** N,O-chelate four coordinate boron compounds **229-238**.

Salicylaldimine based N,O-chelate boron compounds **239-241** were reported by our group in 2014 (**Figure 1.34**).<sup>107</sup> Compounds **239-241** exhibited absorption band at 370-380 nm and emission band at 460-490 nm. Electrochemical study shows that all compounds exhibited two reduction wave. Dhanunjaya *et al.*<sup>108</sup> synthesized two N,O-chelate boron compounds **242** and **243** based on imidazole core (**Figure 1.34**). Compound **242** and **243** were employed as a sensors for picric acid sensing. Stern-

Volmer quenching constant calculated are  $0.7 \times 10^4 \text{ M}^{-1}$  for **242** and  $0.7 \times 10^4 \text{ M}^{-1}$  for **243**. Imidazole and phenanthroimidazole based N,O-chelate boron compounds **244** and **245** were reported by Wang and coworkers (Figure 1.34).<sup>109</sup> Compound **244** and **245** exhibited fluorescence quantum yield of 0.63 and 0.69 respectively. These compounds were used in OLED device fabrication and showed a luminance ( $L_{\text{max}}$ ) of 1412

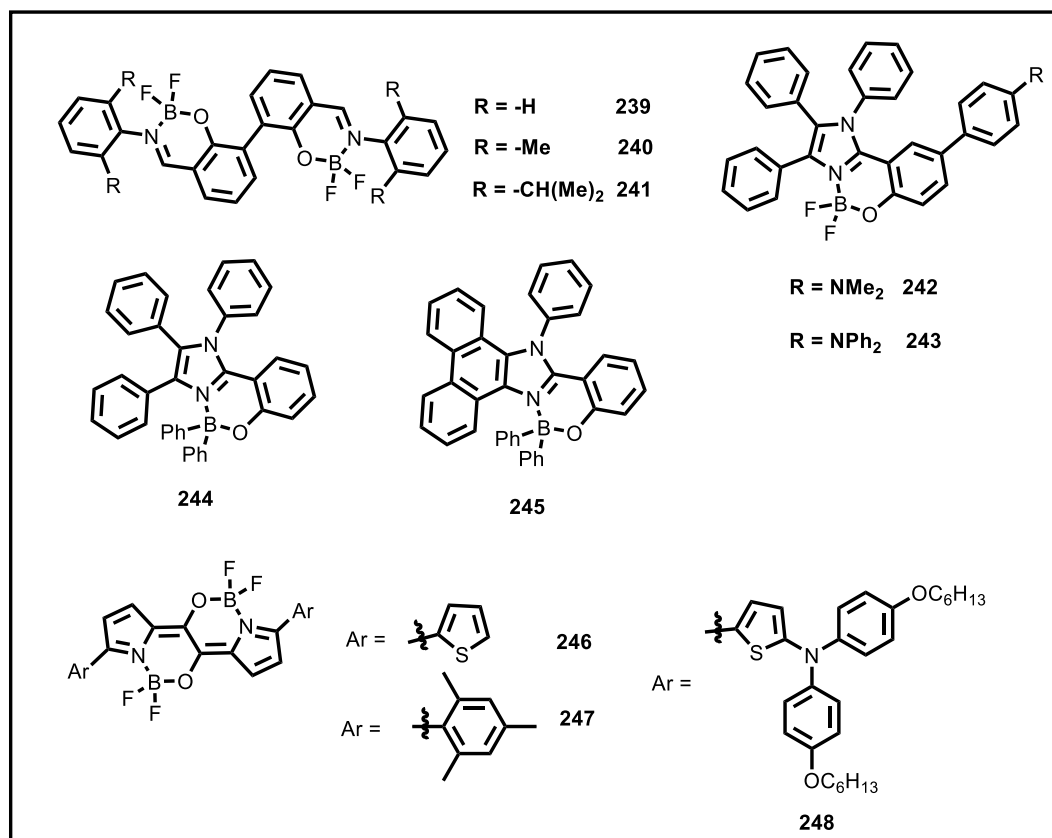


**Figure 1.34:** N,O-chelate four coordinate boron compounds **239-248**.

$\text{cd m}^{-2}$  for **243** and  $2692 \text{ cd m}^{-2}$  for **244**. Wakamiya and coworkers<sup>110</sup> reported azafulvene dimers **246-248** (Figure 1.34). Compounds **246** and **247** showed absorption band at 625 nm and 457 nm where as **247** absorbs at 922 nm. The absorbance of compound **248** remains unaltered upon irradiation of light for 50 h, showed the high photostability. Urban *et al.*<sup>111</sup> reported a series of four coordinate borafuorene compounds **249-256** (Figure 1.35). These compounds showed absorption band in the region of 362-546 nm and emission in the range of 443-604 nm. Recently



naphthalidimine diboron and triboron compounds **257-260** are reported by our group (Figure 1.35).<sup>112</sup> These compounds exhibited absorption band in the range 344-462 nm and emission in the range of 493-562 nm. Electrochemical studies reveal that diboron compounds **257** and **258** exhibited two reduction waves, whereas triboron compounds **259** and **260** exhibited three reduction waves.

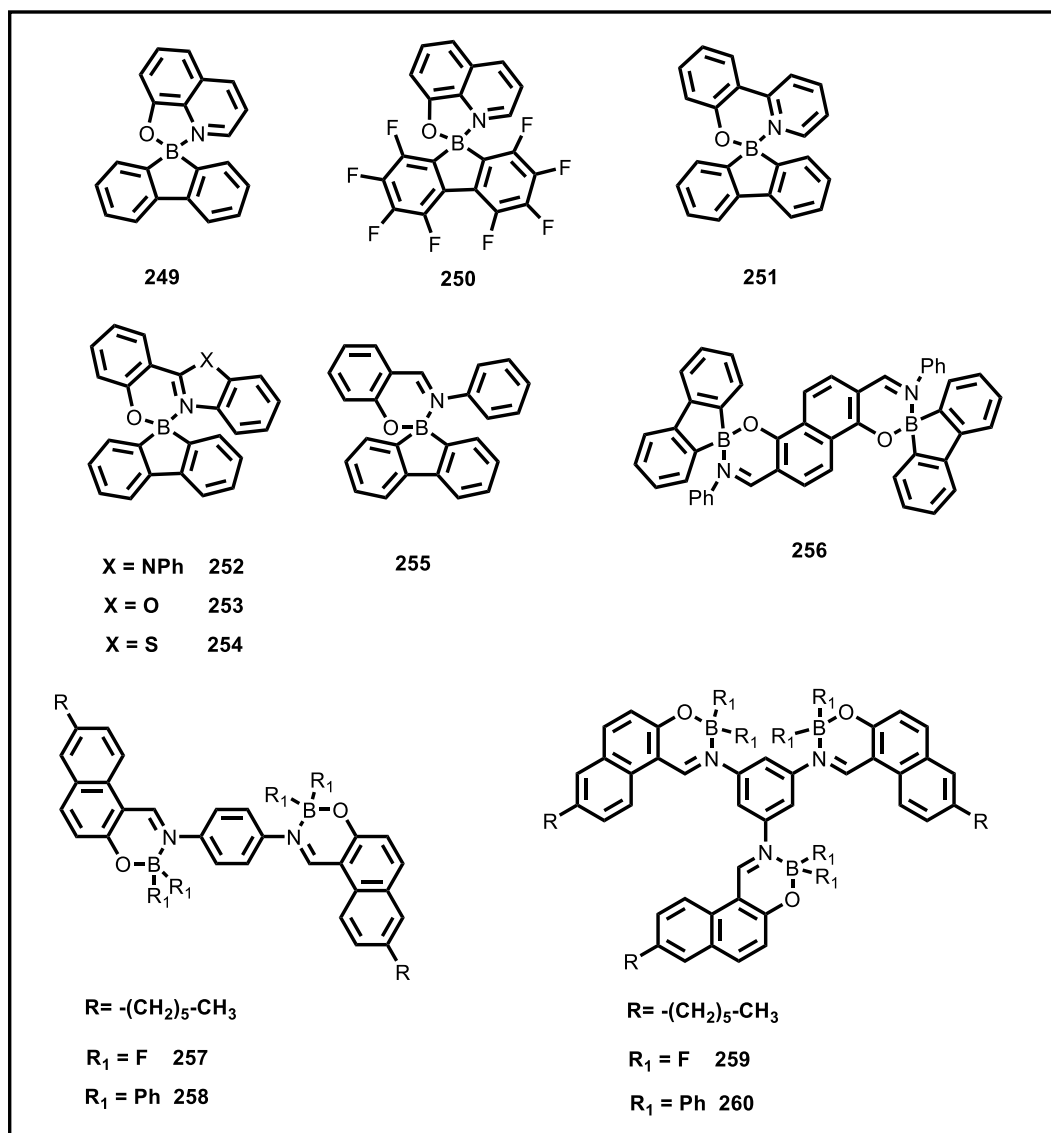


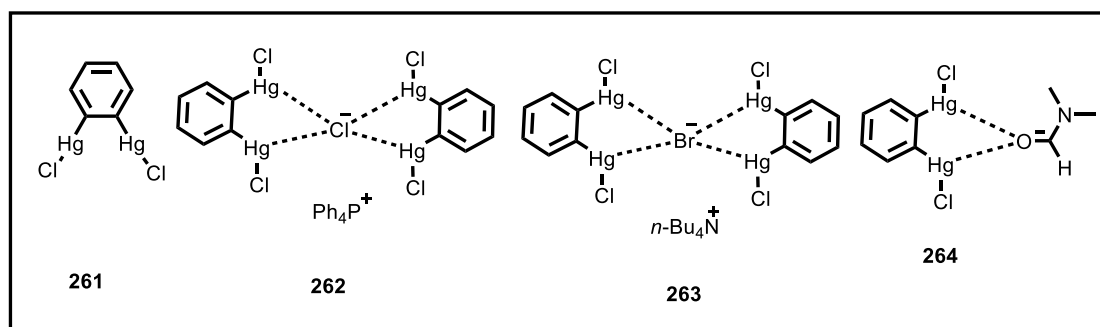
**Figure 1.35:** N,O-chelate four coordinate boron compounds **249-260**.

### 1.3 Main group bidentate Lewis acid

Bidentate Lewis acids possess two binding sites, which can interact simultaneously with the guest molecules. This leads to binding, recognition and activation of guest molecules. In particular, main group bidentate Lewis acids based on mercury and tin atoms have drawn significant research progress in the field of supramolecular chemistry, catalysis and small molecule activation. In this part, I will briefly discuss about bidentate a) mercury , b) tin and boron Lewis acids.

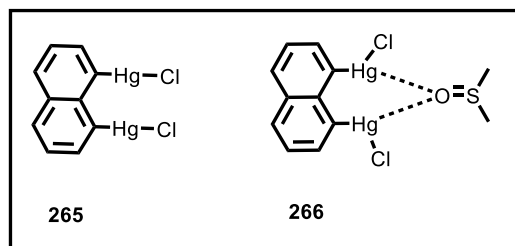
#### 1.3.1 Bidentate mercury Lewis acids

In 1958, Wittig<sup>113</sup> reported the bidentate Lewis acid *o*-phenylene dimercury dihalide complex **261** (Figure 1.36). Wuest and coworkers<sup>114</sup> in 1985 reported the modified procedure for preparation of *o*-phenylene dimercury dihalide and isolated first anionic complexes (**262** and **263**) of *o*-phenylene dimercury dihalide with  $\text{PPh}_4\text{Cl}$  and  $n\text{-Bu}_4\text{NBr}$  with 2:1 ratio (Figure 1.36). Later Wuest and coworkers<sup>115</sup> reported 1:1 complex (**264**) of *o*-phenylene dimercury dihalide with N,N-dimethylformamide (DMF). Single crystal X-ray analysis reveal the presence of intermolecular  $\text{Hg}\cdots\text{Cl}$  interactions (Figure 1.36).



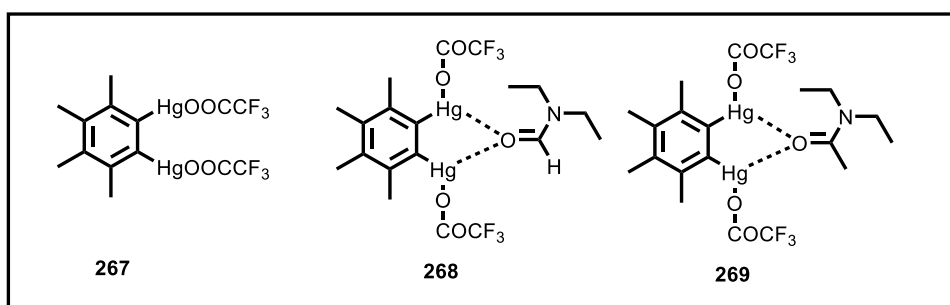
**Figure 1.36:** Bidentate mercury Lewis acid **261** and its adduct **262-263**.

Schimdbaur and coworkers<sup>116</sup> reported the synthesis of 1,8-naphthalenediylbis(mercury chloride) **265** from naphthyllithium and mercuric chloride (Figure 1.37). The mercury complex **266** was obtained from DMSO solution of 1,8-naphthalenediylbis(mercury chloride).



**Figure 1.37:** Bidentate mercury Lewis acid **265** and its adduct **266**.

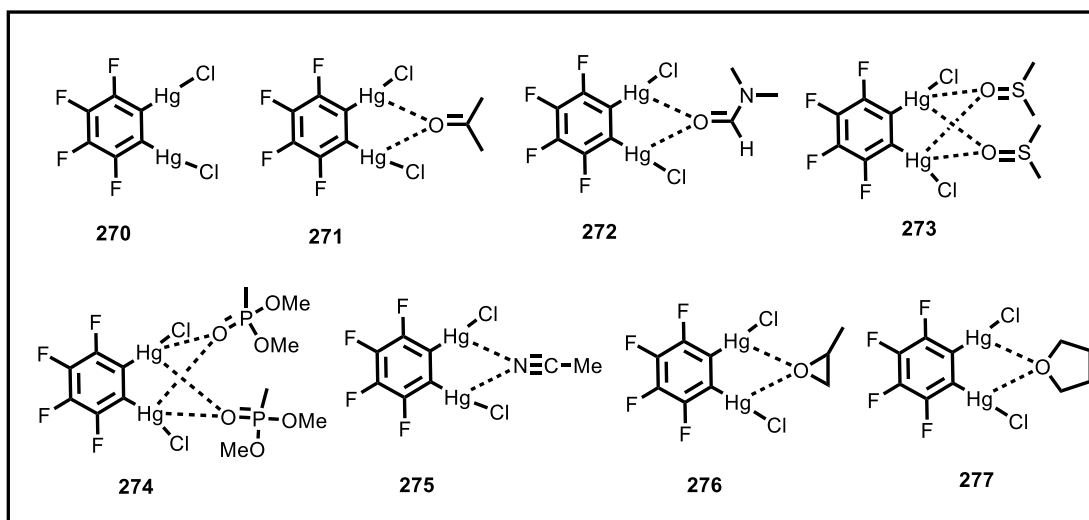
Wuest and coworkers<sup>117</sup> reported the synthesis of 3,4,5,6-tetramethyl-1,2-phenylenedimercury bis(trifluoroacetate) **267** and its complexation with diethylformamide to form complex **268** (Figure 1.38). Later Wuest and coworkers<sup>118</sup> reported the formation of complex **269** in which N,N-diethylacetamide coordinated in a bidentate fashion (Figure 1.38).



**Figure 1.38:** Bidentate mercury Lewis acid **267** and its adduct **268-269**.

Massey *et al.*<sup>119</sup> in 1986 reported 1,2-bis(chloromercurio)tetrafluorobenzene **270** by treating  $(\text{C}_6\text{F}_4\text{Hg})_3$  with mercuric chloride (Figure 1.39). Gabbaï and coworkers<sup>120</sup> reported two 1:1 host-guest complex of 1,2-bis(chloromercurio)tetrafluorobenzene **271** and **272** with acetone and N,N-dimethylformamide respectively (Figure 1.39). The

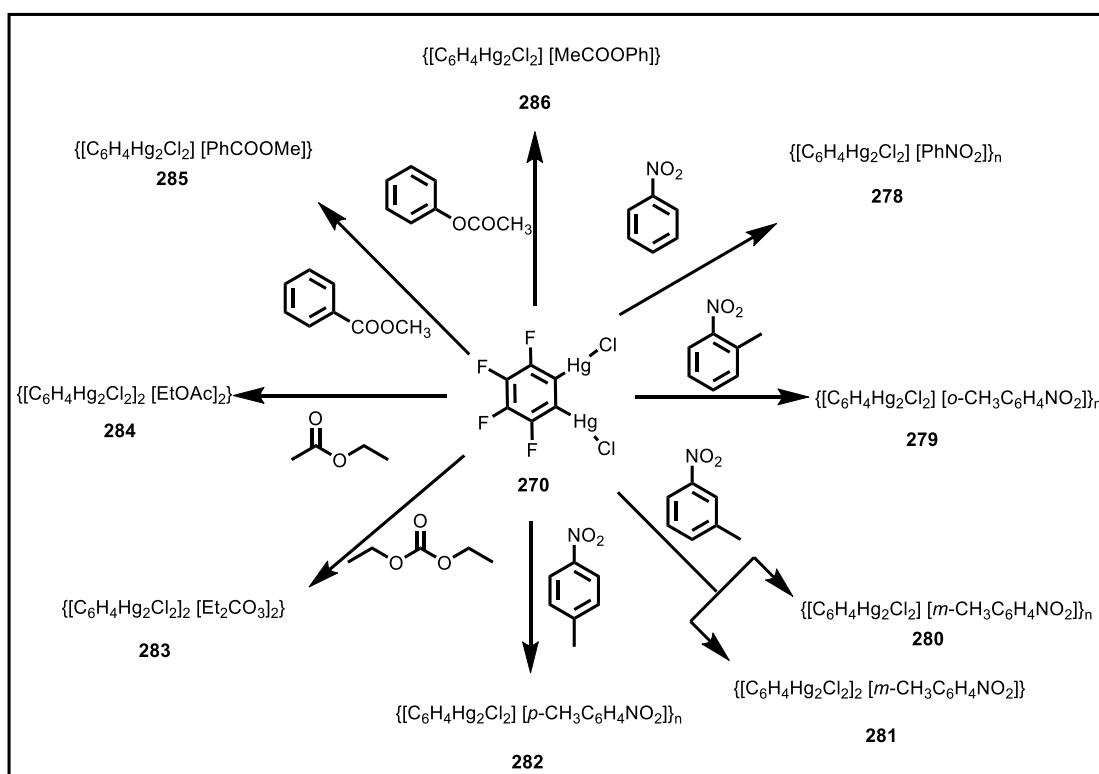
crystal analysis reveals the existence of intermolecular  $\text{Hg}\cdots\text{Cl}$ ,  $\text{Hg}\cdots\text{O}$  and  $\text{Hg}\cdots\text{F}$  contacts. Later Gabbaï and coworkers<sup>121</sup> reported a complex **273** by slow evaporation of DMSO solution of complex **270**, assembles to form microporous solid by retaining the bidentate character (Figure 1.39). The crystal analysis of the complex **273** shows that two DMSO molecules are bridged by two mercury centres and one non coordinating DMSO molecule is also present. From the cell packing examination they found the existence of 2D sheets. Tschinkl *et al.*<sup>122</sup> reported the host-guest complex **274** with coordination of dimethyl methyl phosphonate (DMMP) to complex **270** (Figure 1.39). Cell packing examination reveals the existence of intermolecular  $\text{Hg}\cdots\text{Cl}$  contacts which leads to the formation of polymeric chain like structure. This chain with  $\pi\cdots\pi$  contacts form the layers which sandwich the DMMP molecules.



**Figure 1.39:** Bidentate mercury Lewis acid **270** and its adduct **271-274**.

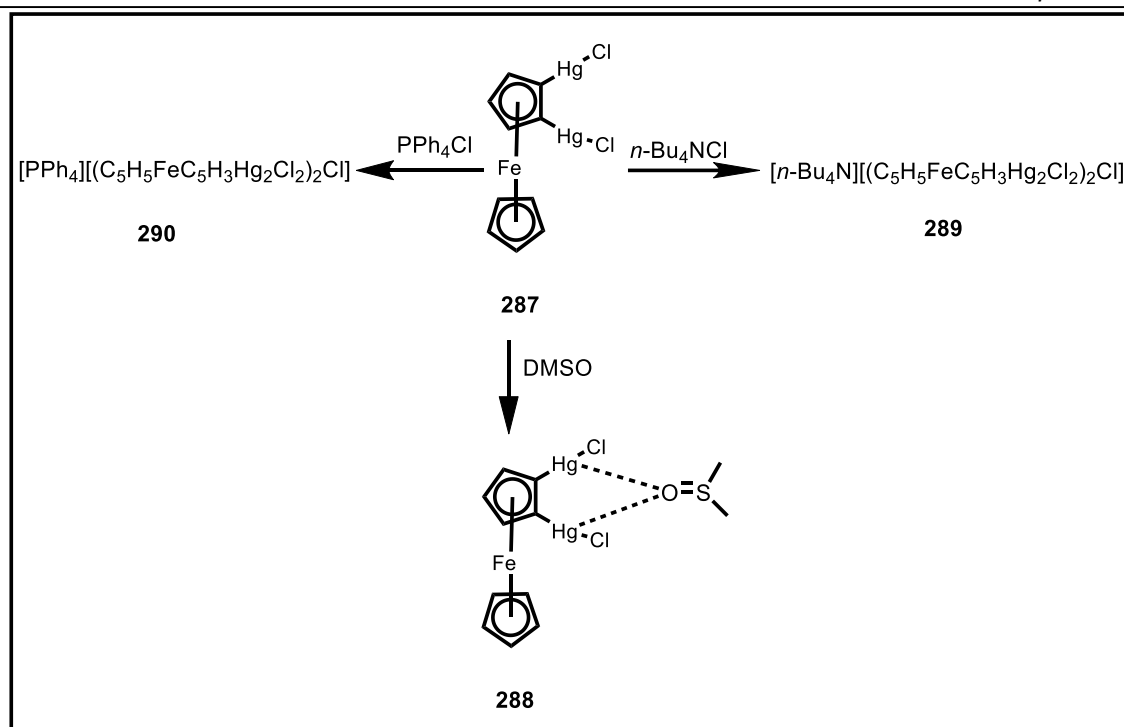
Julie *et al.*<sup>123</sup> reported coordination of acetonitrile and propylene oxide to the bidentate Lewis acid **270**, to form adduct **275** and **276** (Figure 1.40). Both the adduct **275** and **276** forms layered structure with  $\text{Hg}\cdots\text{F}$  and  $\text{Hg}\cdots\text{Cl}$  interaction. Tschinkl *et al.*<sup>124</sup> reported the coordination of tetrahydrofuran to the bidentate Lewis acid **270** to form the adduct **277**, which forms an extended structure with  $\text{Hg}\cdots\text{Cl}$  and  $\pi\cdots\pi$  interaction (Figure

**1.40).** Timofeeva and coworkers<sup>125</sup> have reported a series of adducts **278-282**, with the coordination of nitrobenzenes and nitrotoluenes to **270** (Figure 1.40). Except *m*-isomer other nitrobenzenes and nitrotoluenes forms 1:1 adduct. Later, Timofeeva and coworkers<sup>126</sup> have reported a series of adducts **283-286** by coordination of organic esters (Figure 1.40). Compound **284** and **285** form supramolecular 1D chain like structure while **283** and **286** form supramolecular 2D layer structure.



**Figure 1.40:** Bidentate mercury Lewis acid **270** and its adduct **278-286**.

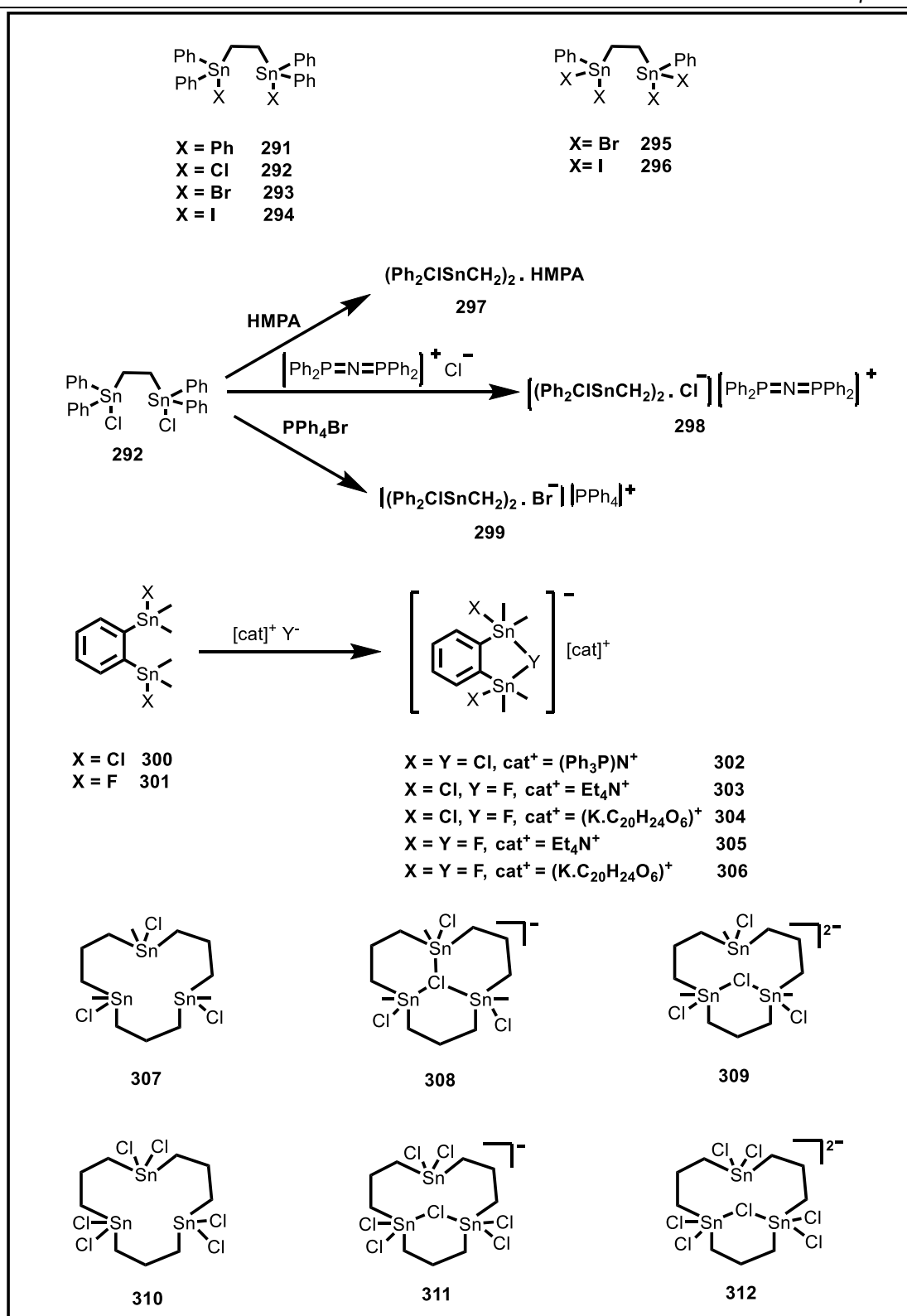
Jäkle and coworkers<sup>127</sup> reported the synthesis of bidentate Lewis acid 1,2-bis(chloromethyl)ferrocene **287** and its complexation with DMSO, *n*-Bu<sub>4</sub>NCl and PPh<sub>4</sub>Cl to form the adducts **288-290** (Figure 1.41). Crystal analysis shows the existence of 1:1 complex with DMSO & 2:1 complex with *n*-Bu<sub>4</sub>NCl and PPh<sub>4</sub>Cl. Layered like structure was observed for [Bu<sub>4</sub>N] and channel like structure for [PPh<sub>4</sub>] counterions.



**Figure 1.41:** Bidentate mercury Lewis acid **287** and its adduct **288-290**.

### 1.3.2 Bidentate tin Lewis acid

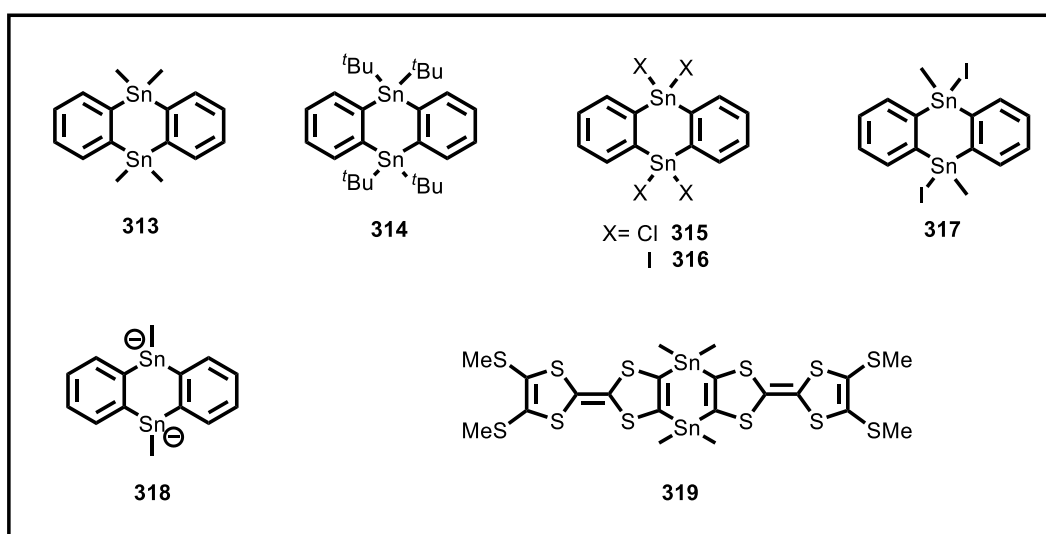
Jurkschat and coworkers<sup>128</sup> reported a series of bidentate tin Lewis acids **291-296**, out of which **292** reacts with hexamethylphosphoramide (HMPA),  $[\text{Ph}_3\text{P}=\text{N}=\text{PPh}_3]^+ [\text{Cl}]^-$  and  $\text{PPh}_4\text{Br}$  to form 1:1 adducts **297-299** respectively (Figure 1.42). Later Jurkschat and coworkers<sup>129</sup> reported two bidentate Lewis acid **300** and **301**, which upon treatment with different chloride and fluoride salts produces 1:1 adducts **302-306** (Figure 1.42). Cyclic bidentate Lewis acids **307** and **308** were also reported by Jurkschat and coworkers<sup>130</sup>. Addition of one equivalent of chloride ion to **307** resulted symmetrical bridged anion species **309** and the addition of two equivalent formed the dianion species **310**, where one chloride is bridged by two tin atoms. However, the addition of one and two equivalent of chloride anion gave the monoanion **311** and dianion **312** respectively (Figure 1.42).



**Figure 1.42:** Bidentate tin Lewis acid and its adduct **291-312**.

Saito *et al.*<sup>131</sup> reported the synthesis of two distannaanthracene **313** and **314**, starting from 1,2-dibromobenzene (Figure 1.42). Crystal analysis reveals the existence of

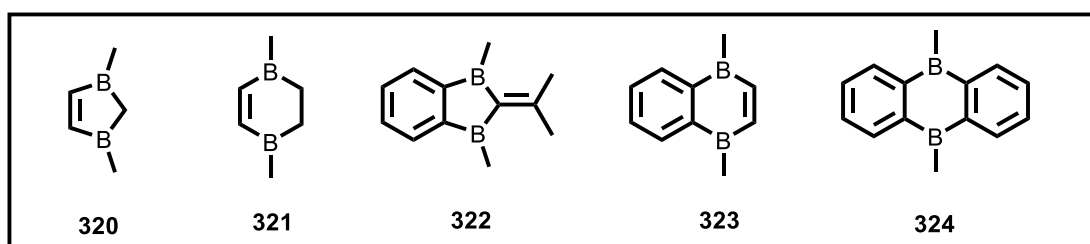
butterfly conformation for central six membered ring in **313** and planar structure for **314**. Later Saito *et al.*<sup>132</sup> reported the tetrahalodistannaanthracenes **315** and **316** (Figure 1.43). The reaction of **316** with methyl lithium gives the dimethyldiiodo derivative **317**. In 2005, Saito and coworkers<sup>133</sup> synthesized the dianion **318**, by treating excess lithium to **317** (Figure 1.43). Shirai *et al.*<sup>134</sup> reported the tin containing tetrathiafulvene dimer **319** (Figure 1.43).



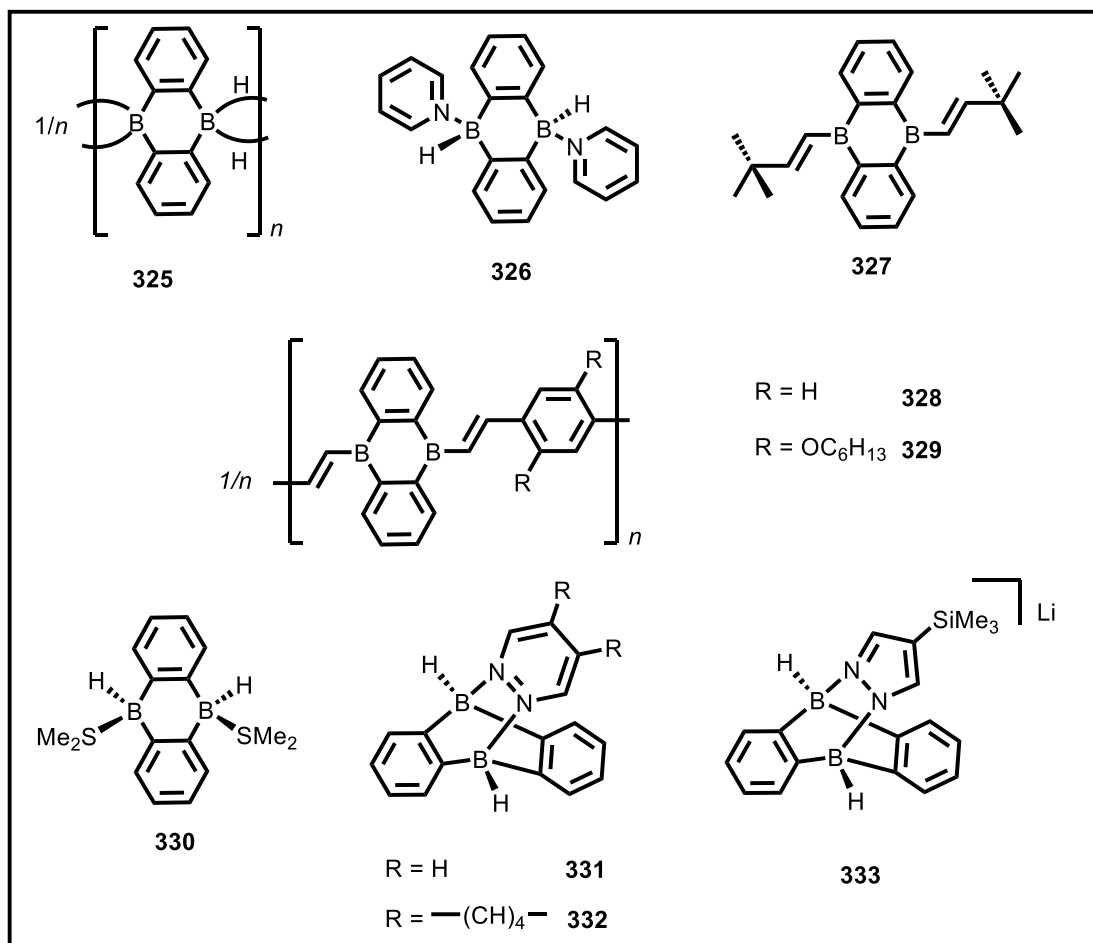
**Figure 1.43:** Bidentate tin Lewis acid **313**-**319**.

### 1.3.3 Bidentate boron Lewis acid

Siebert *et al.* reported the synthesis of 2,3-dihydro-1,3-diborole<sup>135,136</sup> (**320**), 1,4-diboracyclohexene<sup>137,138</sup> (**321**), Benzo-1,3-dihydro-1,3-diborapentafulvene<sup>139</sup> (**322**), 1,4-Dihydro-1,4-diboranaphthalene<sup>139</sup> (**323**), 9,10-dimethyl-9,10-diboraanthracenes<sup>140</sup> (**324**) (Figure 1.44).





**Figure 1.44:** Bidentate boron Lewis acid **320-324**.**Figure 1.45:** Bidentate boron Lewis acid **325-333**.

Wagner and coworkers<sup>141</sup> reported a polymeric 9,10-dihydro-9,10-diboraanthracene **325** which upon treatment with pyridine and acetylene formed the adduct **326** and **327**. Polymer **328** and **329** were formed by treating compound **325** with 1,4-dialkynylbenzene (**Figure 1.45**). Later Wagner and coworkers<sup>142</sup> synthesized the compound **330** by treating compound **325** with dimethyl sulphide (DMS). Compound **330** was further reacted with pyridazine, benzopyridazine and 4-trimethylsilylpyrazolide to give the product **331-333** (**Figure 1.45**). Marder and coworkers<sup>143</sup> have reported three diborane (**334-336**). Compound **336** was used for fluoride sensing, where the fluoride ion was chelated by two boron centres (**Figure**

**1.46).** Marks and coworkers<sup>144</sup> reported two bidentate perfluorodiboranthracene **337** and **338** (Figure **1.46**). Complex **338** was used as a catalyst for polymerisation of ethylene and propylene. Jäkle and coworkers<sup>145</sup> synthesized a bidentate boron Lewis acid **339**, which upon treatment with excess iodine forms the mixed valence species (Figure **1.46**). This shows that ferrocene act as electron withdrawing substituents and enhanced the Lewis acidity of boron centre, which was further proved by coordination of acetonitrile to boron centre to form the dioxidised species. Piers and coworkers<sup>146</sup> reported a benzothiophene fused boron ladder **340**, starting from 2,3-dibromobenzothiophene (Figure **1.46**).

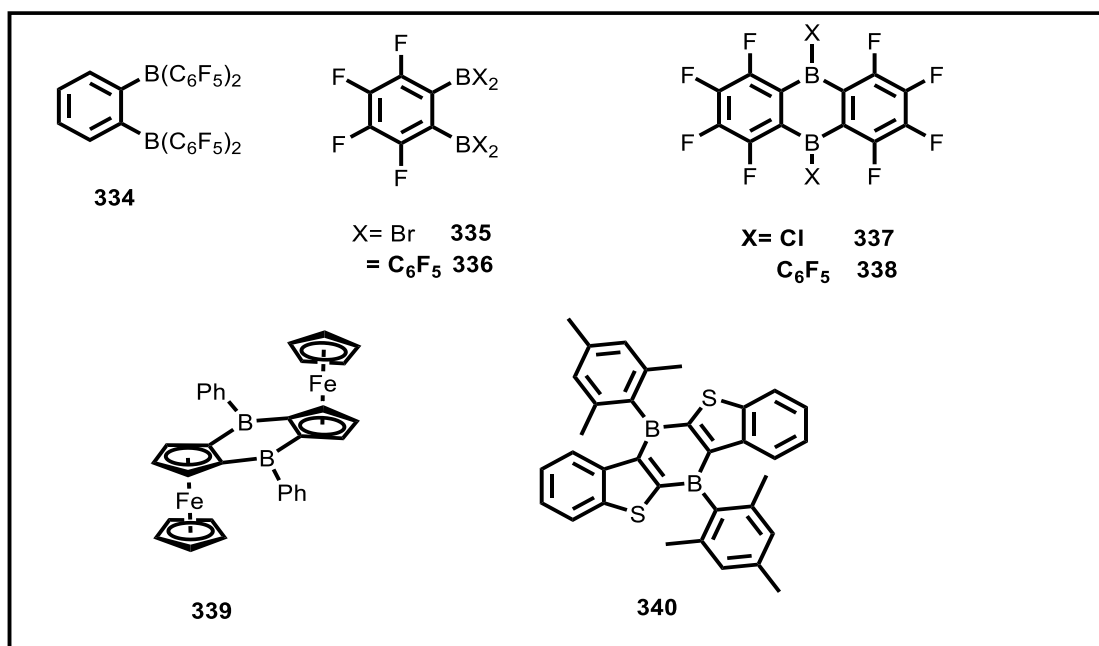


**Figure 1.46:** Bidentate boron Lewis acid **334-340**.

Dehydrogenation of ammonia-borane catalysed by a bidentate Lewis acid **341** was reported by Wegner and coworkers<sup>147</sup> (Figure **1.47**). The using of bidentate Lewis acid catalyst releases 2.46 equiv. of  $\text{H}_2$  per ammonia-borane molecule and the effectiveness of this catalyst is due to the stabilisation of 3c-2e complex with ammonia-borane molecule.

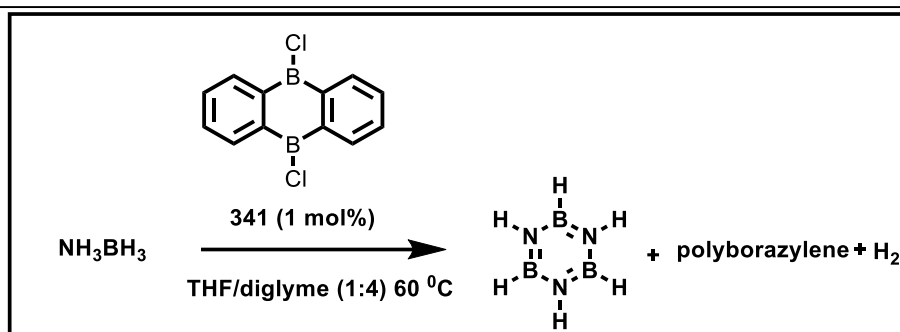


**Figure 1.47:** Bidentate boron Lewis acid **341**.

Wagner and coworkers<sup>148</sup> reported the lithium salts of doubly reduced species **342**, which reduces carbon dioxide to form carbon monoxide and Li<sub>2</sub>CO<sub>3</sub> (Figure 1.48).

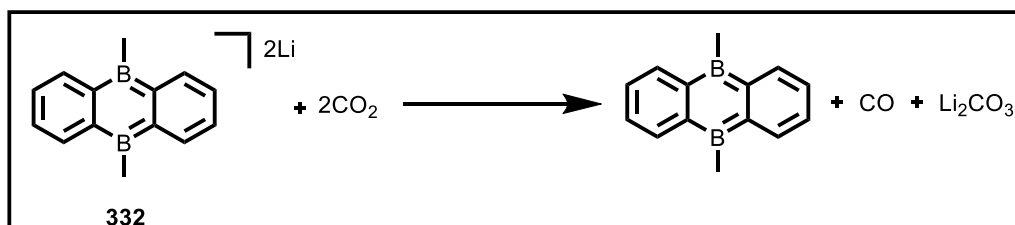


**Figure 1.48:** Bidentate boron Lewis acid **342**.

1,3,2,5-diazadiborene **343** has been reported by Kinjo and coworkers<sup>149</sup>, which forms the adduct **344-347** with MeOTf, phenyl acetylene, carbon dioxide and ethylene respectively (Figure 1.49). The boron centres in **343** behave as both electrophilic and nucleophilic. Later Kinjo and coworkers<sup>150</sup> reported 1,4,2,5-diazadiborinine **348**, in which the boron centre is ambiphilic (Figure 1.49). Compound **348** breaks the C-O, P-H, B-H and Si-H bonds and also undergoes cycloaddition reactions with unsaturated ketones, alkenes, alkynes and nitriles to give the corresponding adduct **349-359** (Figure 1.49). Harman and coworkers<sup>151</sup> have reported 9,10-diboraanthracene (**360**) which is stabilised by a N-heterocyclic carbene (Figure 1.49). Bidentate boron Lewis acid **360** undergoes [4+2] cycloaddition reactions with carbon dioxide (CO<sub>2</sub>), oxygen (O<sub>2</sub>) and ethylene to form the adduct **361-363** respectively.

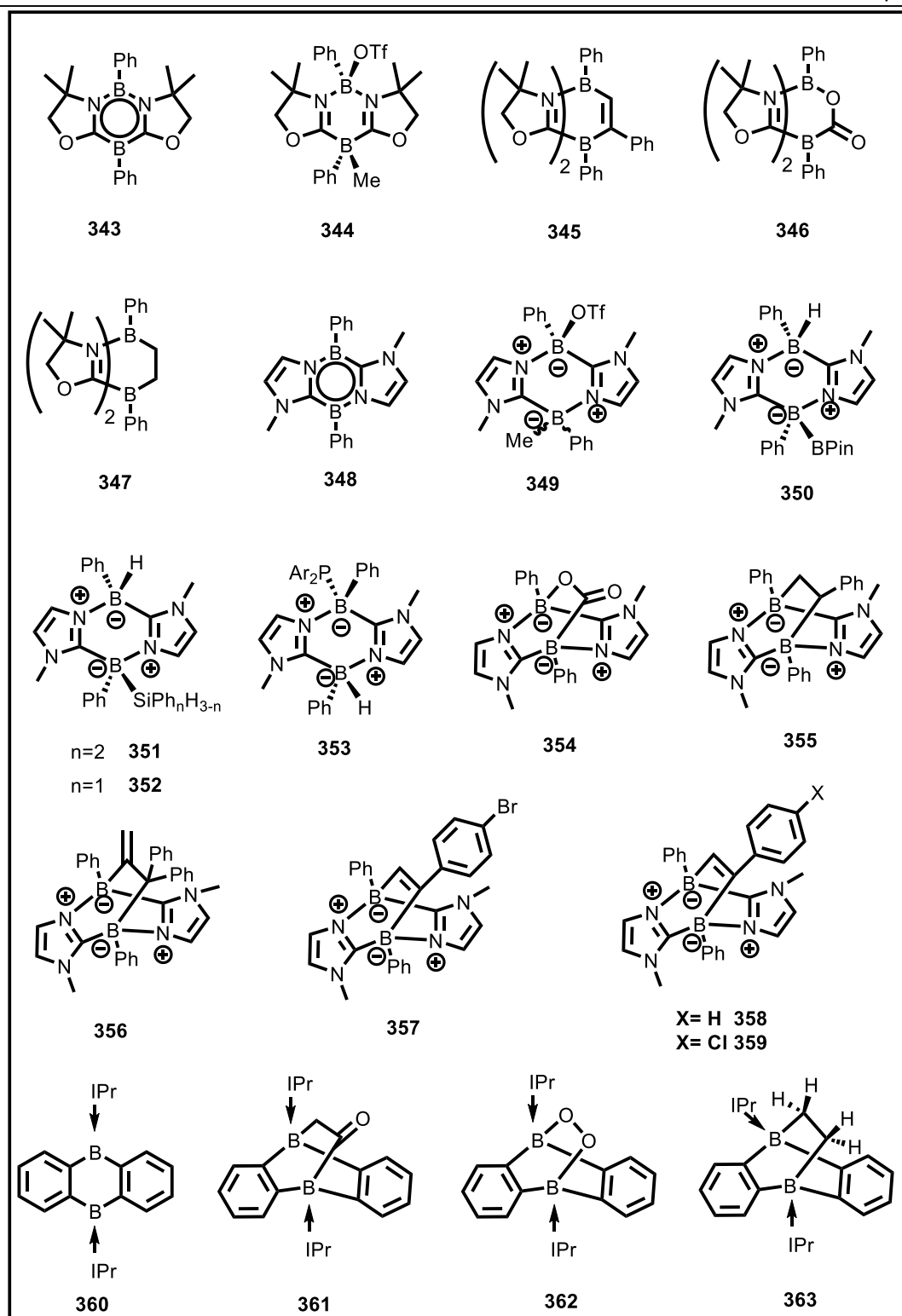


**Figure 1.49:** Bidentate boron Lewis acid and its adduct **343-363**.

Kinjo and coworkers<sup>152</sup> reported 1,4,2,5-diazadiborinine **364**, which on addition with elemental selenium gives the bicyclic product **365** (Figure 1.50). Later Kinjo and

coworkers<sup>153</sup> reported the adduct **366-367**, by treating compound **348** with oxygen and TEMPO respectively. Treatment of **366** with bidentate Lewis acid **348** and pinacolborane gave the product **368** and **369** respectively (Figure 1.50).

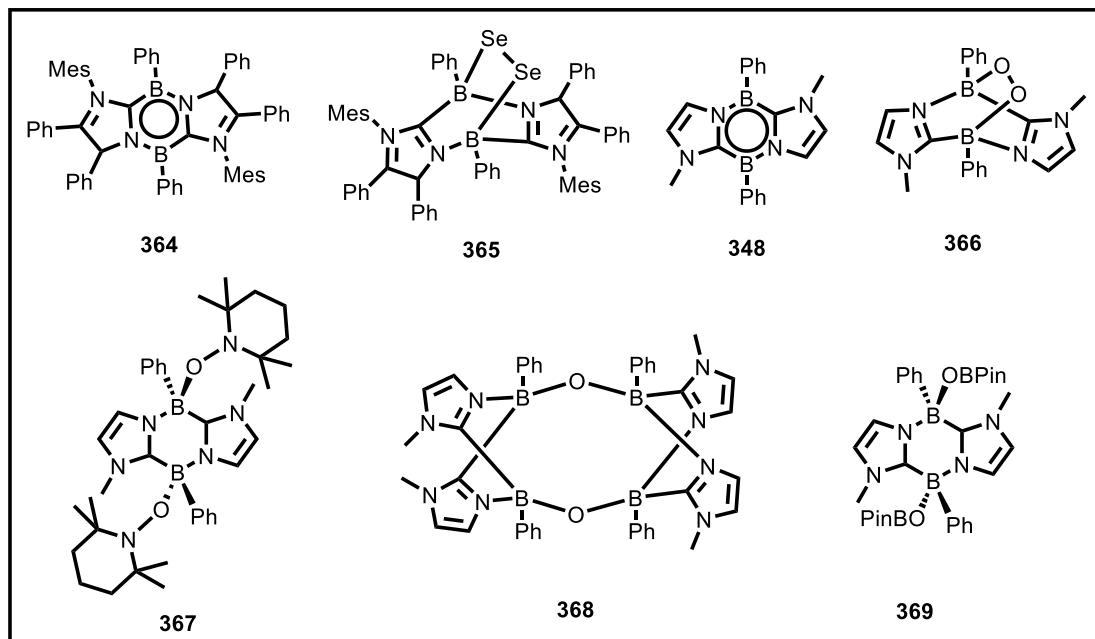


**Figure 1.50:** Bidentate boron Lewis acid and its adduct **364-369**.

## References

- (1) Anthony, J. E. *Chem. Rev.* **2006**, *106*, 5028.
- (2) Bendikov, M.; Wudl, F.; Perepichka, D. F. *Chem. Rev.* **2004**, *104*, 4891.
- (3) Kanis, D. R.; Ratner, M. A.; Marks, T. J.; Zerner, M. C. *Chem. Mater.* **1991**, *3*, 19.
- (4) Kanis, D. R.; Ratner, M. A.; Marks, T. J. *Chem. Rev.* **1994**, *94*, 195.
- (5) Sharma, K.; Sharma, V.; Sharma, S. S. *Nanoscale Res. Lett.* **2018**, *13*, 381.
- (6) Boschloo, G. *Front. Chem.* **2019**, *7*.
- (7) Qian, J.; Tang, B. Z. *Chem.* **2017**, *3*, 56.
- (8) Yuan, L.; Lin, W.; Zheng, K.; He, L.; Huang, W. *Chem. Soc. Rev.* **2013**, *42*, 622.
- (9) Yang, Z.; Mao, Z.; Xie, Z.; Zhang, Y.; Liu, S.; Zhao, J.; Xu, J.; Chi, Z.; Aldred, M. P. *Chem. Soc. Rev.* **2017**, *46*, 915.
- (10) Mei, J.; Leung, N. L. C.; Kwok, R. T. K.; Lam, J. W. Y.; Tang, B. Z. *Chem. Rev.*

---

**2015**, *115*, 11718.

(11) Narita, A.; Wang, X.-Y.; Feng, X.; Müllen, K. *Chem. Soc. Rev.* **2015**, *44*, 6616.

(12) Stępień, M.; Gońka, E.; Żyła, M.; Sprutta, N. *Chem. Rev.* **2017**, *117*, 3479.

(13) Ji, L.; Griesbeck, S.; Marder, T. B. *Chem. Sci.* **2017**.

(14) Hudson, Z. M.; Wang, S. *Acc. Chem. Res.* **2009**, *42*, 1584.

(15) Entwistle, C. D.; Marder, T. B. *Chem. Mater.* **2004**, *16*, 4574.

(16) Li, S.-Y.; Sun, Z.-B.; Zhao, C.-H. *Inorg. Chem.* **2017**, *56*, 8705.

(17) Anzenbacher, P.; Jursíková, K.; Sessler, J. L. *J. Am. Chem. Soc.* **2000**, *122*, 9350.

(18) Anzenbacher, P.; Try, A. C.; Miyaji, H.; Jursíková, K.; Lynch, V. M.; Marquez, M.; Sessler, J. L. *J. Am. Chem. Soc.* **2000**, *122*, 10268.

(19) Yamaguchi, S.; Akiyama, S.; Tamao, K. *J. Am. Chem. Soc.* **2001**, *123*, 11372.

(20) Yamaguchi, S.; Shirasaka, T.; Akiyama, S.; Tamao, K. *J. Am. Chem. Soc.* **2002**, *124*, 8816.

(21) Liu, Z.-Q.; Shi, M.; Li, F.-Y.; Fang, Q.; Chen, Z.-H.; Yi, T.; Huang, C.-H. *Org. Lett.* **2005**, *7*, 5481.

(22) Hudnall, T. W.; Gabbai, F. P. *J. Am. Chem. Soc.* **2007**, *129*, 11978.

(23) Schmidt, H. C.; Reuter, L. G.; Hamacek, J.; Wenger, O. S. *J. Org. Chem.* **2011**, *76*, 9081.

(24) Cheng, F.; Bonder, E. M.; Jäkle, F. *J. Am. Chem. Soc.* **2013**, *135*, 17286.

(25) Song, K. C.; Kim, H.; Lee, K. M.; Lee, Y. S.; Do, Y.; Lee, M. H. *Sensors and Actuators B: Chemical* **2013**, *176*, 850.

- 
- (26) Kumar, G. R.; Thilagar, P. *Dalton Trans.* **2014**, 43, 7200.
- (27) Misra, R.; Jadhav, T.; Dhokale, B.; Mobin, S. M. *Dalton Trans.* **2015**, 44, 16052.
- (28) Brazeau, A. L.; Yuan, K.; Ko, S.-B.; Wyman, I.; Wang, S. *ACS Omega* **2017**, 2, 8625.
- (29) Lee, H.; Jana, S.; Kim, J.; Lee, S. U.; Lee, M. H. *Inorg. Chem.* **2020**, 59, 1414.
- (30) Jiménez, C. C.; Enríquez-Cabrera, A.; González-Antonio, O.; Ordóñez-Hernández, J.; Lacroix, P. G.; Labra-Vázquez, P.; Farfán, N.; Santillan, R. *Inorganics* **2018**, 6, 131.
- (31) Yuan, Z.; Taylor, N. J.; Marder, T. B.; Williams, I. D.; Kurtz, S. K.; Cheng, L.-T. *J. Chem. Soc., Chem. Commun.* **1990**, 1489.
- (32) Branger, C.; Lequan, M.; Lequan, R. M.; Barzoukas, M.; Fort, A. *J. Mater. Chem.* **1996**, 6, 555.
- (33) Liu, Z.-q.; Fang, Q.; Wang, D.; Cao, D.-x.; Xue, G.; Yu, W.-t.; Lei, H. *Chem. Eur. J.* **2003**, 9, 5074.
- (34) Liu, Z.-Q.; Fang, Q.; Cao, D.-X.; Wang, D.; Xu, G.-B. *Org. Lett.* **2004**, 6, 2933.
- (35) Collings, J. C.; Poon, S.-Y.; Le Droumaguet, C.; Charlot, M.; Katan, C.; Pålsson, L.-O.; Beeby, A.; Mosely, J. A.; Kaiser, H. M.; Kaufmann, D.; Wong, W.-Y.; Blanchard-Desce, M.; Marder, T. B. *Chem. Eur. J.* **2009**, 15, 198.
- (36) Chen, P.; Marshall, A. S.; Chi, S.-H.; Yin, X.; Perry, J. W.; Jäkle, F. *Chem. Eur.*
-

---

*J.* **2015**, *21*, 18237.

(37) Griesbeck, S.; Michail, E.; Rauch, F.; Ogasawara, H.; Wang, C.; Sato, Y.; Edkins, R. M.; Zhang, Z.; Taki, M.; Lambert, C.; Yamaguchi, S.; Marder, T. B. *Chem. Eur. J.* **2019**, *25*, 13164.

(38) Griesbeck, S.; Michail, E.; Wang, C.; Ogasawara, H.; Lorenzen, S.; Gerstner, L.; Zang, T.; Nitsch, J.; Sato, Y.; Bertermann, R.; Taki, M.; Lambert, C.; Yamaguchi, S.; Marder, T. B. *Chem. Sci.* **2019**, *10*, 5405.

(39) Pelter, A.; Pardasani, R. T.; Pardasani, P. *Tetrahedron* **2000**, *56*, 7339.

(40) Baik, C.; Hudson, Z. M.; Amarne, H.; Wang, S. *J. Am. Chem. Soc.* **2009**, *131*, 14549.

(41) Rao, Y.-L.; Amarne, H.; Zhao, S.-B.; McCormick, T. M.; Martić, S.; Sun, Y.; Wang, R.-Y.; Wang, S. *J. Am. Chem. Soc.* **2008**, *130*, 12898.

(42) Murphy, S. K.; Baik, C.; Lu, J.-S.; Wang, S. *Org. Lett.* **2010**, *12*, 5266.

(43) Ge, Y.; Ando, N.; Liu, L.; Wang, X.; Sauriol, F.; Yamaguchi, S.; Wu, G.; Wang, S. *Org. Lett.* **2020**, *22*, 3258.

(44) Iida, A.; Saito, S.; Sasamori, T.; Yamaguchi, S. *Angew. Chem. Int. Ed.* **2013**, *52*, 3760.

(45) Ando, N.; Fukazawa, A.; Kushida, T.; Shiota, Y.; Itoyama, S.; Yoshizawa, K.; Matsui, Y.; Kuramoto, Y.; Ikeda, H.; Yamaguchi, S. *Angew. Chem. Int. Ed.* **2017**, *56*,



---

12210.

- (46) Rao, Y.-L.; Hörl, C.; Braunschweig, H.; Wang, S. *Angew. Chem. Int. Ed.* **2014**, *53*, 9086.
- (47) Wang, S. *Coord. Chem. Rev.* **2001**, *215*, 79.
- (48) Li, D.; Zhang, H.; Wang, Y. *Chem. Soc. Rev.* **2013**, *42*, 8416.
- (49) Tanaka, K.; Chujo, Y. *Npg Asia Mater.* **2015**, *7*, e223.
- (50) Rao, Y.-L.; Wang, S. *Inorg. Chem.* **2011**, *50*, 12263.
- (51) Frath, D.; Massue, J.; Ulrich, G.; Ziessel, R. *Angew. Chem. Int. Ed. Engl.* **2014**, *53*, 2290.
- (52) Rao, Y.-L.; Amarne, H.; Wang, S. *Coord. Chem. Rev.* **2012**, *256*, 759.
- (53) Wakamiya, A.; Taniguchi, T.; Yamaguchi, S. *Angew. Chem.* **2006**, *45*, 3170.
- (54) Amarne, H.; Baik, C.; Murphy, S. K.; Wang, S. *Chem. Eur. J.* **2010**, *16*, 4750.
- (55) Li, D.; Zhang, Z.; Zhao, S.; Wang, Y.; Zhang, H. *Dalton Trans.* **2011**, *40*, 1279.
- (56) Zhao, Z.; Chang, Z.; He, B.; Chen, B.; Deng, C.; Lu, P.; Qiu, H.; Tang, B. Z. *Chem.* **2013**, *19*, 11512.
- (57) Chen, J.; Lalancette, R. A.; Jäkle, F. *Chem. Eur. J.* **2014**, *20*, 9120.
- (58) Yusuf, M.; Liu, K.; Guo, F.; Lalancette, R. A.; Jäkle, F. *Dalton Trans.* **2016**, *45*, 4580.
- (59) Yang, D.-T.; Shi, Y.; Peng, T.; Wang, S. *Organometallics* **2017**, *36*, 2654.
- (60) Liu, K.; Lalancette, R. A.; Jäkle, F. *J. Am. Chem. Soc.* **2017**, *139*, 18170.
- (61) Liu, K.; Lalancette, R. A.; Jäkle, F. *J. Am. Chem. Soc.* **2019**, *141*, 7453.
- (62) Dhanunjayarao, K.; Sa, S.; Aradhyula, B. P. R.; Venkatasubbaiah, K. *Tetrahedron* **2018**, *74*, 5819.

- 
- (63) Vanga, M.; Sa, S.; Kumari, A.; Murali, A. C.; Nayak, P.; Das, R.; Venkatasubbaiah, K. *Dalton Trans.* **2020**, 49, 7737.
- (64) Li, C.; Mellerup, S. K.; Wang, X.; Wang, S. *Organometallics* **2018**, 37, 3360.
- (65) Mellerup, S. K.; Li, C.; Wang, X.; Wang, S. *J. Org. Chem.* **2018**, 83, 11970.
- (66) Li, Y.; Meng, H.; Yan, D.; Li, Y.; Pang, B.; Zhang, K.; Luo, G.; Huang, J.; Zhan, C. *Tetrahedron* **2018**, 74, 4308.
- (67) Ryu, K. Y.; Sung, D.-B.; Won, S.-Y.; Jo, A.; Ahn, K.; Kim, H. Y.; ArulKashmir, A.; Kwak, K.; Lee, C.; Kim, W.-S.; Kim, K. *Dyes and Pigments* **2018**, 149, 858.
- (68) Dash, B. P.; Hamilton, I.; Tate, D. J.; Crossley, D. L.; Kim, J.-S.; Ingleson, M. J.; Turner, M. L. *J. Mater. Chem. C* **2019**, 7, 718.
- (69) Li, Y.; Pang, B.; Meng, H.; Xiang, Y.; Li, Y.; Huang, J. *Tetrahedron Lett.* **2019**, 60, 151286.
- (70) Kunchala, D.; Sa, S.; Nayak, P.; Ponniah S, J.; Venkatasubbaiah, K. *Organometallics* **2019**, 38, 870.
- (71) Mukundam, V.; Sa, S.; Kumari, A.; Das, R.; Venkatasubbaiah, K. *J. Mater. Chem. C* **2019**, 7, 12725.
- (72) Mukundam, V.; Lalancette, R. A.; Jäkle, F. *Chem. Eur. J.* **2019**, 25, 10133.
- (73) He, Z.; Liu, L.; Zhao, Z.; Mellerup, S. K.; Ge, Y.; Wang, X.; Wang, N.; Wang, S. *Chem. Eur. J.* **2020**, 26, 12403.
- (74) Koch, R.; Sun, Y.; Orthaber, A.; Pierik, A. J.; Pammer, F. *Org. Chem. Front.* **2020**, 7, 1437.
- (75) Lu, H.; Nakamuro, T.; Yamashita, K.; Yanagisawa, H.; Nureki, O.; Kikkawa, M.; Gao, H.; Tian, J.; Shang, R.; Nakamura, E. *J. Am. Chem. Soc.* **2020**, 142, 18990.
- (76) Loudet, A.; Burgess, K. *Chem. Rev.* **2007**, 107, 4891.
- (77) Ulrich, G.; Ziesel, R.; Harriman, A. *Angew. Chem. Int. Ed.* **2008**, 47, 1184.
-

- 
- (78) Ziessel, R.; Ulrich, G.; Harriman, A. *New J. Chem.* **2007**, 31, 496.
- (79) Yamada, K.; Nomura, Y.; Citterio, D.; Iwasawa, N.; Suzuki, K. *J. Am. Chem. Soc.* **2005**, 127, 6956.
- (80) Zeng, L.; Miller, E. W.; Pralle, A.; Isacoff, E. Y.; Chang, C. J. *J. Am. Chem. Soc.* **2006**, 128, 10.
- (81) Qi, X.; Jun, E. J.; Xu, L.; Kim, S.-J.; Joong Hong, J. S.; Yoon, Y. J.; Yoon, J. *J. Org. Chem.* **2006**, 71, 2881.
- (82) Baruah, M.; Qin, W.; Basarić, N.; De Borggraeve, W. M.; Boens, N. *J. Org. Chem.* **2005**, 70, 4152.
- (83) Baruah, M.; Qin, W.; Vallée, R. A. L.; Beljonne, D.; Rohand, T.; Dehaen, W.; Boens, N. *Org. Lett.* **2005**, 7, 4377.
- (84) Tillo, A.; Bartelmess, J.; Chauhan, V. P.; Bell, J.; Rurack, K. *Anal. Chem.* **2019**, 91, 12980.
- (85) Golovkova, T. A.; Kozlov, D. V.; Neckers, D. C. *J. Org. Chem.* **2005**, 70, 5545.
- (86) Trieflinger, C.; Rurack, K.; Daub, J. *Angew. Chem. Int. Ed.* **2005**, 44, 2288.
- (87) Luo, Y.; Prestwich, G. D. *Bioconjugate Chem.* **1999**, 10, 755.
- (88) Karolin, J.; Johansson, L. B. A.; Strandberg, L.; Ny, T. *J. Am. Chem. Soc.* **1994**, 116, 7801.
- (89) Merino, E. J.; Weeks, K. M. *J. Am. Chem. Soc.* **2005**, 127, 12766.
- (90) Tahtaoui, C.; Parrot, I.; Klotz, P.; Guillier, F.; Galzi, J.-L.; Hibert, M.; Ilien, B. *J. Med. Chem.* **2004**, 47, 4300.
- (91) Lawrie, G.; Grøndahl, L.; Battersby, B.; Keen, I.; Lorentzen, M.; Surawski, P.; Trau, M. *Langmuir* **2006**, 22, 497.
- (92) Lakshmi, V.; Ravikanth, M. *J. Org. Chem.* **2011**, 76, 8466.
-

- 
- (93) Burghart, A.; Thoresen, L. H.; Chen, J.; Burgess, K.; Bergstrom, F.; Johansson, L. B. A. *Chem. Commun.* **2000**, 2203.
- (94) Ge, Y.; O'Shea, D. F. *Chem. Soc. Rev.* **2016**, *45*, 3846.
- (95) Zhang, D.; Wen, Y.; Xiao, Y.; Yu, G.; Liu, Y.; Qian, X. *Chem. Commun.* **2008**, 4777.
- (96) Liu, Q.; Mudadu, M. S.; Schmider, H.; Thummel, R.; Tao, Y.; Wang, S. *Organometallics* **2002**, *21*, 4743.
- (97) Liu, Q. D.; Mudadu, M. S.; Thummel, R.; Tao, Y.; Wang, S. *Adv. Funct. Mater.* **2005**, *15*, 143.
- (98) Araneda, J. F.; Piers, W. E.; Heyne, B.; Parvez, M.; McDonald, R. *Angew. Chem. Int. Ed.* **2011**, *50*, 12214.
- (99) Suresh, D.; Ferreira, B.; Lopes, P. S.; Gomes, C. S. B.; Krishnamoorthy, P.; Charas, A.; Vila-Viçosa, D.; Morgado, J.; Calhorda, M. J.; Maçanita, A. L.; Gomes, P. T. *Dalton Trans.* **2016**, *45*, 15603.
- (100) Wang, T.; Dou, C.; Liu, J.; Wang, L. *Chem. Eur. J.* **2018**, *24*, 13043.
- (101) Li, L.; Gao, Y.; Dou, C.; Liu, J. *Chin. Chem. Lett.* **2020**, *31*, 1193.
- (102) Min, Y.; Dou, C.; Tian, H.; Liu, J.; Wang, L. *Chem. Commun.* **2019**, *55*, 3638.
- (103) Min, Y.; Dou, C.; Liu, D.; Dong, H.; Liu, J. *J. Am. Chem. Soc.* **2019**, *141*, 17015.
- (104) Cao, Y.; Zhu, C.; Barlóg, M.; Barker, K. P.; Ji, X.; Kalin, A. J.; Al-Hashimi, M.; Fang, L. *J. Org. Chem.* **2021**, *86*, 2100.
- (105) Min, Y.; Dou, C.; Tian, H.; Liu, J.; Wang, L. *Chem. Eur. J.* **2021**, *27*, 4364.
- (106) Frath, D.; Azizi, S.; Ulrich, G.; Retailleau, P.; Ziesel, R. *Org. Lett.* **2011**, *13*, 3414.
- (107) Dhanunjayarao, K.; Mukundam, V.; Ramesh, M.; Venkatasubbaiah, K. *Eur. J. Inorg. Chem.* **2014**, *2014*, 539.
-

- 
- (108) Dhanunjayarao, K.; Mukundam, V.; Venkatasubbaiah, K. *Inorg. Chem.* **2016**, *55*, 11153.
- (109) Zhang, Z.; Zhang, Z.; Zhang, H.; Wang, Y. *Dalton Trans.* **2018**, *47*, 127.
- (110) Shimogawa, H.; Murata, Y.; Wakamiya, A. *Org. Lett.* **2018**, *20*, 5135.
- (111) Urban, M.; Durka, K.; Górka, P.; Wiosna-Sałyga, G.; Nawara, K.; Jankowski, P.; Luliński, S. *Dalton Trans.* **2019**, *48*, 8642.
- (112) Chinta, R. V. R. N.; Aradhyula, B. P. R.; Murali, A. C.; Venkatasubbaiah, K. *J. Organomet. Chem.* **2019**, *891*, 20.
- (113) Wittig, G.; Bickelhaupt, F. *Chem. Ber.* **1958**, *91*, 883.
- (114) Wuest, J. D.; Zacharie, B. *Organometallics* **1985**, *4*, 410.
- (115) Beauchamp, A. L.; Olivier, M. J.; Wuest, J. D.; Zacharie, B. *Organometallics* **1987**, *6*, 153.
- (116) Schmidbaur, H.; Öller, H.-J.; Wilkinson, D. L.; Huber, B.; Müller, G. *Chem. Ber.* **1989**, *122*, 31.
- (117) Simard, M.; Vaugeois, J.; Wuest, J. D. *J. Am. Chem. Soc.* **1993**, *115*, 370.
- (118) Vaugeois, J.; Wuest, J. D. *J. Am. Chem. Soc.* **1998**, *120*, 13016.
- (119) Massey, A. G.; Al-Jabar, N. A. A.; Humphries, R. E.; Deacon, G. B. *J. Organomet. Chem.* **1986**, *316*, 25.
- (120) Tschinkl, M.; Schier, A.; Riede, J.; Gabbaï, F. P. *Organometallics* **1999**, *18*, 1747.
- (121) Tschinkl, M.; Schier, A.; Riede, J.; Gabbaï, F. P. *Angew Chem. Int. Ed.* **1999**, *38*, 3547.
- (122) Tschinkl, M.; Bachman, R. E.; Gabbaï, F. P. *Organometallics* **2000**, *19*, 2633.
- (123) Beckwith, J. D.; Tschinkl, M.; Picot, A.; Tsunoda, M.; Bachman, R.; Gabbaï, F. *P. Organometallics* **2001**, *20*, 3169.
-

- 
- (124) Tschinkl, M.; Gabbai, F. P. *J. Chem. Crystallogr.* **2003**, 33, 595.
- (125) Yakovenko, A. A.; Gallegos, J. H.; Antipin, M. Y.; Timofeeva, T. V. *Cryst. Growth Des.* **2009**, 9, 66.
- (126) Yakovenko, A. A.; Gallegos, J. H.; Antipin, M. Y.; Masunov, A.; Timofeeva, T. V. *Cryst. Growth Des.* **2011**, 11, 3964.
- (127) Venkatasubbaiah, K.; Bats, J. W.; Rheingold, A. L.; Jäkle, F. *Organometallics* **2005**, 24, 6043.
- (128) Jurkschat, K.; Hesselbarth, F.; Dargatz, M.; Lehmann, J.; Kleinpeter, E.; Tzschach, A.; Meunier-Piret, J., *J. Organomet. Chem.* **1990**, 388, 259-271.
- (129) Altmann, R.; Jurkschat, K.; Schürmann, M.; Dakternieks, D.; Duthie, A. *Organometallics* **1998**, 17, 5858-5866.
- (130) Jurkschat, K.; Kuivila, H. G.; Liu, S.; Zubieta, J. A., *Organometallics* **1989**, 8, 2755-2759.
- (131) Saito, M.; Nitta, M.; Yoshioka, M. *Organometallics* **2001**, 20, 749.
- (132) Saito, M.; Henzan, N.; Yoshioka, M. *Phosphorus, Sulfur, and Silicon and the Related Elements* **2004**, 179, 957.
- (133) Saito, M.; Henzan, N.; Yoshioka, M. *Chem. Lett.* **2005**, 34, 1018.
- (134) Shirai, M.; Hasegawa, M.; Sato, H.; Mazaki, Y. *Chem. Lett.* **2014**, 43, 592.
- (135) Siebert, W. *Angew. Chem., Int. Ed.* **1985**, 24, 943.
- (136) Siebert, W. *Adv. Organomet. Chem.* **1993**, 35, 187.
- (137) Wörner, K.-F. ; Siebert, W. *Z. Naturforsch.* **1989**, 44b, 1211.
- (138) Wörner, K.-F.; Uhm, J.-K.; Pritzkow, H.; Siebert, W. *Chem. Ber.* **1990**, 123, 1239.
-

- 
- (139) Febenbecker, A.; Schulz, H.; Pritzkow, H.; Siebert, W. *Chem. Ber.* **1990**, *123*, 2273.
- (140) Schulz, H.; Pritzkow, H.; Siebert, W. *Chem. Ber.* **1991**, *124*, 2203.
- (141) Lorbach, A.; Bolte, M.; Li, H.; Lerner, H.-W.; Holthausen, M. C.; Jäkle, F.; Wagner, M. *Angew. Chem. Int. Ed.* **2009**, *48*, 4584-4588.
- (142) Lorbach, A.; Bolte, M.; Lerner, H.-W.; Wagner, M. *Chem. Commun.* **2010**, *46*, 3592-3594.
- (143) Williams, V. C.; Piers, W. E.; Clegg, W.; Elsegood, M. R. J.; Collins, S.; Marder, T. B. *J. Am. Chem. Soc.* **1999**, *121*, 3244.
- (144) Metz, M. V.; Schwartz, D. J.; Stern, C. L.; Nickias, P. N.; Marks, T. J., *Angew. Chem. Int. Ed.* **2000**, *39*, 1312.
- (145) Venkatasubbaiah, K.; Nowik, I.; Herber, R. H.; Jäkle, F. *Chem. Commun.* **2007**, 2154.
- (146) Mercier, L. G.; Piers, W. E.; Harrington, R. W.; Clegg, W. *Organometallics* **2013**, *32*, 6820.
- (147) Lu, Z.; Schweighauser, L.; Hausmann, H.; Wegner, H. A. *Angew. Chem. Int. Ed.* **2015**, *54*, 15556.
- (148) von Grotthuss, E.; Prey, S. E.; Bolte, M.; Lerner, H.-W.; Wagner, M. *Angew. Chem. Int. Ed.* **2018**, *57*, 16491.
- (149) Wu, D.; Kong, L.; Li, Y.; Ganguly, R.; Kinjo, R. *Nat. Commun.* **2015**, *6*, 7340.
- (150) Wang, B.; Li, Y.; Ganguly, R.; Hirao, H.; Kinjo, R. *Nat. Commun.* **2016**, *7*, 11871.
- (151) Taylor, J. W.; McSkimming, A.; Guzman, C. F.; Harman, W. H. *J. Am. Chem. Soc.* **2017**, *139*, 11032.
- (152) Goh, G. K. H.; Li, Y.; Kinjo, R. *Dalton Trans.* **2019**, *48*, 7514.
-

(153) Wang, B.; Kinjo, R. *Chem. Sci.* **2019**, *10*, 2088.



## CHAPTER 2

### **Synthesis of bidentate Lewis acid 3,4-bis(chloromercurio)2,5-dimethylthiophene and its complexation behavior with neutral (THF & DMSO) and anionic nucleophiles (Et<sub>4</sub>NCl)**

<b>2.1 Introduction</b>	63
<b>2.2 Results and discussion</b>	64
<b>2.2.1 Synthesis and characterisation</b>	64
<b>2.2.2 Solid state studies</b>	68
<b>2.3 Conclusions</b>	76
<b>2.4 Experimental section</b>	77
<b>2.4.1 General information</b>	77
<b>2.4.2 Synthetic procedures and spectral characterisations</b>	77
<b>2.5 References</b>	79



## 2.1 Introduction

Multidentate Lewis acids especially arylmercury compounds have gained much interest in the field of catalysis,<sup>1,2</sup> molecular recognition,<sup>3-8</sup> ion sensing<sup>9,10</sup> and as building blocks for supramolecular architecture<sup>11,12</sup>. Multidentate Lewis acids behave as a host for the coordination of neutral as well as anionic substrates. Structural diversity has a significant impact on the binding capabilities of these multidentate arylmercury Lewis acids. Different backbones have been studied to realize the binding capabilities of the multidentate arylmercury compounds. For example, Wuest and co-workers<sup>13-16</sup> explored the complexation and catalytic behavior of 1,2-phenylenedimercury dichloride (Figure 2.1.A), Gabbai and co-workers<sup>17-21</sup> extensively studied, fluorinated analogue of 1,2-phenylenedimercury dichloride namely 1,2-bis(chloromercurio)tetrafluorobenzene (Figure 2.1.B) as a host for different neutral and anionic moieties. The chelating capability of 1,8-bis(chloromercurio)naphthalene (Figure 2.1.C) was studied by Schmidbaur<sup>22</sup> *et. al.*. Synthesis, complexation and functionalization of 1,2- bis(chloromercury)ferrocene (Figure 2.1.D) was reported by Jäekle and coworkers<sup>23</sup>. While, Hawthorne and co-workers<sup>24-29</sup> utilized mercuracarborands, Shur and coworkers<sup>30-33</sup> have investigated polymercury containing macrocycles as ligands for anions. The trapping tendency of copper using a mercuramacrocycle was elegantly shown by Singh and co-workers.<sup>34</sup> Recently, Timofeeva and co-workers<sup>35</sup> used bis(chloromercurio)tetrafluorobenzene as a guest for forming adducts with organic esters. More recently, Thilagar and Swamy<sup>36</sup> showed the selective detection of nitroaromatic explosives using a -HgCl decorated porphyrin system. Fluorinated organomercurials<sup>37-42</sup> have been studied extensively because of their affinity towards binding of not only anionic substrates but also for neutral substrates. However, the complexation behavior of heterocycle based organomercurials

are rarely explored in the literature. Herein, we report the synthesis of 3,4-bis(chloromercurio)2,5-dimethylthiophene and its complexation studies with neutral substrates (THF and DMSO) and anionic substrate ( $\text{Et}_4\text{NCl}$ ).

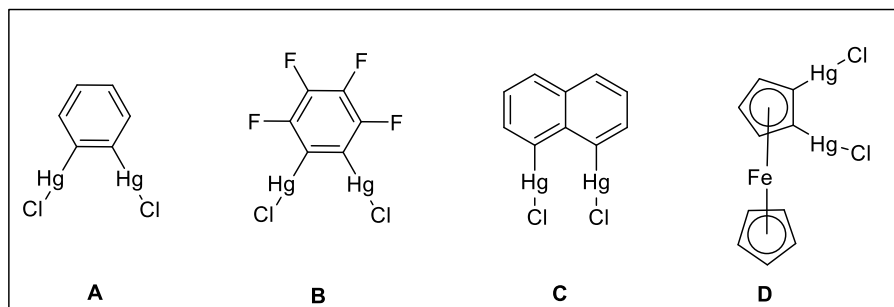


**Figure 2.1:** 1,2-Phenylenedimercury dichloride (A), 1,2-bis(chloromercurio)tetrafluorobenzene (B), 1,8-bis(chloromercurio)naphthalene (C), 1,2-bis(chloromercury)ferrocene (D).

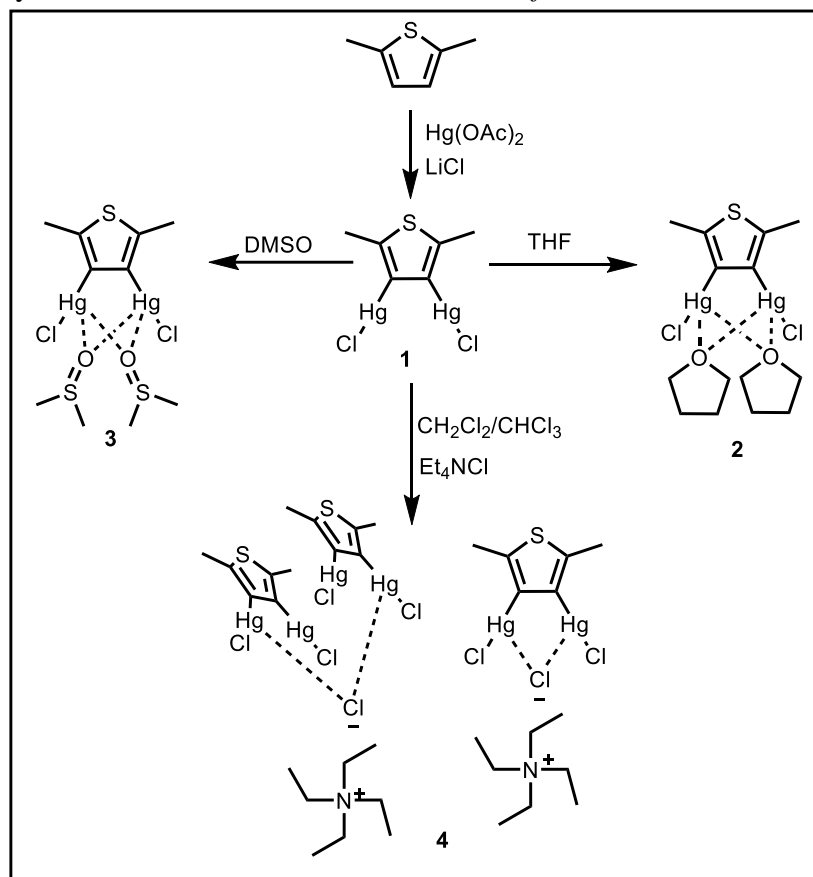
## 2.2 Results and discussion

### 2.2.1 Synthesis and characterisation

Compound **1** was synthesized by treating 2,5-dimethylthiophene with mercuric acetate in methanol followed by the addition of lithium chloride in methanol (**Scheme 2.1**). The formation of compound **1** was characterized by  $^1\text{H}$ , and  $^{13}\text{C}$  NMR. The  $^1\text{H}$  NMR spectrum in  $\text{DMSO}-d_6$  shows a singlet at 2.41 ppm, and the disappearance of signal corresponding to the aromatic proton of 2,5-dimethylthiophene in the aromatic region confirms the formation of compound **1** (Figure 2.2). HRMS studies and elemental analysis further confirm the formation of compound **1** (Figure 2.3).

Slow evaporation of a THF and DMSO solution of compound **1** gives colorless crystals of compound **2** and **3** respectively as determined by elemental analysis (**Scheme 2.1**). The  $^1\text{H}$  NMR of the crystals (without drying) of compound **2** reveals the presence of THF. Compound **2** is stable at ambient temperature, however the crystal of

compound **2** becomes opaque after one day. Compound **3** was analyzed using IR spectroscopy, which shows the anticipated sulfoxide (S=O) stretching band at  $1012\text{ cm}^{-1}$ .<sup>38</sup> Thermogravimetric analysis reveal that compound **2** & **3** undergoes weight loss of 20 % and 21 % at below  $100\text{ }^{\circ}\text{C}$  and  $150\text{ }^{\circ}\text{C}$  respectively (Figure 2.5). The molecular structures of compounds **2** & **3** were further confirmed by single crystal X-ray crystallography studies which will be discussed *vide infra*.



**Scheme 2.1:** Synthesis of thiophene based bidentate Lewis acid and its complexes.

Compound **4** was prepared by treatment of compound **1** with  $\text{Et}_4\text{NCl}$  (**Scheme 2.1**). Slow evaporation of a solvent mixture of dichloromethane and chloroform yields colorless crystals of compound **4**. Formation of compound **4** was confirmed by  $^1\text{H}$  NMR and elemental analysis.  $^1\text{H}$  NMR spectrum of compound **4** (crystals dissolved in  $\text{DMSO-}d_6$ ) shows a triplet at 1.16 ppm and a quartet at 3.20 ppm corresponds to the  $[\text{Et}_4\text{N}]^+$  unit (Figure 2.4). The single crystal structure analysis of compound **4** further

confirms the formation of 3:2 complex. To the best of our knowledge this is the first report of such type of 3:2 complex.

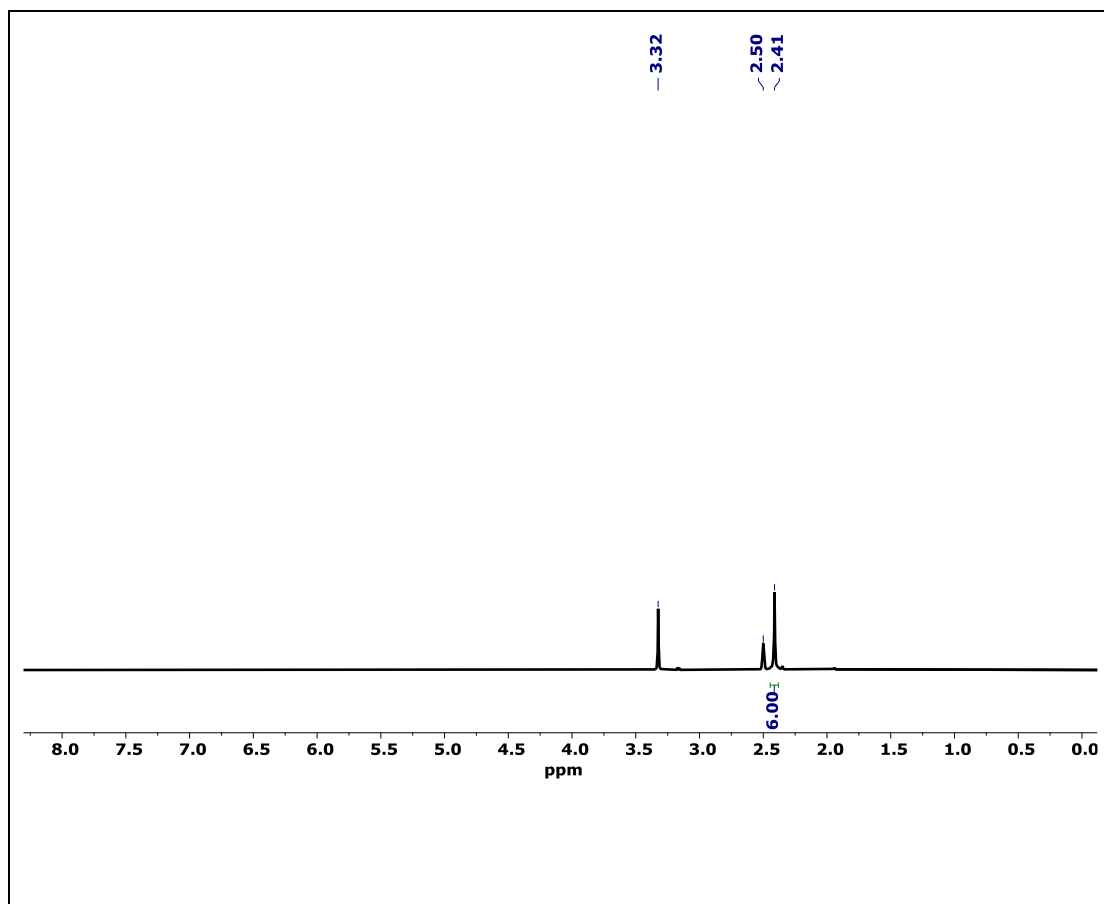


**Figure 2.2:**  $^1\text{H}$  NMR spectrum of compound 1 in  $\text{DMSO-}d_6$ .

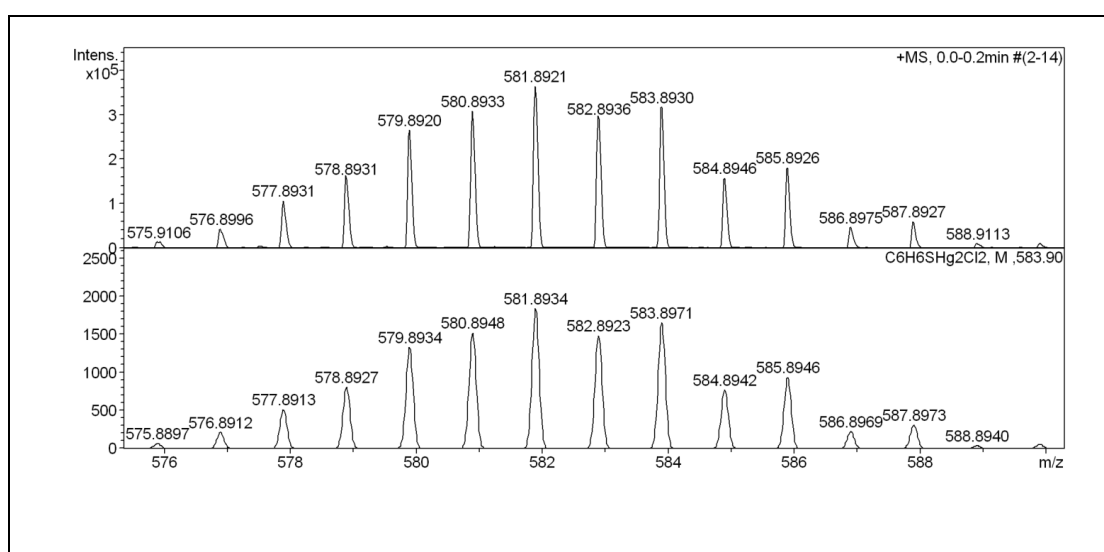


**Figure 2.3:** HRMS spectrum of compound 1.

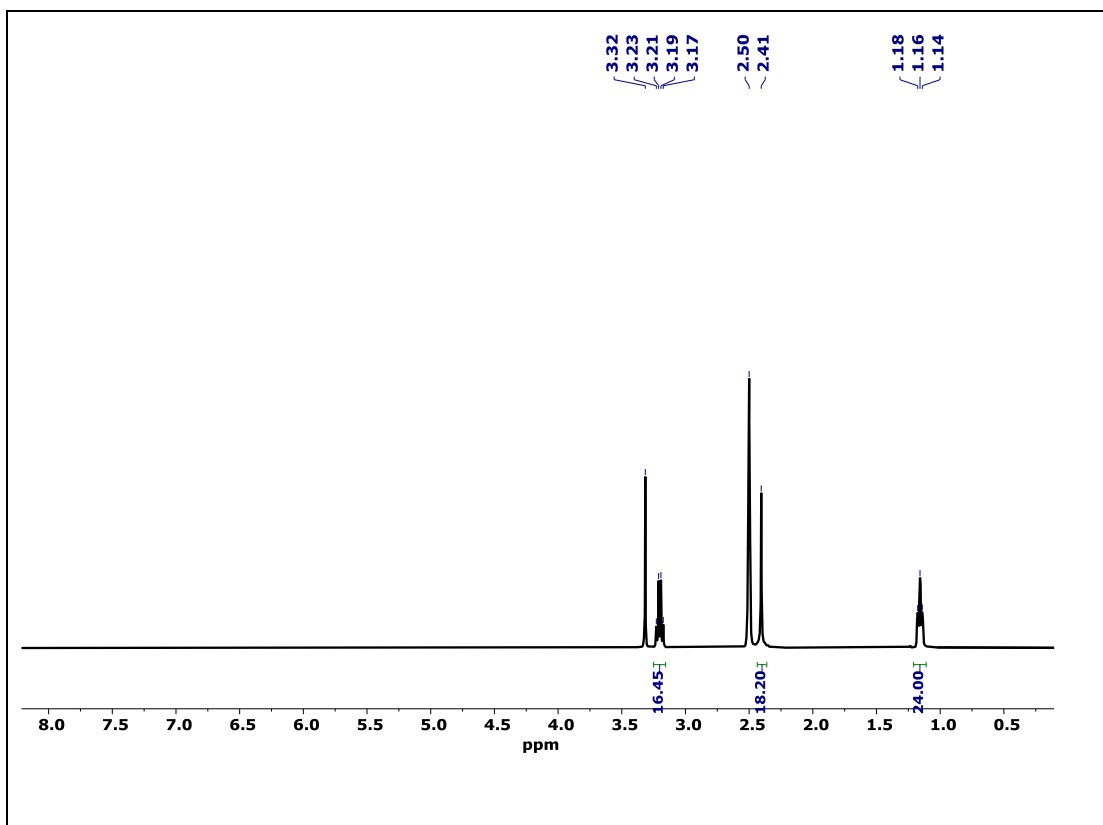


**Figure 2.4:** <sup>1</sup>H NMR spectrum of compound **4** in DMSO-*d*<sub>6</sub>.

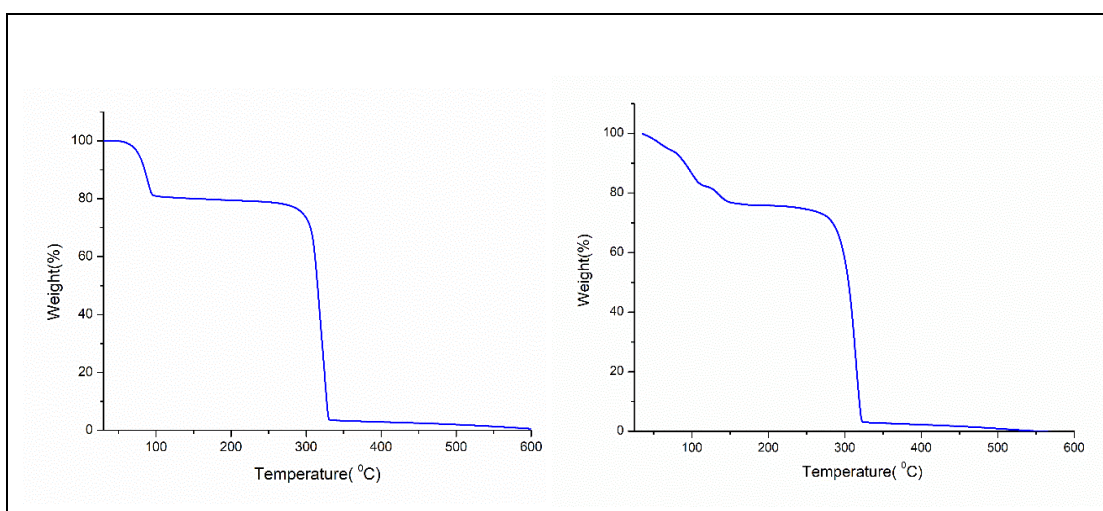


**Figure 2.5:** TGA curves for compound **2** (left) and **3** (Right) under N<sub>2</sub> at a heating rate of 10 °C min<sup>-1</sup>.

### 2.2.2 Solid state studies

X-ray quality crystals of compound **1** were grown by slow evaporation of a DMF solution and determined by X-ray diffraction analysis. Compound **1** crystallizes in the monoclinic  $P2_1/c$  space group. The molecular structure of compound **1** is presented in figure 2.6. Examination of cell packing of compound **1** reveals that it contains intermolecular Hg $\cdots$ Cl contacts (Hg1-Cl1 3.332(5); Hg2-Cl1 3.326(6); Hg2-Cl2 3.414(6)). The observed Hg $\cdots$ Cl contacts (Figure 2.6) are shorter than the sum of the van der Waals radii of mercury (1.73-2.00 Å)<sup>43</sup> and chlorine (1.58-1.78 Å)<sup>44</sup>. Apart from that compound **1** also possess weak hydrogen bonding interactions (C-H $\cdots$ Cl 2.780(4) and 2.869(5)) which lead to the formation of 1D polymeric network as shown in figure 2.7. The Hg $\cdots$ Cl contacts in combination with C-H $\cdots$ Cl interactions lead to the formation of 3D network as shown in figure 2.7.

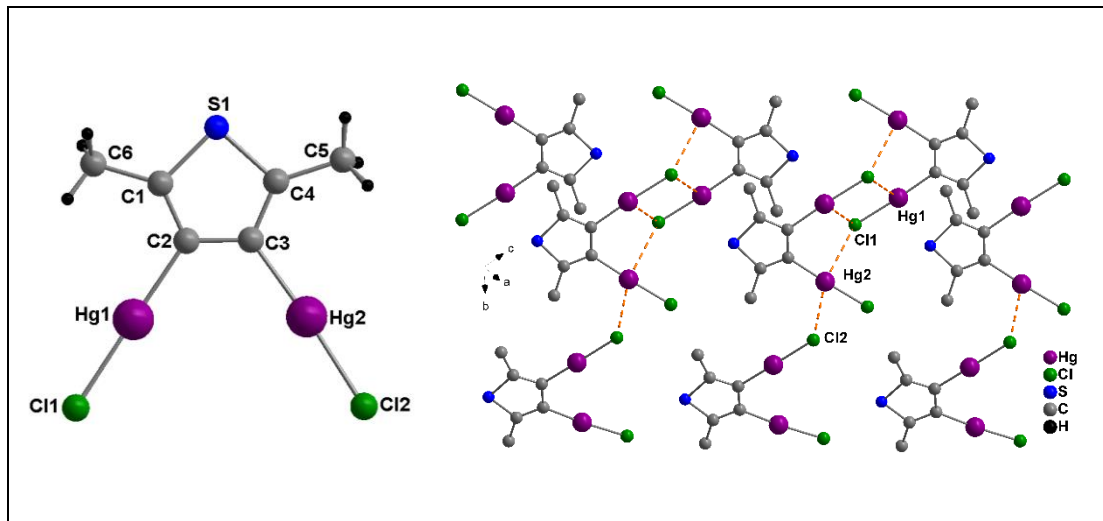


**Figure 2.6:** Molecular structure of compound **1** (left) and its 1D polymeric network via Hg $\cdots$ Cl interactions (right, all hydrogen atoms are omitted for clarity). Selected bond lengths (Å) and bond angles (°): Hg1-C2 2.063(15), Hg2-C3 2.047(15), Hg1-Cl1 2.318(4), Hg2-Cl2 2.297(4), C2-Hg1-Cl1 176.0(4) and C3-Hg2-Cl2:177.0(4).



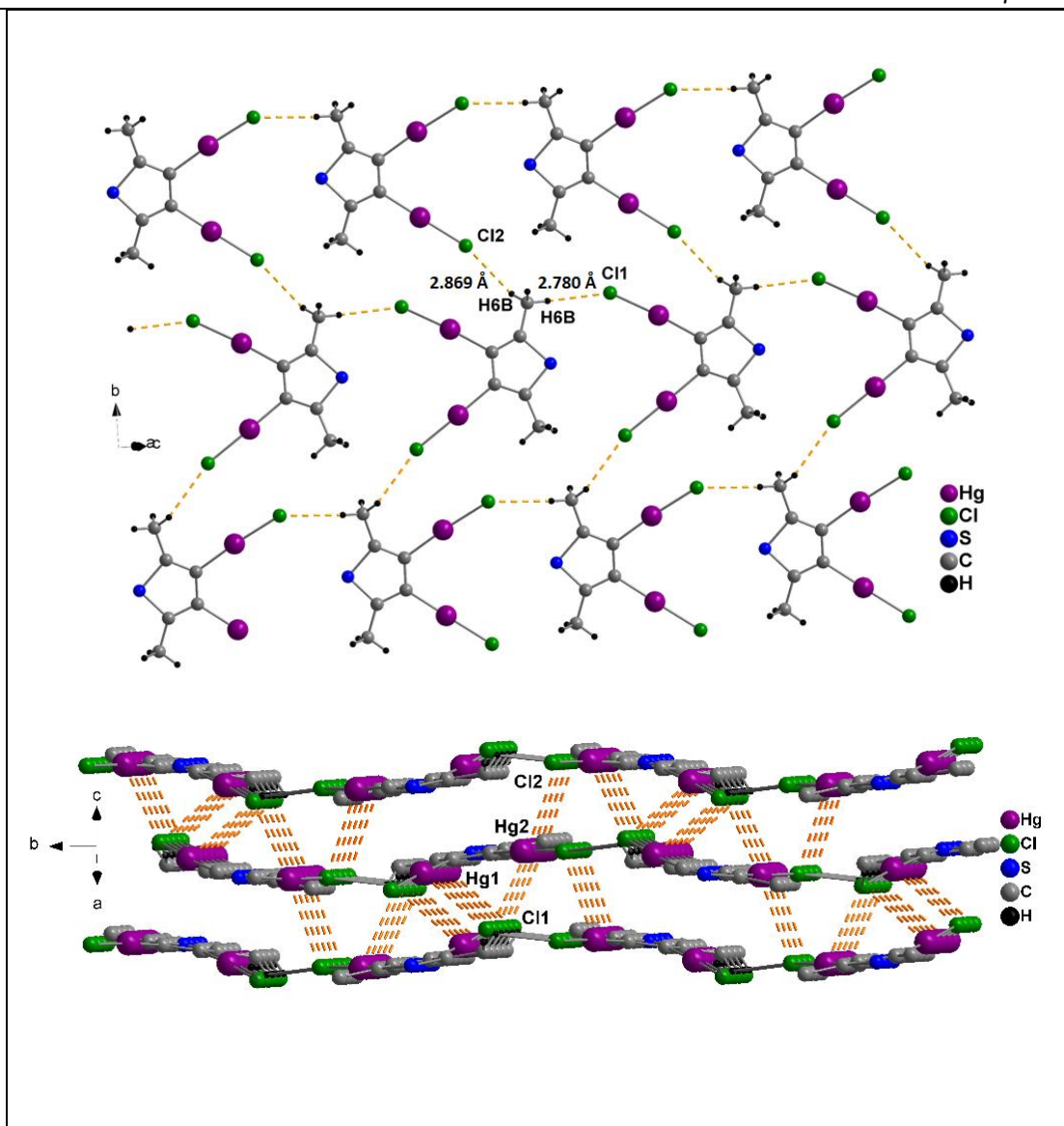


**Figure 2.7:** Portion of a chain like structure of compound **1** through C-H...Cl hydrogen bonding (top); 3D network of compound **1** (bottom) through C-H...Cl hydrogen bonding and Hg...Cl interactions.

Compound **2** & **3** forms 1:2 complexes with THF and DMSO respectively (Figure 2.8 & 2.9). Compound **2** crystallizes in monoclinic space group  $C2/c$  whereas compound **3** crystallises in triclinic space group  $P-1$ . The Hg-O bond distances (Hg1-O1 2.810(6) Å and Hg1\*-O1 2.838(6) Å for compound **2** and Hg1-O2 2.852(4) Å and Hg2-O2 2.816(4) Å for compound **3** (disordered DMSO

bond lengths are not considered) are within the sum of the van der Waals radii for oxygen (1.54 Å)<sup>43</sup> and mercury (1.73-2.00 Å).<sup>44</sup> The observed Hg-O contacts are comparable with the literature reported complexes such as 1,2-bis(chloromercury)ferrocene.DMSO,<sup>12</sup> 1,2-bis(chloromercurio)tetrafluorobenzene.(DMSO)<sub>2</sub>,<sup>12</sup> 1,2-bis(chloromercurio)benzene.(DMF),<sup>13</sup> 1,8-bis(chloromercurio)naphthalene.DMSO,<sup>22</sup> 1,2-bis(chloromercurio)tetrafluorobenzene.(THF),<sup>20</sup> 1,2-bis(chloromercurio)tetrafluorobenzene.(DMF)<sup>17,21</sup> and 1,2-bis(chloromercurio)tetrafluorobenzene.(acetone).<sup>17,21</sup> The Hg-O bonds are nearly perpendicular (C1-Hg1-O1 93.1(2)° and C1\*-Hg1\*-O1 91.2(2)° for compound **2**; C3-Hg2-O2 88.4(2)° and C2-Hg1-O2 86.3(2)°) to the corresponding C-Hg-Cl sequences and the coordination environment around the oxygen center is distorted tetrahedral geometry with an acute angle of 81.1(2)° for compound **2** and 79.5(1)° for compound **3**.

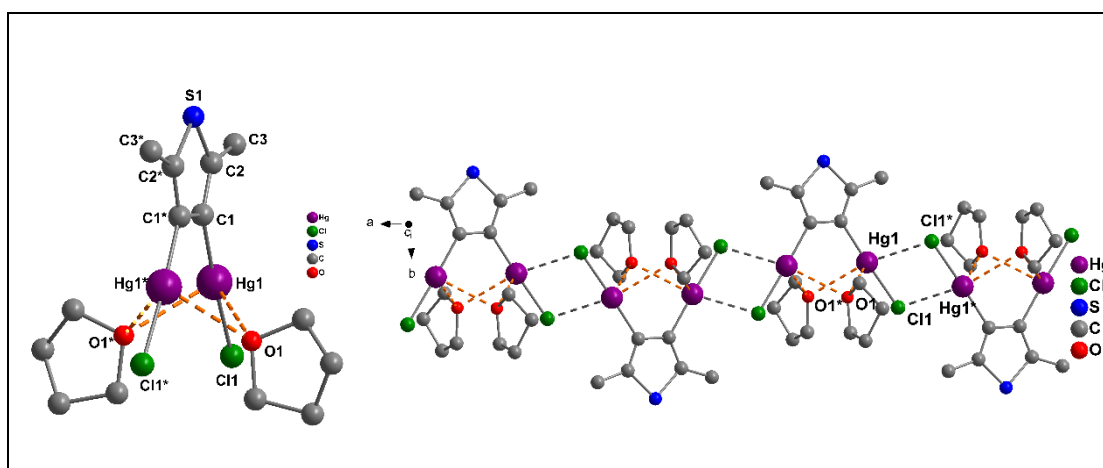


**Figure 2.8:** Molecular structure of compound **2** (left) and its 1D polymeric network *via* Hg...Cl interactions (right, all hydrogen atoms are omitted for clarity). Selected bond lengths (Å) and bond angles (°): Hg1-C1 2.033(5), Hg1-Cl1 2.318(15), C1-Hg1-Cl1 176.63(16), Hg1-O1-Hg1\* 81.1(2).

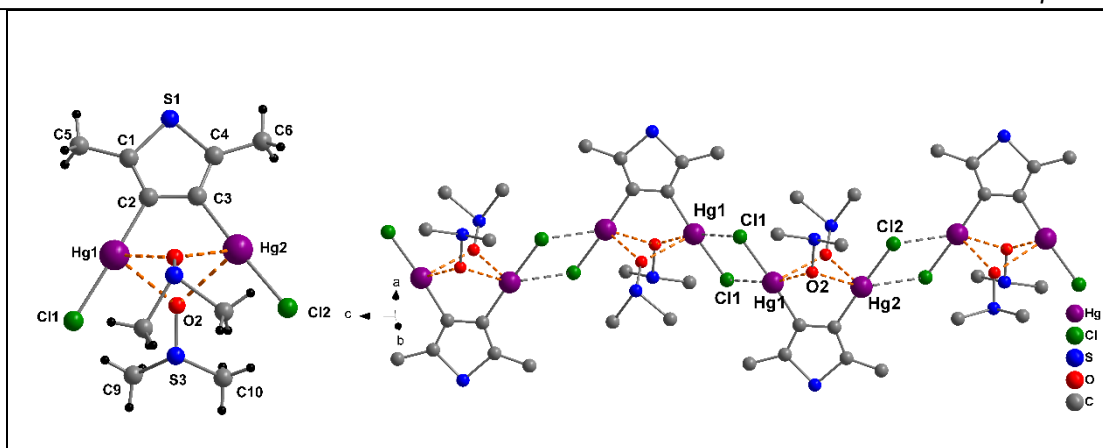


**Figure 2.9:** Molecular structure of compound **3** (left) and its 1D polymeric network *via* Hg...Cl interactions (right, all hydrogen atoms are omitted for clarity). Selected bond lengths (Å) and bond angles (°): Hg1-C2 2.043(6), Hg2-C3 2.047(6), Hg1-Cl1 2.314(2), Hg2-Cl2 2.320(2), C2-Hg1-Cl1 175.8(2), C3-Hg2-Cl2 175.0(2), Hg2-O1A-Hg1 84.8(2), and Hg2-O2-Hg1 79.5(1).

The packing diagram of compound **2** and **3** reveal the existence of Hg...Cl interactions. Formation of Hg<sub>2</sub>Cl<sub>2</sub> bridges are noticed in both compounds as observed in other organomercurio halides.<sup>20,21,23</sup> The intermolecular Hg...Cl bond distance observed for compound **2** is shorter over compound **3** and comparable to the sum of the van der Waals radii of the respective elements ( $r_{\text{vdw}}(\text{Cl})=1.58\text{--}1.78\text{ Å}$ ,<sup>43</sup>  $r_{\text{vdw}}(\text{Hg})=1.73\text{--}2.00\text{ Å}$ <sup>44</sup>). Additionally, compound **2** and **3** also possess weak hydrogen bonding interactions. The weak intermolecular C-H...Cl interactions between THF (or) DMSO and Cl lead to the formation of 3D network in compound **2** (Figure 2.10) and sheet like structure in case of compound **3** (Figure 2.11).

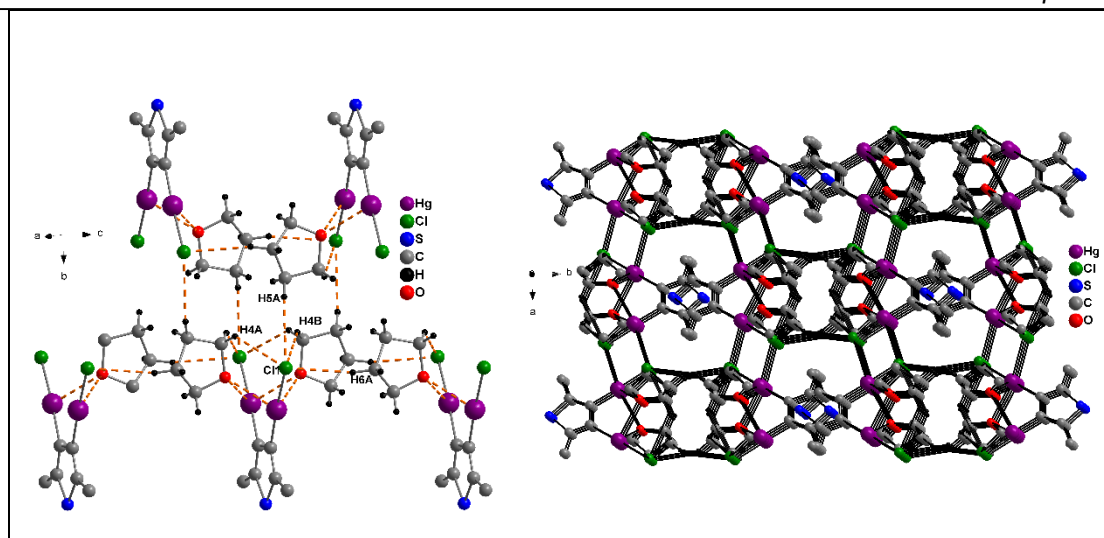


**Figure 2.10:** Portion of chain like structure of compound **2**(left) and its 3D polymeric network *via* C-H...Cl interactions.

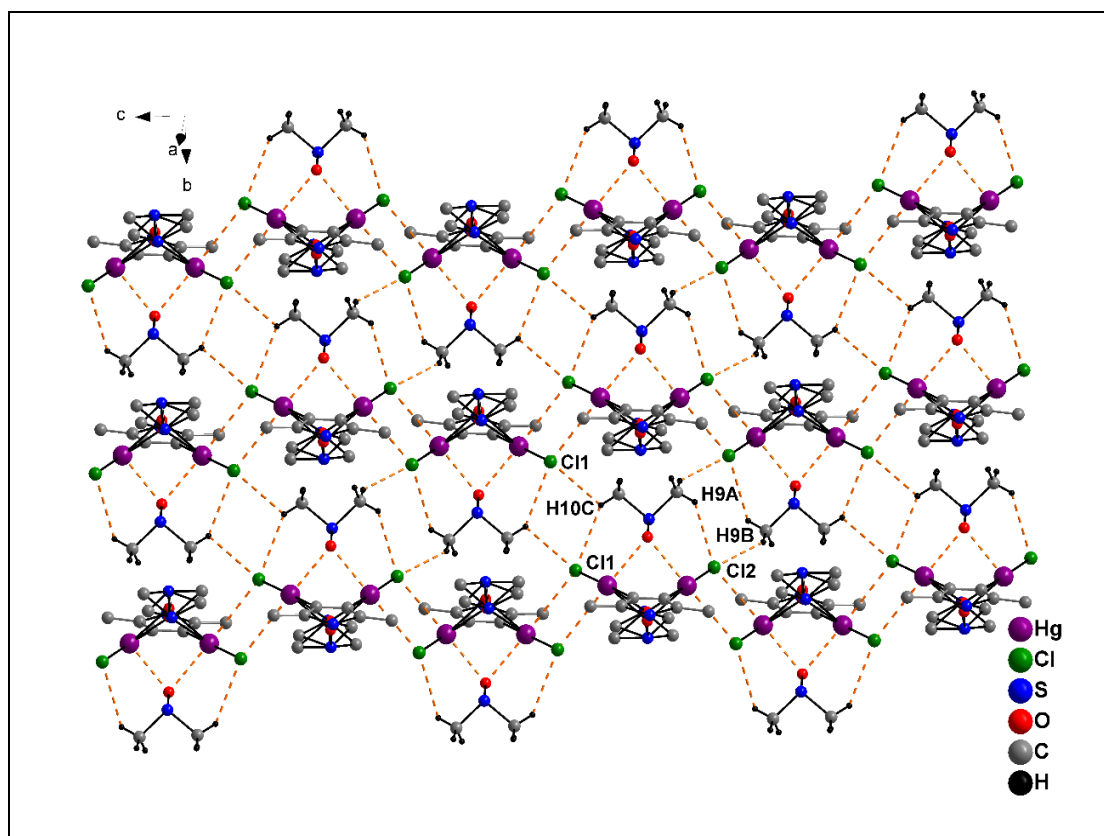


**Figure 2.11:** View of sheet like network in compound **3**.

The molecular structure of compound **4** is shown in figure 2.12. The molecular structure of compound **4** reveals the presence of two chloride anions bridged by three molecules of compound **1**. Chloride anion Cl15 has two short Hg...Cl (Hg1-Cl15 2.882(3) Å & Hg2-

Cl5 2.956(3) Å) contacts and two relatively long Hg-Cl contacts (Hg3-Cl5 3.229(3) Å & Hg4-Cl5 3.339(3) Å). The short contact of Hg1...Cl5 relates to the significant deviation from linearity of C2-Hg1-Cl5 (163.6°(3)) and a long Hg1-Cl1 distance of 2.334(3) Å. Similarly the Hg2...Cl5 contact of 2.956(3) Å relates to deviation from linearity of C3-Hg2-Cl2 (166.1(3)°) and a relatively shorter Hg2-Cl2 distance of 2.327(3) Å. The chloride anion Cl6 is also bridged by four mercury atoms from two molecules of compound **1**, the Hg...Cl (Hg3-Cl6 3.145(3) Å & Hg4-Cl6 2.932(11) Å) distances are nearly equal. The Hg-C and Hg-Cl distances vary from 2.033 Å to 2.071

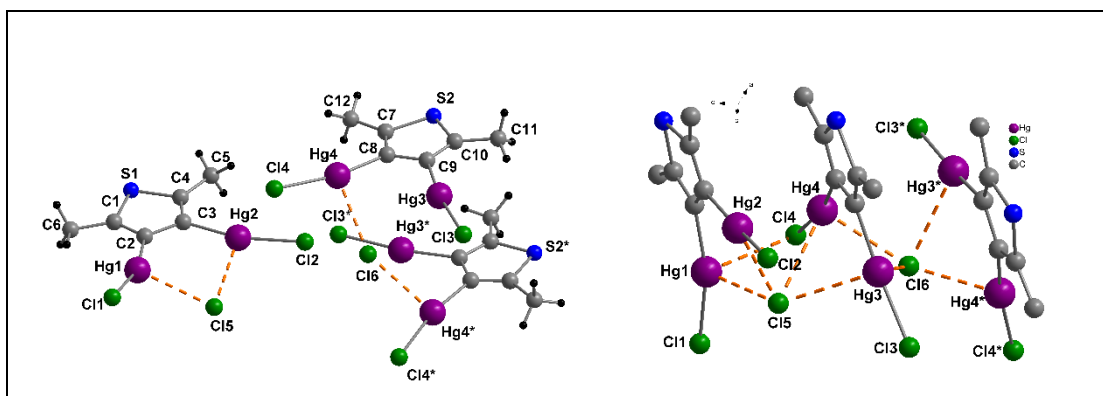


**Figure 2.12:** Molecular structure of compound **4** (left) and its ball and stick model showing 3:2 complex with four Hg...Cl contacts (right, all hydrogen atoms are omitted for clarity). Selected bond lengths (Å) and bond angles (°): Hg1-C2 2.071(10), Hg2-C3 2.066(9), Hg1-Cl1 2.334(3), Hg2-Cl2 2.327(3), Hg4-C9 2.033(10), Hg3-C8 2.055(9), Hg3-C13 2.331(3), Hg4-Cl6 2.932(1), Hg4-Cl4 2.339(3), C2-Hg1-Cl1 163.6(3), C3-Hg2-Cl2 166.1(3), C9-Hg4-Cl4 169.0(3), C8-Hg3-Cl3 171.1(3), Hg1-Cl5-Hg2 81.88(7), Hg4\*-Cl6-Hg4 149.3(1).

Å and 2.327 Å to 2.339 Å respectively and is in the range as those reported in the literature.<sup>20-21,23,45,46</sup> A striking difference between the Wuest's 1,2-phenylenedimercury dichloride and Jäkle's 1,2-bis(chloromercury)ferrocene and our

3,4-bis(chloromercurio)2,5-dimethylthiophene system is that in the former the complexation was formed in 2:1 ratio, whereas in our system it is 3:2 ratio.

Examination of the packing diagram of compound **4** reveals the presence of several C-H $\cdots$ Cl interactions between [Et<sub>4</sub>N]<sup>+</sup> counterion H atoms and the chlorine atoms. These weak interactions lead to the formation of a *zigzag* network as shown in figure 2.13.

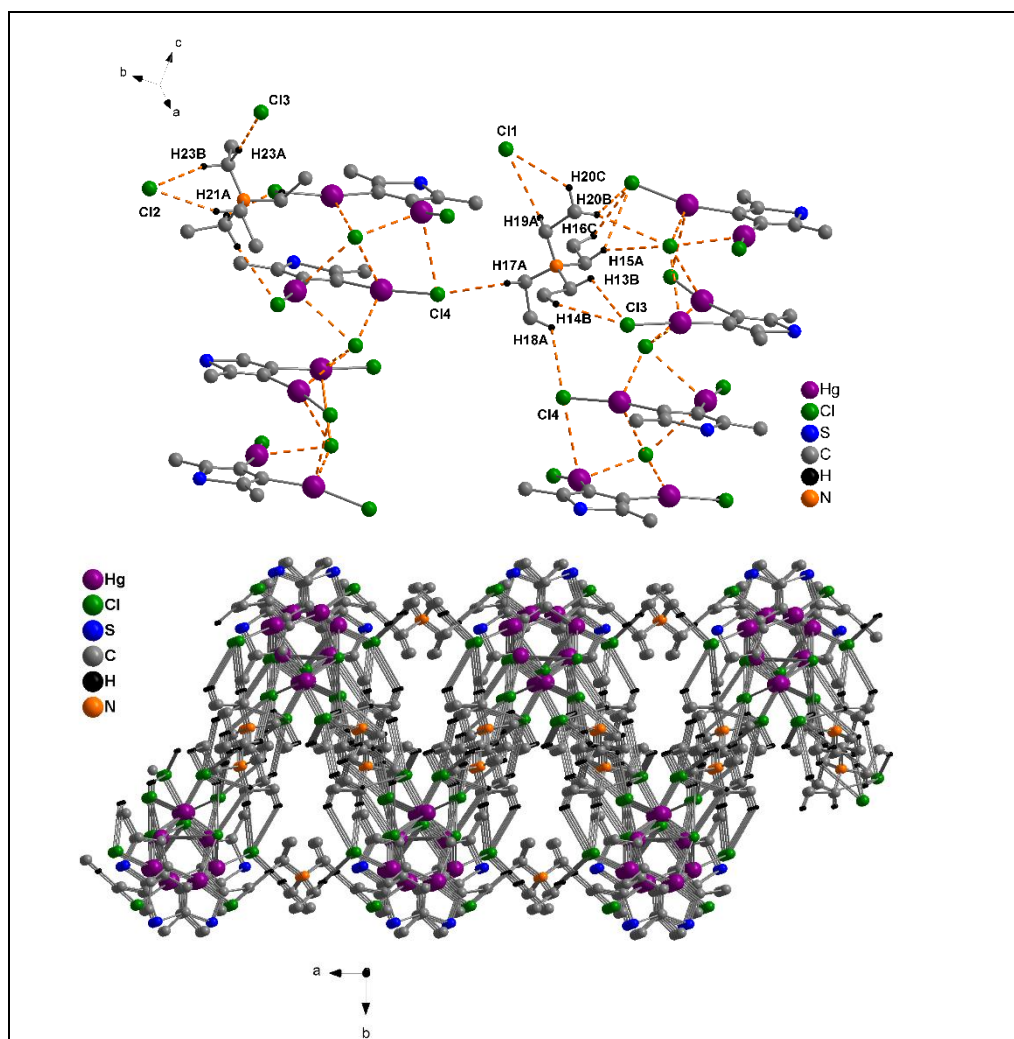


**Figure 2.13:** View of extended structure in compound **4** via Hg $\cdots$ Cl & C-H $\cdots$ Cl interactions (top) and its 3D-polymeric network (bottom).

**Table 2.1:** Crystal data and structure refinement parameters for compound **1** and **2**.

	Compound <b>1</b>	Compound <b>2</b>
Empirical formula	C <sub>6</sub> H <sub>6</sub> Cl <sub>2</sub> Hg <sub>2</sub> S	C <sub>14</sub> H <sub>22</sub> Cl <sub>2</sub> Hg <sub>2</sub> O <sub>2</sub> S

MW	582.25	726.45
T,K	296.15	296.15
Wavelength, Å	0.71073	0.71073
Crystal system	monoclinic	monoclinic
Space group	P2 <sub>1</sub> /c	C2/c
a, Å	7.9428(4)	15.6583(10)
b, Å	17.0079(9)	15.2459(10)
c, Å	7.8225(4)	8.6890(6)
$\alpha$ , deg	90	90
$\beta$ , deg	110.911(3)	115.848(5)
$\gamma$ , deg	90	90
V, Å <sup>3</sup>	987.14(9)	1866.8(2)
Z	4	4
$\rho$ calc, gcm <sup>-3</sup>	3.918	2.585
$\mu$ (Mo K $\alpha$ ), mm <sup>-1</sup>	31.753	16.827
F(000)	1008	1328
$\theta$ range, deg	4.79-55.076	3.936-61.272
limiting indices	$-10 \leq h \leq 9$	$-22 \leq h \leq 22$
	$-22 \leq k \leq 22$	$-21 \leq k \leq 20$
	$-10 \leq l \leq 10$	$-12 \leq l \leq 12$
no. of reflns collected	8315	20347
no. of indepe reflns	2256[Rint=0.0622]	2887[Rint=0.0802]
absorption correction	SADABS-2008/1 (Bruker,2008)	SADABS-2014/5 (Bruker,2014/5)
refinement method	Full matrix least square on F <sup>2</sup>	Full matrix least square on F <sup>2</sup>
No. of datas/restraints/params	2256/0/102	2887/0/98
Goodness-of-fit on F <sup>2</sup>	1.070	1.061
final R indices [ $I \geq 2\sigma(I)$ ]	R <sub>1</sub> =0.0721	R <sub>1</sub> =0.0406
	wR <sub>2</sub> =0.2089	wR <sub>2</sub> =0.1063
R indices (all data)	R <sub>1</sub> =0.0839	R <sub>1</sub> =0.0456
	wR <sub>2</sub> =0.2255	wR <sub>2</sub> =0.1097
peakmax/holemin (e Å <sup>-3</sup> )	5.18/-6.53	5.07/-4.27

**Table 2.2:** Crystal data and structure refinement parameters for compound **3** and **4**.

	Compound <b>3</b>	Compound <b>4</b>
Empirical formula	C <sub>10</sub> H <sub>18</sub> Cl <sub>2</sub> Hg <sub>2</sub> O <sub>2</sub> S <sub>3</sub>	C <sub>51</sub> H <sub>84</sub> Cl <sub>11</sub> Hg <sub>8</sub> N <sub>3</sub> OS <sub>4</sub>
MW	738.50	2878.12
T,K	296.15	296.15
Wavelength, Å	0.71073	0.71073
Crystal system	Triclinic	monoclinic
Space group	P-1	P2/n
a, Å	8.1789(3)	14.5886(9)
b, Å	8.6550(3)	20.4083(13)
c, Å	14.4520(5)	14.9353(10)
$\alpha$ , deg	89.512(2)	90
$\beta$ , deg	85.505(2)	118.440(4)

$\gamma$ , deg	68.884(2)	90
$V, \text{\AA}^3$	951.19(6)	3910.0
$Z$	2	2
$\rho$ calc, gcm <sup>-3</sup>	2.578	2.445
$\mu(\text{Mo K}\alpha)$ , mm <sup>-1</sup>	16.725	16.159
$F(000)$	672	2620.0
$\theta$ range, deg	5.365-61.066	1.996-50.744
limiting indices	$-11 \leq h \leq 11$	$-17 \leq h \leq 17$
	$-12 \leq k \leq 12$	$-24 \leq k \leq 24$
	$-20 \leq l \leq 19$	$-17 \leq l \leq 17$
no. of reflns collected	16904	43061
no. of indepe reflns	5786[Rint=0.0549]	7147[Rint=0.1306]
absorption correction	SADABS-2008/1 (Bruker,2008)	SADABS-2014/5 (Bruker,2014/5)
refinement method	Full matrix least square on $F^2$	Full matrix least square on $F^2$
No. of datas/restraints/params	5786/82/218	7147/0/353
Goodness-of-fit on $F^2$	1.023	1.034
final R indices [ $I \geq 2\sigma(I)$ ]	$R_1=0.0367$	$R_1=0.0413$
	$wR_2=0.0733$	$wR_2=0.0938$
R indices (all data)	$R_1=0.0633$	$R_1=0.0723$
	$wR_2=0.0817$	$wR_2=0.1173$
peakmax/holemin (e $\text{\AA}^{-3}$ )	1.53/-1.39	1.54/-1.41

## 2.3 Conclusions

In summary, we have developed a new method for the synthesis of a bidentate Lewis acid 3,4-bis(chloromercurio)2,5-dimethylthiophene (**1**) by direct mercuration of 2,5-dimethylthiophene using  $\text{Hg}(\text{OAc})_2$  followed by treatment with  $\text{LiCl}$ . Compound **1** readily interacts with neutral nucleophiles such as THF and DMSO to form compounds **2** & **3** in 1:2 ratio and with anionic nucleophile ( $\text{Cl}^-$ ) to yield a unique compound **4** in 3:2 ratio. Compounds **1-4** have been found to form supramolecular assemblies in the solid state. Especially, compounds **1-3** form  $\text{Hg}_2\text{Cl}_2$  bridges along with  $\text{C-H}\cdots\text{Cl}$  interactions. Compound **4** forms *zigzag* 3D network with the assistance of  $\text{C-H}\cdots\text{Cl}$  weak interactions. The potential application of compound **1** as a precursor for making other bidentate Lewis acids through transmetalation, will be discussed in the following chapters.



---

## 2.4 Experimental section

### 2.4.1 General information

All reagents and starting materials were purchased from Sigma-Aldrich, Alfa Aesar and Spectrochem chemical companies and used as received unless otherwise noted. THF and toluene were distilled from Na/benzophenone prior to use. Dichloromethane, N,N-dimethylformamide and dimethylsulfoxide were distilled from CaH<sub>2</sub>. All 400 MHz <sup>1</sup>H, and 100 MHz <sup>13</sup>C spectra were recorded on a Bruker ARX 400 spectrometer operating at 400 MHz. All <sup>1</sup>H and <sup>13</sup>C NMR spectra were referenced internally to solvent signals. ESI mass spectra were recorded using a Bruker microTOF-QII mass spectrometer. Single-crystal X-ray diffraction data were collected on a Bruker APEX-II diffractometer equipped with an Oxford Instruments low-temperature attachment. The data were collected using Mo-K $\alpha$  radiation (0.71073 Å). Crystallographic data for **1-4** and details of X-ray diffraction experiments and crystal structure refinements are given in Table **2.1** and **2.2**. SADABS absorption corrections were applied in both cases. The structures were solved and refined with SHELX suite of programs or Olex. All non-hydrogen atoms were refined with anisotropic displacement coefficients. The H atoms were placed at calculated positions and were refined as riding atoms. Thermogravimetric analyses (TGA) were recorded on a PerkinElmer Pyris 6 TGA model in a nitrogen atmosphere at a heating rate of 20 °C min<sup>-1</sup>. (Caution: Organomercurials are highly toxic, hence appropriate handling should be followed for their generation and disposal).

### 2.4.2 Synthetic procedures and spectral characterisations

#### 2.4.2.1 Synthesis of 3,4-bis(chloromercurio)2,5-dimethylthiophene (1)

In a 250 mL round bottomed flask 2,5-dimethylthiophene (0.985 g, 8.77 mmol) was taken in 10 mL of dichloromethane. Mercuric acetate (5.59 g, 17.54 mmol) in methanol solution was added dropwise to the reaction mixture and stirred at room temperature for 4h to give white suspension. LiCl (1.487 g, 35.08 mmol) in methanol solution was added dropwise to the reaction mixture and stirred at room temperature for 12h. The white precipitate was filtered and washed several times with dichloromethane to give 3,4-bis(chloromercurio)2,5-dimethylthiophene. Yield: 2.50 g (48%).  $^1\text{H}$  NMR (400 MHz, DMSO-*d*6)  $\delta$  = 2.41 (s, 6H).  $^{13}\text{C}$  NMR (101 MHz, DMSO-*d*6)  $\delta$  = 17.71, 138.46, 150.87. HR-MS (ESI): calculated for  $\text{C}_6\text{H}_6\text{Cl}_2\text{Hg}_2\text{S}$  ( $[\text{M}]^+$ ): 583.8971, observed: 583.8930. IR (KBr):  $\nu(\text{cm}^{-1})$  = 2908(m), 1434(s), 1142(m), 813(m), 698(m).

#### 2.4.2.2 Synthesis of compound 2

A THF (10 mL) solution containing 0.200 g of compound **1** was placed in a vial and allowed to stand at room temperature over a period of 7 days. Yield: 0.228 g (91%).  $^1\text{H}$  NMR (400 MHz, DMSO-*d*6)  $\delta$  1.76 (t,  $J$ =8.0, 8H), 2.41(s, 6H), 3.60 (t,  $J$ =7.2, 8H).  $^{13}\text{C}$  NMR (101 MHz, DMSO-*d*6)  $\delta$  17.70, 25.14, 67.03, 138.49, 150.88. Anal.Calcd for  $\text{C}_{14}\text{H}_{22}\text{Cl}_2\text{Hg}_2\text{O}_2\text{S}$ : C, 23.15; H, 3.05; S, 4.41. Found: C, 23.038; H, 3.047; S, 5.161. IR(KBr):  $\nu(\text{cm}^{-1})$  = 2909(m), 1716(s), 1437(s), 1376(m), 1139(s), 814(m), 695(m).

#### 2.4.2.3 Synthesis of compound 3

A DMSO (10 mL) solution containing 0.200 g of compound **1** was placed in a vial and allowed to stand at room temperature over a period of 3 weeks, from which single crystals of DMSO complex **3** isolated. Yield: 0.213 g (94%).  $^1\text{H}$  NMR (400 MHz, DMSO-*d*6)  $\delta$  2.42 (s, 6H), 2.54 (s, 7H).  $^{13}\text{C}$  NMR (101 MHz, DMSO-*d*6)  $\delta$  17.56, 40.43, 138.43, 150.74. Anal. Calcd for  $\text{C}_8\text{H}_{12}\text{Cl}_2\text{Hg}_2\text{O}_2\text{S}_3$ : C, 16.26; H, 2.46; S, 13.02. Found: C, 17.227; H, 2.471; S, 13.483. IR (KBr):  $\nu(\text{cm}^{-1})$  = 2905(m), 1433(m), 1401(m), 1309(s), 1138(m), 1012(s), 954(m), 813(m), 708(m).

#### 2.4.2.4 Synthesis of compound 4

To a suspension of compound **1** (0.100 g) in dichloromethane was added Et<sub>4</sub>NCl (0.014 g) in chloroform. Compound **1** is insoluble in dichloromethane, but forms a homogeneous solution after the addition of Et<sub>4</sub>NCl. Slow evaporation of the mixture gives the colourless crystal of the 3:2 complex **4**. Yield: 0.098 g (57%). <sup>1</sup>H NMR (400 MHz, DMSO-*d*<sub>6</sub>) δ 1.16 (t, *J*=7.2, 24H), 2.41 (s, 18H), 3.21(q, *J*=7.3, 16H). <sup>13</sup>C NMR (101 MHz, DMSO-*d*<sub>6</sub>) δ 7.07, 17.78, 51.37, 138.20, 151.61. Anal.Calcd for C<sub>34</sub>H<sub>58</sub>Cl<sub>8</sub>Hg<sub>6</sub>N<sub>2</sub>S<sub>3</sub>: C, 19.65; H, 2.81; N, 1.35; S, 4.63. Found: C, 19.373; H, 2.708; N, 1.483; S, 5.160. IR(KBr): ν(cm<sup>-1</sup>) = 2980(s), 2945(m), 2908(m), 1456(s), 1392(m), 1182(s), 1004(s), 787(s), 759(m).

#### 2.5 References

1. Lee, H.; Diaz, M.; Hawthorne, M. F.; *Tetrahedron Lett.* **1999**, 40, 7651-7655.
2. Oh, T.; Lopez, P.; Reilly, M. *Eur. J. Org. Chem.* **2000**, 2901-2903.
3. Hawthorne, M. F.; Zheng, Z. *Acc. Chem. Res.* **1997**, 30, 267-276.
4. Wuest, J. D. *Acc. Chem. Res.* **1999**, 32, 81-89.
5. Tsunoda, M.; Gabbaï, F. P. *J. Am. Chem. Soc.* **2000**, 122, 8335-8336.
6. Tschinkl, M.; Schier, A.; Riede, J.; Gabbaï, F. P. *Inorg. Chem.* **1997**, 36, 5706-5711.
7. Schmidtchen, F. P.; Berger, M. *Chem. Rev.* **1997**, 97, 1609-1646.
8. Beer, P. D.; Smith, D. K. *Progress in Inorganic Chemistry*; Karlin, K. D.; Wiley: New York, **1997**; Vol. 46, pp 1-96.
9. Badr, I. H. A.; Johnson, R. D.; Diaz, M.; *Anal. Chem.* **2000**, 72, 4249-4254.
10. Badr, I. H. A.; Diaz, M.; Hawthorne, M. F.; Bachas, L. G. *Anal. Chem.* **1999**, 71, 1371-1377.

- 
11. Tschinkl, M.; Schier, A.; Riede, J.; Gabbaï, F. P. *Angew. Chem. Int.Ed.* **1999**, *38*, 3547-3549.
  12. Rot, N.; de Kanter, F. J. J.; Bickelhaupt, F.; Smeets, W. J. J.; Spek, A. L., *J. Organomet. Chem.* **2000**, *593–594*, 369–379.
  13. Beauchamp, A.L.; Olivier, M.J.; Wuest, J.D.; Zacharie, B. *Organometallics* **1987**, *6*, 153-156.
  14. Wuest, J. D.; Zacharie, B. *J. Am. Chem. Soc.* **1987**, *109*, 4714-4715.
  15. Beauchamp, A. L.; Olivier, M. J.; Wuest, J. D.; Zacharie, B. *J. Am. Chem. Soc.* **1986**, *108*, 73-77.
  16. Wuest, J. D.; Zacharie, B. *Organometallics* **1985**, *4*, 410-411.
  17. Tschinkl, M.; Schier, A.; Riede, J.; Gabbaï, F. P. *Organometallics* **1999**, *18*, 1747-1753.
  18. Tschinkl, M.; Bachman, R. E.; Gabbaï, F. P. *Organometallics* **2000**, *19*, 2633-2636.
  19. Beckwith, J. D.; Tschinkl, M.; Picot, A.; Tsunoda, M.; Bachman, R.; Gabbaï, F. P. *Organometallics* **2001**, *20*, 3169-3174.
  20. Tschinkl, M.; Gabbaï, F. P. *J. Chem. Crystallogr.* **2003**, *33*, 595-598.
  21. Gardinier, J.R.; Gabbaï, F. P. *J. Chem. Soc., Dalton Trans.* **2000**, 2861–2865.
  22. Schimdbaur, H.; Oller, H-J.; Wilkinson, D. L.; Huber, B.; Muller, G. *Chem.Ber.* **1989**, *122*, 31-36.
  23. Venkatasubbaiah, K., Bats, J.W.; Rheingold, A.L.; Jäkle, F. *Organometallics* **2005**, *24*, 6043-6050.
  24. Zheng, Z.; Yang, X.; Knobler, C. B.; Hawthorne, M. F. *J. Am. Chem. Soc.* **1993**, *115*, 5320-5321.
-

- 
25. Yang, X.; Knobler, C. B.; Zheng, Z.; Hawthorne, M. F. *J. Am. Chem. Soc.* **1994**, *116*, 7142-7159.
26. Zheng, Z.; Knobler, C. B.; Hawthorne, M. F. *J. Am. Chem. Soc.* **1995**, *117*, 5105-5113.
27. Hawthorne, M. F.; Zheng, Z. *Acc. Chem. Res.* **1997**, *30*, 267-276.
28. Lee, H.; Knobler, C. B.; Hawthorne, M. F. *J. Am. Chem. Soc.* **2001**, *123*, 8543-8549.
29. Bayer, M. J.; Jalissatgi, S. S.; Smart, B.; Herzog, A.; Knobler, C.B.; Hawthorne, M. F. *Angew. Chem. Int. Ed.* **2004**, *43*, 1854 –1857.
30. Tikhonova, I. A.; Dolgushin, F. M.; Tugashov, K. I.; Petrovskii, P.V.; Furin, G. G.; Shur, V. B. *J. Organomet. Chem.* **2002**, *654*, 123-131.
31. Chistyakov, A. L.; Stankevich, I.V.; Gambaryan, N. P.; Struchkov, Yu. T.; Yanovsky, A.I.; Tikhonova, I. A.; Shur, V.B. *J. Organomet. Chem.* **1997**, 413-424.
32. Shur, V. B.; Tikhonova, I. A. *Russ. Chem. Bull.* **2003**, *52*, 2539-2554.
33. Shur, V. B.; Tikhonova, I. A.; Dolgushin, F. M.; Yanovsky, A. I.; Struchkov, Y. T.; Volkonsky, A. Y.; Solodova, E. V.; Panov, S. Y.; Petrovskii, P. V.; Volpin, M. E. *J. Organomet. Chem.* **1993**, *443*, C19-C21.
34. Patel, U.; Singh, H. B.; Wolmerhauser, G. *Angew. Chem. Int. Ed.* **2005**, *44*, 1715 – 1717.
35. Yakovenko, A. A.; Gallegos, J. H.; Antipin, M. Y.; Masunov, A.; Timofeeva, T. V. *Cryst. Growth Des.* **2011**, *11*, 3964–3978.
36. Thilagar, P.; Swamy P, C. A. *Chem. Eur. J.* **2015**, *21*, 8874 – 8882.
37. Tschinkl, M.; Schier, A.; Riede, J.; Gabbaï, F. P. *Organometallics* **1999**, *18*, 2040-2042.
38. Taylor, T.J.; Burrell, C.N.; Gabbaï, F. P. *Organometallics* **2007**, *26*, 5252-5263.
-

- 
39. Korpar-Colig, B.; Popovic, Z.; Bruvo, M.; Vickovic, I. *Inorg. Chim. Acta* **1988**, *150*, 113-118.
40. Viets, D.; Lork, E.; Watson, P. G.; Mews, R. *Angew. Chem. Int. Ed. Engl.* **1997**, *36*, 623-624.
41. Schulz, F.; Pantenburg, I.; Naumann, D. Z. *Anorg. Allg. Chem.* **2003**, *629*, 2312-2316.
42. Powell, H. B.; Maung, M. T.; Lagowski, J. J. *J. Chem. Soc.* **1963**, 2484-2487.
43. Nyburg, S. C.; Faerman, C. H. *Acta Crystallogr., Sect. B*, **1985**, *41*, 274-279.
44. Canty, A. J.; Deacon, G. B. *Inorg. Chim. Acta*, **1980**, *45*, L225-L227.
45. Sathesh, V.; Chinta, R. V. G. N.; Mamidala, R.; Mukundam, V.; Dhanunjayarao, K.; Venkatasubbaiah, K. *J. Organomet. Chem.* **2017**, *853*, 74-80.
46. Rupf, S. M.; Schröder, G.; Sievers, R.; Malischewski, M. *Chem. Eur. J.* **2021**, *27*, 5125-5129.

## **CHAPTER 3**

### **Synthesis and characterisation of distannadithiophenes analogues of 9,10-distannanthracene and their application towards hydroboration of carbonyl compounds**

<b>3.1 Introduction</b>	85
<b>3.2 Results and discussion</b>	86
<b>3.2.1 Synthesis and characterisation</b>	86
<b>3.2.2 Single crystal analysis</b>	88
<b>3.2.3 Hydroboration of carbonyl compounds</b>	92
<b>3.3 Conclusions</b>	98
<b>3.4 Experimental section</b>	99
<b>3.4.1 General information</b>	99
<b>3.4.2 Synthetic procedures and spectral characterisations</b>	99
<b>3.5 References</b>	107





---

### 3.1 Introduction

Main-group organometallic compounds have received considerable attention owing to their structural diversity and potential applications in a wide-range of areas. In recent years the main-group elements based compounds gained momentum in catalysis as replacement for transition metal based catalysts. Among the different main-group elements studied, organotin compounds are employed as catalysts for the synthesis of a wide variety of organic compounds such as polyester, lactones, fatty acid alkyl ester and so on.<sup>1-10</sup> Apart from that organotin compounds with more than one Lewis acidic centre *i.e.* bi- and multidentate Lewis acids have seen growing interest owing to their role in anion recognition,<sup>11</sup> interesting optical properties<sup>12</sup> and unusual structural motifs<sup>13-16</sup>.

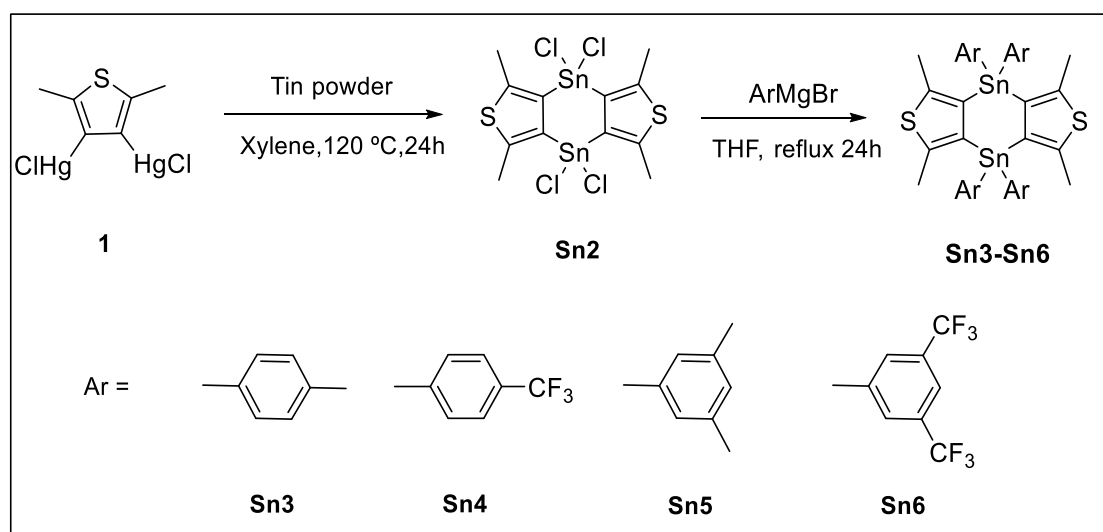
Boronate esters acts as important intermediates for the synthesis of various alcohols, which can be prepared by the hydroboration of carbonyl compounds. Over the past several decades notable progress have been made for the design and synthesis of various catalysts that includes main group metal complexes, transition metal complexes, f-block complexes, alkali and alkaline earth metal complexes<sup>17-30</sup> for hydroboration of carbonyl compounds. Base catalysed<sup>31-33</sup> and catalysis free<sup>34</sup> hydroboration of carbonyl compounds were also investigated. Among the different main-group elements, tin based compounds also studied for this important reaction. For example, Jones and coworkers<sup>35</sup> have reported low coordinate Sn(II) complexes for the hydroboration of carbonyl compounds. Recently, use of N-heterocyclic stannylene as a catalyst for the hydroboration of carbonyl compounds was reported.<sup>36</sup> However, to the best of our knowledge organotin(IV) compounds have not been studied for hydroboration of carbonyl compounds owing to the low reactivity. This chapter describes the synthesis

of distannadithiophenes analogues of 9,10-distannaanthracene and their catalytic activity towards hydroboration of carbonyl compounds.

### 3.2 Results and discussion

#### 3.2.1 Synthesis and characterisation

3,4-Bis(chloromercurio)2,5-dimethylthiophene (compound **1**) was prepared in good yield according to the procedure discussed in chapter 2. Compound **Sn2** was synthesized by a transmetallation reaction between 3,4-bis(chloromercurio)2,5-dimethylthiophene and tin powder in dry xylene. Compound **Sn2** was characterized using  $^1\text{H}$  NMR,  $^{13}\text{C}$  NMR and  $^{119}\text{Sn}$  NMR. The reaction of compound **Sn2** with  $\text{ArMgBr}$  produced the desired compounds **Sn3-Sn6** (Scheme 3.1). All the complexes are stable in air at ambient temperature and were purified through silica gel column chromatography. Compounds **Sn3-Sn6** were characterized using multinuclear NMR ( $^1\text{H}$ ,  $^{13}\text{C}$ ,  $^{19}\text{F}$ ,  $^{119}\text{Sn}$ ) and HRMS analysis. For an illustration the  $^1\text{H}$  NMR spectrum of compound **Sn3** is shown in figure 3.1, which showed two singlets at 2.40 and 2.37 ppm corresponds to the methyl attached to the thiophene ring and the aromatic ring (Ar).  $^{119}\text{Sn}$  NMR spectra of compounds **Sn3-Sn6** showed a signal ranging from -150.0 to -161.8



**Scheme 3.1:** Synthesis of compounds **Sn3-Sn6**.

ppm, which are comparable to the values observed for distannaanthracenes. A representative  $^{119}\text{Sn}$  NMR spectrum of the compound **Sn3** is shown in figure 3.2.

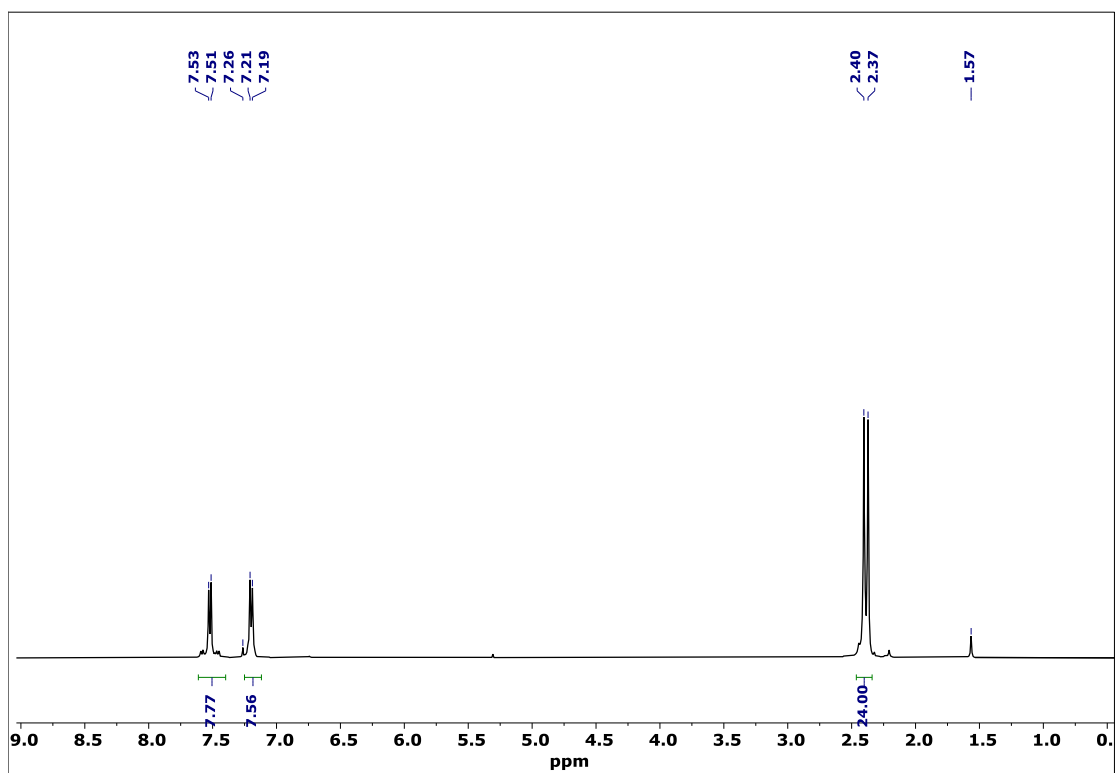


**Figure 3.1:**  $^1\text{H}$  NMR spectrum of **Sn3** in  $\text{CDCl}_3$ .

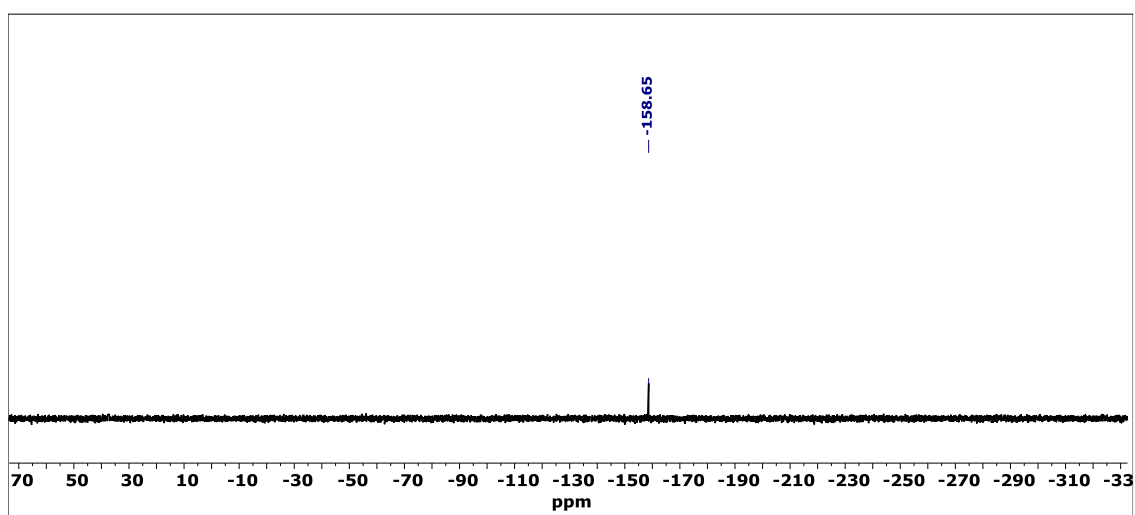


**Figure 3.2:**  $^{119}\text{Sn}$  NMR spectrum of **Sn3** in  $\text{CDCl}_3$ .

### 3.2.2 Single crystal analysis

X-ray quality single crystals of **Sn3**, **Sn4** and **Sn6** were obtained from slow evaporation of a mixture of dichloromethane and ethanol solution and studied using single crystal X-ray diffraction analysis. **Sn3** was crystallized in triclinic space group of *P*-1 while **Sn4** and **Sn6** were crystallized in monoclinic space group of *C*12/m1 and *P*2<sub>1</sub>/n respectively. In all these compounds tin centre adopts a distorted tetrahedral geometry. Molecular structure of **Sn3**, **Sn4** and **Sn6** are presented in figure (3.4-3.6). The Sn-C bond distance falls in the range of 2.127(2) Å to 2.154(2) Å, which are comparable with the values reported in the literature.<sup>14-20</sup> The molecular structure of these complexes shows the formation of a new six membered ring having two tin atoms fused by thiophene carbon atoms. The six membered C<sub>4</sub>Sn<sub>2</sub> ring is coplanar with respect to the thiophene rings. The distance between the two tin atoms in **Sn3**, **Sn4** and **Sn6** are 3.92(2) Å, 3.90(2) Å and 3.86(2) Å respectively. The dihedral angle between the phenyl rings (plane A and plane B) are 51.43 °, 44.77 ° and 38.42 ° in **Sn3**, **Sn4** and **Sn6** respectively (Table 3.1).

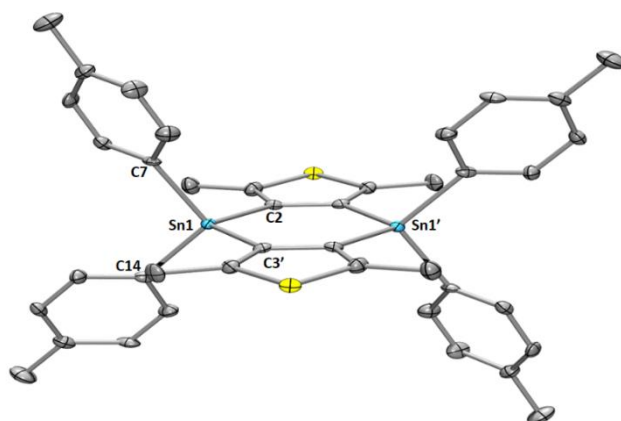


**Figure 3.3:** Molecular structure of **Sn3** (Selected bond distances (Å): C2-Sn1: 2.140(2), C7-Sn1: 2.144(2), C14-Sn1: 2.147(2), C3'-Sn1: 2.130(2). Bond angles (°): C7-Sn1-C2: 110.2(2), C14-Sn1-C7: 108.5(2), C14-Sn1-C3': 113.7(2), C2-Sn1-C3': 108.5(2)).

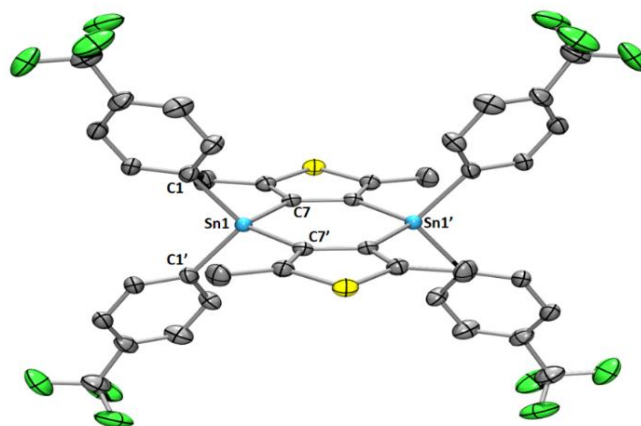


**Figure 3.4:** Molecular structure of **Sn4** (Selected bond distances (Å): C7-Sn1: 2.127(2), C1-Sn1: 2.154(2), C1'-Sn1: 2.154(2), C7'-Sn1: 2.127(2). Bond angles (°): C7-Sn1-C1: 111.4(2), C1-Sn1-C1': 109.6(2), C7-Sn1-C7': 109.5(2), C1-Sn1-C7': 111.4(2).

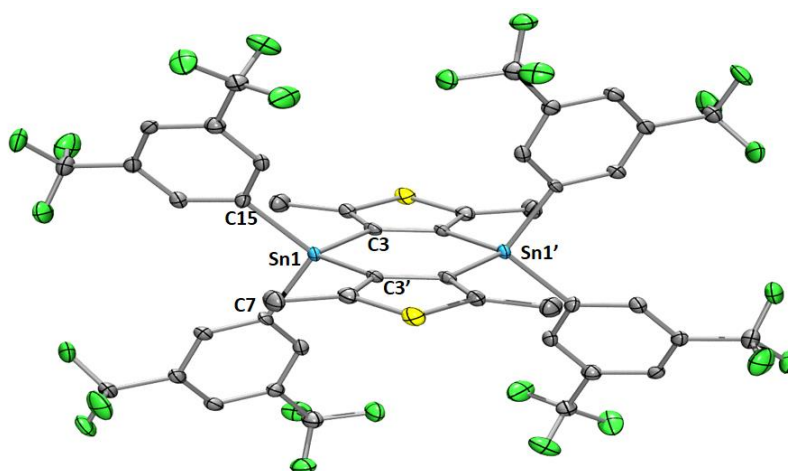
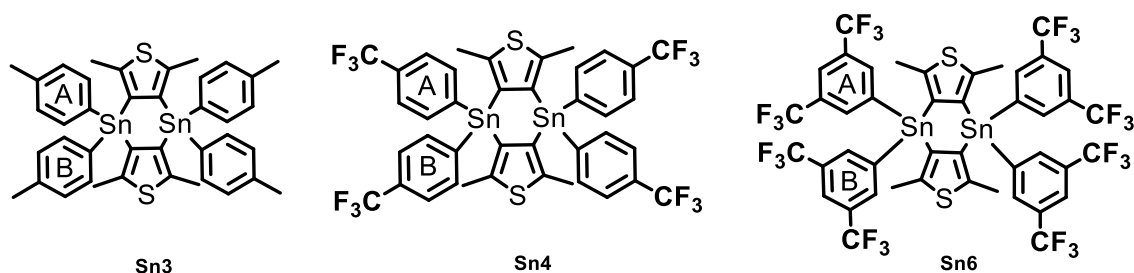


**Figure 3.5:** Molecular structure of **Sn6** (Selected bond distances (Å): C3-Sn1: 2.125(2), C15-Sn1: 2.152(2), C7-Sn1: 2.147(2), C2'-Sn1: 2.124(2). Bond angles (°): C15-Sn1-C3: 106.7(2), C15-Sn1-C7: 110.2(2), C7-Sn1-C2': 112.8(2), C3-Sn1-C2': 110.4 (2)).

**Table 3.1:** Comparison of distance between the two tin atoms (Å) and interplanar angles (°) for **Sn3**, **Sn4** and **Sn6**



Compound	Sn3	Sn4	Sn6
Distance between two tin atom (Å)	3.92(2)	3.90(2)	3.86(2)
Plane A // Plane B (°)	51.43	46.54	37.90
Plane A // C4Sn2 (°)	71.58	76.71	80.74
Plane A // C4Sn2 (°)	71.98	76.71	73.58
Thiophene// C4Sn2 (°)	3.5(2)	1.5(2)	3.7(2)

**Table 3.2:** Crystal data and structure refinement parameters for **Sn3**, **Sn4** & **Sn6**

	Sn3	Sn4	Sn6
Empirical formula	C <sub>40</sub> H <sub>40</sub> S <sub>2</sub> Sn <sub>2</sub>	C <sub>40</sub> H <sub>28</sub> F <sub>12</sub> S <sub>2</sub> Sn <sub>2</sub>	C <sub>88</sub> H <sub>48</sub> F <sub>48</sub> S <sub>4</sub> Sn <sub>4</sub>
MW	822.22	1038.12	2620.26
T, K	100.00(10)	100.0	100.00(11)
Wavelength, Å	1.54184	1.54178	1.54184
Crystal system	triclinic	monoclinic	monoclinic
Space group	<i>P</i> -1	<i>C</i> 1 2/m 1	<i>P</i> 2 <sub>1</sub> /n
a, Å	7.60310(10)	12.1586(3)	10.8980(3)
b, Å	11.5500(2)	25.6687(6)	7.8949(2)
c, Å	12.0225(2)	7.5308(2)	26.5995(10)
α, deg	116.449(2)	90	90

B,deg	105.5400(10)	98.8680(10)	95.889(3)
$\gamma$ ,deg	94.9950(10)	90	90
Volume, $\text{\AA}^3$	884.25(3)	2322.23(10)	2276.51(12)
Z	1	2	1
$\rho$ calc,gcm $^{-3}$	1.544	1.485	1.911
$\mu(\text{Mo K}\alpha)$ , mm $^{-1}$	12.526	10.053	10.812
F(000)	412.0	1016	1272.0
$\theta$ range, deg	4.3660 -75.0890	3.44 - 72.07	4.246 - 74.500
limiting indices	$-6 \leq h \leq 9$	$-14 \leq h \leq 14$	$-13 \leq h \leq 13$
	$-14 \leq k \leq 14$	$-31 \leq k \leq 31$	$-9 \leq k \leq 4$
	$-14 \leq l \leq 14$	$-9 \leq l \leq 9$	$-33 \leq l \leq 31$
no. of reflns collected	12759	25450	18040
no. of indepe reflns	3547 [ $R_{\text{int}} = 0.0736$ ]	2311 [ $R_{\text{int}} = 0.0682$ ]	4637 [ $R_{\text{int}} = 0.0703$ ]
refinement method	Full matrix least square on $F^2$	Full matrix least square on $F^2$	Full matrix least square on $F^2$
No. of datas/restraints/params	3547/0/203	2333/0/130	4637/0/327
Goodness-of-fit on $F^2$	1.057	1.094	1.091
final R indices [ $I \geq 2\sigma(I)$ ]	$R_1 = 0.0654$ ,	$R_1 = 0.0441$ ,	$R_1 = 0.0530$
	$wR_2 = 0.1818$	$wR_2 = 0.1308$	$wR_2 = 0.1477$
R indices (all data)	$R_1 = 0.0655$	$R_1 = 0.0444$	$R_1 = 0.0538$
	$wR_2 = 0.1821$	$wR_2 = 0.1311$	$wR_2 = 0.1485$
peakmax/holemin (e $\text{\AA}^{-3}$ )	5.81/-2.63	7.40/-1.257	3.22/-1.71

All three distannadithiophenes adopts a planar geometry (central six membered ring) unlike distannaanthracenes where both boat & planar confirmation were realised.

Examination of cell packing diagram of **Sn4** shows the presence of intermolecular C-H $\cdots$ F interaction with a distance of 2.55(2) Å between CF<sub>3</sub> group and H-atom of aryl group attached to the tin atom (Figure 3.6).

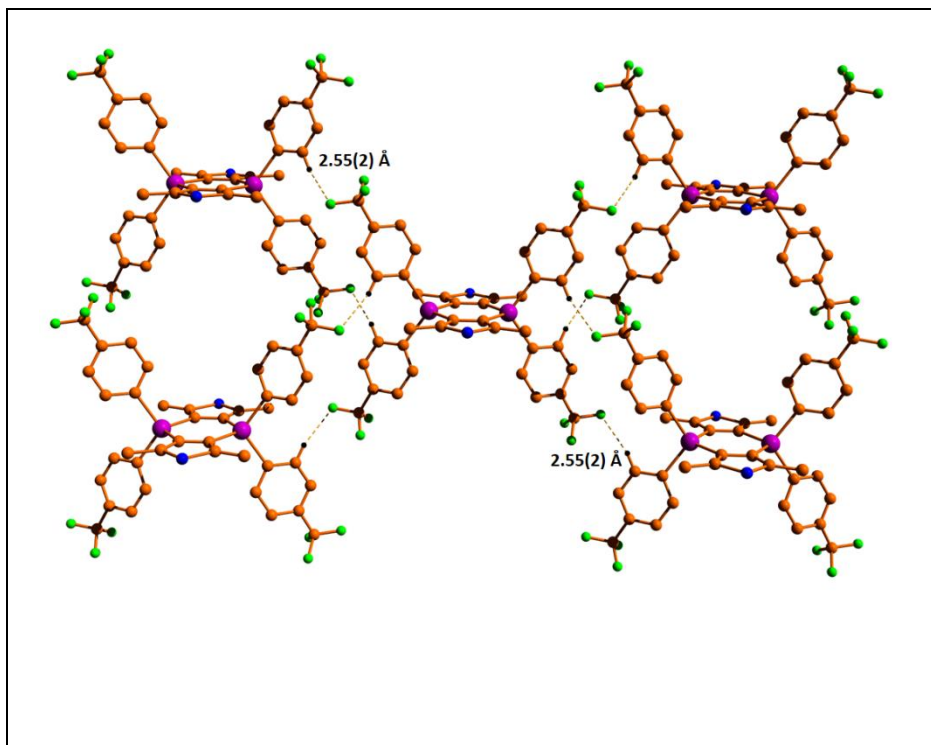


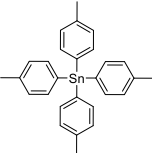
**Figure 3.6:** Packing diagram in **Sn4** (C-H $\cdots$ F distance 2.55(2) Å).

### 3.2.3 Hydroboration of carbonyl compounds

The potential application of the distannadithiophenes were studied for the hydroboration reaction. In the initial screening, 4-methoxybenzaldehyde, HBpin and **Sn3** (2.5 mol%) were taken. The hydroboration reaction was carried out smoothly at room temperature and completed in 24h by giving the desired product in an excellent yield (Table 3.3, entry 1). However compounds **Sn4**, **Sn5** and **Sn6** gave low yield and conversions under similar reaction conditions (Table 3.3, entries 2-4). This is probably due to the existence of high dihedral angle (51.43 °) and distance between the two tin atoms in the six membered ring (3.92 Å) of compound **Sn3**.



**Table 3.3:** Optimization reaction condition

Entry	Catalyst	Cat. Load. (mol%)	Solvent	Time	Conversion	Yield
1	Sn3	2.5	Toluene	24h	99	98
2	Sn4	2.5	Toluene	24h	81	75
3	Sn5	2.5	Toluene	24h	44	32
4	Sn6	2.5	Toluene	24h	60	56
5	Sn3	2.0	Toluene	24h	99	99
6	Sn3	1.5	Toluene	24h	95	90
7	Sn3	1.0	Toluene	24h	74	68
8	Sn3	2.0	Toluene	12h	99	99
9	Sn3	2.0	Toluene	6h	84	81
10	Sn3	2.0	Toluene	3h	58	57
11	Sn3	2.0	Toluene	1h	30	29
12	Sn3	2.0	THF	12h	89	85
13	Sn3	2.0	DCE	12h	38	35
14		4.0	Toluene	12h	60	58
15	Me <sub>2</sub> SnCl <sub>2</sub>	4.0	Toluene	12h	66	63

After screening the time and catalyst loading, the reaction conditions was optimized with catalyst loading of 2 mol% at room temperature for 12h (Table 3.3, entry 8). Additional reactions were carried out using 4mol% of Sn(Tol)<sub>4</sub> and commercially available Me<sub>2</sub>SnCl<sub>2</sub> as catalysts under the optimized conditions (Table 3.3, entries 14 & 15). In both cases, the yields observed were lower than the yields observed using compound **Sn3**, which suggest that there is a cooperative effect involved in case of compound **Sn3**.

To monitor the course of the reaction, we have performed kinetic study and analysed the conversion and product formation using <sup>1</sup>H NMR spectroscopy (Figure 3.7). The progress of the reaction and the decreasing concentration of 4-methoxybenzaldehyde is

presented in figure 3.7 (left). The cooperative nature of catalyst **Sn3** was evaluated for the hydroboration reaction. As shown in figure 3.7, the dimeric catalyst gave 80% conversion in 6h, where as the monomeric catalyst gave only 40% conversion at the same time and same catalyst loading.

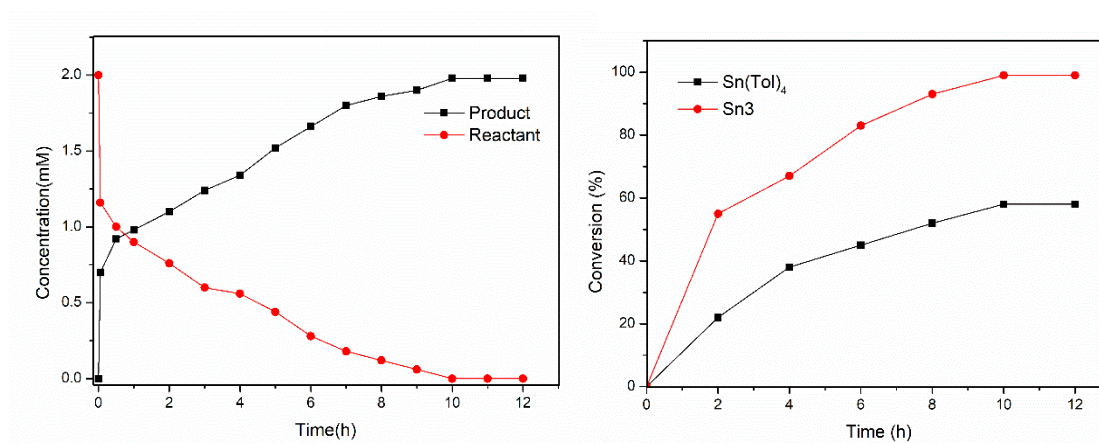


**Figure 3.7:** (Left) Reaction progress of 4-methoxybenzaldehyde monitored by  $^1\text{H}$  NMR spectroscopy. (Right) Comparison of conversion percentage with **Sn3** (2eq) and  $\text{Sn}(\text{Tol})_4$ (4eq).

With the optimized conditions in hand, we performed the hydroboration of a variety of aldehydes and ketones. Benzaldehyde, 2-methoxybenzaldehyde, 3-methoxybenzaldehyde and 4-methoxybenzaldehyde were reduced to their respective boronate esters in 12h at room temperature (Table 3.4, entries 1-4). The reduction of *o*-tolualdehyde, *m*-tolualdehyde and *p*-tolualdehyde to the corresponding boronate esters were proceeded smoothly (Table 3.4, entries 5-7). To our delight compound **Sn3** also showed impressive functional group tolerance. Substrates with electron withdrawing groups(- $\text{CF}_3$ , -Br, -F) were converted completely to the desired products (Table 3.4, entries 12-15). Heteroaromatic substrates such as 2-thiophenecarboxaldehyde, furfural and pyrrole-2-carboxaldehyde were smoothly reduced to their boronate esters (Table

**3.4**, entries **9-11**). Aliphatic aldehyde such as cyclohexane carboxaldehyde also converted to the corresponding boronate ester (Table **3.4**, entry **8**).

With this success, we further examined a variety of ketones under the optimized conditions. Acetophenone, 4-methylacetophenone, benzophenone and 4-methoxyacetophenone were converted easily to their esters (Table **3.5**, entries **1-4**). To our surprise, ketones with electron withdrawing substrates such as -F, -Cl, -Br and -I at the *ortho*, *meta*, *para* positions were reacted effectively to produce excellent yields of the desired product (Table **3.5**, entries **5-10**).

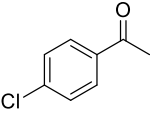
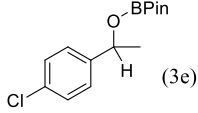
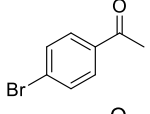
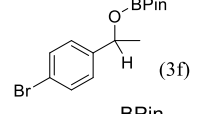
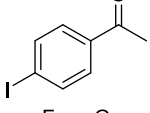
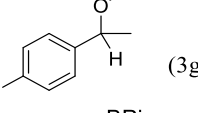
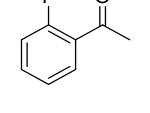
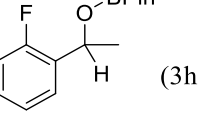
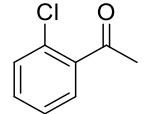
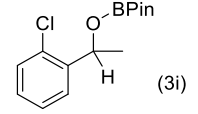
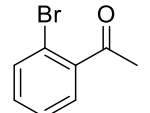
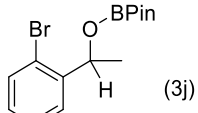
**Table 3.4:** Scope of hydroboration of aldehydes catalysed by **Sn3**

Sl. No.	Substrate	Catalyst (mol%)	Time(h)	Product	Yield (%)
1		2	12	(2a)	99
2		2	12	(2b)	99
3		2	12	(2c)	99
4		2	12	(2d)	99
5		2	12	(2e)	99
6		2	12	(2f)	99

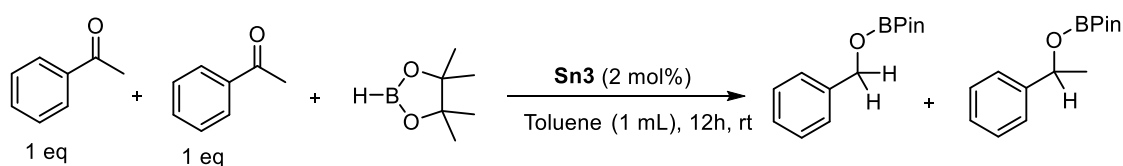
7		2	12		99
8		2	12		99
9		2	12		99
10		2	12		99
11		2	12		99
12		2	12		99
13		2	12		99
14		2	12		99
15		2	12		99

**Table 3.5:** Scope of hydroboration of ketones catalysed by **Sn3**.

Sl. No.	Substrate	Catalyst (mol%)	Time(h)	Product	Yield
1		2	12		99
2		2	12		99
3		2	12		99
4		2	12		99

5		2	12		99
6		2	12		99
7		2	12		99
8		2	12		99
9		2	12		99
10		2	12		99

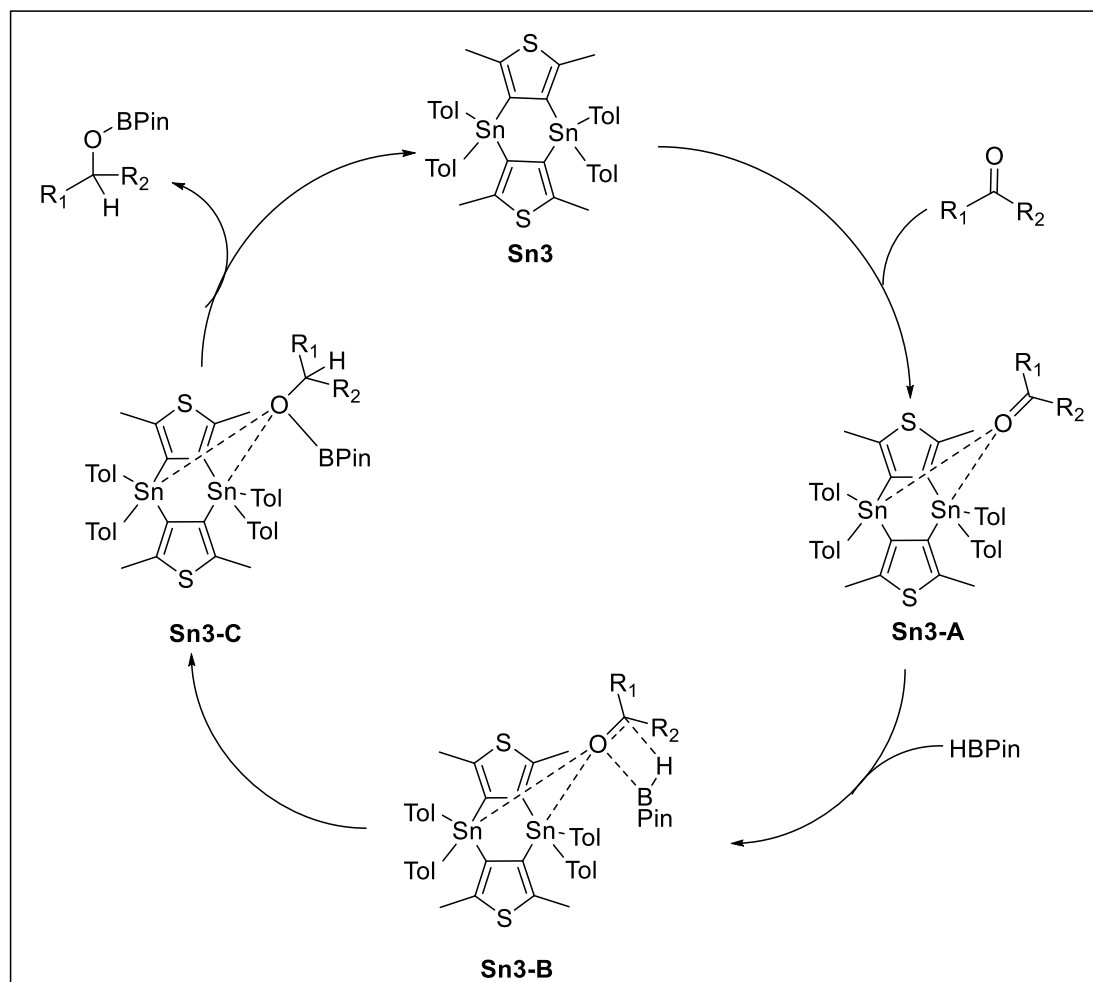
To investigate selectivity on a competitive intermolecular hydroboration reaction, we performed a reaction using a equimolar quantities of benzaldehyde (0.5 mmol) and acetophenone (0.5 mmol)(Scheme 3.2). Benzaldehyde reduced selectively converted (99%) to the desired product, suggesting that aldehydes are more reactive compared to ketones under the experimental conditions.



**Scheme 3.2:** Selectivity study for intermolecular hydroboration of aldehydes and ketones.

Based on the literature reports<sup>37-39</sup> we propose a plausible mechanism (Scheme 3.3). The first step involves a Lewis acid-base interaction of carbonyl oxygen to the tin centre forming an adduct (**Sn3-A**). This leads to the polarisation of carbonyl bond and increases the electrophilicity of carbonyl centre. In the second step, nucleophilic attack

by HBPIn to form a four membered cyclic transition state (**Sn3-B**). Finally, the hydride ion was added to carbon centre and forms the intermediate (**Sn3-C**), from which the boronate ester was eliminated.



**Scheme 3.3:** Plausible catalytic cycles for hydroboration of carbonyl compounds catalysed by **Sn3**.

### 3.3 Conclusions

In summary, we have synthesized and characterised a series of thiophene fused distannadithiophenes (**Sn3** - **Sn6**) using transmetallation approach from compound **1**. X-ray crystallography analysis shows that these compounds are planar with respect to thiophene. We have utilised these compounds for hydroboration of carbonyl

compounds. Compound **Sn3** showed better catalytic activity compared to other compounds and converted a wide variety of carbonyl compounds to boronate esters. Ditin compound (**Sn3**) showed superior activity over monotin compound ( $\text{Sn}(\text{Tol})_4$ ) owing to the cooperative nature.

### 3.4 Experimental section

#### 3.4.1 General information

All reagents and starting materials were purchased from Sigma-Aldrich, Alfa Aesar and Spectrochem chemical companies and used as received unless otherwise noted. THF and xylene were distilled from Na/benzophenone prior to use. All 400 MHz  $^1\text{H}$ , 100 MHz  $^{13}\text{C}$ , 377 MHz  $^{19}\text{F}$  and 149 MHz  $^{119}\text{Sn}$  NMR spectra were recorded on a Bruker ARX 400 spectrometer and JEOL 400 MHz spectrometer operating at 400 MHz. All  $^1\text{H}$  and  $^{13}\text{C}$  NMR spectra were referenced internally to solvent signals. ESI mass spectra were recorded using a Bruker microTOF-QII mass spectrometer. Single-crystal X-ray diffraction data were collected on a Rigaku Oxford X-ray diffractometer. The data were collected using  $\text{CuK}\alpha$  radiation (1.54184 Å). Crystallographic data for **Sn3**, **Sn4**, **Sn6** and details of X-ray diffraction experiments and crystal structure refinements are given in table 3.2. SADABS absorption corrections were applied in both cases. The structures were solved and refined with SHELX suite of programs or Olex. All non-hydrogen atoms were refined with anisotropic displacement coefficients. The H atoms were placed at calculated positions and were refined as riding atoms.

#### 3.4.2 Synthetic procedures and spectral characterisations

##### 3.4.2.1 Synthesis of Sn2

Compound **1** (5.00 g, 8.59 mmol) and metallic tin powder (2.45 g, 20.61 mmol) were refluxed in dry xylene (50 mL) for 24h in a two necked round bottomed flask. After

removing the metallic mercury and excess tin powder through filtration, the reaction mixture was concentrated in vacuo. The compound was washed with hexanes and dried under high vacuum. Yield: 1.20 g (23%).  $^1\text{H}$  NMR (400 MHz,  $\text{DMSO}-d_6$ )  $\delta$  2.68 (s, 12H).  $^{13}\text{C}$  NMR (101 MHz,  $\text{DMSO}-d_6$ )  $\delta$  143.64 (d,  $J = 55.0$  Hz), 125.09, 15.87.  $^{119}\text{Sn}$  NMR (149 MHz,  $\text{DMSO}-d_6$ )  $\delta$  -250.79.

### 3.4.2.2 General procedure for synthesis of Sn3- Sn6

To a suspensions of **Sn2** in 20 mL THF, aryl magnesium bromide in THF was added and the reaction mixture was refluxed for 24h. After removing THF, water was added and extracted using dichloromethane (3 x 50 mL). The extracted organic phase was dried over sodium sulphate. The mixture was concentrated in vacuo and the product was purified using silica gel column chromatography using EtOAc/*n*-hexane (2:98) as mobile phase.

### 3.4.2.3 Synthesis of Sn3

The quantities involved are as follows: **Sn2** (0.50 g, 0.833 mmol), tolyl magnesium bromide (3.67 mL, 3.67 mmol). Yield: 0.160 g (23%).  $^1\text{H}$  NMR (400 MHz,  $\text{CDCl}_3$ )  $\delta$  = 7.52 (d,  $J=7.6$ , 8H), 7.20 (d,  $J=7.3$ , 8H), 2.40 (s, 12H), 2.37 (s, 12H).  $^{13}\text{C}$  NMR (101 MHz,  $\text{CDCl}_3$ )  $\delta$ = 145.65, 138.87, 138.72, 137.01(s/d,  $J(^{117/119}\text{Sn},\text{C})= 43$  Hz), 135.53, 129.54(s/d,  $J(^{117/119}\text{Sn},\text{C})= 55$  Hz), 21.62, 17.56.  $^{119}\text{Sn}$  NMR (149 MHz,  $\text{CDCl}_3$ )  $\delta$ = -158.65. IR (KBr):  $\nu(\text{cm}^{-1})$  2916(m), 1492(m), 1435(m), 1187(m), 1069(m), 793(s), 480(s). HR-MS (ESI): calcd for  $\text{C}_{40}\text{H}_{40}\text{S}_2\text{Sn}_2$   $[\text{M}+\text{H}]^+$ : 825.0690, Found: 825.1066.

### 3.4.2.4 Synthesis of Sn4

The quantities involved are as follows: **Sn2** (0.50 g, 0.833 mmol), 4- $\text{CF}_3$ benzyl magnesium bromide (3.67 mL, 3.67 mmol). Yield: 0.295 g (34%).  $^1\text{H}$  NMR (400 MHz,  $\text{CDCl}_3$ )  $\delta$  = 7.71 – 7.69 (m, 8H), 7.62 (d,  $J=8.1$ , 8H), 2.37 (s, 12H).  $^{13}\text{C}\{^{19}\text{F}$  decoupled} NMR (101 MHz,  $\text{CDCl}_3$ )  $\delta$ = 147.13, 143.55, 137.11(s/d,  $J(^{117/119}\text{Sn},\text{C})= 51$  Hz), 136.60,



131.63, 125.39(s/d,  $J(^{117/119}\text{Sn},\text{C})=60\text{ Hz}$ ), 17.71.  $^{19}\text{F}$  NMR (377 MHz,  $\text{CDCl}_3$ )  $\delta = -63.04$ .  $^{119}\text{Sn}$  NMR (149 MHz,  $\text{CDCl}_3$ )  $\delta = -150.00$ . IR (KBr):  $\nu(\text{cm}^{-1})$  2920(m), 1391(m), 1326(m), 1169(m), 1050(m), 823(m), 681(m). HR-MS (ESI): calcd for  $\text{C}_{40}\text{H}_{28}\text{F}_{12}\text{S}_2\text{Sn}_2$   $[\text{M}+\text{H}]^+$ : 1040.9559, Found: 1040.3605.

### 3.4.2.5 Synthesis of Sn5

The quantities involved are as follows: **Sn2** (0.50 g, 0.833 mmol), 3,5-xylyl magnesium bromide (3.67 mL, 3.67 mmol). Yield: 0.274 g (37%).  $^1\text{H}$  NMR (400 MHz,  $\text{CDCl}_3$ )  $\delta = 7.20$  (s, 8H), 6.97 (s, 4H), 2.38 (s, 12H), 2.26 (s, 24H).  $^{13}\text{C}$  NMR (101 MHz,  $\text{CDCl}_3$ )  $\delta = 145.60$ , 139.17, 139.07, 137.84(s/d,  $J(^{117/119}\text{Sn},\text{C})=46\text{ Hz}$ ), 134.66(s/d,  $J(^{117/119}\text{Sn},\text{C})=41\text{ Hz}$ ), 130.74, 21.57, 17.68.  $^{119}\text{Sn}$  NMR (149 MHz,  $\text{CDCl}_3$ )  $\delta = -161.89$ . IR (KBr):  $\nu(\text{cm}^{-1})$  2913(m), 1591(m), 1436(m), 1127(m), 1038(m), 839(m), 692(m). HR-MS (ESI): calcd for  $\text{C}_{44}\text{H}_{48}\text{S}_2\text{Sn}_2$   $[\text{M}+\text{H}]^+$ : 881.1316, Found: 881.1297.

### 3.4.2.6 Synthesis of Sn6

The quantities involved are as follows: **Sn2** (0.50 g, 0.833 mmol), 3,5- $\text{CF}_3$ benzyl magnesium bromide (3.67 mL, 3.67 mmol). Yield: 0.316 g (29%).  $^1\text{H}$  NMR (400 MHz,  $\text{CDCl}_3$ )  $\delta = 7.93$  (s, 12H), 2.39 (s, 12H).  $^{13}\text{C}\{^{19}\text{F}\text{ decoupled}\}$  NMR (101 MHz,  $\text{CDCl}_3$ )  $\delta = 148.66$ , 140.73, 136.21(s/d,  $J(^{117/119}\text{Sn},\text{C})=46\text{ Hz}$ ), 134.37, 132.22(s/d,  $J(^{117/119}\text{Sn},\text{C})=54\text{ Hz}$ ), 123.98, 17.88.  $^{19}\text{F}$  NMR (376 MHz,  $\text{CDCl}_3$ )  $\delta = -62.98$ .  $^{119}\text{Sn}$  NMR (149 MHz,  $\text{CDCl}_3$ )  $\delta = -156.70$ . IR (KBr):  $\nu(\text{cm}^{-1})$  2918(m), 1615(m), 1354(m), 1285(m), 1123(m), 890(m), 682(m). HR-MS (ESI): calcd for  $\text{C}_{44}\text{H}_{24}\text{F}_{24}\text{S}_2\text{Sn}_2$   $[\text{M}+\text{H}]^+$ : 1312.9055, Found: 1312.4310.

### 3.4.2.7 Typical procedure for hydroboration reaction

In a nitrogen filled glovebox, aldehyde/ ketone (0.5 mmol), pinacolborane (1.0 mmol), **Sn3** (2 mol%) were added to the teflon stopper pressure tube. Toluene (1 mL) was

added to it and the mixture was stirred at room temperature for 12hr. The reaction mixture was evaporated to dryness under reduced pressure and the products were analysed through  $^1\text{H}$ ,  $^{13}\text{C}$  and  $^{11}\text{B}$  NMR spectroscopy.

#### 3.4.2.8 Analytical data for hydroboration of aldehydes

##### *2-(Benzyloxy)pinacolborane(2a) (Table 3.4, entry 1)<sup>22</sup>*

$^1\text{H}$  NMR (400 MHz,  $\text{CDCl}_3$ )  $\delta$  = 7.36–7.27 (m, 5H), 4.95 (s, 2H), 1.28 (s, 12H).  $^{13}\text{C}$  NMR (101 MHz,  $\text{CDCl}_3$ )  $\delta$  = 139.20, 128.26, 127.36, 126.71, 82.96, 66.67, 24.59.  $^{11}\text{B}$  NMR (128 MHz,  $\text{CDCl}_3$ )  $\delta$  = 22.39.

##### *2-(4-Methoxybenzyloxy)pinacolborane(2b) (Table 3.4, entry 2)<sup>35</sup>*

$^1\text{H}$  NMR (400 MHz,  $\text{CDCl}_3$ )  $\delta$  = 7.28 (d,  $J$ =8.6, 2H), 6.87 (d,  $J$ =8.8, 2H), 4.85 (s, 2H), 3.79 (s, 3H), 1.26 (s, 12H).  $^{13}\text{C}$  NMR (101 MHz,  $\text{CDCl}_3$ )  $\delta$  = 159.08, 131.51, 128.59, 113.73, 82.97, 66.50, 55.31, 24.68.  $^{11}\text{B}$  NMR (128 MHz,  $\text{CDCl}_3$ )  $\delta$  = 21.37.

##### *2-(3-Methoxybenzyloxy)pinacolborane(2c) (Table 3.4, entry 3)<sup>37</sup>*

$^1\text{H}$  NMR (400 MHz,  $\text{CDCl}_3$ )  $\delta$  = 7.23 (d,  $J$ =8.1, 1H), 6.92 (dd,  $J$ =4.0, 2.5, 2H), 6.81 (dd,  $J$ =8.2, 2.3, 1H), 4.91 (s, 2H), 3.80 (s, 3H), 1.27 (s, 12H).  $^{13}\text{C}$  NMR (101 MHz,  $\text{CDCl}_3$ )  $\delta$  = 129.35, 118.91, 113.27, 111.95, 83.07, 66.63, 55.25, 24.68.  $^{11}\text{B}$  NMR (128 MHz,  $\text{CDCl}_3$ )  $\delta$  = 21.40.

##### *2-(2-Methoxybenzyloxy)pinacolborane(2d) (Table 3.4, entry 4)<sup>17</sup>*

$^1\text{H}$  NMR (400 MHz,  $\text{CDCl}_3$ )  $\delta$  = 7.43 (d,  $J$ =8.3, 1H), 7.24 (d,  $J$ =7.5, 1H), 6.96 (t,  $J$ =7.5, 1H), 6.84 (d,  $J$ =8.2, 1H), 5.00 (s, 2H), 3.81 (s, 3H), 1.28 (s, 12H).  $^{13}\text{C}$  NMR (101 MHz,  $\text{CDCl}_3$ )  $\delta$  = 156.54, 128.27, 127.73, 127.37, 120.36, 109.85, 82.87, 62.30, 55.20, 24.65.  $^{11}\text{B}$  NMR (128 MHz,  $\text{CDCl}_3$ )  $\delta$  = 21.43.

##### *2-(4-Methylbenzyloxy)pinacolborane(2e) (Table 3.4, entry 5)<sup>17</sup>*

$^1\text{H}$  NMR (400 MHz,  $\text{CDCl}_3$ )  $\delta$  = 7.26 (d,  $J$ =8.0, 2H), 7.16 (d,  $J$ =8.0, 2H), 4.91 (s, 2H), 2.35 (s, 3H), 1.28 (s, 12H).  $^{13}\text{C}$  NMR (101 MHz,  $\text{CDCl}_3$ )  $\delta$  = 137.03, 136.31, 129.01, 126.92, 82.97, 66.65, 24.66, 21.18.  $^{11}\text{B}$  NMR (128 MHz,  $\text{CDCl}_3$ )  $\delta$  = 21.13.

***2-(3-Methylbenzyloxy)pinacolborane(2f) (Table 3.4, entry 6)<sup>40</sup>***

$^1\text{H}$  NMR (400 MHz,  $\text{CDCl}_3$ )  $\delta$  = 7.24 – 7.20 (m, 2H), 7.16 (d,  $J$ =7.6, 1H), 7.09 (d,  $J$ =7.4, 1H), 4.92 (s, 2H), 2.36 (s, 3H), 1.29 (s, 12H).  $^{13}\text{C}$  NMR (101 MHz,  $\text{CDCl}_3$ )  $\delta$  = 139.21, 137.94, 128.25, 128.14, 127.51, 123.81, 83.01, 66.73, 24.68, 21.40.  $^{11}\text{B}$  NMR (128 MHz,  $\text{CDCl}_3$ )  $\delta$  = 21.40.

***2-(2-Methylbenzyloxy)pinacolborane(2g) (Table 3.4, entry 7)<sup>32</sup>***

$^1\text{H}$  NMR (400 MHz,  $\text{CDCl}_3$ )  $\delta$  = 7.44 – 7.42 (m, 1H), 7.23 – 7.16 (m, 3H), 4.97 (s, 2H), 2.35 (s, 3H), 1.30 (s, 12H).  $^{13}\text{C}$  NMR (101 MHz,  $\text{CDCl}_3$ )  $\delta$  = 137.18, 135.65, 130.00, 127.50, 127.26, 125.87, 82.99, 65.02, 24.65, 18.69.  $^{11}\text{B}$  NMR (128 MHz,  $\text{CDCl}_3$ )  $\delta$  = 21.22.

***2-(Cyclohexylmethoxy)pinacolborane(2h) (Table 3.4, entry 8)<sup>22</sup>***

$^1\text{H}$  NMR (400 MHz,  $\text{CDCl}_3$ )  $\delta$  = 3.64 (d,  $J$ =6.4, 2H), 1.84 – 1.54 (m, 6H), 1.24 (s, 12H), 1.18 (s, 2H), 0.93 (dd,  $J$ =11.7, 3.0, 2H).  $^{13}\text{C}$  NMR (101 MHz,  $\text{CDCl}_3$ )  $\delta$  = 82.70, 70.50, 39.43, 29.45, 26.67, 25.91, 24.69.  $^{11}\text{B}$  NMR (128 MHz,  $\text{CDCl}_3$ )  $\delta$  = 22.12.

***2-(Methoxythiophene)pinacolborane(2i) (Table 3.4, entry 9)<sup>27</sup>***

$^1\text{H}$  NMR (400 MHz,  $\text{CDCl}_3$ )  $\delta$  = 7.24 (d,  $J$ =1.4, 1H), 7.02 (d,  $J$ =4.4, 1H), 6.95 (d,  $J$ =1.6, 1H), 5.04 (s, 2H), 1.27 (s, 12H).  $^{13}\text{C}$  NMR (101 MHz,  $\text{CDCl}_3$ )  $\delta$  = 142.04, 126.64, 125.94, 125.56, 83.18, 77.48, 76.84, 61.68, 24.67.  $^{11}\text{B}$  NMR (128 MHz,  $\text{CDCl}_3$ )  $\delta$  = 21.38.

***2-(Methoxyfuran)pinacolborane(2j) (Table 3.4, entry 10)<sup>17</sup>***

$^1\text{H}$  NMR (400 MHz,  $\text{CDCl}_3$ )  $\delta$  = 7.36 (s, 1H), 6.31 – 6.29 (m, 2H), 4.81 (s, 2H), 1.25 (s, 12H).  $^{13}\text{C}$  NMR (101 MHz,  $\text{CDCl}_3$ )  $\delta$  = 152.54, 142.52, 110.32, 108.38, 83.15, 59.27, 24.65.  $^{11}\text{B}$  NMR (128 MHz,  $\text{CDCl}_3$ )  $\delta$  = 22.34.

***2-(Methoxypyrrole)pinacolborane(2k) (Table 3.4, entry 11)<sup>27</sup>***

$^1\text{H}$  NMR (400 MHz,  $\text{CDCl}_3$ )  $\delta$  = 8.71 (s, 1H), 6.76 (m, 1H), 6.14 (m, 2H), 4.86 (s, 2H), 1.29 (s, 12H).  $^{13}\text{C}$  NMR (101 MHz,  $\text{CDCl}_3$ )  $\delta$  = 129.47, 118.32, 108.14, 107.71, 83.19, 59.86, 24.72.  $^{11}\text{B}$  NMR (128 MHz,  $\text{CDCl}_3$ )  $\delta$  = 21.47.

***2-(4-Trifluoromethylbenzyloxy)pinacolborane(2l) (Table 3.4, entry 12)<sup>28</sup>***

$^1\text{H}$  NMR (400 MHz,  $\text{CDCl}_3$ )  $\delta$  = 7.58 (d,  $J$ =8.1, 2H), 7.45 (d,  $J$ =8.0, 2H), 4.98 (s, 2H), 1.27 (s, 12H).  $^{13}\text{C}$  NMR (101 MHz,  $\text{CDCl}_3$ )  $\delta$  = 143.37, 129.82 (t,  $J$ =32), 126.72, 125.35 (t,  $J$ =4), 122.97 (t,  $J$ =270), 83.33, 66.00, 24.64.  $^{19}\text{F}$  NMR (377 MHz,  $\text{CDCl}_3$ )  $\delta$  = -62.37.  $^{11}\text{B}$  NMR (128 MHz,  $\text{CDCl}_3$ )  $\delta$  = 21.43.

***2-(4-Bromobenzyloxy)pinacolborane(2m) (Table 3.4, entry 13)<sup>22</sup>***

$^1\text{H}$  NMR (400 MHz,  $\text{CDCl}_3$ )  $\delta$  = 7.44 (d,  $J$ =8.4, 2H), 7.21 (d,  $J$ =8.4, 2H), 4.86 (s, 2H), 1.25 (s, 12H).  $^{13}\text{C}$  NMR (101 MHz,  $\text{CDCl}_3$ )  $\delta$  = 138.30, 131.44, 128.48, 121.28, 83.18, 66.03, 24.67.  $^{11}\text{B}$  NMR (128 MHz,  $\text{CDCl}_3$ )  $\delta$  = 22.31.

***2-(4-Fluorobenzyloxy)pinacolborane(2n) (Table 3.4, entry 14)<sup>17</sup>***

$^1\text{H}$  NMR (400 MHz,  $\text{CDCl}_3$ )  $\delta$  = 7.33 – 7.29 (m, 2H), 7.00 (t,  $J$ =8.7, 2H), 4.87 (s, 2H), 1.25 (s, 12H).  $^{13}\text{C}$  NMR (101 MHz,  $\text{CDCl}_3$ )  $\delta$  = 162.26 (d,  $J$ =245.1), 136.92, 128.70 (d,  $J$ =8.1), 115.15 (d,  $J$ =21.4), 83.11, 66.11, 24.63.  $^{19}\text{F}$  NMR (377 MHz,  $\text{CDCl}_3$ )  $\delta$  = -115.26.  $^{11}\text{B}$  NMR (128 MHz,  $\text{CDCl}_3$ )  $\delta$  = 22.31.

***2-(2-Fluorobenzyloxy)pinacolborane(2o) (Table 3.4, entry 15)<sup>40</sup>***

$^1\text{H}$  NMR (400 MHz,  $\text{CDCl}_3$ )  $\delta$  = 7.49 – 7.42 (m, 1H), 7.22 (dd,  $J$ =7.7, 2.2, 1H), 7.15 – 7.09 (m, 1H), 7.05 – 6.97 (m, 1H), 5.01 (s, 2H), 1.27 (s, 12H).  $^{13}\text{C}$  NMR (101 MHz,  $\text{CDCl}_3$ )  $\delta$  = 160.25 (d,  $J$ =246.5), 129.08 (d,  $J$ =8.2), 128.88 (d,  $J$ =4.5), 124.06, 115.06 (d,  $J$ =20.7), 83.17, 60.90 (d,  $J$ =4.9), 24.67.  $^{19}\text{F}$  NMR (376 MHz,  $\text{CDCl}_3$ )  $\delta$  = -119.07.  $^{11}\text{B}$  NMR (128 MHz,  $\text{CDCl}_3$ )  $\delta$  = 21.43.

### 3.4.2.9 Analytical data for hydroboration of ketones

#### *2-(1-Phenylethoxy)pinacolborane(3a) (Table 3.5, entry 1)*<sup>22</sup>

$^1\text{H}$  NMR (400 MHz,  $\text{CDCl}_3$ )  $\delta$  = 7.38 (d,  $J$ =8.1, 2H), 7.32 (t,  $J$ =7.5, 2H), 7.24 (s, 1H), 5.26 (q,  $J$ =6.4, 1H), 1.51 (d,  $J$ =6.5, 3H), 1.25 (s, 6H), 1.22 (s, 6H).  $^{13}\text{C}$  NMR (101 MHz,  $\text{CDCl}_3$ )  $\delta$  = 144.64, 128.26, 127.18, 125.41, 82.82, 72.66, 25.53, 24.59.  $^{11}\text{B}$  NMR (128 MHz,  $\text{CDCl}_3$ )  $\delta$  = 22.21.

#### *2-(1-(p-Tolyl)ethoxy)pinacolborane(3b) (Table 3.5, entry 2)*<sup>22</sup>

$^1\text{H}$  NMR (400 MHz,  $\text{CDCl}_3$ )  $\delta$  = 7.28 (d,  $J$ =8.1, 2H), 7.14 (d,  $J$ =5.6, 1H), 5.25 (q,  $J$ =6.4, 1H), 2.35 (s, 3H), 1.50 (d,  $J$ =6.5, 3H), 1.26 (s, 6H), 1.24 (s, 6H).  $^{13}\text{C}$  NMR (101 MHz,  $\text{CDCl}_3$ )  $\delta$  = 141.71, 136.69, 128.91, 125.36, 82.75, 72.50, 25.51, 24.59, 21.14.  $^{11}\text{B}$  NMR (128 MHz,  $\text{CDCl}_3$ )  $\delta$  = 22.19.

#### *2-(Diphenylmethoxy)pinacolborane(3c) (Table 3.5, entry 3)*<sup>22</sup>

$^1\text{H}$  NMR (400 MHz,  $\text{CDCl}_3$ )  $\delta$  = 7.44 (d,  $J$ =7.0, 4H), 7.33 (t,  $J$ =7.5, 4H), 7.26 (t,  $J$ =7.3, 2H), 6.24 (s, 1H), 1.24 (s, 12H).  $^{13}\text{C}$  NMR (101 MHz,  $\text{CDCl}_3$ )  $\delta$  = 143.22, 128.28, 127.34, 126.60, 83.04, 78.02, 24.57.  $^{11}\text{B}$  NMR (128 MHz,  $\text{CDCl}_3$ )  $\delta$  = 22.47.

#### *2-(1-(4-Methoxyphenyl)ethoxy)pinacolborane(3d) (Table 3.5, entry 4)*<sup>22</sup>

<sup>1</sup>H NMR (400 MHz, CDCl<sub>3</sub>) δ 7.30 (d, *J* = 8.7 Hz, 2H), 6.86 (d, *J* = 8.7 Hz, 2H), 5.21 (q, *J* = 6.4 Hz, 1H), 3.79 (s, 3H), 1.48 (d, *J* = 6.5 Hz, 3H), 1.24 (s, 6H), 1.22(s, 6H). <sup>13</sup>C NMR (101 MHz, CDCl<sub>3</sub>) δ 158.81, 136.90, 126.71, 113.63, 82.77, 72.31, 55.31, 25.41, 24.65, 24.59. <sup>11</sup>B NMR (128 MHz, CDCl<sub>3</sub>) δ = 22.11.

**2-(1-(4-Chlorophenyl)ethoxy)pinacolborane(3e) (Table 3.5, entry 5)<sup>20</sup>**

<sup>1</sup>H NMR (400 MHz, CDCl<sub>3</sub>) δ = 7.36 – 7.25 (m, 1H), 5.20 (q, *J*=6.4, 1H), 1.46 (d, *J*=6.5, 3H), 1.24 (s, 6H), 1.21(s, 6H). <sup>13</sup>C NMR (101 MHz, CDCl<sub>3</sub>) δ = 143.29, 132.93, 128.46, 126.93, 82.99, 72.09, 25.39, 24.63. <sup>11</sup>B NMR (128 MHz, CDCl<sub>3</sub>) δ = 22.30.

**2-(1-(4-Bromophenyl)ethoxy)pinacolborane(3f) (Table 3.5, entry 6)<sup>22</sup>**

<sup>1</sup>H NMR (400 MHz, CDCl<sub>3</sub>) δ = 7.43 (d, *J*=8.4, 2H), 7.23 (d, *J*=8.4, 2H), 5.19 (q, *J*=6.5, 1H), 1.45 (d, *J*=6.5, 3H), 1.23 (s, 6H), 1.20(s, 6H). <sup>13</sup>C NMR (101 MHz, CDCl<sub>3</sub>) δ = 143.71, 131.37, 127.23, 120.95, 82.96, 72.06, 25.39, 24.63. <sup>11</sup>B NMR (128 MHz, CDCl<sub>3</sub>) δ = 21.19.

**2-(1-(4-Iodophenyl)ethoxy)pinacolborane(3g) (Table 3.5, entry 7)<sup>41</sup>**

<sup>1</sup>H NMR (400 MHz, CDCl<sub>3</sub>) δ = 7.64 (d, *J*=8.2, 2H), 7.11 (d, *J*=8.2, 2H), 5.18 (q, *J*=6.4, 1H), 1.45 (d, *J*=6.5, 3H), 1.24 (s, 6H), 1.21 (s, 6H). <sup>13</sup>C NMR (101 MHz, CDCl<sub>3</sub>) δ = 144.39, 137.34, 129.49, 127.49, 82.97, 72.12, 25.42, 24.65. <sup>11</sup>B NMR (128 MHz, CDCl<sub>3</sub>) δ = 22.09.

**2-(1-(2-Fluorophenyl)ethoxy)pinacolborane(3h) (Table 3.5, entry 8)<sup>42</sup>**

<sup>1</sup>H NMR (400 MHz, CDCl<sub>3</sub>) δ = 7.58 – 7.46 (m, 1H), 7.24 – 7.07 (m, 2H), 7.01 – 6.93 (m, 1H), 5.56 (q, *J*=6.4, 1H), 1.49 (d, *J*=6.5, 3H), 1.25 (s, 6H), 1.22(s, 6H). <sup>13</sup>C NMR (101 MHz, CDCl<sub>3</sub>) δ = 159.16 (d, *J*=245.5), 131.76 (d, *J*=13.5), 128.46 (d, *J*=8.2), 126.68 (d, *J*=4.4), 124.13 (d, *J*=3.4), 114.94 (d, *J*=21.6), 82.88, 66.71 (d, *J*=2.9), 24.53, 24.29. <sup>19</sup>F NMR (377 MHz, CDCl<sub>3</sub>) δ = -119.58. <sup>11</sup>B NMR (128 MHz, CDCl<sub>3</sub>) δ = 22.15.

**2-(1-(2-Chlorophenyl)ethoxy)pinacolborane(3i) (Table 3.5, entry 9)<sup>18</sup>**

<sup>1</sup>H NMR (400 MHz, CDCl<sub>3</sub>) δ = 7.64 (d, *J*=9.8, 1H), 7.30 (d, *J*=7.8, 1H), 7.20 – 7.12 (m, 2H), 5.59 (q, *J*=6.3, 1H), 1.49 (d, *J*=6.4, 3H), 1.25 (s, 6H), 1.22(s, 6H). <sup>13</sup>C NMR (101 MHz, CDCl<sub>3</sub>) δ = 142.32, 131.18, 129.20, 128.23, 127.13, 126.73, 82.99, 69.63, 24.62, 23.98. <sup>11</sup>B NMR (128 MHz, CDCl<sub>3</sub>) δ = 22.24.

**2-(1-(2-Bromophenyl)ethoxy)pinacolborane(3j) (Table 3.5, entry 10)**

<sup>1</sup>H NMR (400 MHz, CDCl<sub>3</sub>) δ = 7.62 (d, *J*=9.7, 1H), 7.48 (d, *J*=7.9, 1H), 7.30 (t, *J*=8.3, 1H), 7.12 – 7.05 (m, 1H), 5.52 (q, *J*=6.3, 1H), 1.48 (d, *J*=6.3, 3H), 1.24 (s, 6H), 1.21(s, 6H). <sup>13</sup>C NMR (101 MHz, CDCl<sub>3</sub>) δ = 143.85, 132.44, 128.56, 127.73, 126.98, 121.15, 82.95, 71.79, 24.58, 24.05. <sup>11</sup>B NMR (128 MHz, CDCl<sub>3</sub>) δ = 22.18.

**3.4.2.10 Typical procedure for selective hydroboration of aldehyde vs ketone**

In a nitrogen filled glovebox, benzaldehyde (0.5 mmol), acetophenone (0.5 mmol), pinacolborane (1.0 mmol), **Sn3** (2 mol%) were added to the teflon stoppered pressure tube. Toluene (1 mL) was added to it and the reaction mixture was stirred at room temp. for 12h. The reaction mixture was evaporated to dryness under high vacuum and the products were analysed through <sup>1</sup>H NMR spectroscopy.

**3.5 References**

1. Barbosa, A. S. L.; Guedes, J. d. S.; da Silva, D. R.; Meneghetti, S. M. P.; Meneghetti, M. R.; da Silva, A. E.; de Araujo, M. V.; Alexandre-Moreira, M. S.; de Aquino, T. M.; de Siqueira Junior, J. P.; de Araújo, R. S. A.; da Cruz, R. M. D.; Mendonça-Junior, F. J. B. *J. Inorg. Biochem.* **2018**, 180, 80.
2. Vinayak, R.; Dey, D.; Ghosh, D.; Chattopadhyay, D.; Ghosh, A.; Nayek, H. P. *Appl. Organomet. Chem.* **2018**, 32, e4122.
3. Wen, G.-H.; Zhang, R.-F.; Li, Q.-L.; Zhang, S.-L.; Ru, J.; Du, J.-Y.; Ma, C.-L. *J. Organomet. Chem.* **2018**, 861, 151.

- 
4. Brito, Y. C.; Ferreira, D. A. C.; Fragoso, D. M. d. A.; Mendes, P. R.; Oliveira, C. M. J. d.; Meneghetti, M. R.; Meneghetti, S. M. P. *Appl. Catal. A: Gen.* **2012**, 443-444, 202.
  5. Meneghetti, M. R.; Meneghetti, S. M. P. *Catal. Sci. Tech.* **2015**, 5, 765.
  6. Shiina, I. *Chem. Rev.* **2007**, 107, 239.
  7. Deshayes, G.; Mercier, F. A. G.; Degée, P.; Verbruggen, I.; Biesemans, M.; Willem, R.; Dubois, P. *Chem. Eur. J.* **2003**, 9, 4346.
  8. Zubair, M.; Sirajuddin, M.; Haider, A.; Hussain, I.; Tahir, M. N.; Ali, S. *Appl. Organomet. Chem.* **2020**, 34, e5305.
  9. da Silva, M. A.; dos Santos, A. S. S.; dos Santos, T. V.; Meneghetti, M. R.; Meneghetti, S. M. P. *Catal. Sci. Tech.* **2017**, 7, 5750.
  10. da Silva, D. S.; Altino, F. M. R. S.; Bortoluzzi, J. H.; Meneghetti, S. M. P., *Mol. Catal.* **2020**, 494, 111130.
  11. Naseer, M. M.; Jurkschat, K. *Chem. Commun.* **2017**, 53, 8122.
  12. Tanaka, D.; Ohshita, J.; Ooyama, Y.; Kobayashi, N.; Higashimura, H.; Nakanishi, T.; Hasegawa, Y. *Organometallics* **2013**, 32, 4136.
  13. Adachi, Y.; Ohshita, J. Main Group Strategies towards Functional Hybrid Materials, 2017; pp 237-264.
  14. Lee, K.-H.; Ohshita, J.; Tanaka, D.; Tominaga, Y.; Kunai, A. *J. Organomet. Chem.* **2012**, 710, 53.
  15. Saito, M.; Shiratake, M.; Tajima, T.; Guo, J. D.; Nagase, S. *J. Organomet. Chem.* **2009**, 694, 4056.
  16. Saito, M.; Nitta, M.; Yoshioka, M. *Organometallics* **2001**, 20, 749.
  17. Bisai, M. K.; Das, T.; Vanka, K.; Sen, S. S. *Chem. Commun.* **2018**, 54, 6843.
  18. Yan, D.; Dai, P.; Chen, S.; Xue, M.; Yao, Y.; Shen, Q.; Bao, X. *Org. Biomol. Chem.* **2018**, 16, 2787.
-



- 
19. Osseili, H.; Mukherjee, D.; Spaniol, T. P.; Okuda, J. *Chem. Eur. J.* **2017**, *23*, 14292.
  20. Peddaraao, T.; Sarkar, N.; Nembenna, S. *Inorg. Chem.* **2020**, *59*, 4693.
  21. Shegavi, M. L.; Bose, S. K. *Catal. Sci. Tech.* **2019**, *9*, 3307.
  22. Anga, S.; Acharya, J.; Chandrasekhar, V. *J. Org. Chem.* **2021**, *86*, 2224.
  23. Kuciński, K.; Hreczycho, G. *Green Chem.* **2020**, *22*, 5210.
  24. Chong, C. C.; Kinjo, R. *ACS Catal.* **2015**, *5*, 3238.
  25. Jakhar, V. K.; Barman, M. K.; Nembenna, S. *Org. Lett.* **2016**, *18*, 4710.
  26. Kaithal, A.; Chatterjee, B.; Gunanathan, C. *Org. Lett.* **2015**, *17*, 4790.
  27. Harinath, A.; Bhattacharjee, J.; Nayek, H. P.; Panda, T. K. *Dalton Trans.* **2018**, *47*, 12613.
  28. Zeng, H.; Wu, J.; Li, S.; Hui, C.; Ta, A.; Cheng, S.-Y.; Zheng, S.; Zhang, G. *Org. Lett.* **2019**, *21*, 401.
  29. Tamang, S. R.; Bedi, D.; Shafiei-Haghighi, S.; Smith, C. R.; Crawford, C.; Findlater, M. *Org. Lett.* **2018**, *20*, 6695.
  30. Hossain, I.; Schmidt, J. A. R. *Eur. J. Inorg. Chem.* **2020**, *2020*, 1877.
  31. Wu, Y.; Shan, C.; Ying, J.; Su, J.; Zhu, J.; Liu, L. L.; Zhao, Y. *Green Chem.* **2017**, *19*, 4169.
  32. Zhu, Z.; Wu, X.; Xu, X.; Wu, Z.; Xue, M.; Yao, Y.; Shen, Q.; Bao, X. *J. Org. Chem.* **2018**, *83*, 10677.
  33. Ma, D. H.; Jaladi, A. K.; Lee, J. H.; Kim, T. S.; Shin, W. K.; Hwang, H.; An, D. K., *ACS Omega* **2019**, *4*, 15893.
  34. Wang, W.; Luo, M.; Yao, W.; Ma, M.; Pullarkat, S. A.; Xu, L.; Leung, P.-H. *New J. Chem.* **2019**, *43*, 10744.
  35. Hadlington, T. J.; Hermann, M.; Frenking, G.; Jones, C. *J. Am. Chem. Soc.* **2014**, *136*, 3028.

- 
36. Dasgupta, R.; Das, S.; Hiwase, S.; Pati, S. K.; Khan, S. *Organometallics* **2019**, 38, 1429.
37. Baishya, A.; Baruah, S.; Geetharani, K. *Dalton Trans.* **2018**, 47, 9231.
38. Kumar, G. S.; Harinath, A.; Narvariya, R.; Panda, T. K. *Eur. J. Inorg. Chem.* **2020**, 2020, 467.
39. Romero, E. A.; Peltier, J. L.; Jazzar, R.; Bertrand, G. *Chem. Commun.* **2016**, 52, 10563.
40. Stachowiak, H.; Kaźmierczak, J.; Kuciński, K.; Hreczycho, G. *Green Chem.* **2018**, 20, 1738.
41. Bagherzadeh, S.; Mankad, N. P. *Chem. Commun.* **2016**, 52, 3844.
42. Wang, W.; Shen, X.; Zhao, F.; Jiang, H.; Yao, W.; Pullarkat, S. A.; Xu, L.; Ma, M. *J. Org. Chem.* **2018**, 83, 69.

## **CHAPTER 4**

### **Thiophene-fused boracycles as photoactive analogues of diboranthracenes**

<b>4.1 Introduction</b>	113
<b>4.2 Results and discussion</b>	114
<b>4.2.1</b> Synthesis and characterisation	114
<b>4.2.2</b> X-ray crystal analysis	117
<b>4.2.3</b> Photophysical properties	119
<b>4.2.4</b> Electrochemical properties	121
<b>4.2.5</b> Photochromic properties	122
<b>4.3 Conclusions</b>	127
<b>4.4 Experimental section</b>	127
<b>4.4.1</b> General information	127
<b>4.4.2</b> Synthetic procedures and spectral characterisations	128
<b>4.5 References</b>	130



---

## 4.1 Introduction

Organic  $\pi$ -conjugated materials have gained much attention owing to their tunable and diverse properties to use them as organic electronics,<sup>1-4</sup> bio-imaging<sup>5-10</sup> and sensing materials.<sup>11,12</sup> Incorporation of non-carbon elements especially main-group elements such as B, P, Si, S, Sn, Se, Te etc. into the  $\pi$ -conjugated materials has emerged as an attractive method to fine tune the electronic properties and to overcome the shortcomings experienced by pure organic materials.<sup>13-16</sup> Among the different main-group elements doped (or) embedded  $\pi$ -electron system, tri-coordinated boron compounds have gained overwhelming interest owing to their potential applications in organic light emitting diodes,<sup>17-22</sup> non-linear optics,<sup>23-28</sup> fluorescent probes<sup>29-34</sup> and bimolecular probes. Introduction of Lewis acidic boron atom perturbs the electronic structure of the  $\pi$ -conjugated system through the interaction of the  $\pi$ -electron clouds with the p-orbital at the boron center. Among the different types of  $\pi$ -conjugated boranes, fused boracycles and (or) boron embedded cyclic systems gained much attention.<sup>35-41</sup> Notable progress has been made in the development of borafluorene<sup>42</sup>, diboraanthracene derivatives<sup>43</sup> (Figure 4.1.A). Diboron fused aromatic systems has been used to make sandwich complexes,<sup>44</sup> the perfluorinated derivatives studied as activators in Ziegler-Natta olefin polymerization,<sup>45</sup> the ferrocenyl derivative<sup>46</sup> (Figure 4.1.B) was explored for its redox chemistry and Lewis acidity tuning and the boron doped polyaromatics to make boron doped graphene flakes or nano-ribbons.<sup>47</sup>

Thiophene is a five membered aromatic system extensively incorporated as a building block to construct many functional materials. Coplanarity, quinoid character, intermolecular  $\pi$ -stacking and sulphur-sulphur interactions helps to attain unique chemical and electronic characteristics.<sup>48</sup> As alluded in the previous section,

incorporation of boron in between thiophene moieties has turned out to be an attractive method to tune the chemical and electronic properties of the thiophene system.<sup>49</sup> Apart from boron embedded oligo- and polythiophenes, boron incorporated cyclic systems have gained much attention due to their attractive photophysical properties.<sup>50-52</sup> For example, Yamaguchi and co-workers<sup>53</sup> reported thiophene fused boroles with high antiaromaticity. Piers and co-workers<sup>54</sup> reported benzothiophene fused diborane which emits red light. Siebert and coworkers<sup>55</sup> reported the reactivity of diiododiboradithiophene. Recently, Tovar and co-workers<sup>56</sup> explored the synthesis of dithienoborepins, in which boron is fused in a seven-membered ring system. In spite of these exciting results, the study of thiophene fused diboradithiophene derivatives are very limited, especially the synthesis of diboradithiophene fused in the 3,4-positions of thiophene not explored (Figure 4.1.C). This chapter describes the synthesis of thiophene analogue of diboraanthracene *i.e.* diboradithiophene.

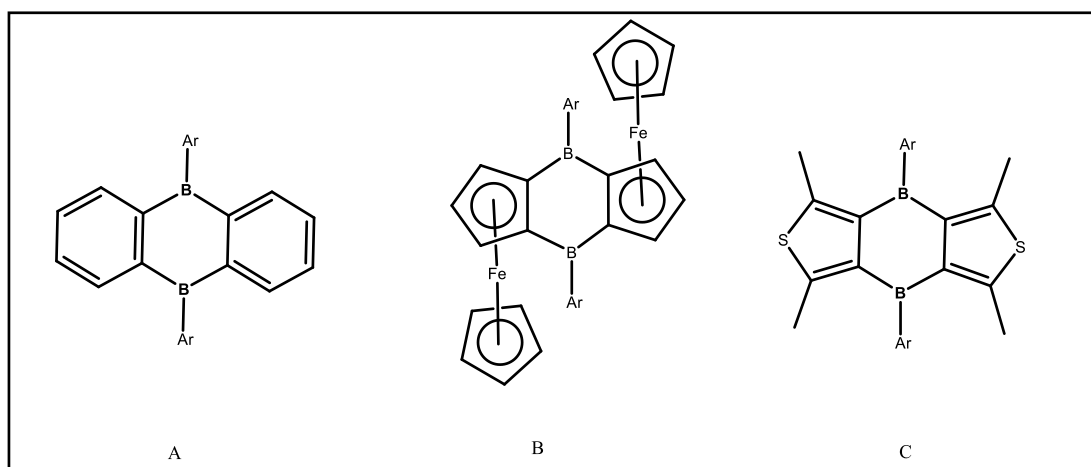
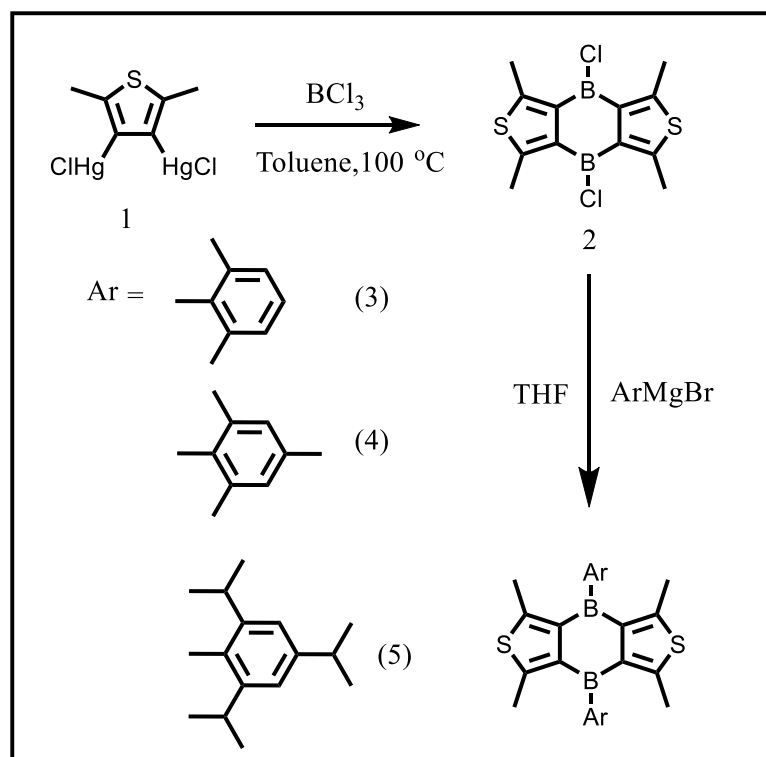


**Figure 4.1:** Examples of diboracycles (A) diboraanthracene, (B) diboradiferrocene, (C) diboradithiophene

## 4.2 Results and discussion

### 4.2.1 Synthesis and characterisation

The synthesis of diboradithiophenes is shown in scheme 4.1. Reaction of compound **1** with  $\text{BCl}_3$  in toluene gave a moderate yield of dihalodiboradithiophene. The presence of B-Cl bonds allows compound **2** to be used as a precursor for the synthesis of other diboradithiophenes. Reaction of compound **2** with  $\text{ArMgBr}$  provides compounds **3-5** in moderate yields. Compounds **3-5** were purified by column chromatography on silica gel. Compounds **2-5** were fully characterised by  $^1\text{H}$ ,  $^{13}\text{C}$ ,  $^{11}\text{B}$  NMR and elemental analysis. These compounds are also confirmed by HRMS analysis. The  $^1\text{H}$  NMR spectrum of compound **4** displays three sets of signal at aliphatic region, 1.97 and 2.33 ppm for mesityl  $-\text{CH}_3$  group. The peak at 2.12 ppm corresponds to  $-\text{CH}_3$  group attached to thiophene ring (Figure 4.2). The  $^{11}\text{B}$  NMR spectra of compounds **3-5** display a broad signal at around  $\sim 56$  ppm which falls in the region of tri-coordinated organo boron compounds. For an illustration the  $^{11}\text{B}$  NMR spectrum of compound **4** is shown in figure 4.3.



**Scheme 4.1:** Synthesis of diboradithiophene derivatives.

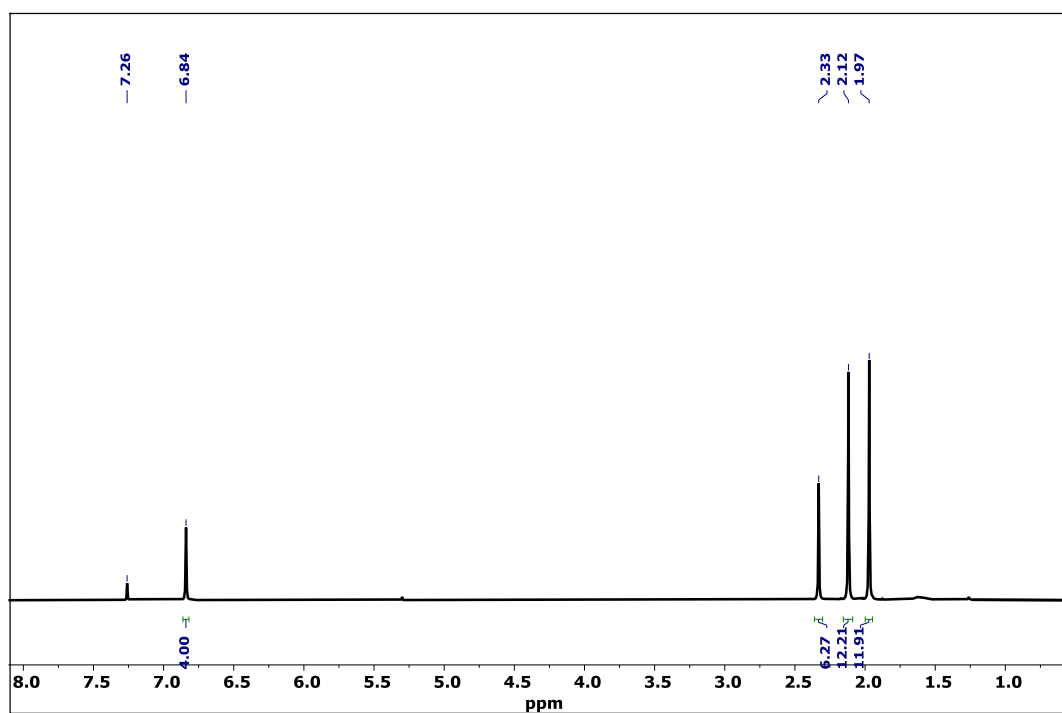


**Figure 4.2:** <sup>1</sup>H NMR spectrum of compound **4** in CDCl<sub>3</sub>.

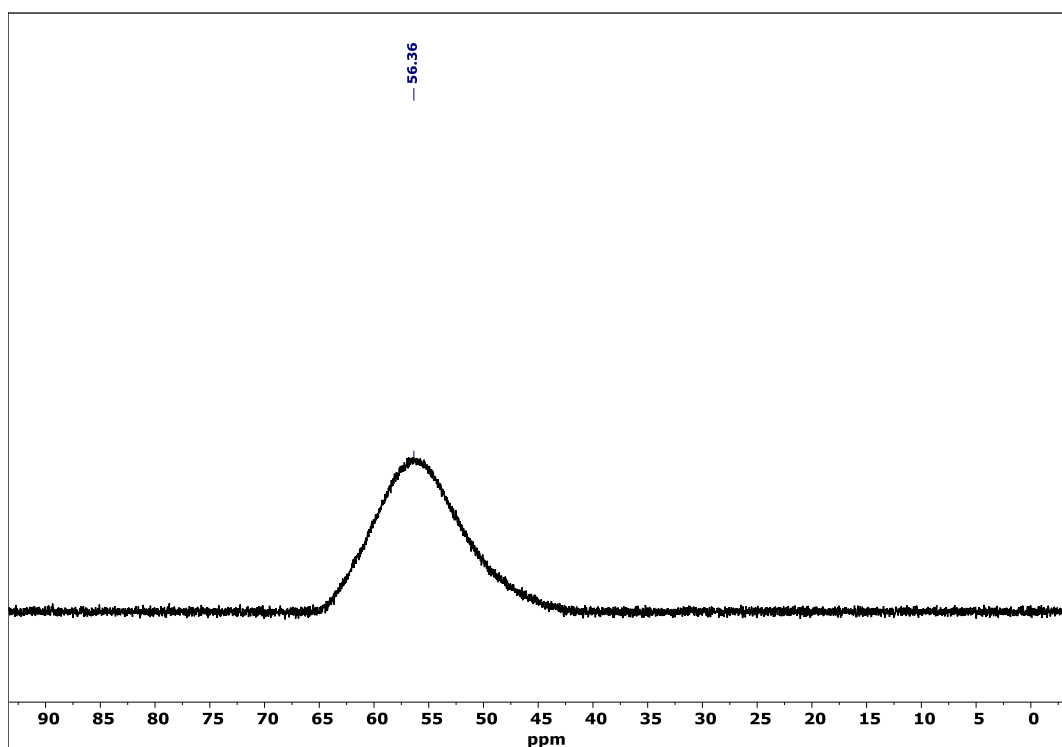


**Figure 4.3:** <sup>11</sup>B NMR spectrum of compound **4** in CDCl<sub>3</sub>.



### 4.2.2 X-ray crystal analysis

Single crystals of compounds **3** and **4** were obtained from slow evaporation of a mixture of dichloromethane and ethanol solution. The molecular structure of compounds **3** & **4** were determined by single crystal X-ray diffraction analysis (Figure 4.4 and Table 4.1). Compounds **3** & **4** were crystallized in a centrosymmetric space group of *P21/c* and *P21/n* respectively. As shown in figure 4.5, the aryl group ('xylyl' in **3** and 'mesityl' in **4**) attached to the boron atom is almost perpendicular to the ring/plane C4B2. The dihedral angle between the C4B2 plane and the aryl group is 89.9 and 89.2 ° in **3** and **4** respectively. The central C4B2 planes of compound **3** & **4** are almost coplanar with respect to the thiophene units (0.9 ° for **3** and 1.8 ° for **4**). The C-B-C bond angles and B-C bond lengths in **3** and **4** are similar to those observed in other diboracycles.<sup>43,46</sup> The B-C bonds to the thiophene rings (1.550 (3) & 1.553(3) for compound **3**; 1.552(2) & 1.551(2) for compound **4**) are considerably shorter than the B-C bonds to the exocyclic 'xylyl' and 'mesityl' groups (1.584 (3) for compound **3**; 1.581(2) for compound **4**), which suggests considerable carbon-boron  $\pi$ -bonding in the C4B2 plane.

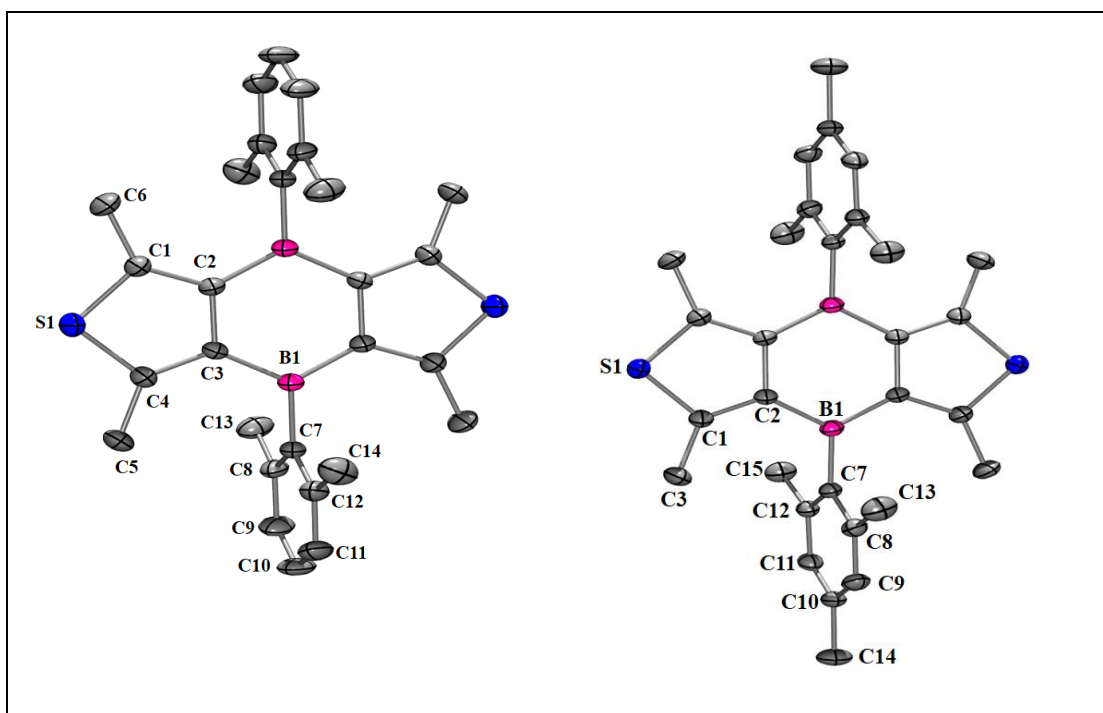


**Figure 4.4:** Molecular structure of compound **3** (Left) and **4** (Right). (thermal ellipsoids at 30 % probability). Hydrogen atoms are omitted for clarity. Selected interatomic distances (Å) and angles (°): For compound **3**, B1-C7 1.584(3), B1-C3 1.553(3), B1\*-C2 1.550(3), C3-B1-C7 121.9(2), C2\*-B-C3 116.7 (2), C2\*-B1-C7 121.3 (2), Ar//C4B2 89.9 (7), Thio//C4B2 0.9(5); For compound **4**, B1-C7 1.581(2), B1-C2 1.552(2), B1-C4 1.551(2), C4-B1-C7 120.8(1), C4-B1-C2 116.7 (1), C2-B1-C7 122.4(1), Ar//C4B2 89.3 (3), Thio//C4B2 1.9(5).

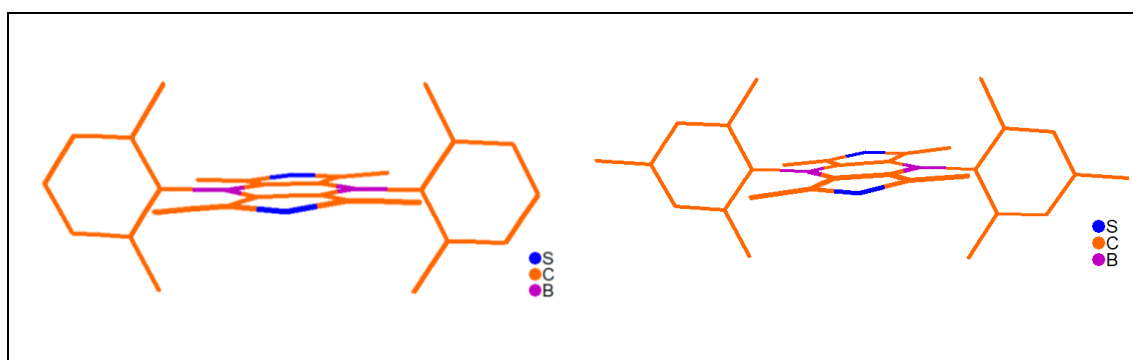


**Figure 4.5:** Side view of **3** and **4**.

**Table 4.1:** Crystal data and structure refinement parameters for compound **3** and **4**

Compound	<b>3</b>	<b>4</b>
Empirical formula	C <sub>28</sub> H <sub>30</sub> B <sub>2</sub> S <sub>2</sub>	C <sub>30</sub> H <sub>34</sub> B <sub>2</sub> S <sub>2</sub>
Formula weight	452.26	480.31
Temperature/K	297.6(8)	296.15
Crystal system	monoclinic	monoclinic
Space group	P2 <sub>1</sub> /c	P2 <sub>1</sub> /n
a/Å	10.54815(16)	7.3621(3)
b/Å	14.5492(2)	16.4766(7)
c/Å	8.34333(15)	11.3205(5)
α/°	90	90
β/°	97.4946(16)	93.878(2)
γ/°	90	90
Volume/Å <sup>3</sup>	1269.49(4)	1370.06(10)
Z	2	2
ρ <sub>calc</sub> /cm <sup>3</sup>	1.183	1.164
μ/mm <sup>-1</sup>	1.979	0.211
F(000)	480.0	512.0

Radiation	CuK $\alpha$ ( $\lambda$ = 1.54184)	MoK $\alpha$ ( $\lambda$ = 0.71073)
2 $\theta$ range for data collection/ $^\circ$	8.454 to 150.788	4.372 to 56.714
Index ranges	$-13 \leq h \leq 12$ , $-17 \leq k \leq 9$ , $-9 \leq l \leq 10$	$-9 \leq h \leq 9$ , $-21 \leq k \leq 21$ , $-15 \leq l \leq 15$
Reflections collected	9588	22133
Independent reflections	2563 [ $R_{\text{int}} = 0.0963$ , $R_{\text{sigma}} = 0.0555$ ]	3394 [ $R_{\text{int}} = 0.0345$ , $R_{\text{sigma}} = 0.0218$ ]
Data/restraints/parameters	2563/0/150	3394/0/159
Goodness-of-fit on F <sup>2</sup>	1.112	1.022
Final R indexes [ $I \geq 2\sigma(I)$ ]	$R_I = 0.0680$ , $wR_2 = 0.1955$	$R_I = 0.0467$ , $wR_2 = 0.1309$
Final R indexes [all data]	$R_I = 0.0749$ , $wR_2 = 0.2030$	$R_I = 0.0610$ , $wR_2 = 0.1429$
Largest diff. peak/hole / e $\text{\AA}^{-3}$	0.31 and -0.32	0.31 and -0.23

#### 4.2.3 Photophysical properties

The photophysical properties of compounds **3-5** were studied using UV-Vis absorption and emission spectroscopy in cyclohexane, dichloromethane and THF. All three compounds exhibited strong absorption band at around 275 nm (Figure 4.6). The slight hypsochromic shift of compound **5** relative to compounds **3** & **4** is due to the strong electron donating nature of the isopropyl group. Compounds **3-5** showed a bimodal emission spectrum (Figure 4.6). The emission bands remain unaltered by changing the solvent polarity (cyclohexane, THF and dichloromethane) (Table 4.2). Compounds **3-5** emit in the blue region with a quantum yield of ~5 % (4.7 for **3**; 5.2 for **4** and 6.2 for **5**) in the solution state and ~2 % (2.04% for **3**; 1.94% for **4**; 1.95% for **5**) in the thin film state (Figure 4.7).

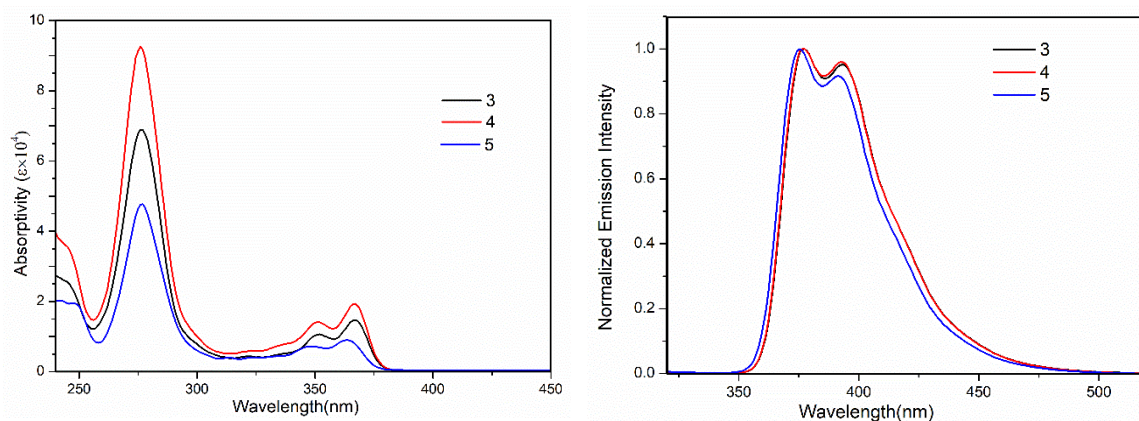


**Figure 4.6:** (left) Absorption spectra of compounds **3-5** in  $10^{-5}$  M THF, (right) Normalized emission spectra of compounds **3-5** in  $10^{-5}$  M THF.

**Table 4.2:** Photophysical properties of compounds **3-5**

Compound	Solvent	$\lambda_{\text{max}}$ (nm)	$\epsilon_{\text{max}}$ ( $\text{M}^{-1} \text{cm}^{-1} \times 10^4$ )	$\lambda_{\text{em}}$ (nm)	$\Phi_{\text{F}}$	Stokes Shift (nm)	$\tau$ (ns)
<b>3</b>	$\text{CH}_2\text{Cl}_2$	275	7.495	378,395	5.89	103,120	
	THF	275	6.892	377,394	4.73	102,119	0.54
	Cyclohexane	277	8.970	372,390	5.22	95,113	
	Thin Film			397	2.04		
<b>4</b>	$\text{CH}_2\text{Cl}_2$	275	5.310	378,395	5.37	103,120	
	THF	275	9.249	376,394	5.23	101,119	0.52
	Cyclohexane	276	5.887	373,390	4.69	97,114	
	Thin Film			397	1.94		
<b>5</b>	$\text{CH}_2\text{Cl}_2$	275	5.756	376,393	7.06	101,118	0.53
	THF	275	5.989	375,392	6.24	100,117	
	Cyclohexane	277	6.083	371,388	4.35	94,111	
	Thin Film			396	1.95		



**Figure 4.7:** Photograph of compounds **3-5** in 2% PMMA film under handheld UV lamp irradiated at 365 nm.

#### 4.2.4 Electrochemical properties

Cyclic voltammograms of the compounds **3-5** were studied in dimethoxyethane (DME) solution using  $[n\text{Bu}_4\text{N}][\text{PF}_6]$  as a supporting electrolyte (Figure 4.8). All three boron compounds exhibit two quasi reversible redox processes (Table 4.3). The redox potential (Table 4.3) are highly negative in comparison with most of the substituted diboraanthracene<sup>57-59</sup> and diboradiferrocene<sup>60-61</sup> derivatives, which suggest that

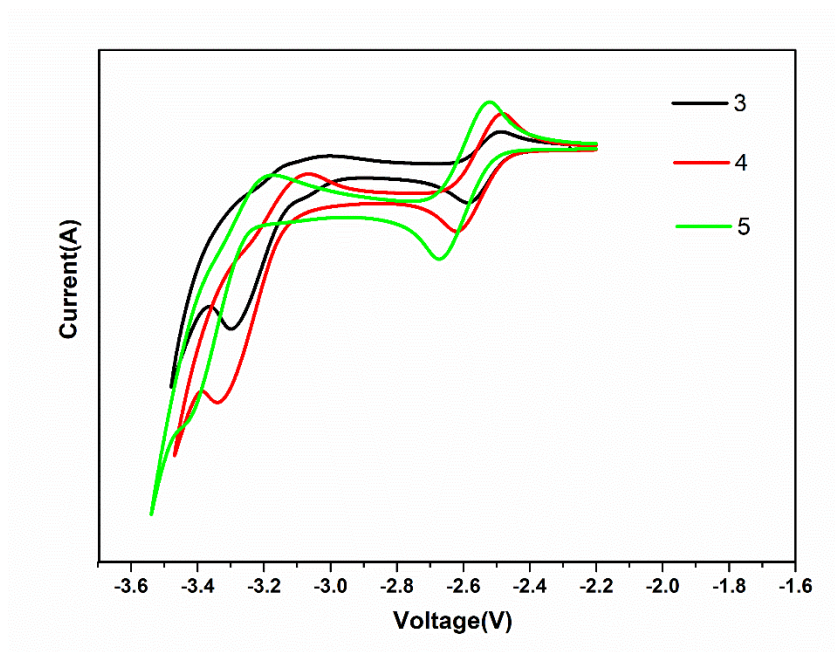


**Figure 4.8:** Cyclic voltammogram of compounds **3-5** (vs. Ferrocene/Ferrocenium) with 0.1 M  $\text{Bu}_4\text{NPF}_6$  as the supporting electrolyte (scan rate 100 mV/s) in DME.

diboradithiophenes are considerably more electron-rich. The HOMO-LUMO energy gaps were calculated from the onset of absorption and onset of reduction potentials. The HOMO-LUMO energy gaps were calculated from the onset absorption and onset reduction potentials (Table 4.3).

**Table 4.3:** Electrochemical data and frontier orbital energies [eV] derived from the UV/Vis onset absorption and electrochemical data.

Compound	$E_{1/2}$ (V)	HOMO-LUMO gap <sup>[a]</sup>	LUMO <sup>[b]</sup>	HOMO <sup>[c]</sup>
<b>3</b>	-2.53, -3.21	3.28	-2.01	-5.29
<b>4</b>	-2.55, -3.20	3.28	-2.03	-5.31
<b>5</b>	-2.59, -3.30	3.30	-1.98	-5.28

[a] Estimated from the absorption onset of the longest-wavelength absorption band. [b]

Calculated from the  $E_{pc}$  of the first reduction wave referenced to  $Fc/Fc^+$ . [c] Calculated from the HOMO–LUMO gap and the LUMO.

#### 4.2.5 Photochromic properties

We envisioned that our boron compounds **3-5** would act as photochromic materials to detect UV radiation. Wang and co-workers<sup>62-67</sup> explored several tetra-coordinated boranes as photochromic materials. Recently, Yamaguchi and co-workers<sup>68</sup> elegantly showed the photoinduced cyclization of dimesityl(hetero)arylboranes using experimental and theoretical studies. In order to investigate the photochromic properties, compound **4** was irradiated using UV light (365 nm) in THF solution and the response was monitored using absorption and emission spectroscopy. Upon sequential irradiation, the bands at 275, 351 and 367 nm in the absorption and the bands at 377 nm and 394 nm in the emission were steadily decreased with time and completely disappeared after 35 minutes of UV exposure (Figure 4.9). A similar phenomenon was also observed when we tested compounds **3** and **5** (Figure 4.10 & 4.11).



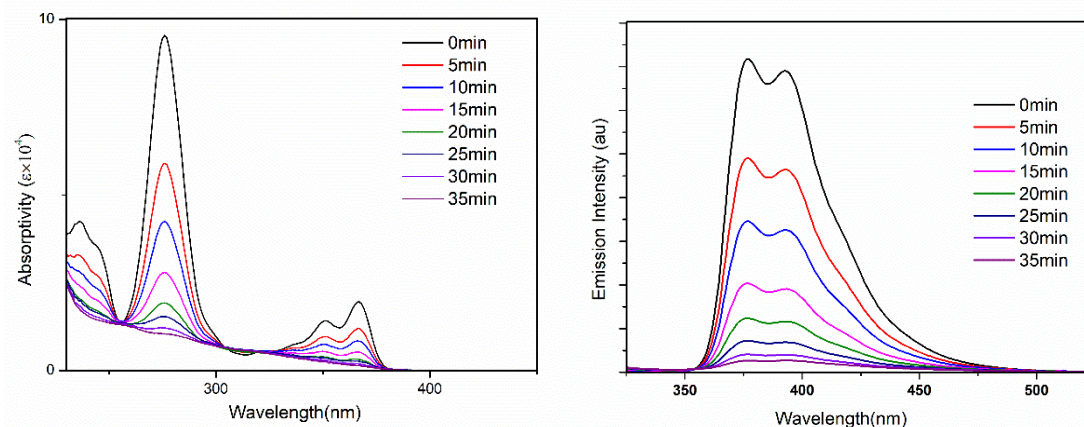


**Figure 4.9:** Absorption (left) and emission spectra (right) of compound **4** in THF (10<sup>-5</sup> M) after passing of UV light (365 nm).

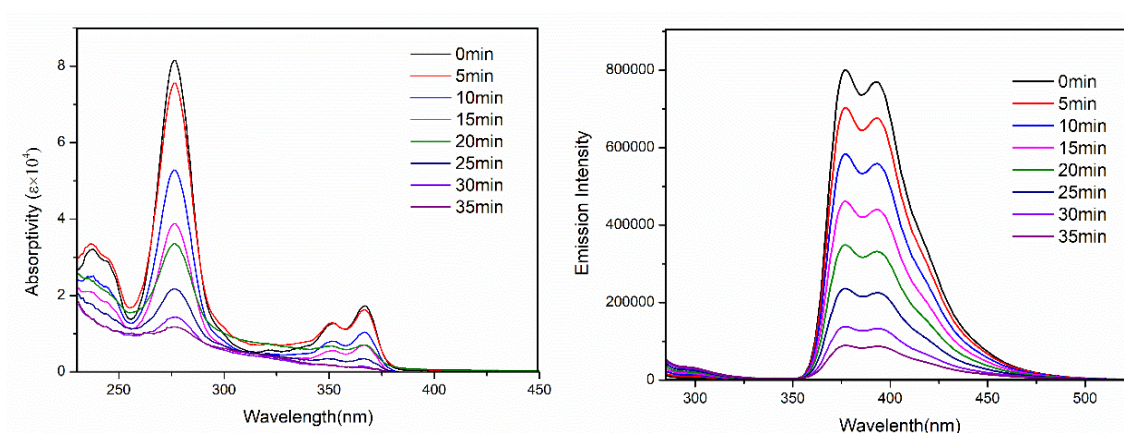


**Figure 4.10:** Absorption (left) and emission spectra (right) of compound **3** in THF (10<sup>-5</sup> M) after passing of UV light (365 nm).

It is worth noting that compound **5** showed quick response over compound **3** and **4**; although the reasons for this quick response is not known, we think that better electron donating nature of 'isopropyl' makes it more reactive under the conditions mentioned above.

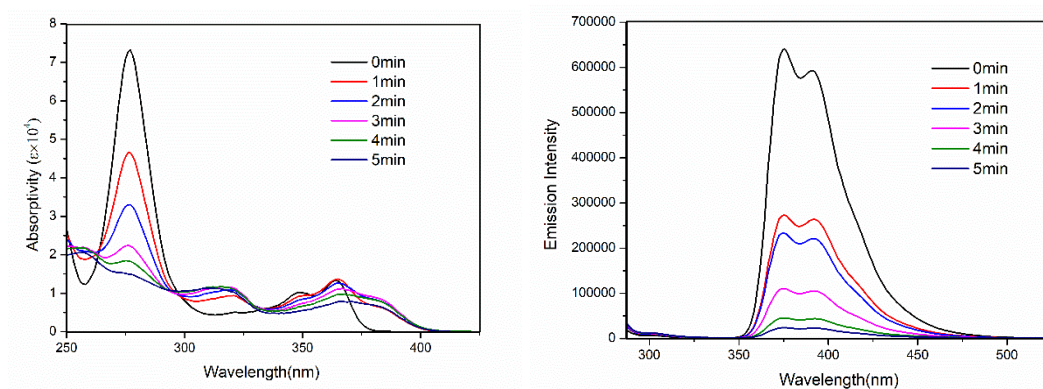


**Figure 4.11:** Absorption (left) and emission spectra (right) of compound **5** in THF ( $10^{-5}$  M) after passing of UV light (365 nm).

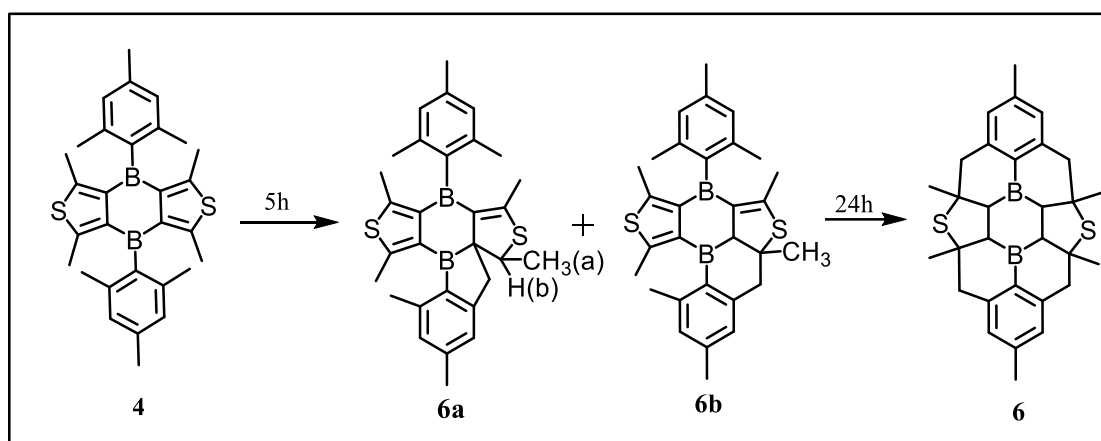


**Figure 4.12:** Plausible product formation after photoirradiation of compound **4**.

To investigate the species formed upon irradiation at 365 nm, the  $^1\text{H}$  NMR of compound **4** in  $\text{C}_6\text{D}_6$  was recorded after 5h irradiation (Figure 4.13). After 5h, the  $^1\text{H}$  and  $^{13}\text{C}$  DEPT-135 experiment reveals the presence of two species **6a** and **6b** (Figure 4.12). Formation of a doublet (Figure 4.13,  $\text{CH}_3$  (a)) at 1.26 ppm and quartet at 3.38 ppm (H(b)) was observed, which corresponds to species **6a**. The observed pattern is similar to the product reported by Yamaguchi and co-workers<sup>68</sup> for the photochemical intramolecular 1,6-sigmatropic rearrangement reaction of dimesityl(2,5-dimethyl-3-thienyl)borane (Figure 4.13). In addition to that presence of two carbons ( $-\text{CH}_2-$ ) with different environment was also observed using  $^{13}\text{C}$  DEPT-135 experiment (Figure



**4.14**), which suggest that more than one species is formed during the photoirradiation.

The second species is assigned as **6b**.

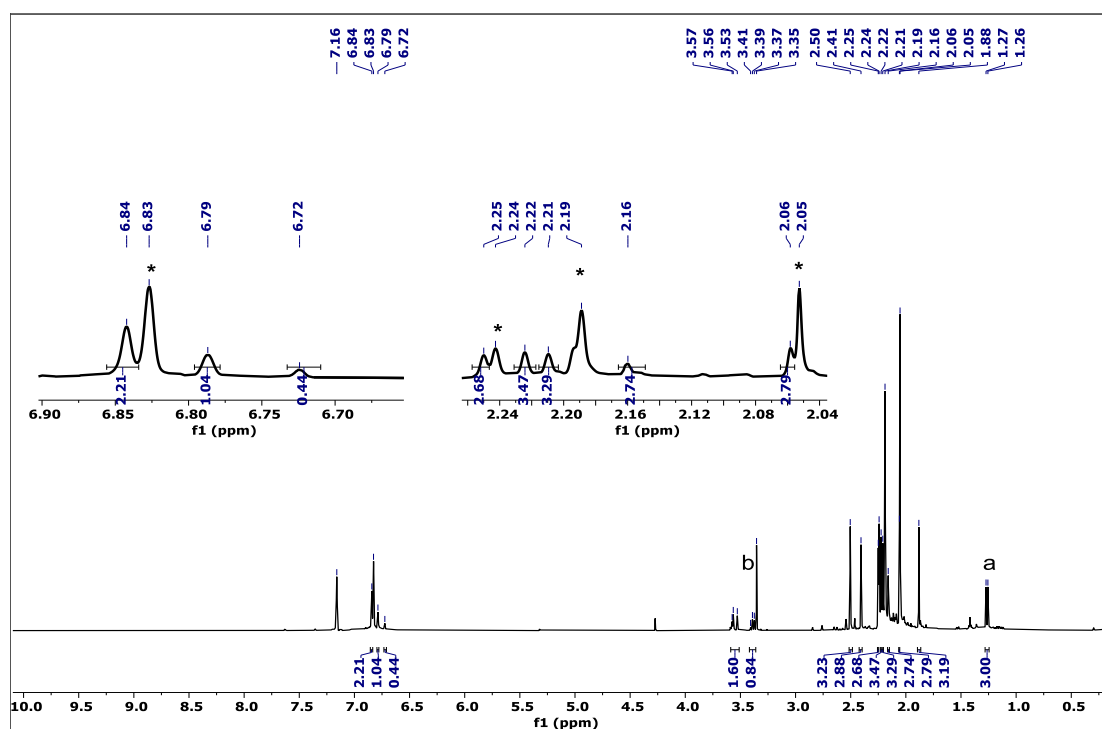


**Figure 4.13:**  $^1\text{H}$  NMR spectrum of compound **4** in  $\text{C}_6\text{D}_6$  after irradiation of UV light for 5h. Starting material peaks are marked with asterisk (\*).

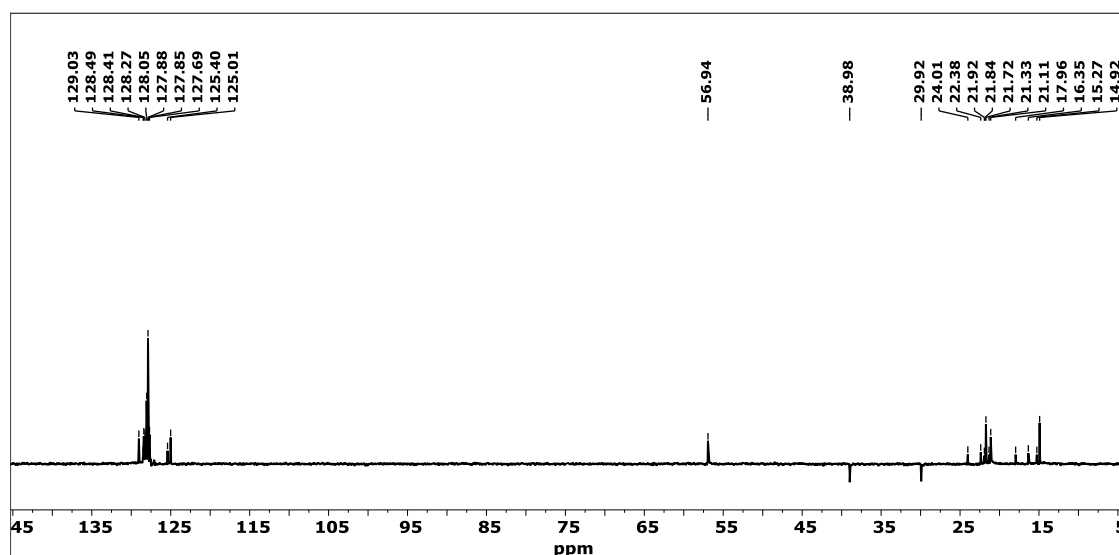


**Figure 4.14:**  $^{13}\text{C}$  DEPT-135 NMR spectrum of compound **4** in  $\text{C}_6\text{D}_6$  after irradiation of UV light for 5h.

However, after 24h photoirradiation, presence of a symmetrical product **6** was observed. Product **6** was confirmed by  $^1\text{H}$  and  $^{13}\text{C}$  DEPT-135 NMR experiment (Figure 4.15 and figure 4.16). A similar phenomenon was observed for compound **3** and **5**. Our attempts to revert the reaction by heating or passing visible light were not successful. Further studies are needed to reveal the pathways involved in this process and also other species involved in the processes.

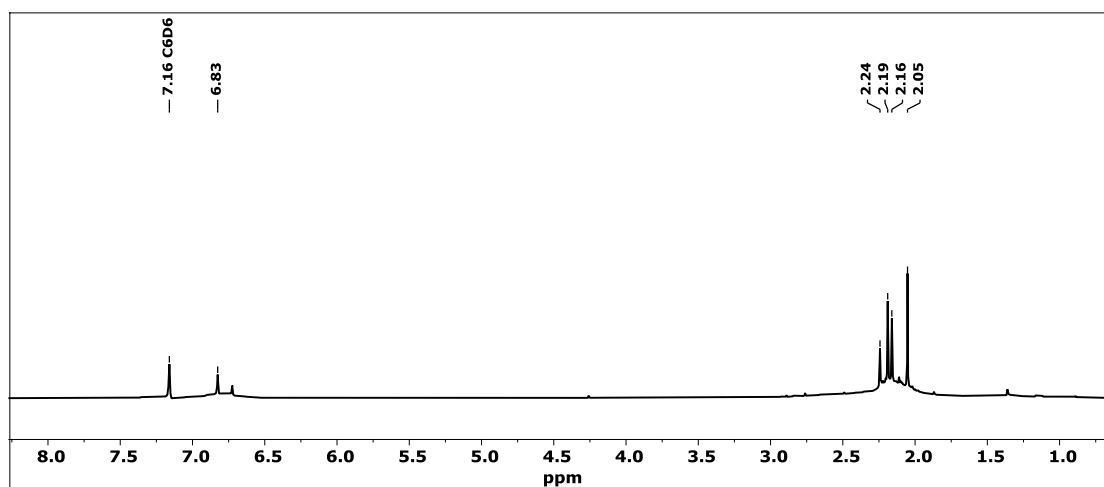


**Figure 4.15:**  $^1\text{H}$  NMR of compound **4** in  $\text{C}_6\text{D}_6$  after irradiation of UV light for 24h.

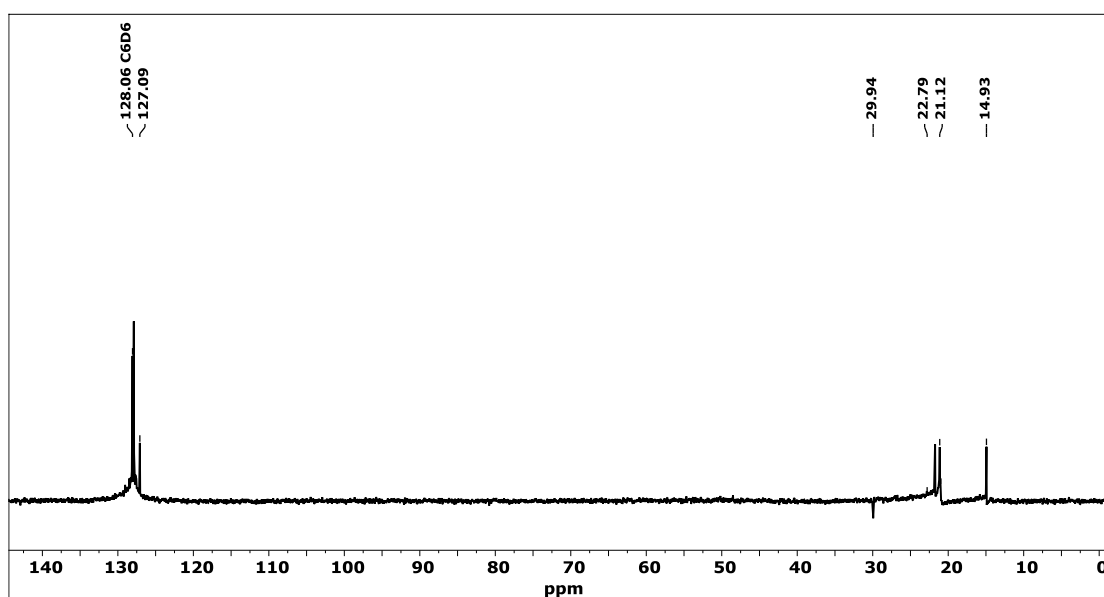


**Figure 4.16:**  $^{13}\text{C}$  DEPT-135 NMR spectrum of compound **4** in  $\text{C}_6\text{D}_6$  after irradiation of UV light for 24h.

---

### 4.3 Conclusions

In conclusion, we established a synthetic route to the thiophene fused analogues diboraanthracenes starting from 3,4-bis(chloromercurio)2,5-dimethylthiophene. The halogenated dichlorodiboradithiophene (**2**) serves as a precursor to make other derivatives **3-5**. The diboradithiophene's **3-5** are stable in air, and showed interesting optical and electrochemical properties. Upon photoirradiation, the absorption and the emission intensity of compounds **3-5** decreases gradually which was exploited for the detection of UV radiation.

### 4.4 Experimental section

#### 4.4.1 General information

All reagents and starting materials were purchased from Sigma-Aldrich, Alfa-Aesar and Spectrochem chemical companies and used as received unless otherwise noted. Dichloromethane was distilled from  $\text{CaH}_2$ . Cyclohexane, THF, DME and toluene were distilled from Na/benzophenone prior to use. All 400 MHz  $^1\text{H}$ , 100 MHz  $^{13}\text{C}$ , NMR spectra were recorded on a Bruker ARX 400 spectrometer operating at 400 MHz. All  $^1\text{H}$  and  $^{13}\text{C}$  NMR spectra were referenced internally to solvent signals. All NMR spectra were recorded at ambient temperature. ESI mass spectra were recorded on Bruker, microTOF-QII mass spectrometer. The absorbance spectra were recorded on a JASCO V-730 UV-Visible spectrometer. The fluorescence spectra were recorded using Edinburgh FS5 spectrofluorometer. Absolute fluorescence quantum yields of compounds **3-5** were measured by integrating sphere method using Edinburgh FS30 spectrofluorometer. The fluorescence spectra are corrected for the instrumental response. Cyclic voltammetry measurements were performed with a conventional three electrode cell using an electrochemical workstation (CH Instrument, Model: 1100A)

The three-electrode system consisted of a Glassy carbon working electrode, a Pt wire as the secondary electrode, and a Ag wire as the reference electrode. The voltammograms were recorded with ca.  $1.0 \times 10^{-3}$  M solution in DME containing  $\text{Bu}_4\text{NPF}_6$  (0.1 M) as the supporting electrolyte. The scans were referenced after the addition of a small amount of ferrocene as the internal standard. Single-crystal X-ray diffraction data for compound **3** were collected on a Rigaku SuperNova fine-focused dual diffractometer, with Cu  $K\alpha$  radiation ( $\lambda = 1.54178 \text{ \AA}$ ) equipped with a PILATUS200K detector and for compound **4** were collected on a Bruker APEX-II diffractometer using Mo- $K\alpha$  radiation ( $0.71073 \text{ \AA}$ ). Using Olex2, the structures were solved with the ShelXS structure solution program using Direct Methods and refined with the ShelXL refinement package using Least Squares minimization. All non-hydrogen atoms were refined with anisotropic displacement coefficients. The H atoms were placed at calculated positions and were refined as riding atoms.

#### 4.4.2 Synthetic procedures and spectral characterisations

##### 4.4.2.1 Synthesis of compound **2**

To a suspension of 3,4-bis(chloromercurio)2,5-dimethylthiophene (**1**) (2.00 g, 3.42 mmol) in toluene (50 mL) in a seal tube was added  $\text{BCl}_3$  (4 mL in  $\text{CH}_2\text{Cl}_2$ ) inside a glovebox. The tube was closed and heated at  $100^\circ\text{C}$  in an oil bath for 12h. After cooling to room temp, the resulting mixture was filtered inside the glovebox and kept for crystallization. Fluffy white needles formed were filtered to give compound **2**. Yield: 0.322 g (30%).  $^1\text{H}$  NMR (400 MHz,  $\text{CDCl}_3$ )  $\delta$  2.82 (s, 12H).  $^{13}\text{C}$  NMR (101 MHz,  $\text{CDCl}_3$ )  $\delta$ =155.27, 128.38, 17.35.  $^{11}\text{B}$  NMR (128 MHz,  $\text{CDCl}_3$ )  $\delta$ =49.96.

##### General procedure for the synthesis of compounds **3-5**

A solution of arylmagnesium bromide (6 mL, 1M in THF) was added to a solution of compound **2** (0.50 g) in toluene (20 mL) in a sealed tube. The resulting mixture was

then refluxed for 12h. After 12h, the compound was extracted with water and dichloromethane (3 x 50 mL). The organic phase was collected and dried over anhydrous sodium sulphate. The solvent was concentrated and the product was purified using silica gel column chromatography (EtOAc/ *n*-hexane (5:95)).

#### 4.4.2.2 Synthesis of compound 3

The quantities involved are as follows, xylylmagnesium bromide (6 mL, 1M in THF), compound **2** (0.50 g), and toluene (20 mL). Yield: 0.298 g (41%). Mp: 248 °C. <sup>1</sup>H NMR (400 MHz, CDCl<sub>3</sub>) δ= 7.18 - 7.14 (m, 2H), 7.01 (d, *J* = 4.0 Hz, 4H), 2.17 (s, 12H), 1.96 (s, 12H). <sup>13</sup>C NMR (101 MHz, CDCl<sub>3</sub>) δ=156.29, 145.14, 136.17, 126.83, 126.58, 21.97, 14.97. <sup>11</sup>B NMR (128 MHz, CDCl<sub>3</sub>) δ=56.71. HR-MS (ESI): calcd for C<sub>28</sub>H<sub>30</sub>B<sub>2</sub>S<sub>2</sub>[M+H]<sup>+</sup>: 453.2058, Found: 453.2042. Anal. Calcd for C<sub>28</sub>H<sub>30</sub>B<sub>2</sub>S<sub>2</sub>: C 74.36; H 6.69; S 14.18. Found: C 75.28; H 6.50; S 15.48 IR (KBr): ν (cm<sup>-1</sup>) = 2959(m), 2912(m), 1607(m), 1463(m), 1259(m), 1104(m), 761(m), 699(m).

#### 4.4.2.3 Synthesis of compound 4

The quantities involved are as follows, mesitylmagnesium bromide (6 mL, 1M in THF), compound **2** (0.50 g), and toluene (20 mL). Yield: 0.312g (40%). Mp: 253 °C. <sup>1</sup>H NMR (400 MHz, CDCl<sub>3</sub>) δ = 6.84 (s, 4H), 2.33 (s, 6H), 2.12 (s, 12H), 1.97 (s, 12H). <sup>13</sup>C NMR (101 MHz, CDCl<sub>3</sub>) δ = 156.26, 145.49, 144.24, 136.26, 136.16, 127.57, 21.98, 21.37, 15.10. <sup>11</sup>B NMR (128 MHz, CDCl<sub>3</sub>) δ = 56.36. HR-MS (ESI): calcd for C<sub>30</sub>H<sub>34</sub>B<sub>2</sub>S<sub>2</sub>[M+H]<sup>+</sup>: 481.2371, Found: 481.2348. Anal. Calcd for C<sub>30</sub>H<sub>34</sub>B<sub>2</sub>S<sub>2</sub>: C 75.02; H 7.13; S 13.35. Found: C 74.89; H 7.037; S 13.525. IR (KBr): ν (cm<sup>-1</sup>) = 2959(m), 2910(m), 1605(m), 1465(m), 1302(m), 1255(m), 1104(m), 851(m), 794(m), 681(m).

#### 4.4.2.4 Synthesis of compound 5

The quantities involved are as follows, 2,4,6-triisopropylphenylmagnesium bromide (6 mL, 1M in THF), compound **2** (0.50 g), and toluene (20 mL). Yield: 0.328g (32%). Mp:

255 °C.  $^1\text{H}$  NMR (400 MHz,  $\text{CDCl}_3$ )  $\delta$  = 7.00 (s, 4H), 2.92 (h,  $J$  = 8 Hz, 2H), 2.61 (h,  $J$  = 8 Hz, 4H), 1.98 (s, 12H), 1.29 (d,  $J$  = 8 Hz, 2H), 1.11 (d,  $J$  = 8 Hz, 24H).  $^{13}\text{C}$  NMR (101 MHz,  $\text{CDCl}_3$ )  $\delta$  = 156.12, 148.40, 146.96, 120.44, 34.94, 34.34, 24.41, 24.33, 15.87.  $^{11}\text{B}$  NMR (128 MHz,  $\text{CDCl}_3$ )  $\delta$  = 57.79. HR-MS (ESI): calcd for  $\text{C}_{42}\text{H}_{58}\text{B}_2\text{S}_2[\text{M}+\text{Na}]^+$ : 671.4072, Found: 671.4033. Anal. Calcd for  $\text{C}_{42}\text{H}_{58}\text{B}_2\text{S}_2$ : C, 77.77; H, 9.01; S, 9.88. Found: C, 76.168; H, 8.68; S, 10.107. IR (KBr):  $\nu$  ( $\text{cm}^{-1}$ ) = 2959(m), 2925(m), 1602(m), 1455(m), 1247(m), 1090(m), 876(m), 790(m), 689(m).

#### 4.5 References

1. Anthony, J. E. *Chem. Rev.* **2006**, *106*, 5028.
2. Bendikov, M.; Wudl, F.; Perepichka, D. F. *Chem. Rev.* **2004**, *104*, 4891.
3. Wu, J.; Pisula, W.; Müllen, K. *Chem. Rev.* **2007**, *107*, 718.
4. Fukazawa, A.; Yamaguchi, S. *Chem. Asian J.* **2009**, *4*, 1386.
5. Carter, K. P.; Young, A. M.; Palmer, A. E. *Chem. Rev.* **2014**, *114*, 4564.
6. Lavis, L. D.; Raines, R. T. *ACS Chem. Bio.* **2014**, *9*, 855.
7. Yang, Y.; Zhao, Q.; Feng, W.; Li, F. *Chem. Rev.* **2013**, *113*, 192.
8. Chan, J.; Dodani, S. C.; Chang, C. J. *Nat. Chem.* **2012**, *4*, 973.
9. Ni, Y.; Wu, J. *Org. Biomol. Chem.* **2014**, *12*, 3774.
10. Gorka, A. P.; Nani, R. R.; Schnermann, M. J. *Org. Biomol. Chem.* **2015**, *13*, 7584.
11. Zheng, H.; Zhan, X.-Q.; Bian, Q.-N.; Zhang, X.-J. *Chem. Commun.* **2013**, *49*, 429.
12. Chen, X.; Pradhan, T.; Wang, F.; Kim, J. S.; Yoon, J. *Chem. Rev.* **2012**, *112*, 1910.
13. Dhbaibi, K.; Favereau, L.; Crassous, J. *Chem. Rev.* **2019**, *119*, 8846.
14. Hirai, M.; Tanaka, N.; Sakai, M.; Yamaguchi, S. *Chem. Rev.* **2019**, *119*, 8291.
15. Narita, A.; Wang, X.-Y.; Feng, X.; Müllen, K. *Chem. Soc. Rev.* **2015**,

---

44,6616.

16. Stępień, M.; Gońka, E.; Żyła, M.; Sprutta, N. *Chem. Rev.* **2017**, *117*, 3479.
17. Jia, W.-L.; Bai, D.-R.; McCormick, T.; Liu, Q.-D.; Motala, M.; Wang, R.-Y.; Seward, C.; Tao, Y.; Wang, S. *Chem. Eur. J.* **2004**, *10*, 994.
18. Noda, T.; Ogawa, H.; Shirota, Y. *Adv. Mater.* **1999**, *11*, 283.
19. Shirota, Y.; Kinoshita, M.; Noda, T.; Okumoto, K.; Ohara, T. *J. Am. Chem. Soc.* **2000**, *122*, 11021.
20. Lin, S.-L.; Chan, L.-H.; Lee, R.-H.; Yen, M.-Y.; Kuo, W.-J.; Chen, C.-T.; Jeng, R.-J. *Adv. Mater.* **2008**, *20*, 3947.
21. Jia, W. L.; Feng, X. D.; Bai, D. R.; Lu, Z. H.; Wang, S.; Vamvounis, G. *Chem. Mater.* **2005**, *17*, 164.
22. Yang, T.; Cheng, Z.; Li, Z.; Liang, J.; Xu, Y.; Li, C.; Wang, Y. *Adv. Funct. Mater.* **2020**, *30*, 2002681.
23. Yuan, Z.; Entwistle, C. D.; Collings, J. C.; Albesa-Jové, D.; Batsanov, A. S.; Howard, J. A. K.; Taylor, N. J.; Kaiser, H. M.; Kaufmann, D. E.; Poon, S.-Y.; Wong, W.-Y.; Jardin, C.; Fathallah, S.; Boucekkine, A.; Halet, J.-F.; Marder, T. B. *Chem. Eur. J.* **2006**, *12*, 2758.
24. Yuan, Z.; Collings, J. C.; Taylor, N. J.; Marder, T. B.; Jardin, C.; Halet, J.-F. *J. Solid State Chem.* **2000**, *154*, 5.
25. Yuan, Z.; Taylor, N. J.; Marder, T. B.; Williams, I. D.; Kurtz, S. K.; Cheng, L.-T. *J. Chem. Soc. Chem. Commun.* **1990**, 1489.
26. Yuan, Z.; Taylor, N. J.; Ramachandran, R.; Marder, T. B. *Appl. Organomet. Chem.* **1996**, *10*, 305.
27. Branger, C.; Lequan, M.; Lequan, R. M.; Barzoukas, M.; Fort, A. *J. Mater. Chem.* **1996**, *6*, 555.

- 
28. Sa, S.; Mukundam, V.; Kumari, A.; Das, R.; Venkatasubbaiah, K. *Dalton Trans.* **2021**, *50*, 6204.
29. Yamaguchi, S.; Akiyama, S.; Tamao, K. *J. Am. Chem. Soc.* **2001**, *123*, 11372.
30. Parab, K.; Venkatasubbaiah, K.; Jäkle, F. *J. Am. Chem. Soc.* **2006**, *128*, 12879.
31. Zhou, G.; Baumgarten, M.; Müllen, K. *J. Am. Chem. Soc.* **2008**, *130*, 12477.
32. Bai, D.-R.; Liu, X.-Y.; Wang, S. *Chem. Eur. J.* **2007**, *13*, 5713.
33. Kim, Y.; Gabbaï, F. P. *J. Am. Chem. Soc.* **2009**, *131*, 3363.
34. Melaimi, M.; Gabbaï, F. P. *J. Am. Chem. Soc.* **2005**, *127*, 9680.
35. Chai, J.; Wang, C.; Jia, L.; Pang, Y.; Graham, M.; Cheng, S. Z. D. *Synth. Met.* **2009**, *159*, 1443.
36. Lorbach, A.; Bolte, M.; Li, H.; Lerner, H.-W.; Holthausen, M. C.; Jäkle, F.; Wagner, M. *Angew. Chem. Int. Ed.* **2009**, *48*, 4584.
37. Lorbach, A.; Bolte, M.; Lerner, H.-W.; Wagner, M. *Chem. Commun.* **2010**, *46*, 3592.
38. Januszewski, E.; Lorbach, A.; Grewal, R.; Bolte, M.; Bats, J. W.; Lerner, H.-W.; Wagner, M. *Chem. Eur. J.* **2011**, *17*, 12696.
39. Hoffend, C.; Diefenbach, M.; Januszewski, E.; Bolte, M.; Lerner, H.-W.; Holthausen, M. C.; Wagner, M. *Dalton Trans.* **2013**, *42*, 13826.
40. Durka, K.; Głowacki, I.; Luliński, S.; Łuszczynska, B.; Smętek, J.; Szczepanik, P.; Serwatowski, J.; Wawrzyniak, U. E.; Wesela-Bauman, G.; Witkowska, E.; Wiosna-Sałyga, G.; Woźniak, K. *J. Mater. Chem. C* **2015**, *3*, 1354.
41. Kirschner, S.; Mewes, J.-M.; Bolte, M.; Lerner, H.-W.; Dreuw, A.; Wagner, M. *Chem. Eur. J.* **2017**, *23*, 5104.
42. Su, X.; Bartholome, T. A.; Tidwell, J. R.; Pujol, A.; Yruegas, S.; Martinez, J. J.; Martin, C. D. *Chem. Rev.* **2021**, *121*, 4147.
-



- 
43. Agou, T.; Sekine, M.; Kawashima, T. *Tetrahedron Lett.* **2010**, *51*, 5013.
44. Böhnke, J.; Braunschweig, H.; Jiménez-Halla, J. O. C.; Krummenacher, I.; Stennett, T. E. *J. Am. Chem. Soc.* **2018**, *140*, 848.
45. Chen, E. Y.-X.; Marks, T. J. *Chem. Rev.* **2000**, *100*, 1391.
46. Venkatasubbaiah, K.; Pakkirisamy, T.; Lalancette, R. A.; Jäkle, F. *Dalton Trans.* **2008**, 4507.
47. Senkovskiy, B. V.; Usachov, D. Y.; Fedorov, A. V.; Marangoni, T.; Haberer, D.; Tresca, C.; Profeta, G.; Caciuc, V.; Tsukamoto, S.; Atodiresei, N.; Ehlen, N.; Chen, C.; Avila, J.; Asensio, M. C.; Varykhalov, A. Y.; Nefedov, A.; Wöll, C.; Kim, T. K.; Hoesch, M.; Fischer, F. R.; Grüneis, A. *ACS Nano* **2018**, *12*, 7571.
48. Novoa, J. J.; Rovira, M. C.; Rovira, C.; Veciana, J.; Tarrés, J. *Adv. Mater.* **1995**, *7*, 233.
49. Ren, Y.; Jäkle, F. *Dalton Trans.* **2016**, *45*, 13996.
50. Chen, P.; Lalancette, R. A.; Jäkle, F. *J. Am. Chem. Soc.* **2011**, *133*, 8802.
51. Yin, X.; Guo, F.; Lalancette, R. A.; Jäkle, F. *Macromolecules* **2016**, *49*, 537.
52. Helten, H. *Chem. Asian J.* **2019**, *14*, 919.
53. Iida, A.; Yamaguchi, S. *J. Am. Chem. Soc.* **2011**, *133*, 6952.
54. Mercier, L. G.; Piers, W. E.; Harrington, R. W.; Clegg, W. *Organometallics* **2013**, *32*, 6820.
55. Asgarouladi, B.; Full, R.; Schaper, K.-J.; Siebert, W. *Chem. Ber.* **1974**, *107*, 34.
56. Levine, D. R.; Messersmith, R. E.; Siegler, M. A.; Tovar, J. D. *Can. J. Chem.* **2017**, *95*, 381.
57. Müller, P.; Huck, S.; Köppel, H.; Pritzkow, H.; Siebert, W. *Z. Naturforsch. B* **1995**, *50*, 1476.
-

- 
58. Chai, J.; Wang, C.; Jia, L.; Pang, Y.; Graham, M.; Cheng, S. Z. D. *Synth. Met.*, **2009**, *159*, 1443.
59. Reus, C.; Weidlich, S.; Bolte, M.; Lerner, H-W; Wagner, M. *J. Am.Chem. Soc.*, **2013**, *135*, 12892.
60. Venkatasubbaiah, K.; Zakharov, L. N.; Kassel, W. S.; Rheingold, A. L.; Jäkle, F. *Angew. Chem., Int. Ed.*, **2005**, *44*, 5428.
61. Venkatasubbaiah, K.; Nowik, I.; Herber, R. H.; Jäkle, F. *Chem. Commun.*, **2007**, 2154.
62. Mellerup, S. K.; Rao, Y. L.; Amarne, H.; Wang, S. *Org. Lett.* **2016**, *18*, 4436.
63. Li, C.; Mellerup, S. K.; Wang, X.; Wang, S. *Organometallics* **2018**, *37*, 3360.
64. Li, H. J.; Mellerup, S. K.; Wang, X.; Wang, S. *Chem. Commun.* **2018**, *54*, 8245.
65. Mellerup, S. K.; Li, C.; Radtke, J.; Wang, X.; Li, Q. S.; Wang, S. *Angew. Chem.* **2018**, *57*, 9634.
66. Radtke, J.; Mellerup, S. K.; Bolte, M.; Lerner, H. W.; Wang, S.; Wagner, M. *Org. Lett.* **2018**, *20*, 3966.
67. Wang, S.; Yuan, K.; Hu, M. F.; Wang, X.; Peng, T.; Wang, N.; Li, Q. S. *Angew. Chem.* **2018**, *57*, 1073.
68. Ando, N.; Fukazawa, A.; Kushida, T.; Shiota, Y.; Itoyama, S.; Yoshizawa, K.; Matsui, Y.; Kuramoto, Y.; Ikeda, H.; Yamaguchi, S. *Angew. Chem. Int. Ed.*, **2017**, *56*, 12210.
-

## **CHAPTER 5A**

### **Tetraaryl pyrazole based four coordinated boron compounds: Synthesis, Characterisation and AIEE Phenomenon**

<b>5A.1 Introduction</b>	137
<b>5A.2 Results and discussion</b>	138
<b>5A.2.1 Synthesis and characterisation</b>	138
<b>5A.2.2 X-Ray studies</b>	141
<b>5A.2.3 Photophysical properties</b>	146
<b>5A.2.4 AIEE studies</b>	150
<b>5A.2.5 Picric acid sensing using compound 18</b>	157
<b>5A.2.6 Electrochemical properties</b>	159
<b>5A.3 Conclusions</b>	160
<b>5A.4 Experimental section</b>	160
<b>5A.4.1 General information</b>	160
<b>5A.4.2 Synthetic procedures and spectral characterisations</b>	161
<b>5A.5 References</b>	171



---

### 5A.1 Introduction

Considerable efforts have been made in the development of new and tunable organic fluorophores due to their low manufacturing cost and potential use in optoelectronic applications. However, many fluorophores suffer from aggregation-caused quenching i.e. fluorophores showed reduced emission in the aggregate state in comparison to their dilute solutions.<sup>1-3</sup> The materials used in making the devices are in the form of solids or thin films, hence it is important to have enhanced emission in the solid state. Aggregation induced emission introduced by Tang and coworkers,<sup>4</sup> exhibit strong emission in the solid state or in the aggregate state. This phenomenon which is opposite of the aggregation caused quenching (ACQ) has attracted many researchers to invent structurally tailored molecules with applications ranging from chemosensing, bioimaging, optoelectronics to stimuli-responsive properties.<sup>5-24</sup>

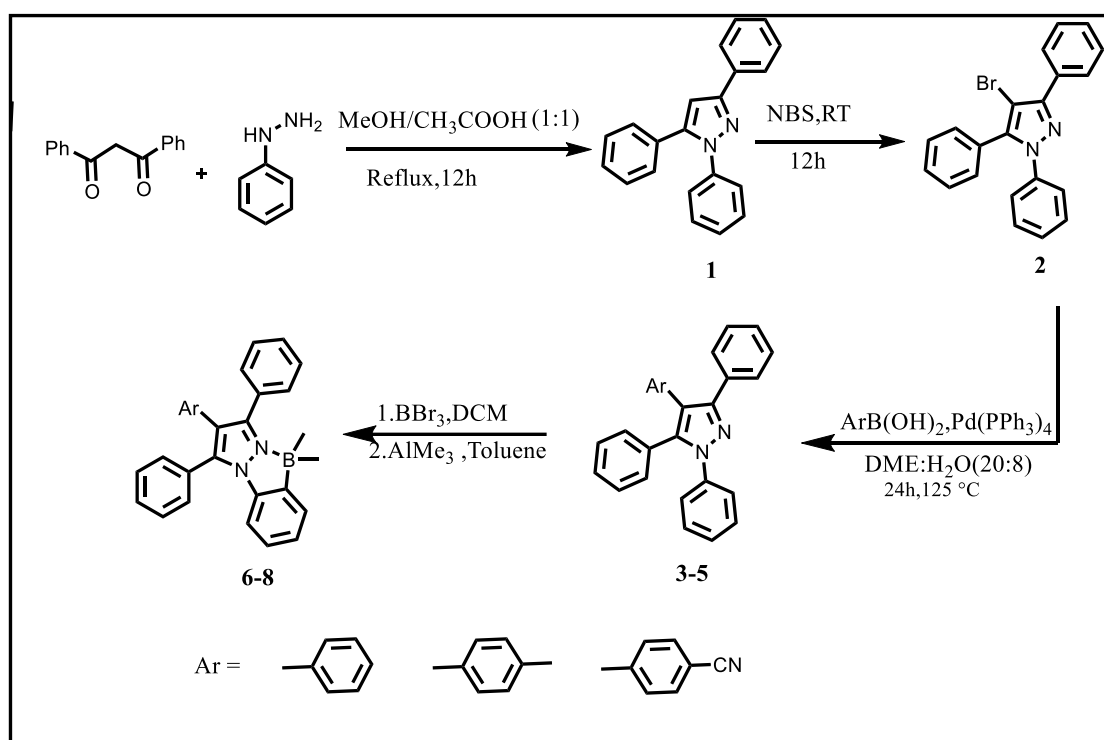
Boron derivatives have received considerable attention due to their exceptional properties such as high stability, light absorption, emission and electron acceptability. These properties made them widely useful in organic light emitting devices, fluorescent sensors, nonlinear optics and biomolecular probes.<sup>25-50</sup> Among various boron containing fluorophores, four-coordinated boron compounds have received particular interest owing to their stability over tri-coordinated boron compounds.<sup>51-56</sup> Of different four coordinated boron compounds, boron dipyrromethene (BODIPY) compounds have received much attention due to their high quantum yields in the solution phase.<sup>57-59</sup> However, most of the boron dipyrromethene compounds show ACQ and small Stokes shift. To overcome this problem, different strategies have been developed, among them synthesis of new AIEE luminogens which attracted many researchers around the world. This strategy helped to make many organic luminogens such as tetraphenylethene,<sup>60</sup> triphenylethene,<sup>61</sup> distyrylanthracene,<sup>62</sup> tetraphenyl-1,4-butadiene<sup>63</sup> and so on.

However, the number of luminogens especially boron containing luminogens with AIEE are still scarce. This chapter describes a new family of B-N coordinated AIEE luminogens based on pyrazoles.

## 5A.2 Results and discussion

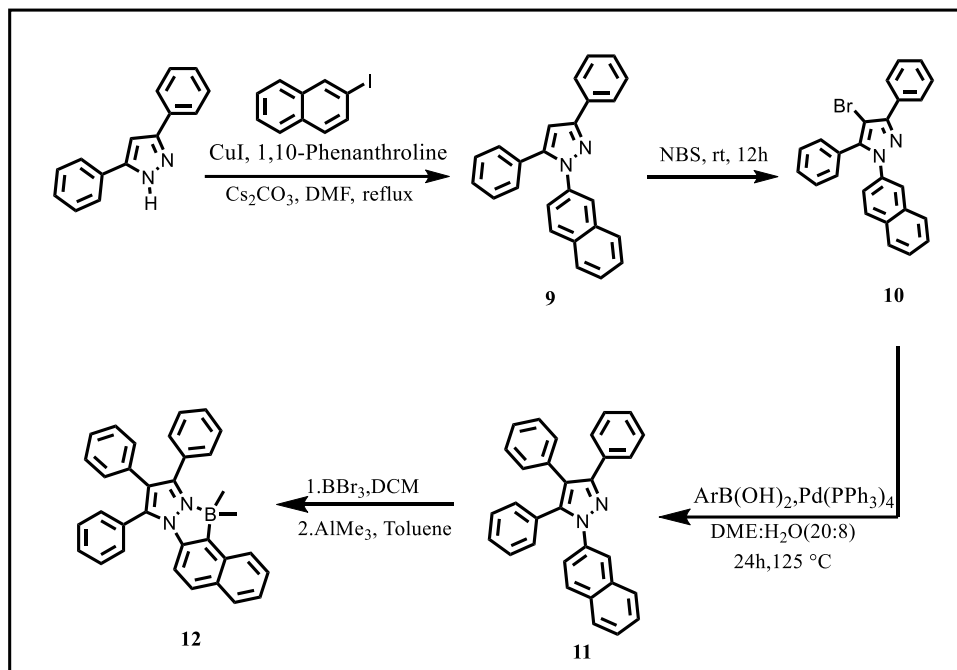
### 5A.2.1 Synthesis and characterisation

The synthetic routes to synthesize tetraaryl pyrazole based four coordinate boron compounds **6-8**, **12** and **18** are illustrated in scheme 5A.1, 5A.2 and 5A.3 respectively. Compound **1** was synthesized using condensation of 1,3-diphenyl-1,3-propanedione with phenyl hydrazine in methanol:acetic acid (1:1) under reflux condition. Bromination of compound **1** using N-bromosuccinimide(NBS) afforded the bromopyrazole compound **2**. Tetraaryl pyrazoles **3-5** were synthesized using Suzuki coupling reaction between compound **2** and different aryl boronic acid.<sup>64,65</sup>



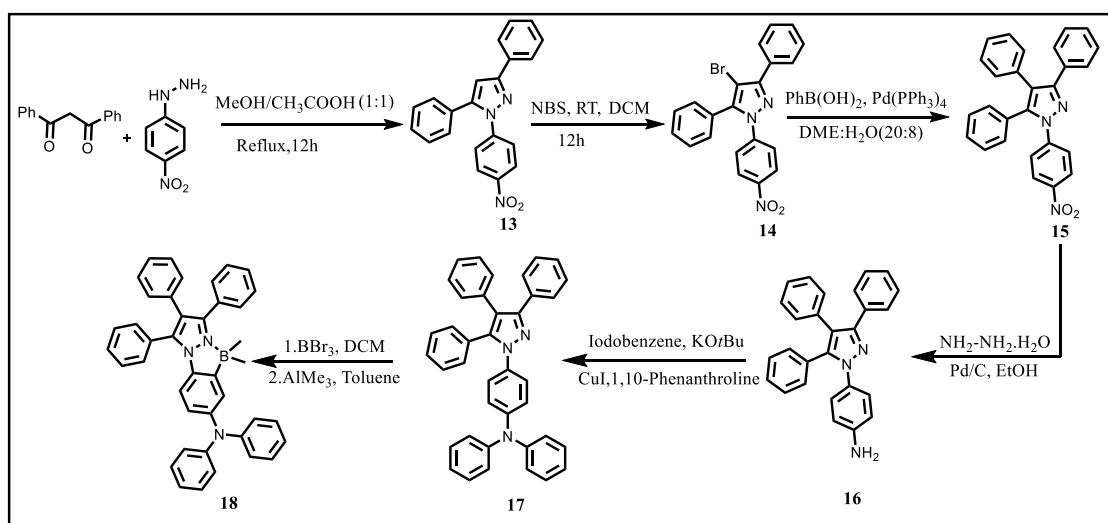
**Scheme 5A.1:** Synthesis of compounds **6-8**.

Compound **9** was prepared using Cu-catalysed Ullman coupling reaction between 3,5-diphenyl-1H-pyrazole and iodonaphthalene. A similar protocol is used as mentioned above( compound **3-5**) for the synthesis of compound **11** in moderate yield.



**Scheme 5A.2:** Synthesis of compound **12**.

Compound **15** was prepared following a similar methodology mentioned above starting from 4-nitrophenylhydrazine as shown in scheme **5A.3**. Reduction of compound **15** using Pd/C and hydrazine monohydrate produces compound **16**.



**Scheme 5A.3:** Synthesis of compound **18**.

Compound **17** was prepared using Ullman coupling between compound **16** and iodobenzene. Electrophilic aromatic borylation of compounds **3-5**, **11** and **17** using  $\text{BBr}_3$  and  $N,N$ -diisopropylethylamine (DIPEA) in dichloromethane yielded the dibromoboron compounds. Without further purification, the dibromoboron compounds were treated with  $\text{AlMe}_3$  to give the tetraryl pyrazole based boron compounds **6-8**, **12** and **18**. These compounds are stable in air and moisture. The crude products were purified through silica gel column chromatography. All the boron compounds were fully characterized with  $^1\text{H}$ ,  $^{13}\text{C}$ ,  $^{11}\text{B}$  NMR and HRMS. The  $^1\text{H}$  NMR of all boron compounds show a signal  $\sim 0.2$  ppm, which corresponds to  $-\text{BMe}_2$  proton. The  $^{11}\text{B}$  NMR of the complexes showed a resonance at  $\sim 1$  ppm, which confirms the presence of a tetracoordinated boron compound. For an illustration,  $^1\text{H}$  and  $^{11}\text{B}$  NMR spectra of compound **6** are shown in figure 5A.1 and figure 5A.2 respectively. All boron compounds showed characteristic  $[\text{M}+\text{H}]^+$  peak in the HRMS. Representative HRMS of compound **6** is given in figure 5A.3.

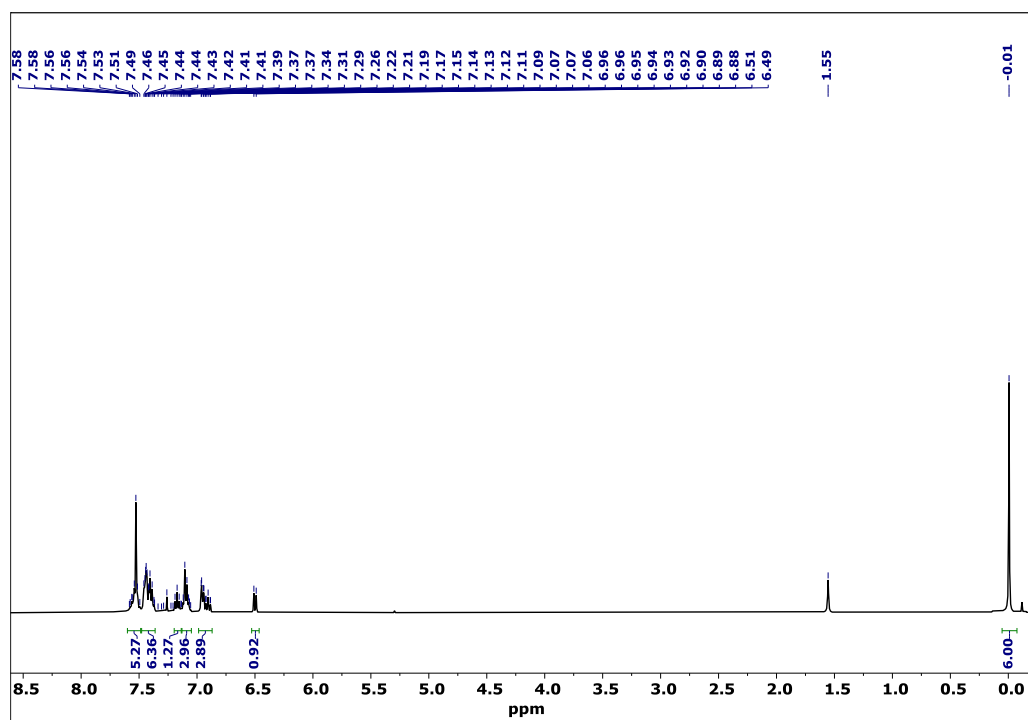


**Figure 5A.1:**  $^1\text{H}$  NMR spectrum of compound **6** in  $\text{CDCl}_3$ .



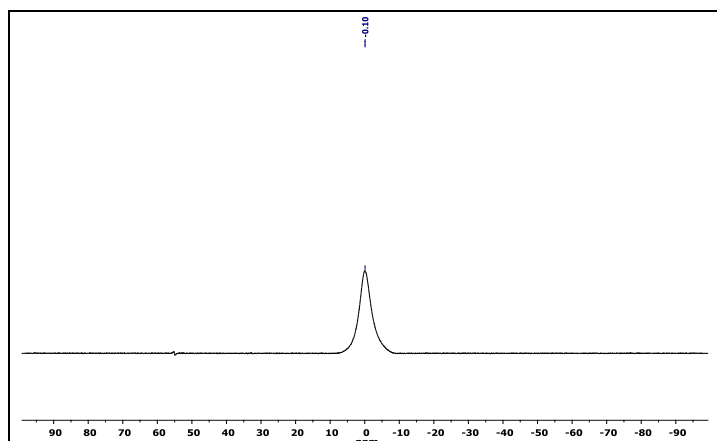


**Figure 5A.2:**  $^{11}\text{B}$  NMR spectrum of compound **6** in  $\text{CDCl}_3$ .

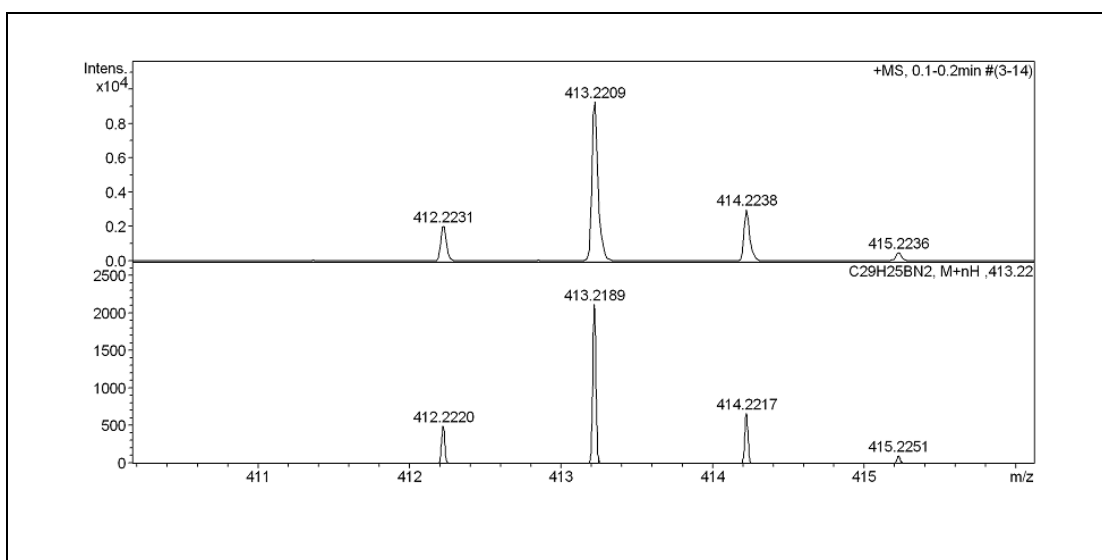


**Figure 5A.3:** HRMS spectrum of compound **6**.

### 5A.2.2 X-Ray studies

Single crystals of boron compounds **6-8** and **12** were grown from slow evaporation of a dichloromethane and hexane mixture. Compounds **6**, **7** and **12** are crystallised in a monoclinic space group of  $P2_1/c$  while compound **8** crystallised in the orthorhombic space group of  $Pca2_1$ . Molecular structure of compounds **6-8** and **12** were presented in figure 5A.4 and 5A.5. In all boron compounds, the boron centre lies in a distorted tetrahedral geometry. The B-N bond distances are 1.654(2) Å for **6**, 1.648(3) Å for **7**, 1.649(2) Å for **8** and 1.646(2) Å for **12**. The B-C bond distances are 1.597-1.613 Å for

**6**, 1.598-1.622 Å for **7**, 1.605-1.628 Å for **8** and 1.607-1.620 Å for **12**. These distances are comparable to the literature reported values.<sup>66-69</sup> The crystallographic data and structure refinement parameters are presented in table **5A.2** and **5A.3**.

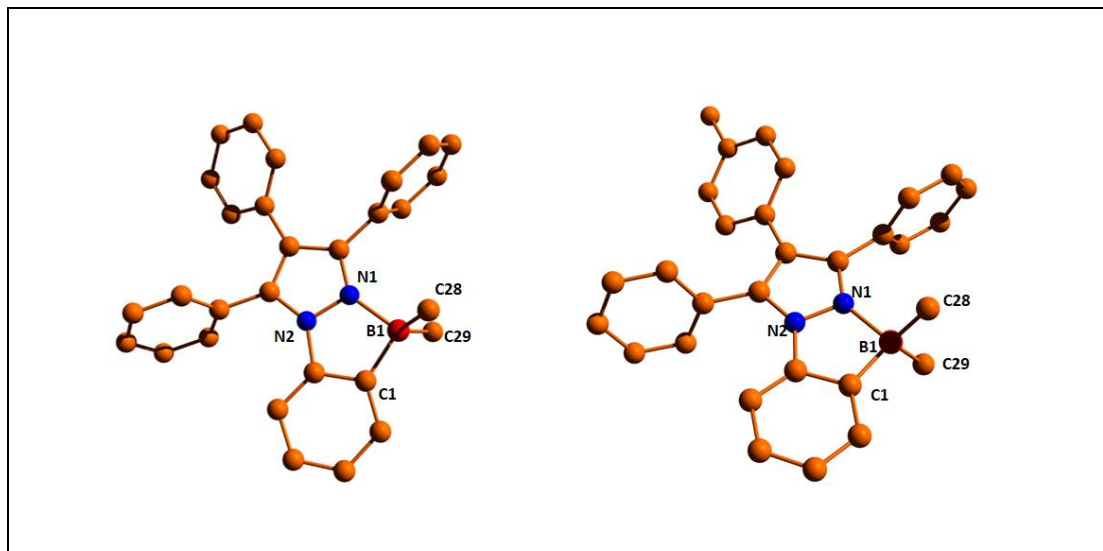


**Figure 5A.4:** Molecular structure of compound **6** (Left): Selected bond distances (Å): B1-N2: 1.654(2), B1-C1: 1.598(3), B1-C28: 1.613(3), B1-C29: 1.612(3). Bond angles (°): C28-B1-N1: 109.1(1), C1-B1-N1: 94.4(2), C1-B1-C29: 114.5(2), C29-B1-C28: 113.2(2) and compound **7** (right): Selected bond distances (Å): B1-N1: 1.649(2), B1-C1: 1.599(4), B1-C29: 1.622(3), B1-C30: 1.608(3). Bond angles (°): C29-B1-N1: 109.6(2), C1-B1-N1: 94.8(2), C30-B1-C1: 114.7(2), C29-B1-C30: 114.2(2).

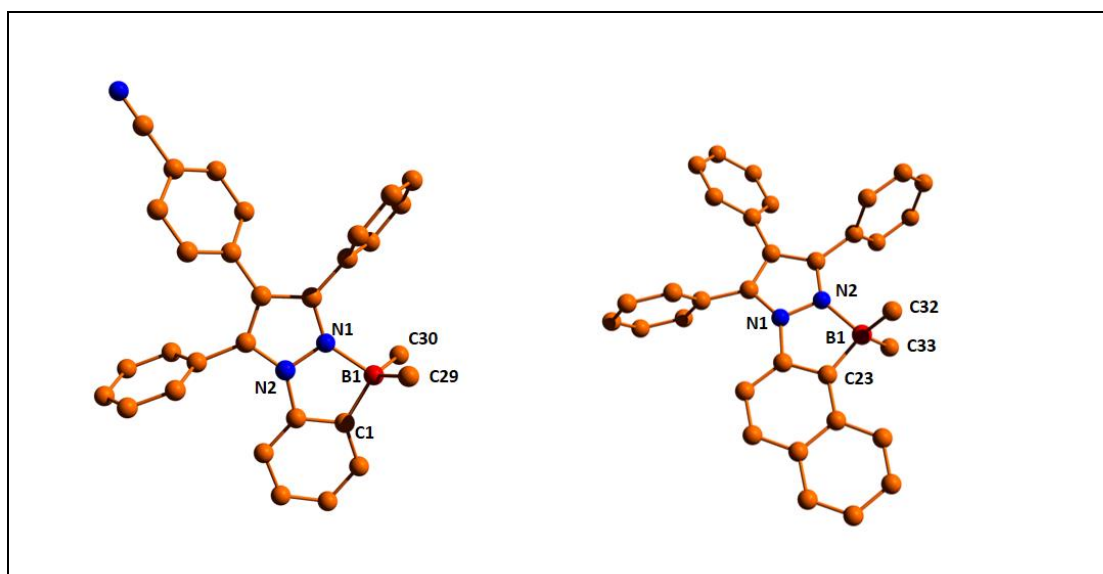
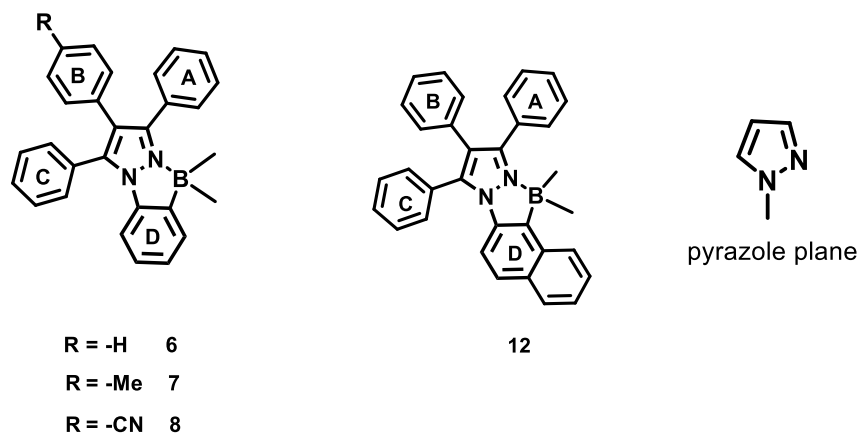


**Figure 5A.5:** Molecular structure of compound **8** (Left): Selected bond distances (Å): B1-N1: 1.650(4), B1-C1: 1.606(5), B1-C30: 1.605(6), B1-C29: 1.628(4). Bond angles (°): C30-B1-N1: 108.2(2), C1-B1-N1: 94.6(2), C30-B1-C29: 113.8(2), C1-B1-C29: 113.7(2) and compound **12** (right): Selected bond distances (Å): B1-N2: 1.646(2), B1-C23: 1.620(2), B1-C32: 1.607(2), B1-C33: 1.6126(2). Bond angles (°): C32-B1-N2: 108.6(2), C23-B1-N2: 94.4(2), C23-B1-C33: 113.3(2), C32-B1-C33: 114.4(2).

The boron atom deviates from the pyrazole plane defined by C<sub>2</sub>N<sub>2</sub>B with a distance ranging from 0.003 to 0.039 Å (Table 5A.1). The interplanar angle between the pyrazole plane and the plane A is 84.83 °(for compound **6**), 82.05 °(for compound **7**), 73.92 °(for compound **8**) and 81.49 °(for compound **12**). Similarly the other interplanar angles are presented in table 5A.1. These interplanar angles suggest that the phenyl ring attached to the pyrazole units are in a propellar shape arrangement. Examination of cell packing reveals the formation of intermolecular C-H... $\pi$  interaction of 2.77 Å for compound **6** and 2.81 Å for compound **7**. These interactions help in enhancing the molecular rigidity and better emission in the aggregate states, which will be discussed in the following sections.

**Table 5A.1:** Comparison of deviation of boron from C<sub>2</sub>N<sub>2</sub>B plane (Å) and interplanar angles (°) for compounds **6-8** and **12**



Compound	6	7	8	12
Deviation of boron (B) from C <sub>2</sub> N <sub>2</sub> B plane (Å)	0.003	0.009	0.039	0.007
Pyrazole // Plane A( °)	84.8(2)	82.0(2)	73.9(2)	81.5(2)
Pyrazole // Plane B( °)	34.7(2)	34.7(2)	39.3(2)	42.7(2)
Pyrazole // Plane C( °)	70.8(2)	72.2(2)	72.8(2)	83.2(2)
Pyrazole // Plane D( °)	2.0(2)	3.5(2)	6.2(2)	3.5(2)

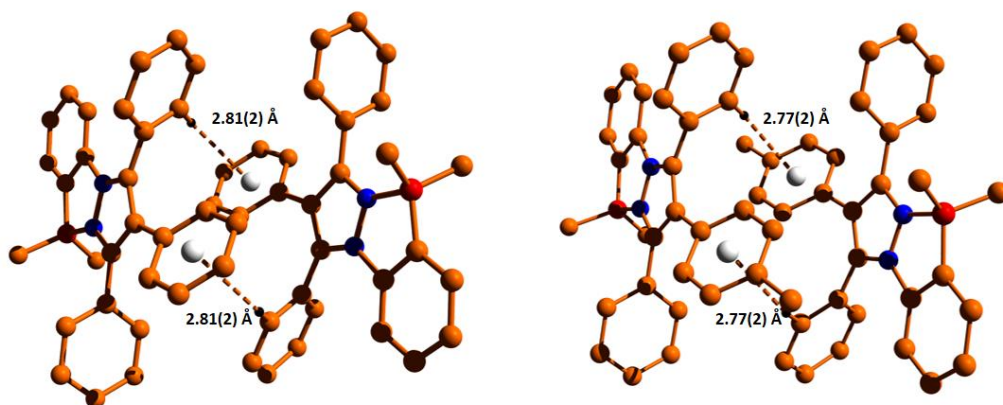


**Figure 5A.6:** Intermolecular interaction in compound **6** (C-H $\cdots$  $\pi$  : 2.81 Å) and **7** (C-H $\cdots$  $\pi$  : 2.81 Å).

**Table 5A.2:** Crystal data and structure refinement parameters for compound **6** and **7**.

	Compound <b>6</b>	Compound <b>7</b>
Empirical formula	C <sub>58</sub> H <sub>50</sub> B <sub>2</sub> N <sub>4</sub>	C <sub>60</sub> H <sub>54</sub> B <sub>2</sub> N <sub>4</sub>
MW	821.84	852.69
T,K	296.15	293(2)
Wavelength, Å	MoK $\alpha$ ( $\lambda$ = 0.71073)	CuK $\alpha$ ( $\lambda$ = 1.54184)
Crystal system	Monoclinic	Monoclinic
Space group	P2 <sub>1</sub> /c	P2 <sub>1</sub> /c
a, Å	25.3018(6)	25.1438(8)
b, Å	21.2949(6)	21.3712(5)
c, Å	8.6077(2)	9.0329(2)
$\alpha$ , deg	90	90
$\beta$ , deg	96.688(2)	98.017(3)
$\gamma$ , deg	90	90

V, Å <sup>3</sup>	4606.3(2)	4806.4(2)
Z	4	4
ρ calc, gcm <sup>-3</sup>	1.185	1.178
μ, mm <sup>-1</sup>	0.068	0.516
F(000)	1740	1808.0
2θ range, deg	3.764 to 52.746	5.45 to 161.868
limiting indices	-31 ≤ h ≤ 31	-31 ≤ h ≤ 23
	-26 ≤ k ≤ 26	-27 ≤ k ≤ 25
	-10 ≤ l ≤ 10	-9 ≤ l ≤ 11
no. of reflns collected	70894	45489
no. of indepe reflns	9433[R <sub>int</sub> = 0.0963]	10058[R <sub>int</sub> = 0.0566]
refinement method	Full matrix least square on F <sup>2</sup>	Full matrix least square on F <sup>2</sup>
No. of datas/restraints/params	9433/0/581	10058/0/601
Goodness-of-fit on F <sup>2</sup>	1.005	1.112
final R indices [I ≥ 2σ(I)]	R <sub>1</sub> = 0.0548	R <sub>1</sub> = 0.0647
	wR <sub>2</sub> = 0.1180	wR <sub>2</sub> = 0.1820
R indices (all data)	R <sub>1</sub> = 0.1183	R <sub>1</sub> = 0.0852
	wR <sub>2</sub> = 0.1468	wR <sub>2</sub> = 0.2148
peakmax/holemin (e Å <sup>-3</sup> )	0.15/-0.16	0.19/-0.31

Table 5A.3: Crystal data and structure refinement parameters for compound **8** and **12**.

	Compound <b>8</b>	Compound <b>12</b>
Empirical formula	C <sub>30</sub> H <sub>24</sub> BN <sub>3</sub>	C <sub>33</sub> H <sub>27</sub> BN <sub>2</sub>
MW	437.33	462.37
T, K	293(2)	293(2)
Wavelength, Å	CuKα (λ = 1.54184)	CuKα (λ = 1.54184)
Crystal system	Orthorhombic	Monoclinic
Space group	Pca2 <sub>1</sub>	P2 <sub>1</sub> /c
a, Å	24.3645(15)	13.1104(6)
b, Å	9.1233(5)	9.0510(4)
c, Å	11.2088(6)	24.4206(12)
α, deg	90	90
β, deg	90	99.279
γ, deg	90	90
V, Å <sup>3</sup>	2491.5(2)	2859.9(2)
Z	4	4
ρ calc, gcm <sup>-3</sup>	1.166	1.074
μ, mm <sup>-1</sup>	0.525	0.062
F(000)	920	976
2θ range, deg	7.256 to 133.96	3.38 to 49.996
limiting indices	-28 ≤ h ≤ 29	-16 ≤ h ≤ 16
	-10 ≤ k ≤ 9	-12 ≤ k ≤ 12
	-11 ≤ l ≤ 13	-31 ≤ l ≤ 30
no. of reflns collected	20474	31191
no. of indepe reflns	4283[R <sub>int</sub> = 0.1282]	5028[R <sub>int</sub> = 0.0485]

refinement method	Full matrix least square on $F^2$	Full matrix least square on $F^2$
No. of datas/restraints/params	4283/1/309	5028/0/328
Goodness-of-fit on $F^2$	1.064	1.068
final R indices [ $I \geq 2\sigma(I)$ ]	$R_1 = 0.0523$	$R_1 = 0.0424$
	$wR_2 = 0.1259$	$wR_2 = 0.1090$
R indices (all data)	$R_1 = 0.0599$	$R_1 = 0.0595$
	$wR_2 = 0.1366$	$wR_2 = 0.1159$
peakmax/holemin ( $e \text{ \AA}^{-3}$ )	0.12/-0.19	0.15/-0.16

### 5A.2.3 Photophysical properties

The photophysical properties of compounds **6-8**, **12** and **18** were investigated in five different solvents with varying polarity and in the solid state (Table 5A.3). THF solutions of compounds **6-8**, **12** and **18** absorb between 300-353 nm with a molar extinction coefficients of  $12710 \text{ cm}^{-1}$  to  $21500 \text{ cm}^{-1}$ . Compound **12** showed red shifted absorption maximum compared to compounds **6-8** due to increased conjugation. Compound **18** showed more red shifted compared to other compounds, owing to the electron donating nature of  $\text{NPh}_2$  group. The absorption spectra of these compounds did not alter with the solvent polarity.

**Table 5A.4:** Photophysical data of compounds **6-8**, **12** and **18**

Compound	Solvent	$\lambda_{\text{max}}^a$ (nm)	$\epsilon_{\text{max}}$ ( $\text{M}^{-1} \text{ cm}^{-1} \times 10^3$ )	$\lambda_{\text{em}}^b$ (nm)	$\Phi_F^c$	Stokes Shift ( $\text{cm}^{-1}$ )	$\tau$ (ns)
<b>6</b>	Toluene	301	20.9	438	0.03	10391	
	THF	300	21.5	430	0.03	10077	0.39
	$\text{CH}_2\text{Cl}_2$	299	21.5	432	0.01	10297	
	$\text{CH}_3\text{CN}$	297	21.3	440	0.01	10942	
	DMF	298	20.2	430	0.03	10301	
	Solid			376	0.14		
<b>7</b>	Toluene	301	22.4	439	0.03	10443	
	THF	300	21.1	436	0.03	10397	0.40
	$\text{CH}_2\text{Cl}_2$	299	17.0	433	0.02	10350	

	CH <sub>3</sub> CN	296	21.3	440	0.01	11056	
	DMF	298	14.2	430	0.02	10301	
	Solid			365	0.13		
<b>8</b>	Toluene	304	23.5	431	0.03	10456	
	THF	302	27.6	422	0.03	9415	0.63
	CH <sub>2</sub> Cl <sub>2</sub>	303	17.9	426	0.04	9529	
	CH <sub>3</sub> CN	298	26.3	431	0.02	10355	
	DMF	301	30.6	426	0.03	9748	
	Solid			474	0.21		
<b>12</b>	Toluene	319	13.75	457	0.26	9466	
	THF	319	12.71	459	0.31	9561	2.13
	CH <sub>2</sub> Cl <sub>2</sub>	326	11.94	459	0.27	8888	
	CH <sub>3</sub> CN	317	15.18	462	0.20	9900	
	DMF	318	14.17	465	0.27	9941	
	Solid			390	0.31		
<b>18</b>	Toluene	360	23.85	511	0.46	8208	4.07
	THF	353	18.17	531	0.31	9496	3.59
	CH <sub>2</sub> Cl <sub>2</sub>	355	19.32	536	0.38	9512	3.99
	CH <sub>3</sub> CN	347	18.8	561	0.13	10993	2.43
	DMF	351	21.39	557	0.16	10536	2.14
	Solid			443	0.67		

<sup>a</sup> Absorption maximum, <sup>b</sup> Excited at absorption maximum, <sup>c</sup> Absolute quantum yields

were measured using integrating sphere.

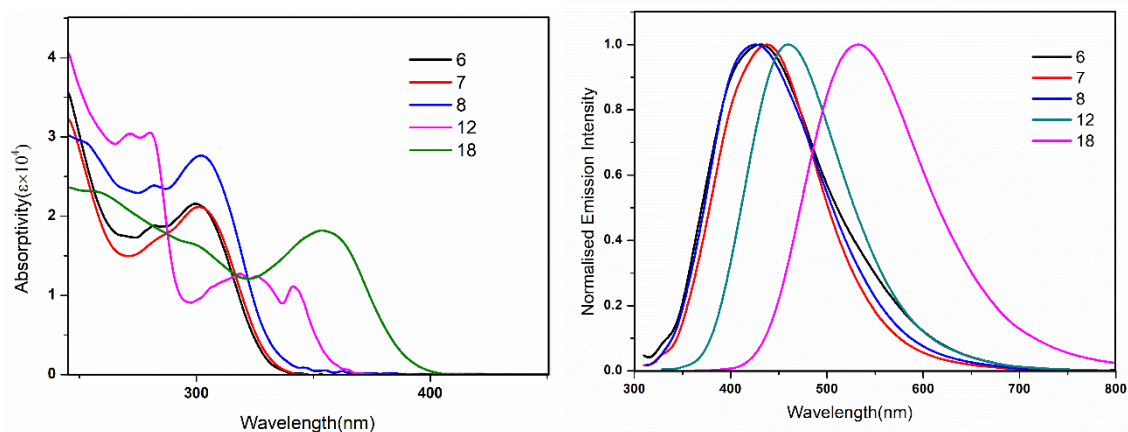


**Figure 5A.7:** (Left) Absorption spectra of compounds **6-8**, **12** and **18** in  $10^{-5}$  M THF. (Right) Normalised emission spectra of compounds **6-8**, **12** and **18** in  $10^{-5}$  M THF.

The emission spectra of compounds **6-8**, **12** and **18** were recorded by exciting at their longest absorption maxima and the relevant data are presented in table 5A.3. THF solutions of these compounds showed emission peak ranged from 422 nm to 531 nm. Compound **18** showed more red shifted emission compared to other compounds and exhibits large Stoke shift ( $9496\text{ cm}^{-1}$ ) due to intramolecular charge transfer from  $\text{NPh}_2$  group. Emission spectra of compounds **6-8** and **12** did not change with varying solvent polarity.

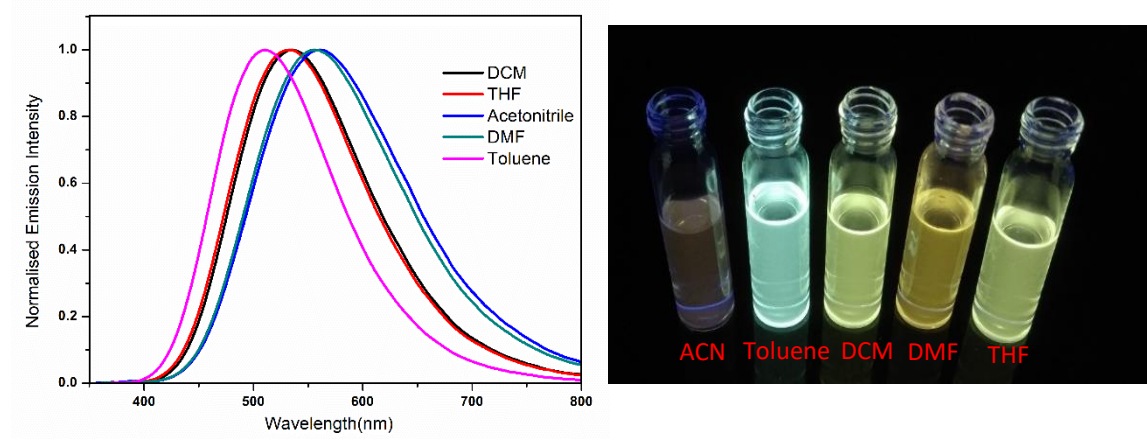


**Figure 5A.8:** (Left) Solvatochromic emission spectra of compound **18**. (Right) Photograph of compound **18** in toluene, dichloromethane (DCM), tetrahydrofuran (THF), dimethylformamide (DMF) and acetonitrile (ACN) under handheld UV lamp irradiated at 365 nm.

The absolute quantum yield of these complexes were measured using integrating sphere. Compounds **6-8** were found to be weakly fluorescent with a quantum yield of less than 5%. However, compound **12** and **18** are moderately fluorescent. Compound **18** showed positive solvatochromism with increasing solvent polarity (Figure 5A.8); from toluene to acetonitrile, it exhibited a red shift of 50 nm. The observed blue shift



in emission and high quantum yield in toluene is due to locally excited (LE) states and red shift in the acetonitrile is due to twisted intramolecular charge transfer (TICT) states.<sup>70</sup> A low quantum yield observed in acetonitrile and dimethylformamide, may be due to the disruption of lewis acid-base adduct(B-N coordination) by the polar solvents, which disturbs the conjugation leading to poor emission. The positive solvatochromism was further supported by Lippert-Mataga plot which shows a linear correlation between the stokes shift and solvent polarity. Lippert-Mataga graph was plotted with Stokes shift ( $\Delta\nu$ ) versus the solvent orientation polarizability ( $\Delta f$ ). (Figure 5A.9)

**Table 5A.5:** Refractive index ( $n$ ), dielectric constant ( $\epsilon$ ), orientation polarizability ( $\Delta f$ ) and Stokes shift ( $\Delta\nu$  ( $\text{cm}^{-1}$ )) of compound **18** as a function of different solvents are shown.

Solvent	$n$	$\epsilon$	$\Delta f$	Stokes Shift(nm)	$\Delta\nu(\text{cm}^{-1})$
Toluene	1.497	2.38	0.013	151	8208
THF	1.407	7.58	0.210	178	9496
$\text{CH}_2\text{Cl}_2$	1.424	8.93	0.217	181	9512
DMF	1.430	36.7	0.274	206	10536
Acetonitrile	1.344	37.5	0.305	214	10993

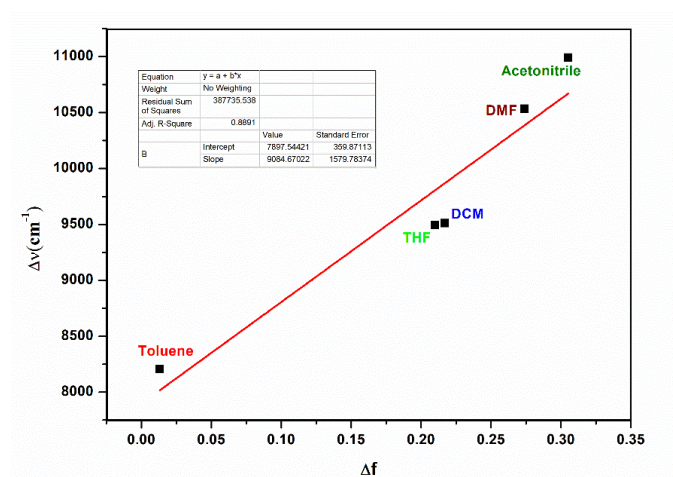


**Figure 5A.9:** Lippert-Mataga plot of compound **18** depicting Stokes shift ( $\Delta\nu$ ) versus the solvent orientation polarizability ( $\Delta f$ ).

Figure **5A.10** depicts the solid state emission spectra of compounds **6-8**, **12** and **18**. Compounds **6-8**, **12** and **18** exhibited blue shifted emission with high quantum yields in the solid state as compared to their solution state. However, compounds **12** exhibited red shifted emission which indicates that excited state of compound **12** is more stabilized in the solid state compared to the solution state.

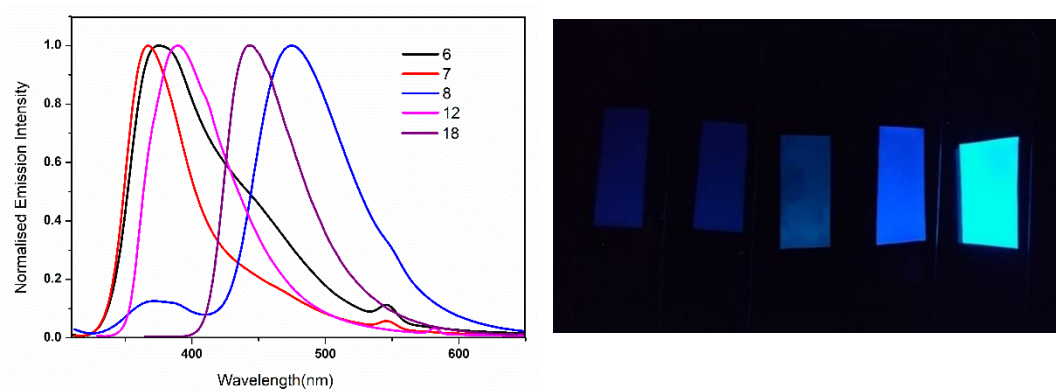


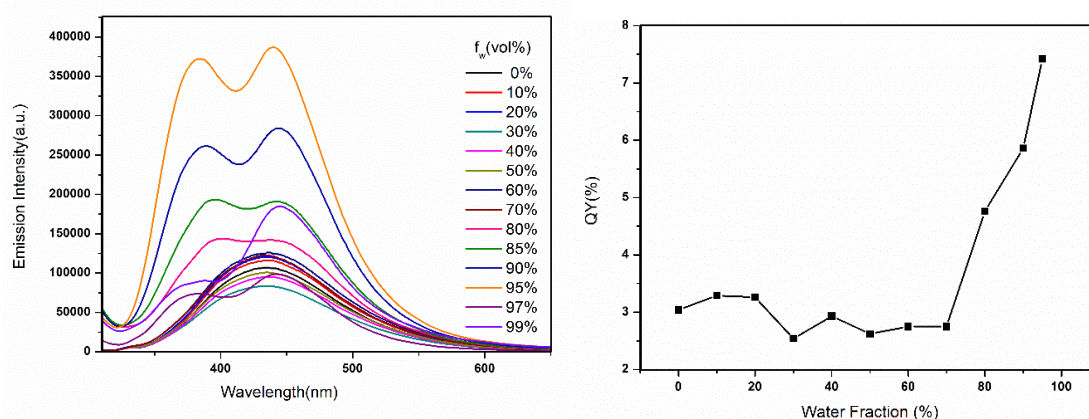
**Figure 5A.10:** (Left) Solid state emission spectra of compounds **6-8**, **12** and **18**. (Right) Photograph of thin film of compounds **6-8**, **12** and **18** (4% PMMA) under handheld UV lamp irradiated at 365 nm.

#### 5A.2.4 AIEE studies

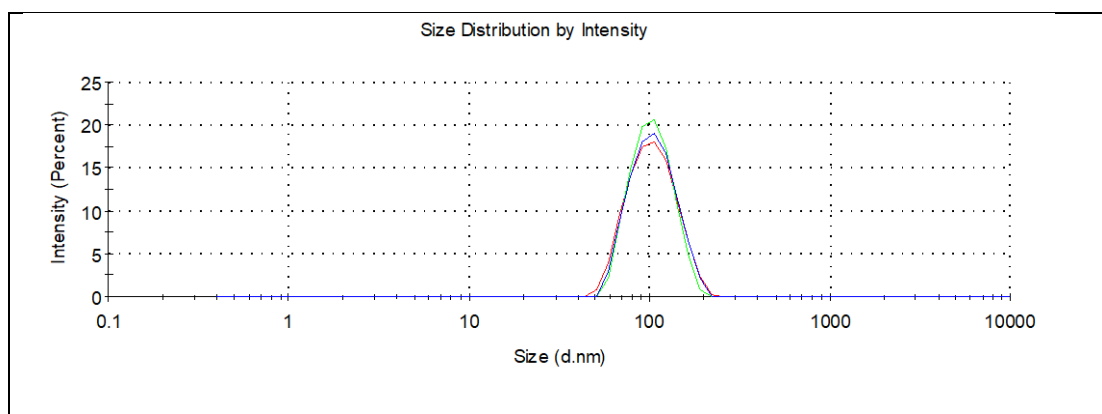
As mentioned in the previous section, the quantum yield of all compounds in the solid state are much higher than their respective solution state quantum yield, is an indication that these molecules could exhibit AIEE phenomenon. To understand whether compounds **6-8**, **12** and **18** are AIEE active or not; fluorescence spectra of compound **6-8**, **12** and **18** were recorded using THF and water mixture (the concentration was maintained). As shown in figure **5A.11** the emission spectrum of compound **6** was slightly affected upto a water content of 70 vol%. Further increase in water fraction

results in enhancement in emission intensity and reaches to a maximum at 95% water.

This is due to the formation of nanoaggregates which was further confirmed by particle size measurement using dynamic light scattering technique (Figure 5A.12). Emission intensity starts decreasing after 95% water fraction because of insolubility of compound in higher water content. Compound **6** in the aggregate state exhibited two emission peak at 383 nm ( $\tau = 0.61$  ns) and 440 nm ( $\tau = 1.02$  ns).



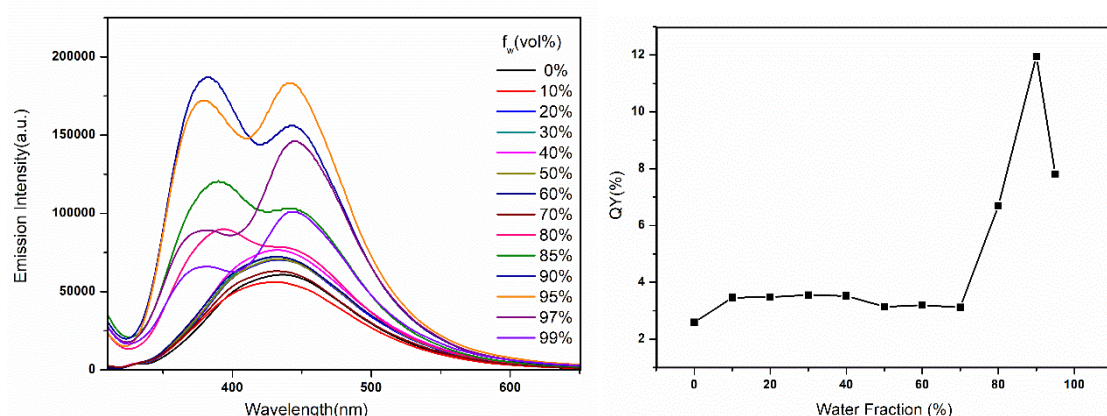
**Figure 5A.11 :** (Left) Fluorescence spectra of compound **6** ( $10^{-5}$  M, excited at 300 nm) in THF:H<sub>2</sub>O mixture. (Right) Variation of quantum yield of compound **6** in THF:H<sub>2</sub>O mixture.



**Figure 5A.12:** Particle size distribution graph of compound **6** in THF:H<sub>2</sub>O (10:90) mixture.

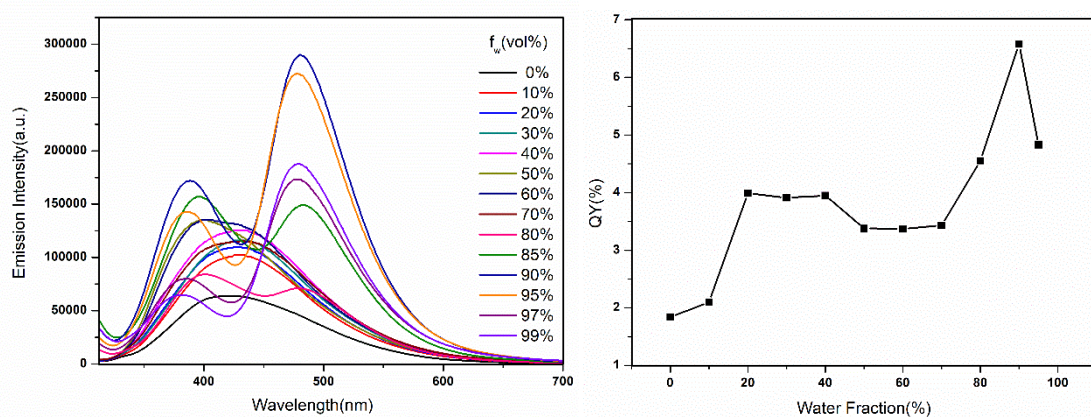
Similar trend was observed in compound **7** as in the case of compound **6**. The fluorescence spectra of compound **7** recorded in THF:H<sub>2</sub>O mixture is shown in figure

**5A.13.** The particle size of the nanoaggregate at 95% water fraction is found to be 92 nm.



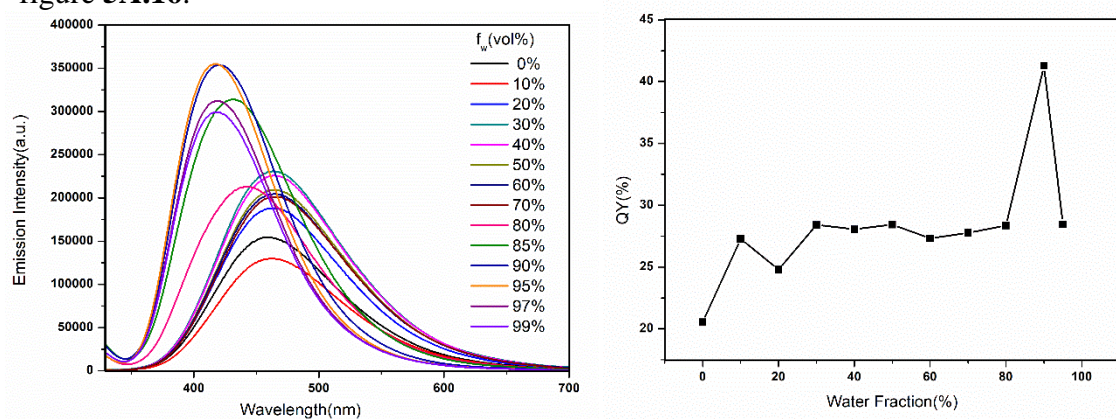
**Figure 5A.13:** (Left) Fluorescence spectra of compound **7** (10<sup>-5</sup> M, excited at 300 nm) in THF:H<sub>2</sub>O mixture. (Right) Variation of quantum yield of compound **7** in THF: H<sub>2</sub>O mixture.

Figure **5A.14** depicts the fluorescence spectra of compound **8** in THF: H<sub>2</sub>O mixture. Compound **8** showed six fold enhancement in emission intensity in 90% THF: H<sub>2</sub>O mixture compared to pure THF. The particle size of the nanoaggregate at 90% water fraction is found to be 102 nm.



**Figure 5A.14:** (Left) Fluorescence spectra of compound **8** (10<sup>-5</sup> M, excited at 302 nm) in THF:H<sub>2</sub>O mixture. (Right) Variation of quantum yield of compound **8** in THF:H<sub>2</sub>O mixture.

The emission spectra of compound **12** in THF:H<sub>2</sub>O mixture is represented in figure 5A.15. Compound **12** showed more than two fold enhancement in emission intensity and blue shifted emission ( $\lambda = 419$  nm,  $\tau = 2.18$  ns). Photograph of compound **12** in THF/H<sub>2</sub>O mixture under a hand held UV lamp irradiated at 365 nm is represented in figure 5A.16.



**Figure 5A.15:** (Left) Fluorescence spectra of compound **12** ( $10^{-5}$  M, excited at 319 nm) in THF:H<sub>2</sub>O mixture. (Right) Variation of quantum yield of compound **12** in THF:H<sub>2</sub>O mixture.

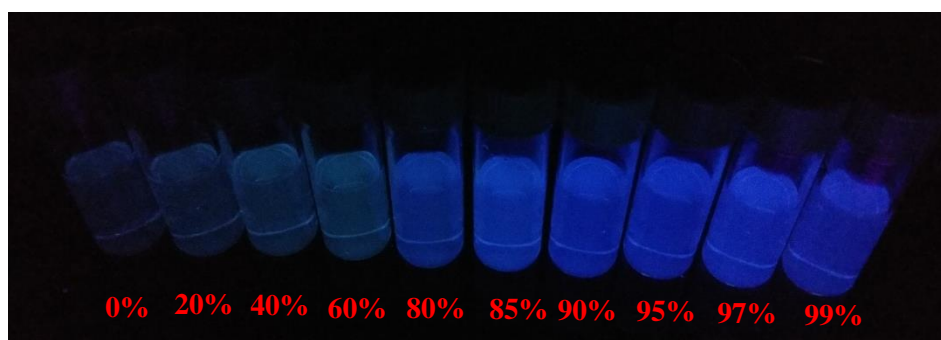


**Figure 5A.16:** Photograph of compound **12** in THF/H<sub>2</sub>O mixture under a handheld UV lamp irradiated at 365 nm.



Fluorescence spectra of compound **18** in THF/water mixture is shown in figure 5A.17. The emission intensity of compound **18** unaltered or showed slight reduction from 0 to 70% of water fraction. Further increase in water fraction, the emission intensity enhances with a blue shifted emission. This may be due to suppression of intramolecular charge transfer (ICT) process. The hydrophobic environment created inside the ICT state and aggregate state can not be stabilized.<sup>70</sup> Thus, ICT effect is suppressed. From pure THF solution to a THF/water mixture with 90% water, the emission intensity increases by 3.5 fold. This confirms that the complex is AIEE active. The fluorescence quantum yield enhances from 0.30 in a pure THF solution to 0.71 in THF/water (10:90). Photograph of compound **18** in THF/H<sub>2</sub>O mixture with increasing water fraction is shown in figure 5A.18.

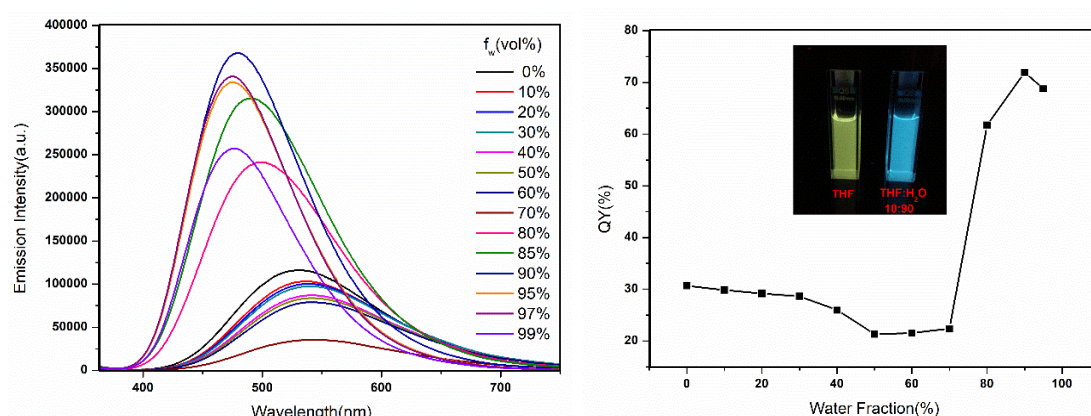


**Figure 5A.17:** (Left) Fluorescence spectra of compound **18** ( $10^{-5}$  M, excited at 353 nm) in THF:H<sub>2</sub>O mixture. (Right) Variation of quantum yield of compound **18** in THF:H<sub>2</sub>O mixture.

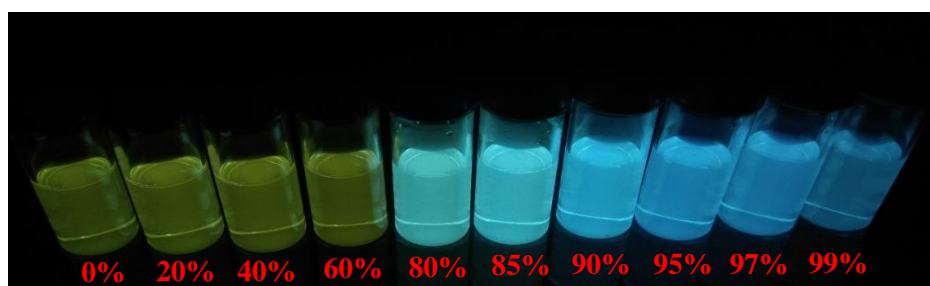


**Figure 5A.18:** Photograph of compound **18** in THF/H<sub>2</sub>O mixture under a handheld UV lamp irradiated at 365 nm.

For the better understanding of the AIEE properties, emission of compounds **6-8**, **12** and **18** were recorded by varying the temperature. Figures **5A.19** - **5A.21** reveal that increase in temperature lowers the emission intensity due to faster molecular rotation at higher temperature. Restriction of intramolecular rotation (RIR) phenomenon plays a vital role at low temperature resulting in enhanced emission intensity.

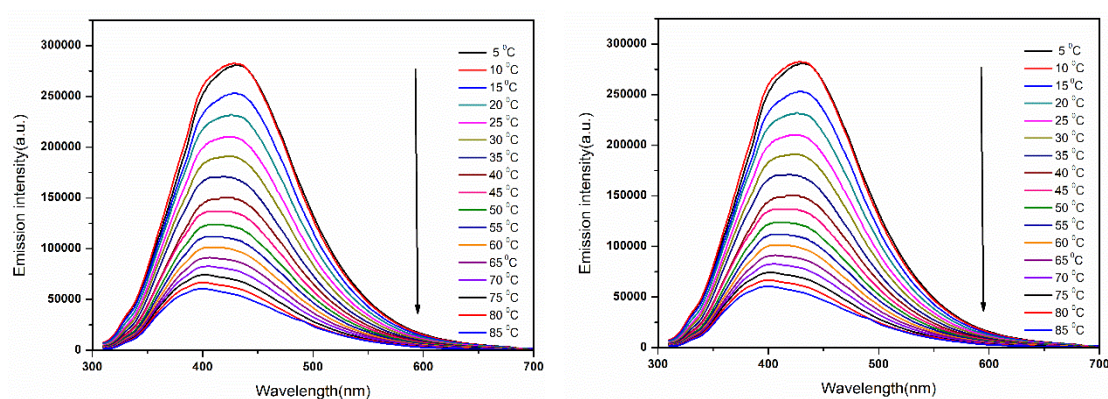


**Figure 5A.19:** Emission spectra of compound **6** (Left) and compound **7** (Right) in  $10^{-5}$  M THF at different temperatures.

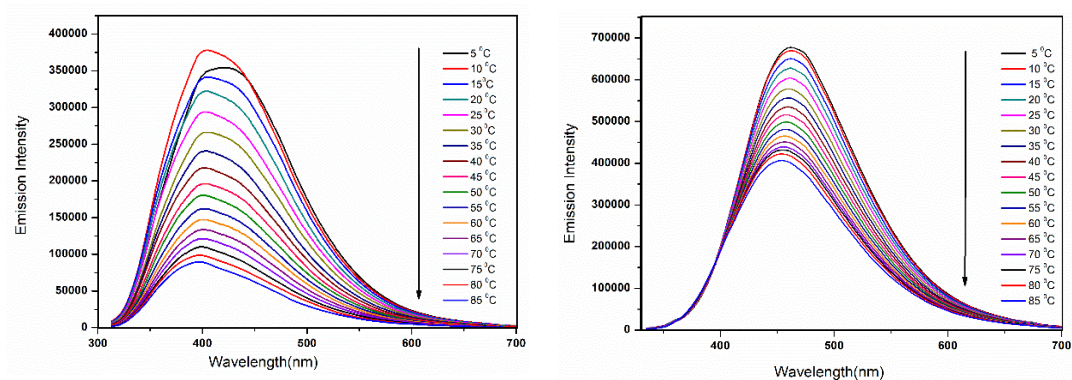


**Figure 5A.20:** Emission spectra of compound **8** (Left) and compound **12** (Right) in  $10^{-5}$  M THF at different temperatures.

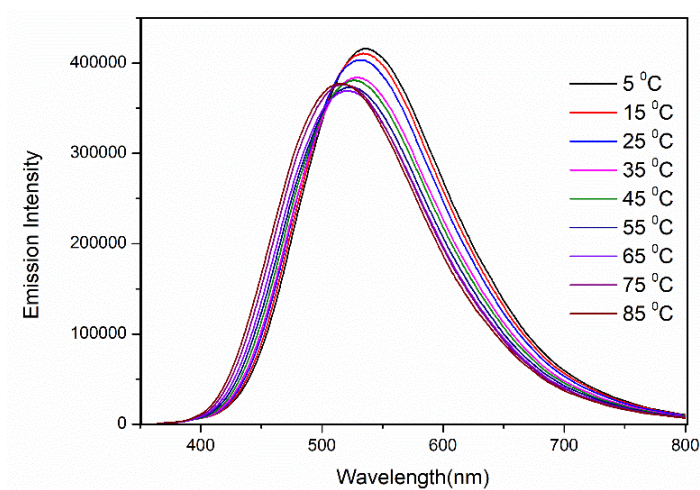


**Figure 5A.21:** Emission spectra of compound **18** in  $10^{-5}$  M THF at different temperatures.

To further support the AIEE mechanism, the emission of compounds **6-8**, **12** and **18** were recorded by blending glycerol with methanol (Figure 5A.22- 5A.24). Emission intensity increases with increase of glycerol fraction due to increase in viscosity of the mixture. The increasing viscosity strengthen the restriction of intramolecular rotation process and further activate the radiative decay.

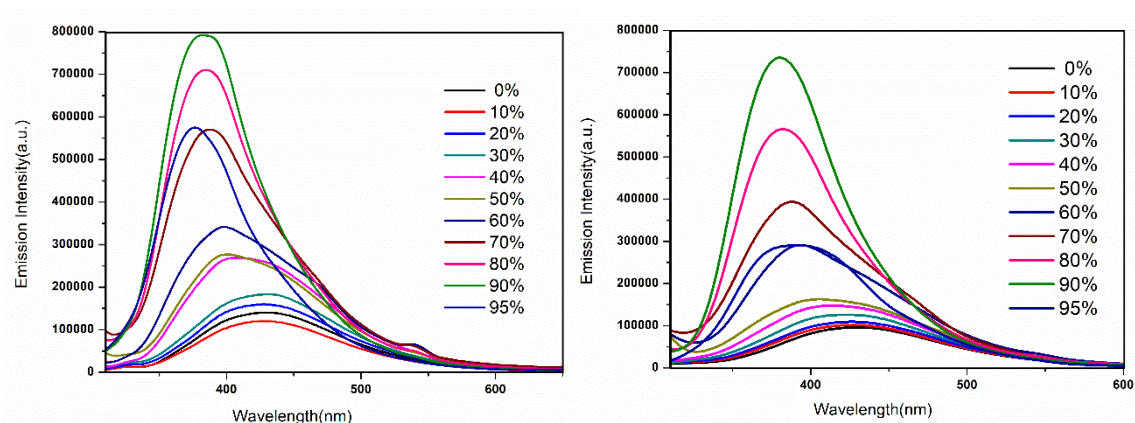


**Figure 5A.22:** Emission spectra of complex **6** (Left) and **7** (Right) in methanol/glycerol mixture with increasing glycerol fraction (0 to 95%).



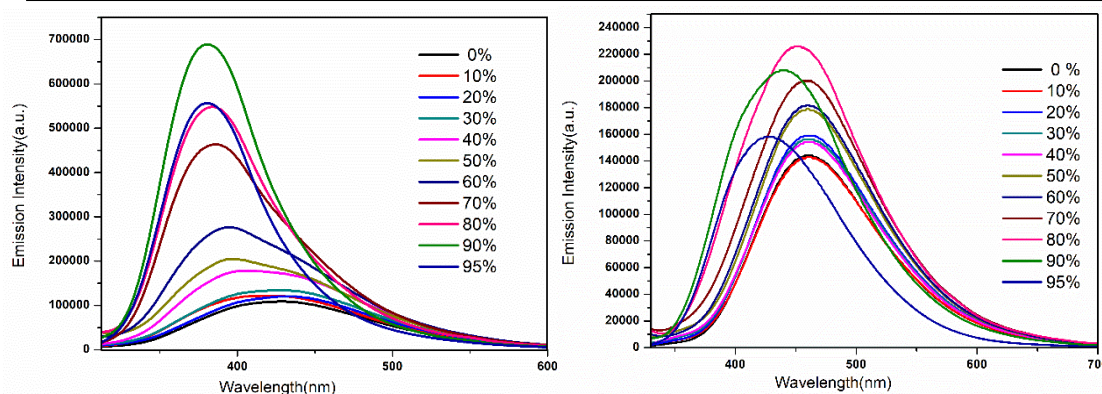


**Figure 5A.23:** Emission spectra of compound **8** (Left) and **12** (Right) in methanol/glycerol mixture with increasing glycerol fraction (0 to 95%).

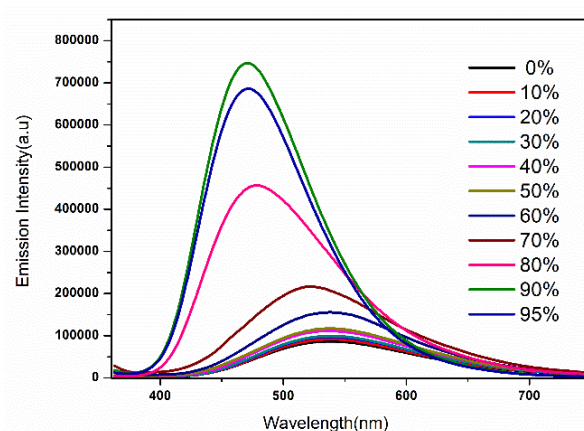


**Figure 5A.24:** Emission spectra of compound **18** in methanol/glycerol mixture with increasing glycerol fraction (0 to 95%).

#### 5A.2.4 Picric acid sensing using compound 18

To show the potential utility, as a proof of concept, compound **18** was used for the detection of picric acid. The sensing and recognition of picric acid has attracted tremendous research attention due to its potential use in terrorism and war activity.<sup>71-75</sup> Picric acid causes serious health affect such as skin allergy, skin irritation, cancer etc.<sup>76,77</sup> Thus, the detection of picric acid is extremely important. Compound **18** in THF/H<sub>2</sub>O (10:90) mixture was used as a probe. Upon gradual addition of picric acid to aggregates of compound **18**, the emission intensity was quenched gradually (Figure

**5A.25).** Quenching in emission intensity upto 91% was observed after adding 8 equivalents of picric acid solution to compound **18**.

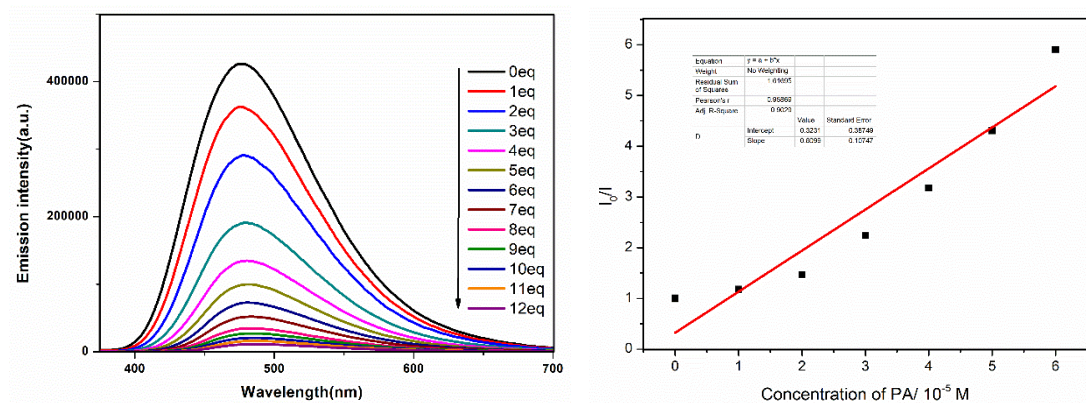


**Figure 5A.25:** (Left) Fluorescence quenching of compound **18** ( $10^{-5}$  M, excited at 352 nm) in a mixed solvent of THF: H<sub>2</sub>O (10 : 90) with different concentrations of PA (0, 1.0, 2.0, 3.0, 4.0, 5.0, 6.0, 7.0, 8.0, 9.0, 10.0, 11.0 and 12.0 equiv. of PA). (Right) Stern-Volmer plot of compound **18** in THF: H<sub>2</sub>O (10 : 90) with different concentrations of PA.

The emission quenching of compound **18** was studied using Stern-Volmer plot. From the Stern-Volmer plot, the quenching constant was calculated and found to be  $8.0 \times 10^4$  M<sup>-1</sup>(**Figure 5A.25**). Time resolved fluorescence measurements was carried out to understand the mode of quenching. Figure **5A.26** shows the fluorescence decay profile graph of compound **18**. Fluorescence lifetime of compound **18** is invariant in the presence of picric acid, which suggests that the mechanism of quenching is static.

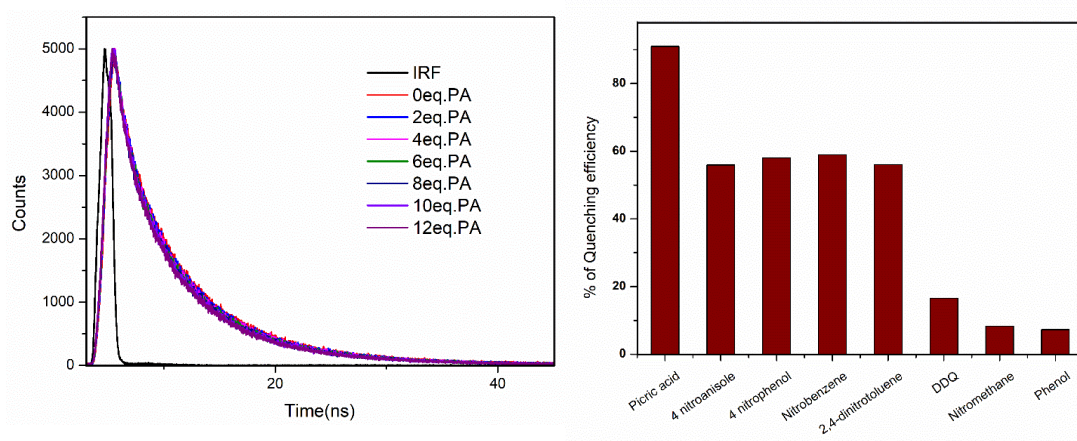


**Figure 5A.26:** (Left) Fluorescence lifetime decay of compound **18** after the addition of 0, 2, 4, 6, 8 and 12 equiv. of PA in THF:H<sub>2</sub>O (10:90) mixture. (Right) Fluorescence quenching efficiencies of compound **18** in THF : H<sub>2</sub>O (10:90) mixture towards of different nitroaromatics (8 equiv).

Fluorescence responses of compound **18** towards different nitroaromatics were tested (Figure 5A.26). Among all, picric acid quenches the emission intensity 91%, while the quenching in other analytes are less compared to picric acid.

### 5A.3 Electrochemical properties

Figure 5A.27 represents the electrochemical properties of boron compounds **6-8**, **12** and **18**. All the boron compounds showed an irreversible reduction peak (-2.88 V for **6**, -2.97 V for **7**, -2.70 V for **8**, -2.84 V for **12** and -2.83 V for **18**). These observed reduction values are more negative compared to reported literature values.<sup>66-69</sup>

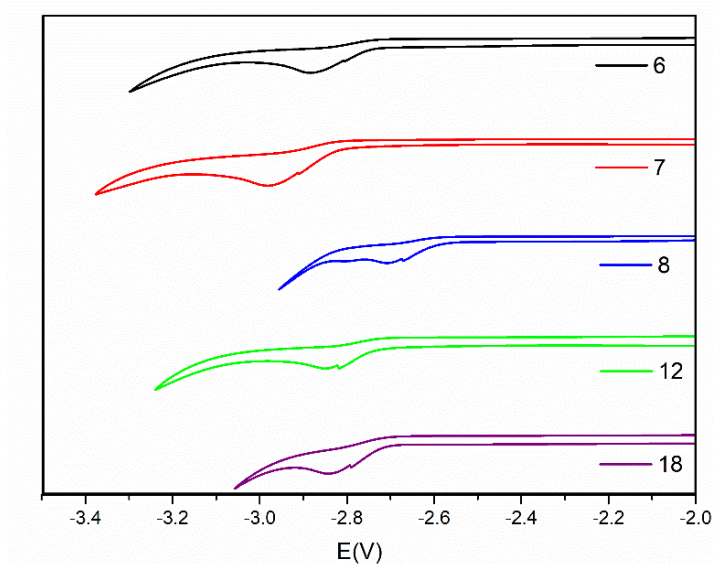


**Figure 5A.27:** Cyclic voltammograms of compounds **6-8**, **12** and **18** (vs. ferrocene/ferrocenium) with 0.1 M Bu<sub>4</sub>NPF<sub>6</sub> in DME as the supporting electrolyte (scan rate 100 mV s<sup>-1</sup>).

---

### 5A.3 Conclusions

In summary, five tetraaryl pyrazole based four coordinate boron complexes have been synthesized and characterized with different technique. All the boron compounds are fluorescent in both solution and solid states. All five boron compounds are found to be AIEE active. From crystal analysis it was observed that the propeller shape arrangement of phenyl group and intermolecular C-H $\cdots\pi$  interactions are responsible for the observed AIEE properties in these compounds. Compound **18** in the aggregate state was used to detect the nitroexplosive (picric acid). The rich electrochemical and photophysical studies suggest the potential use of these compounds as an emitter in organic light emitting diodes (OLEDs).

### 5A.4 Experimental section

#### 5A.4.1 General information

All reagents and starting materials were purchased from Sigma-Aldrich, Alfa-Aesar and Spectrochem chemical companies; and used as received unless otherwise noted. Chlorinated solvents, acetonitrile, and DMF were distilled from CaH<sub>2</sub>. THF and toluene were distilled from Na/benzophenone prior to use. All 400 MHz <sup>1</sup>H, 100 MHz <sup>13</sup>C, NMR spectra were recorded on a Bruker ARX 400 spectrometer operating at 400 MHz. All <sup>1</sup>H and <sup>13</sup>C NMR spectra were referenced internally to solvent signals. All NMR spectra were recorded at ambient temperature. ESI mass spectra were recorded on Bruker, micrOTOF-QII mass spectrometer. The absorbance spectra were recorded on a JASCO V-730 UV-Visible spectrometer. The fluorescence spectra were recorded using Edinburgh FS5 spectrofluorometer. Absolute fluorescence quantum yields of compounds **6-8**, **12** and **18** were measured by integrating sphere method using Edinburgh FS5 spectrofluorometer. The fluorescence spectra are corrected for the instrumental response. Cyclic voltammetry measurements were performed with a

conventional three electrode cell using an electrochemical workstation (CH Instrument, Model: 1100A) The three-electrode system consisted of a Glassy carbon working electrode, a Pt wire as the secondary electrode, and a Ag wire as the reference electrode. The voltammograms were recorded with ca.  $1.0 \times 10^{-3}$  M solution in DME containing Bu<sub>4</sub>NPF<sub>6</sub> (0.1 M) as the supporting electrolyte. The scans were referenced after the addition of a small amount of ferrocene as the internal standard. Single-crystal X-ray diffraction data were collected on a Bruker APEXII diffractometer using Mo-K $\alpha$  radiation (0.71073 Å) and Rigaku Oxford X-ray diffractometer Cu-K $\alpha$  (1.54184 Å). SADABS absorption corrections were applied. The structures were solved and refined with SHELX suite of programs. All non-hydrogen atoms were refined with anisotropic displacement coefficients. The H atoms were placed at calculated positions and were refined as riding atoms.

#### 5A.4.2 Synthetic procedures and spectral characterisations

##### 5A.4.2.1 Synthesis of compound 1

A mixture of 1,3-diphenyl propane dione (4.00 g, 17.83 mmol), phenyl hydrazine (2.20 ml, 21.39 mmol), acetic acid (40 mL) and methanol (40 mL) were refluxed for 24 hours. After completion of the reaction, the product was extracted using water and dichloromethane (3 x 60 mL). The extracted organic phase was washed with aqueous sodium carbonate and dried over anhydrous sodium sulphate. The solvent was concentrated and the product was purified using silica gel column chromatography (n-hexane/EtOAc (98:2)). Yield: 3.40 g (65%). <sup>1</sup>H NMR (400 MHz, CDCl<sub>3</sub>)  $\delta$  = 7.99 – 7.91 (m, 2H), 7.50 – 7.42 (m, 2H), 7.41 – 7.27 (m, 11H), 6.86 – 6.83 (m, 1H). <sup>13</sup>C NMR (101 MHz, CDCl<sub>3</sub>)  $\delta$  152.05, 144.46, 140.22, 133.14, 130.64, 129.02, 128.83, 128.77, 128.59, 128.40, 128.12, 127.53, 125.92, 125.38, 105.33. HR-MS (ESI): Calculated for C<sub>21</sub>H<sub>16</sub>N<sub>2</sub> ([M+H]<sup>+</sup>): 297.1386, Observed : 297.1386.

---

**5A.4.2.2 Synthesis of compound 2**

Compound **1** (2.50 g, 8.42 mmol) and N-bromosuccinimide (1.89 g, 13.08 mmol) were taken in dichloromethane (50 mL). The reaction mixture was stirred at room temperature in dark for 24 h. After completion of the reaction, the product was extracted using water and dichloromethane (3 x 50 mL). The organic phase was collected and dried over anhydrous sodium sulphate. The solvent was concentrated and the product was purified using silica gel column chromatography (n-hexane/EtOAc (95:5)). Yield: 2.40 g (64%).  $^1\text{H}$  NMR (400 MHz,  $\text{CDCl}_3$ )  $\delta$  = 8.04 – 7.98 (m, 2H), 7.48 (t,  $J$ =7.4, 2H), 7.44 – 7.37 (m, 4H), 7.37 – 7.32 (m, 2H), 7.32 – 7.27 (m, 5H).  $^{13}\text{C}$  NMR (101 MHz,  $\text{CDCl}_3$ )  $\delta$  = 149.77, 142.06, 139.83, 132.00, 129.05, 128.92, 128.55, 128.48, 128.40, 128.11, 127.62, 94.95. HR-MS (ESI): Calculated for  $\text{C}_{21}\text{H}_{16}\text{BrN}_2$  ( $[\text{M}+\text{H}]^+$ ): 375.0491, Observed : 375.0520.

**5A.4.2.3 Synthesis of compound 3**

Compound **2** (1.50 g, 3.73 mmol), benzene boronic acid (0.55 g, 4.48 mmol), sodium carbonate (1.19 g, 11.19 mmol) and  $\text{Pd}(\text{PPh}_3)_4$  (0.13 g, 0.11 mmol) were taken in a two necked round bottomed flask. A mixture of THF and water (THF: $\text{H}_2\text{O}$  = 20:8) was degassed for 30 minutes and added to the reaction mixture under nitrogen atmosphere. The reaction mixture was refluxed for 24 h. After completion of the reaction, the compound was extracted with water and dichloromethane (3 x 50 mL). The organic phase was collected and dried over anhydrous sodium sulphate. The solvent was concentrated and the product was purified using silica gel column chromatography (EtOAc/ n-hexane(2:98)). Yield: 0.92 g (66%).  $^1\text{H}$  NMR (400 MHz,  $\text{CDCl}_3$ )  $\delta$  = 7.58 (dd,  $J$ =6.6, 2.9, 2H), 7.41 – 7.30 (m, 8H), 7.30 – 7.21 (m, 6H), 7.16 (dd,  $J$ =6.5, 2.9, 2H), 7.12 (d,  $J$ =6.9, 2H).  $^{13}\text{C}$  NMR (101 MHz,  $\text{CDCl}_3$ )  $\delta$  150.27, 141.42, 140.00, 133.18, 133.15, 130.76, 130.48, 130.11, 128.83, 128.46, 128.33, 128.26, 128.21, 127.69,

127.28, 126.72, 125.37, 120.76. HR-MS (ESI): calculated for  $C_{27}H_{20}N_2$  ( $[M+H]^+$ ): 374.1699, observed : 374.1707.

#### 5A.4.2.4 Synthesis of compound 4

Compound 2 (2.5 g, 6.69 mmol), *p*-tolueneboronic acid (1.18 g, 8.70 mmol), sodium carbonate (2.12 g, 20.0 mmol) and  $Pd(PPh_3)_4$  (0.232 g, 0.20 mmol) were taken in a two necked round bottomed flask. A mixture of THF and water (THF:H<sub>2</sub>O = 20:8) was degassed for 30 minutes and then added to the reaction mixture under nitrogen atmosphere. The reaction mixture was refluxed for 24 h. After completion of the reaction, the compound was extracted with water and dichloromethane (3 x 50 mL). The organic phase was collected and dried over anhydrous sodium sulphate. The solvent was concentrated and the product was purified using silica gel column chromatography (EtOAc/ n-hexane(2:98)). Yield: 1.60 g (62%). <sup>1</sup>H NMR (400 MHz, CDCl<sub>3</sub>)  $\delta$  = 7.58 – 7.51 (m, 2H), 7.36 – 7.18 (m, 11H), 7.11 – 7.06 (m, 2H), 7.01 (d, *J*=5.7, 4H), 2.33 (s, 3H). <sup>13</sup>C NMR (176 MHz, CDCl<sub>3</sub>)  $\delta$  = 150.23, 141.28, 140.03, 136.20, 133.28, 130.52, 130.47, 130.24, 129.98, 128.96, 128.75, 128.41, 128.25, 128.18, 128.08, 127.57, 127.16, 125.32, 120.65, 21.26. HR-MS (ESI): calculated for  $C_{28}H_{22}N_2$  ( $[M+H]^+$ ): 387.1856, observed : 387.1858.

#### 5A.4.2.5 Synthesis of compound 5

Compound 2 (2.0 g, 5.35 mmol), 4-cyanophenylboronic acid (1.02 g, 6.96 mmol), sodium carbonate (1.7 g, 16.07 mmol) and  $Pd(PPh_3)_4$  (0.185 g, 0.16 mmol) were taken in a two necked round bottomed flask. A mixture of THF and water (THF:H<sub>2</sub>O = 20:8) was degassed for 30 minutes and added to the reaction mixture under nitrogen atmosphere. The reaction mixture was refluxed for 24 h. After completion of the reaction, the compound was extracted with water and dichloromethane (3 x 50 mL).

The organic phase was collected and dried over anhydrous sodium sulphate. The solvent was concentrated and the product was purified using silica gel column chromatography (EtOAc/ n-hexane (2:98)). Yield: 0.90 g (42%).  $^1\text{H}$  NMR (400 MHz,  $\text{CDCl}_3$ )  $\delta$  = 7.51 – 7.43 (m, 4H), 7.37 – 7.22 (m, 11H), 7.16 (d,  $J$ =8.3, 2H), 7.08 – 7.01 (m, 2H).  $^{13}\text{C}$  NMR (101 MHz,  $\text{CDCl}_3$ )  $\delta$  150.37, 141.81, 139.54, 138.35, 132.46, 132.0, 131.11, 130.34, 129.39, 128.88, 128.76, 128.66, 128.59, 128.48, 128.15, 127.61, 125.34, 118.99, 118.88. HR-MS (ESI): calculated for  $\text{C}_{28}\text{H}_{19}\text{N}_3$  ( $[\text{M}+\text{H}]^+$ ): 398.1652, observed : 398.1654.

#### 5A.4.2.6 Synthesis of compound 9

3,5-diphenyl-1H-pyrazole (2.62 g, 11.2 mmol), 2-iodonaphthalene (2.02 g, 7.95 mmol), CuI (0.45g, 2.39 mmol), 1,10-phenanthroline (0.57 g, 3.18 mmol),  $\text{Cs}_2\text{CO}_3$  (5.18 g, 15.9 mmol) were taken in a two necked round bottom flask under nitrogen atmosphere and anhydrous degassed DMF was added. The reaction mixture was heated to reflux for 24h. The reaction mixture was cooled to room temperature, diluted with ethyl acetate and passed through silica gel. The solvent was removed under reduced pressure and the resultant residue was purified by silica gel column chromatography using ethyl acetate and n-hexane (5:95) as eluent. Yield: 1.79 g (65%).  $^1\text{H}$  NMR (400 MHz,  $\text{CDCl}_3$ )  $\delta$  = 8.01 – 7.94 (m, 2H), 7.92 (s, 1H), 7.81 (d,  $J$ =8.9, 3H), 7.55 – 7.42 (m, 5H), 7.31 (d,  $J$ =4.7, 6H), 6.89 (s, 1H).  $^{13}\text{C}$  NMR (101 MHz,  $\text{CDCl}_3$ )  $\delta$  152.17, 128.84, 128.79, 128.75, 128.60, 128.46, 128.25, 127.79, 126.73, 125.97, 123.71, 123.52, 105.45. HR-MS (ESI): calculated for  $\text{C}_{25}\text{H}_{18}\text{N}_2$  ( $[\text{M}+\text{H}]^+$ ): 347.1543, observed : 347.1549.

#### 5A.4.2.7 Synthesis of compound 10

A mixture of compound **9** (1.5 g, 4.3 mmol) and N-bromosuccinimide (0.78 g, 5.19 mmol) was taken in dichloromethane (40 mL). The reaction mixture was stirred at room



temperature in dark for 24 h. After completion of the reaction, the product was extracted using water and dichloromethane (3 x 50 mL). The organic phase was collected and dried over anhydrous sodium sulphate. The solvent was concentrated and the product was purified by silica gel column chromatography using ethyl acetate and n-hexane (5:95) as eluent. Yield: 1.40 g (76%).  $^1\text{H}$  NMR (400 MHz,  $\text{CDCl}_3$ )  $\delta$  = 8.07 (t,  $J$ =8.2, 2H), 7.86 – 7.79 (m, 2H), 7.75 (t,  $J$ =6.9, 2H), 7.55 – 7.34 (m, 11H).  $^{13}\text{C}$  NMR (101 MHz,  $\text{CDCl}_3$ )  $\delta$  149.98, 142.27, 137.28, 132.26, 133.14, 131.99, 130.30, 129.13, 129.07, 128.76, 128.62, 128.55, 128.44, 128.22, 128.18, 127.74, 126.81, 126.58, 123.11, 122.99, 95.17. HR-MS (ESI): calculated for  $\text{C}_{25}\text{H}_{17}\text{BrN}_2$  ( $[\text{M}+\text{H}]^+$ ): 425.0648, observed: 425.0652.

#### 5A.4.2.8 Synthesis of compound 11

Compound **10** (1.0 g, 2.3 mmol), benzene boronic acid (0.34 g, 2.82 mmol), sodium carbonate (0.78 g, 7.36 mmol) and  $\text{Pd}(\text{PPh}_3)_4$  (0.08 g, 0.069 mmol) were taken in a two necked round bottomed flask. A mixture of THF and water ( $\text{THF}:\text{H}_2\text{O}$  = 20:8) was degassed for 30 minutes and added to the reaction mixture under nitrogen atmosphere. The reaction mixture was refluxed for 24 h. After completion of the reaction, the compound was extracted with water and dichloromethane (3 x 50 mL). The organic phase was collected and dried over anhydrous sodium sulphate. The solvent was concentrated and the product was purified using silica gel chromatography. Yield: 0.80 g, 82%.  $^1\text{H}$  NMR (400 MHz,  $\text{CDCl}_3$ )  $\delta$  = 7.92 (s, 1H), 7.88 – 7.82 (m, 1H), 7.77 (t,  $J$ =7.5, 2H), 7.60 (dd,  $J$ =6.5, 3.0, 2H), 7.55 – 7.47 (m, 2H), 7.48 – 7.41 (m, 1H), 7.40 – 7.10 (m, 13H).  $^{13}\text{C}$  NMR (101 MHz,  $\text{CDCl}_3$ )  $\delta$  150.50, 141.55, 137.48, 133.24, 133.15, 133.11, 132.12, 130.76, 130.50, 130.10, 128.54, 128.48, 128.38, 128.28, 128.26, 128.21, 127.72, 126.74, 126.64, 126.35, 123.66, 123.48, 120.92. HR-MS (ESI): calculated for  $\text{C}_{31}\text{H}_{22}\text{N}_2$  ( $[\text{M} + \text{H}]^+$ ): 423.1856, observed : 423.1876.

---

**5A.4.2.9 Synthesis of compound 13**

4-nitrophenylhydrazine (6.0 g, 39.14 mmol) and 1,3-diphenylpropane-1,3-dione (7.98 g, 35.58 mmol) were dissolved in methanol / acetic acid (1:1) and heated to reflux for 24 hr. The reaction mixture was cooled to room temperature and poured into water. The mixture was extracted with ethyl acetate and dried over  $\text{Na}_2\text{SO}_4$ . The solvent was removed under reduced pressure and the resulting residue was purified by silica gel column chromatography using ethyl acetate / *n*-hexane as eluent. Yield: 7.28 g, (60%).  $^1\text{H}$  NMR (400 MHz,  $\text{CDCl}_3$ )  $\delta$  = 8.24 – 8.16 (m, 2H), 7.96 – 7.89 (m, 2H), 7.58 – 7.52 (m, 2H), 7.49 – 7.37 (m, 6H), 7.34 – 7.28 (m, 2H), 6.87 (s, 1H).  $^{13}\text{C}$  NMR (101 MHz,  $\text{CDCl}_3$ )  $\delta$  153.42, 145.91, 145.69, 145.06, 145.02, 132.40, 130.21, 129.23, 129.07, 128.96, 128.91, 128.73, 126.04, 124.60, 124.55, 107.33. HR-MS (ESI): calculated for  $\text{C}_{21}\text{H}_{16}\text{N}_3\text{O}_2$  ( $[\text{M}+\text{H}]^+$ ): 342.1237, found : 342.1252.

**5A.4.2.10 Synthesis of compound 14**

A mixture of compound **13** (2.80 g, 8.2 mmol) and N-bromosuccinimide (1.94 g, 9.84 mmol) were taken in dichloromethane. The reaction mixture was stirred at room temperature in dark for 24 h. After completion of the reaction, the product was extracted using water and dichloromethane (3 x 50 mL). The organic phase was collected and dried over anhydrous sodium sulphate. The reaction mixture was concentrated and the product was purified using silica gel column chromatography (*n*-hexane/EtOAc (95:5). Yield: 2.10 g (61%).  $^1\text{H}$  NMR (400 MHz,  $\text{CDCl}_3$ )  $\delta$  = 8.19 – 8.14 (m, 2H), 8.03 – 7.98 (m, 2H), 7.54 – 7.43 (m, 8H), 7.39 – 7.33 (m, 2H).  $^{13}\text{C}$  NMR (101 MHz,  $\text{CDCl}_3$ )  $\delta$  = 151.16, 145.99, 144.45, 142.54, 131.30, 130.10, 129.82, 129.10, 129.01, 128.57, 128.54, 128.10, 97.20. HR-MS (ESI) : calculated for  $\text{C}_{21}\text{H}_{14}\text{BrN}_3\text{O}_2$  ( $[\text{M}+\text{H}]^+$ ): 420.0342, observed : 421.0336.

**5A.4.2.11 Synthesis of compound 15**

A mixture of compound **14** (1.40 g, 3.73 mmol), benzene boronic acid (0.55 g, 4.48 mmol), sodium carbonate (1.19 g, 11.19 mmol) and Pd(PPh<sub>3</sub>)<sub>4</sub> (0.1 g, 0.11 mmol) were taken. A mixture of THF and water (THF:H<sub>2</sub>O = 20:8) was degassed for 30 minutes and added to the reaction mixture under nitrogen atmosphere. The reaction mixture was refluxed for 24 h. After completion of the reaction, the compound was extracted with water and dichloromethane (3 x 50 mL). The organic phase was collected and dried over anhydrous sodium sulphate. The solvent was removed under reduced pressure and the resultant residue was purified using silica gel column chromatography (*n*-hexane/EtOAc) (98:2). Yield: 0.940 g (62%). <sup>1</sup>H NMR (400 MHz, CDCl<sub>3</sub>) δ = 8.17 (d, *J*=9.1, 2H), 7.52 (t, *J*=7.8, 4H), 7.38 – 7.27 (m, 6H), 7.25 – 7.20 (m, 3H), 7.15 – 7.07 (m, 4H). <sup>13</sup>C NMR (101 MHz, CDCl<sub>3</sub>) δ = 151.75, 145.72, 144.85, 141.76, 132.43, 132.26, 130.59, 130.31, 129.60, 128.98, 128.84, 128.35, 128.32, 128.19, 127.11, 124.48, 124.37, 122.57. HR-MS (ESI): calculated for C<sub>27</sub>H<sub>19</sub>N<sub>3</sub>O<sub>2</sub> ([M+H]<sup>+</sup>): 418.1550, observed : 418.1576.

**5A.4.2.12 Synthesis of compound 16**

Compound **15** (0.80 g 1.91 mmol), 10% Pd/C (0.020g, 0.019 mmol) and hydrazine monohydrate (1.11 ml, 23 mmol) were taken in a two necked round bottomed flask and ethanol was added to it. The resulting mixture was heated to reflux for 12h under nitrogen atmosphere and then filtered through celite in hot condition. The filtrate was evaporated to dryness and the obtained residue was purified by silica gel column chromatography using dichloromethane/ *n*-hexane (10:90) as eluent. Yield: 0.7 g (95%). <sup>1</sup>H NMR (400 MHz, CDCl<sub>3</sub>) δ = 7.52 (dd, *J*=6.5, 3.1, 2H), 7.27 (dd, *J*=5.0, 1.7, 3H), 7.23 – 7.16 (m, 6H), 7.14 – 7.03 (m, 6H), 6.61 – 6.56 (m, 2H), 3.69 (s, 2H). <sup>13</sup>C NMR (101 MHz,

$\text{CDCl}_3$ )  $\delta$  = 149.55, 145.81, 141.33, 133.39, 133.35, 131.30, 130.74, 130.49, 130.22, 128.45, 128.20, 128.17, 127.93, 127.50, 126.79, 126.55, 119.96, 114.91. HR-MS (ESI): calculated for  $\text{C}_{27}\text{H}_{21}\text{N}_3$  ( $[\text{M}+\text{H}]^+$ ): 388.1808, observed : 388.1822.

#### 5A.4.2.13 Synthesis of compound 17

Compound **16** (1.5 g, 3.87 mmol), iodobenzene (1.29 mL, 11.61 mmol), potassium *tert*-butoxide (1.3 g, 11.63 mmol), CuI (0.442 g, 2.322 mmol), 1,10-phenanthroline (0.418 g, 2.322 mmol) were taken in a two necked round bottom flask under nitrogen atmosphere and anhydrous degassed toluene was added. The reaction mixture was heated to reflux for 24 h. The reaction mixture was cooled to room temperature, diluted with ethyl acetate and passed through silicagel. The solvent was removed under reduced pressure and the resultant residue was purified by silica gel column chromatography using ethyl acetate and *n*-hexane (5:95) as eluent. Yield: 1.5 g (74 %).  $^1\text{H}$  NMR (400 MHz,  $\text{CDCl}_3$ )  $\delta$  = 7.53 (s, 2H), 7.32 – 7.19 (m, 13H), 7.17 (d,  $J$ =8.1, 2H), 7.10 (s, 8H), 7.01 (dd,  $J$ =21.1, 7.7, 4H).  $^{13}\text{C}$  NMR (101 MHz,  $\text{CDCl}_3$ )  $\delta$  = 149.82, 147.41, 147.00, 141.41, 134.02, 133.13, 130.71, 130.45, 130.06, 129.32, 128.42, 128.18, 127.62, 126.63, 126.24, 124.64, 123.25, 123.07, 120.38. HR-MS (ESI): calculated for  $\text{C}_{39}\text{H}_{29}\text{N}_3$  ( $[\text{M} + \text{H}]^+$ ): 540.2434, observed : 540.2409.

#### General procedure for the synthesis of compounds 6-8, 12 and 18

A three-neck round-bottom flask with a dropping funnel was degassed and after purging with vacuum–nitrogen cycles, dichloromethane solution of compounds **3-5**, **11** and were added. *N,N*-diisopropylethylamine (*i*-Pr<sub>2</sub>NEt) was added to this solution at 0 °C. After 10 minute,  $\text{BBr}_3$  (1.0 M in dichloromethane) was added dropwise at 0 °C and the reaction mixture was heated to room temperature. The reaction mixture was stirred at room temperature for 24 h, a saturated potassium carbonate aqueous solution was added and this mixture was extracted with dichloromethane. The organic layers were washed

with water, dried over sodium sulfate and concentrated using a rotary evaporator to give the dibromoboron compound. This crude dibromoboron product was charged in a round-bottom flask and after purging with vacuum–nitrogen cycles, toluene was added to it. To this stirred solution  $\text{AlMe}_3$  was added. After being stirred at this temperature for 30 min, the reaction was quenched by adding water. The organic layer was separated and dried over  $\text{Na}_2\text{SO}_4$ . The reaction mixture was concentrated and the residue was purified using silica gel column chromatography (dichloromethane/ n-hexane).

#### 5A.4.2.14 Synthesis of compound 6

The quantities involved are as follows: compound **3** (0.8 g, 2.14 mmol), *N,N*-diisopropylethylamine (0.370 mL, 2.14 mmol),  $\text{BBr}_3$  (1.0 M in  $\text{CH}_2\text{Cl}_2$ , 6.44 mL, 6.44 mmol), and  $\text{AlMe}_3$  (2 M in hexane, 2.36 mL, 4.72 mmol). Yield: 0.25 g (56 %).  $^1\text{H}$  NMR (400 MHz,  $\text{CDCl}_3$ )  $\delta$  = 7.54 (q,  $J$ =7.1, 5.7, 5H), 7.48 – 7.36 (m, 6H), 7.16 (q,  $J$ =6.6, 5.9, 1H), 7.10 (q,  $J$ =5.6, 3H), 6.99 – 6.87 (m, 3H), 6.50 (d,  $J$ =8.1, 1H), -0.01 (s, 6H).  $^{13}\text{C}$  NMR (101 MHz,  $\text{CDCl}_3$ )  $\delta$  = 145.97, 138.43, 136.24, 130.72, 130.70, 130.32, 130.15, 130.12, 129.65, 129.16, 129.06, 128.29, 128.10, 127.93, 127.07, 126.63, 124.81, 124.10, 112.21, 9.43.  $^{11}\text{B}$  NMR (128 MHz,  $\text{CDCl}_3$ )  $\delta$  = -0.10. HR-MS (ESI): calculated for  $\text{C}_{29}\text{H}_{25}\text{BN}_2$  ( $[\text{M}+\text{H}]^+$ ): 413.2189, observed : 413.2209. IR (KBr):  $\nu(\text{cm}^{-1})$  = 3226(m), 2082(m), 1636(s), 1104(m), 697(m).

#### 5A.4.2.15 Synthesis of compound 7

The quantities involved are as follows: compound **4** (1.2 g, 3.10 mmol), *N,N*-diisopropylethylamine (0.537 mL, 3.10 mmol),  $\text{BBr}_3$  (1.0 M in  $\text{CH}_2\text{Cl}_2$ , 9.31 mL, 9.31 mmol), and  $\text{AlMe}_3$  (2 M in hexane, 3.41 mL, 6.83 mmol). Yield: 0.6 g (56 %).  $^1\text{H}$  NMR (400 MHz,  $\text{CDCl}_3$ )  $\delta$  = 7.60 – 7.49 (m, 5H), 7.43 (m, 6H), 7.17 (s, 1H), 6.93 – 6.80 (m, 5H), 6.49 (d,  $J$ =8.1, 1H), 2.22 (s, 3H), -0.01 (s, 6H).  $^{13}\text{C}$  NMR (101 MHz,  $\text{CDCl}_3$ )  $\delta$  =

145.89, 138.46, 136.73, 136.10, 130.72, 130.71, 130.07, 129.90, 129.61, 129.20, 120.12, 120.09, 128.85, 128.43, 127.90, 127.27, 126.55, 124.77, 124.04, 112.16, 21.13, 9.43.  $^{11}\text{B}$  NMR (128 MHz,  $\text{CDCl}_3$ )  $\delta = 0.01$ . HR-MS (ESI): calculated for  $\text{C}_{30}\text{H}_{27}\text{BN}_2$  ( $[\text{M}+\text{H}]^+$ ): 427.2345, observed : 427.2355. IR (KBr):  $\nu(\text{cm}^{-1}) = 3420(\text{m})$ ,  $1654(\text{s})$ ,  $1629(\text{m})$ ,  $1450(\text{m})$ ,  $1381(\text{m})$ ,  $1279(\text{m})$ ,  $752(\text{m})$ ,  $696(\text{m})$ ,  $551(\text{m})$ .

#### 5A.4.2.16 Synthesis of compound 8

The quantities involved are as follows: compound **5** (0.9 g, 2.26 mmol), *N,N*-diisopropylethylamine (0.39 mL, 2.26 mmol),  $\text{BBr}_3$  (1.0 M in  $\text{CH}_2\text{Cl}_2$ , 6.79 mL, 6.79 mmol), and  $\text{AlMe}_3$  (2 M in hexane, 2.49 mL, 4.98 mmol). Yield: 0.25 g (25 %).  $^1\text{H}$  NMR (400 MHz,  $\text{CDCl}_3$ )  $\delta = 7.66 - 7.33$  (m, 13H), 7.19 (t,  $J=7.2$ , 1H), 7.01 (d,  $J=8.2$ , 2H), 6.92 (t,  $J=7.7$ , 1H), 6.49 (d,  $J=8.1$ , 1H), -0.02 (s, 6H).  $^{13}\text{C}$  NMR (101 MHz,  $\text{CDCl}_3$ )  $\delta$  145.98, 136.40, 135.40, 131.92, 130.68, 130.56, 130.47, 130.36, 129.76, 129.67, 129.52, 128.31, 128.27, 127.55, 127.02, 124.94, 122.17, 118.56, 112.36, 110.75, 9.30.  $^{11}\text{B}$  NMR (128 MHz,  $\text{CDCl}_3$ )  $\delta = -0.38$ . HR-MS (ESI): calculated for  $\text{C}_{30}\text{H}_{24}\text{BN}_3$  ( $[\text{M}+\text{H}]^+$ ): 438.2141, observed : 438.2144. IR (KBr):  $\nu(\text{cm}^{-1}) = 3472(\text{m})$ ,  $3411(\text{m})$ ,  $1719(\text{m})$ ,  $1511(\text{m})$ ,  $753(\text{m})$ ,  $699(\text{m})$ .

#### 5A.4.2.17 Synthesis of compound 12

The quantities involved are as follows: compound **11** (0.8 g, 1.89 mmol), *N,N*-diisopropylethylamine (0.327 mL, 1.89 mmol),  $\text{BBr}_3$  (1.0 M in  $\text{CH}_2\text{Cl}_2$ , 5.68 mL, 5.68 mmol), and  $\text{AlMe}_3$  (2 M in hexane, 2.07 mL, 4.15 mmol). Yield: 0.6 g (69 %).  $^1\text{H}$  NMR (400 MHz,  $\text{CDCl}_3$ )  $\delta = 8.17$  (d,  $J=8.3$ , 1H), 7.78 (d,  $J=8.1$ , 1H), 7.66 – 7.37 (m, 13H), 7.10 (d,  $J=6.7$ , 3H), 6.97 (d,  $J=7.5$ , 2H), 6.73 (d,  $J=8.8$ , 1H), 0.22 (s, 6H).  $^{13}\text{C}$  NMR (101 MHz,  $\text{CDCl}_3$ )  $\delta$  145.97, 135.92, 134.91, 134.63, 132.39, 130.97, 130.46, 130.24, 129.28, 129.25, 129.22, 128.60, 128.56, 128.48, 128.18, 128.05, 127.12, 126.20,

125.84, 125.42, 124.16, 112.33, 77.48, 77.16, 76.84, 9.79.  $^{11}\text{B}$  NMR (128 MHz,  $\text{CDCl}_3$ )  $\delta = 0.93$ . HR-MS (ESI): calculated for  $\text{C}_{33}\text{H}_{27}\text{BN}_2$  ( $[\text{M}+\text{H}]^+$ ): 463.2346, observed : 463.2329. IR (KBr):  $\nu(\text{cm}^{-1}) = 3359(\text{m}), 2068(\text{m}), 1635(\text{s}), 1109(\text{m}), 697(\text{m})$ .

#### 5A.4.2.18 Synthesis of compound 18

The quantities involved are as follows: compound **17** (1.5 g, 2.77 mmol), *N,N*-diisopropylethylamine (0.479 mL, 2.77 mmol),  $\text{BBr}_3$  (0.788 mL, 8.31 mmol, 1.0 M in  $\text{CH}_2\text{Cl}_2$ ), and  $\text{AlMe}_3$  (3 mL, 6.09 mmol, 2 M in hexane). Yield: 1.05 g (66 %).  $^1\text{H}$  NMR (400 MHz,  $\text{CDCl}_3$ )  $\delta = 7.55 - 7.35$  (m, 10H), 7.25 – 7.17 (m, 5H), 7.09 (q,  $J=7.7$ , 6.5, 7H), 6.96 (td,  $J=9.3$ , 7.7, 4.7, 4H), 6.56 (d,  $J=7.4$ , 1H), 6.35 (d,  $J=8.6$ , 1H), -0.07 (s, 6H).  $^{13}\text{C}$  NMR (176 MHz,  $\text{CDCl}_3$ )  $\delta = 148.05, 145.64, 135.58, 130.68, 130.38, 130.04, 129.09, 128.26, 128.05, 127.90, 126.98, 125.19, 124.06, 123.70, 122.37, 120.92, 112.79, 9.36$ .  $^{11}\text{B}$  NMR (128 MHz,  $\text{CDCl}_3$ )  $\delta = 0.78$ . HR-MS (ESI): calculated for  $\text{C}_{41}\text{H}_{34}\text{BN}_3$  ( $[\text{M}+\text{H}]^+$ ): 580.2926, observed : 580.2905. IR (KBr):  $\nu(\text{cm}^{-1}) = 3180(\text{m}), 2060(\text{m}), 1638(\text{s}), 1115(\text{m}), 754(\text{m})$ .

#### 5A.5 References

1. Zhelev, Z.; Ohba, H.; Bakalova, R. *J. Am. Chem. Soc.* **2006**, *128*, 6324.
2. Bakalova, R.; Zhelev, Z.; Aoki, I.; Ohba, H.; Imai, Y.; Kanno, I. *Anal. Chem.* **2006**, *78*, 5925.
3. Birks, J. B. *Photophysics of Aromatic Molecules*, Wiley, London, 1970.
4. Luo, J.; Xie, Z.; Lam, J. W. Y.; Cheng, L.; Chen, H.; Qiu, C.; Kwok, H. S.; Zhan, X.; Liu, Y.; Zhu, D.; Tang, B. Z. *Chem. Commun.* **2001**, 1740.
5. Shimizu, M.; Tatsumi, H.; Mochida, K.; Shimono, K.; Hiyama, T. *Chem. - Asian J.* **2009**, *4*, 1289.
6. Hu, R.; Lam, J. W. Y.; Liu, Y.; Zhang, X.; Tang, B. Z. *Chem. Eur. J.* **2013**, *19*,

---

5617.

7. Zhang, Z.; Xu, B.; Su, J.; Shen, L.; Xie, Y.; Tian, H. *Angew. Chem. Int. Ed.* **2011**, *50*, 11654.
8. Yang, L.; Ye, J.; Xu, L.; Yang, X.; Gong, W.; Lin, Y.; Ning, G. *RSC Adv.* **2012**, *2*, 11529.
9. Zhang, X.; Ye, J.; Xu, L.; Yang, L.; Deng, D.; Ning, G. *J. Lumin.* **2013**, *139*, 28.
10. An, B.-K.; Gierschner, J.; Park, S. Y. *Acc. Chem. Res.* **2012**, *45*, 544.
11. Tracy, H. J.; Mullin, J. L.; Klooster, W. T.; Martin, J. A.; Haug, J.; Wallace, S.; Rudloe, I.; Watts, K. *Inorg. Chem.* **2005**, *44*, 2003.
12. Tang, W.; Xiang, Y.; Tong, A. *J. Org. Chem.* **2009**, *74*, 2163.
13. Qian, Y.; Cai, M.; Zhou, X.; Gao, Z.; Wang, X.; Zhao, Y.; Yan, X.; Wei, W.; Xie, L.; Huang, W. *J. Phys. Chem. C* **2012**, *116*, 12187.
14. Upamali, K. A. N.; Estrada, L. A.; De, P. K.; Cai, X.; Krause, J. A.; Neckers, D. *C. Langmuir* **2011**, *27*, 1573.
15. Bandrowsky, T. L.; Carroll, J. B.; Braddock-Wilking, J. *Organometallics* **2011**, *30*, 3559.
16. Mutai, T.; Tomoda, H.; Ohkawa, T.; Yabe, Y.; Araki, K. *Angew. Chem. Int. Ed.* **2008**, *47*, 9522.
17. Yu, Z.; Duan, Y.; Cheng, L.; Han, Z.; Zheng, Z.; Zhou, H.; Wu, J.; Tian, Y. *J. Mater. Chem.* **2012**, *22*, 16927.
18. Liu, G.; Yang, M.; Wang, L.; Zheng, J.; Zhou, H.; Wu, J.; Tian, Y. *J. Mater. Chem. C* **2014**, *2*, 2684.
19. Yao, B.; Mei, J.; Li, J.; Wang, J.; Wu, H.; Sun, J. Z.; Qin, A.; Tang, B. Z. *Macromolecules* **2014**, *47*, 1325.
20. Huang, G.; Ma, B.; Chen, J.; Peng, Q.; Zhang, G.; Fan, Q.; Zhang, D. *Chem. Eur.*



---

*J.* **2012**, *18*, 3886.

21. Ma, C.; Ling, Q.; Xu, S.; Zhu, H.; Zhang, G.; Zhou, X.; Chi, Z.; Liu, S.; Zhang, Y.; Xu, J. *Macromol. Biosci.* **2014**, *14*, 235.

22. Shiraishi, K.; Kashiwabara, T.; Sanji, T.; Tanaka, M. *New J. Chem.* **2009**, *33*, 1680.

23. Arseneault, M.; Leung, N. L. C.; Fung, L. T.; Hu, R.; Morin, J.-F.; Tang, B. Z. *Polym. Chem.* **2014**, *5*, 6087.

24. Sun, H.-L.; Jiang, R.; Li, Z.; Dong, Y. Q.; Du, M. *CrystEngComm* **2013**, *15*, 1669.

25. Jäkle, F. *Chem. Rev.* **2010**, *110*, 3985.

26. Gabbai, F. P. *Angew. Chem. Int. Ed.* **2012**, *51*, 6316.

27. Li, S. Y. ; Sun, Z. B.; Zhao, C. H. *Inorg. Chem.* **2017**, *56*, 8705.

28. Møllerup, S. K. ; Wang, S. *Trends Chem.* **2019**, *1*, 77.

29. Kirschner, S.; Mewes, J.-M.; Bolte, M.; Lerner, H.-W.; Dreuw A. ; Wagner, M. *Chem. –Eur. J.*, **2017**, *23*, 5104.

30. John, A.; Bolte, M. ; Lerner H. W.; Wagner, M. *Angew. Chem. Int. Ed.* **2017**, *56*, 5588.

31. Hu, K. ; Zhang, Z.; Burke J. ; Qin, Y. *J. Am. Chem. Soc.* **2017**, *139*, 11004.

32. Yoshii, R.; Hirose, A.; Tanaka K.; Chujo, Y. *J. Am. Chem. Soc.* **2014**, *136*, 18131.

33. Kushida, T.; Shuto, A.; Yoshio, M.; Kato, T.; Yamaguchi, S. *Angew. Chem. Int. Ed.* **2015**, *54*, 6922.

34. Møllerup, S. K.; Wang, S. *Chem. Soc. Rev.* **2019**, *48*, 3537.

35. Pandey, U. P.; Thilagar, P. *Adv. Opt. Mater.* **2020**, 1902145.

36. Riensch, N. A.; Fritze, L.; Schindler, T. ; Kremer, M. ; Helten, H. *Dalton Trans.* **2018**, *47*, 10399.

37. Lin, H.; Patel, S.; Jäkle, F. *Macromolecules* **2020**, *53*, 10601.

- 
38. Ji, L.; Griesbeck, S.; Marder, T. B.; *Chem. Sci.* **2017**, 8, 846..
39. Pagidi, S.; Kalluvettukuzhy, N. K.; Thilagar, P. *Inorg. Chem.*, **2020**, 59, 3142.
40. Yuan, K.; Kahan, R. J.; Si, C.; Williams, A.; Kirschner, S.; Uzelac, M. ; Zysman-Colman, E.; Ingleson, M. *Chem. Sci.* **2020**, 11, 3258.
41. K. Mishiba, Y. Tanaka and M. Akita, *Chem. –Eur. J.*, **2021**, 27, 1.
42. Ji, L.; Krummenacher, I.; Friedrich, A.; Lorbach, A.; Haehnel, M.; Edkins, K.; Braunschweig, H.; Marder, T. B. *J. Org. Chem.* **2018**, 83, 3599.
43. Griesbeck, S.; Michail, E.; Rauch, F.; Ogasawara, H.; Wang, C. ; Sato, Y.; Edkins, R. M.; Zhang, Z.; Taki, M.; Lambert, C.; Yamaguchi, S.; Marder, T. B. *Chem. – Eur. J.*, **2019**, 25, 13164.
44. Griesbeck, S.; Michail, E.; Wang, C.; Ogasawara, H.; Lorenzen, S.; Gerstner, L.; Zang, T.; Nitsch, J.; Sato, Y.; Taki, M.; Lambert, C.; Yamaguchi, S.; Marder, T. B. *Chem. Sci.*, **2019**, 10, 5405.
45. Zhang, F.; Noda, T. ; Kageyama, H.; Shirota, Y. *Proc. SPIE*, **2009**, 7213(1–5), 721302.
46. Yamaguchi, S. ; Akiyama S.; Tamao, K. *J. Am. Chem. Soc.*, **2001**, 123, 11372.
47. Parab, K.; Venkatasubbaiah, K.; Jäkle, F.; *J. Am. Chem. Soc.*, **2006**, 128, 12879.
48. Møllerup, S. K.; Rao, Y.-L.; Amarne, H.; Wang, S. *Org. Lett.*, **2016**, 18, 4436.
49. Swamy, C. A.; Mukherjee, P. S.; Thilagar, P. *Inorg. Chem.*, **2014**, 53, 4813.
50. Lee, H.; Jana, S.; Kim, J.; Lee, S. U.; Lee, M. H. *Inorg. Chem.*, **2020**, 59, 1414.
51. Wang, S. *Coord. Chem. Rev.* **2001**, 215, 79.
52. Li, D.; Zhang, H.; Wang, Y. *Chem. Soc. Rev.* **2013**, 42, 8416.
53. Tanaka, K.; Chujo, Y. *Npg Asia Mater.* **2015**, 7, e223.
54. Rao, Y.-L.; Wang, S. *Inorg. Chem.* **2011**, 50, 12263.
-

- 
55. Frath, D.; Massue, J.; Ulrich, G.; Ziessel, R. *Angew. Chem. Int. Ed. Engl.* **2014**, *53*, 2290.
56. Rao, Y.-L.; Amarne, H.; Wang, S. *Coord. Chem. Rev.* **2012**, *256*, 759.
57. Loudet, A.; Burgess, K. *Chem. Rev.* **2007**, *107*, 4891.
58. Ulrich, G.; Ziessel, R.; Harriman, A. *Angew. Chem. Int. Ed.* **2008**, *47*, 1184.
59. Ziessel, R.; Ulrich, G.; Harriman, A. *New J. Chem.* **2007**, *31*, 496.
60. Zhao, Z.; Lam, J. W. Y.; Tang, B. Z. *J. Mater. Chem.* **2012**, *22*, 23726-23740.
61. Xu, B. J.; Chi, Z. G.; Yang, Z. Y.; Chen, J. B.; Deng, S. Z.; Li, H. Y.; Li, X. F.; Zhang, Y.; Xu, N. S.; Xu, J. R. *J. Mater. Chem.* **2010**, *20*, 4135-4141.
62. He, J. T.; Xu, B.; Chen, F. P.; Xia, H. J.; Li, K. P.; Ye, L.; Tian, W. *J. J. Phys. Chem. C* **2009**, *113*, 9892-9899.
63. Zhang, Y.; Xu, H.; Xu, W.; Zhang, C.; Shi, J.; Tong, B.; Cai, Z.; Dong, Y. *Sci. China Chem.* **2019**, *62*, 1393-1397.
64. Mukundam, V. PhD thesis, National Institute of Science Education and Research (NISER), India, **2017**.
65. Sahoo, A. MSc thesis, National Institute of Science Education and Research (NISER), India, **2019**.
66. Dhanunjayarao, K.; Sa, S.; Nayak, P.; Ponniah S. J.; Venkatasubbaiah, K. *Organometallics*, **2019**, *38*, 870.
67. Dhanunjayarao, K.; Sa, S.; Aradhyula, B. P. R.; Venkatasubbaiah, K. *Tetrahedron*, **2018**, *74*, 5819.
68. Mukundam, V.; Sa, S.; Kumari, A.; Das, R.; Venkatasubbaiah, K. *J. Mater. Chem. C*, **2019**, *7*, 12725.
-

- 
69. Mukundam, V.; Sa, S.; Kumari, A.; Murali, A. C.; Nayak, P.; Das, R.; Venkatasubbaiah, K. *Dalton Trans.*, **2020**, 49, 7737.
70. Liang, Z.-Q.; Wang, X.-M.; Dai, G.-L.; Ye, C.-Q.; Zhou, Y.-Y.; Tao, X.-T. *New J. Chem.* **2015**, 39, 8874.
71. Caygill, J. S.; Davi, F.; Higson, S. P. J. *Talanta*, **2012**, 88, 14.
72. Salinas, Y.; Martinez-Manez, R.; Marcos, M. D.; Sancenon, F.; Costero, A. M.; Parra M.; Gil, S. *Chem. Soc. Rev.*, **2012**, 41, 1261.
73. Germain, M. E.; Knapp, M. J. *Chem. Soc. Rev.*, **2009**, 38, 2543.
74. Sohn, H.; Calhoun, R. M.; Sailor, M. J.; Trogler, W. C. *Angew. Chem., Int. Ed.*, **2001**, 40, 2104.
75. Akhavan, J. *The Chemistry of Explosives*, The Royal Society of Chemistry, London, 2nd edn, **2004**.
76. Ashbrook, P. C.; Houts, T. A. *Chem. Health Saf.*, **2003**, 10, 27.
77. Wollin, K. M.; Dieter, H. H. *Arch. Environ. Contam. Toxicol.*, **2005**, 49, 18.

## **CHAPTER 5B**

### **Boron doped tetraarylpyrazole AIEgens: Synthesis, Characterisation and Optical properties**

<b>5B.1 Introduction</b>	179
<b>5B.2 Results and discussion</b>	180
<b>5B.2.1 Synthesis and characterisation</b>	180
<b>5B.2.2 X-Ray studies</b>	181
<b>5B.2.3 Photophysical properties</b>	187
<b>5B.2.4 AIEE phenomenon</b>	190
<b>5B.2.5 Thermal studies</b>	195
<b>5B.2.6 Electrochemical properties</b>	196
<b>5B.3 Conclusions</b>	196
<b>5B.4 Experimental section</b>	197
<b>5B.4.1 General information</b>	197
<b>5B.4.2 Synthetic procedures and spectral characterisations</b>	198
<b>5B.5 References</b>	201



---

## 5B.1 Introduction

The growing demand for OLEDs<sup>1-3</sup> and energy efficient lighting<sup>4-8</sup> have drawn attention to develop new organic electronic materials.<sup>9</sup> Organic  $\pi$ -conjugated materials have shown intense emission in the dilute solution; however they are weakly emissive in the solid state due to aggregation which is known as aggregation-caused quenching (ACQ).<sup>10,11</sup> This effect hampered the fabrication of light emitting diodes using organic luminogen. To mitigate the obstacle caused by ACQ, anti-ACQ fluorophoric systems have been developed by several research groups. Aggregation induced emission (AIE) and aggregation induced enhanced emission (AIEE) are two phenomenon developed by Tang group<sup>12</sup> and Park group<sup>13</sup> to tackle the problem caused by ACQ. Since this seminal discovery, AIE and AIEE materials have gained momentum in the fabrication of OLEDs,<sup>14-18</sup> bioprobes<sup>19-21</sup> and chemosensors.<sup>22-24</sup>

Pyrazole is an important heterocyclic ring system and its chemistry has attracted tremendous research attention due to its application in pharmaceutical chemistry<sup>25-30</sup>, as building blocks for heterocycle synthesis<sup>31,32</sup>, as ligands for supramolecular chemistry and catalysis<sup>33-38</sup>, as efficient blue emitters for light emitting diodes.<sup>39-41</sup> Tetraaryl pyrazoles have been reported by several research groups.<sup>42-45</sup> For instance Peruncheralathan<sup>46</sup> and coworkers have reported a series of tetraaryl pyrazole molecules, with AIEE phenomenon. Their finding shows that phenyl rings are necessary to demonstrate the AIEE phenomenon. Our interest is to investigate whether AIEE phenomenon can be preserved with superior photophysical properties in B-N embedded tetraaryl pyrazoles. We believe that B-N coordination increases the planarity and rigidity of the  $\pi$ -conjugated scaffold which leads to intense luminescence.<sup>54-66</sup>

## 5B.2 Results and discussion

### 5B.2.1 Synthesis and characterisation

Ligands **1a-4a** and boron compounds **1b-4b** were prepared as described in chapter 5A. Target boron compounds **1-4** were prepared by addition of phenyl magnesium bromide solution to the precursor **1b-4b** (Scheme 5B.1). All the four B-N coordinated boron compounds were stable in air and can be purified through silica gel column chromatography. All the boron compounds were fully characterised using  $^1\text{H}$  NMR,  $^{13}\text{C}$  NMR,  $^{11}\text{B}$  NMR and HRMS analysis. The  $^{11}\text{B}$  NMR spectra of compounds **1-4** showed a peak at 1-3.2 ppm which suggest the formation of a tetracoordinated boron. An illustration example of boron NMR of compound **4** is shown in Figure 5B.1.

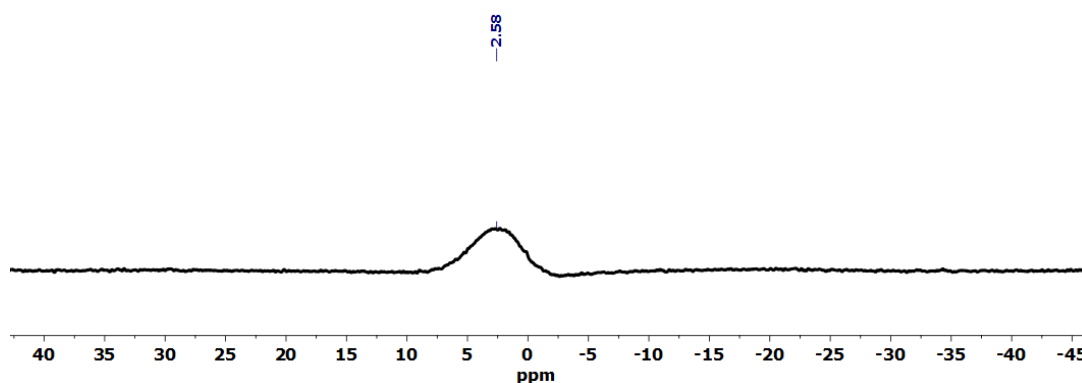
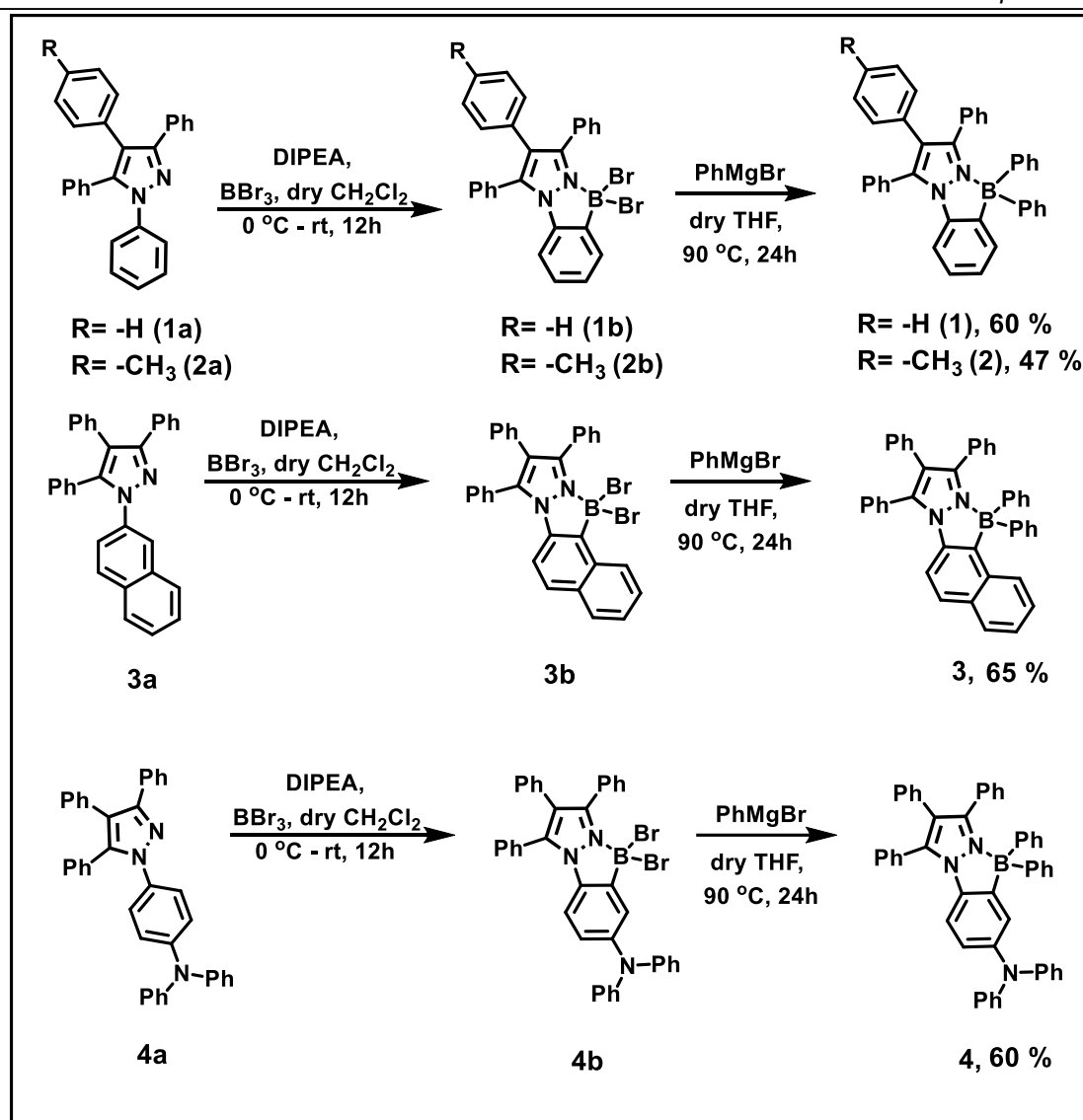


**Figure 5B.1:**  $^{11}\text{B}$  NMR spectrum of compound **4**.





**Scheme 5B.1:** Synthetic route to boron compounds **1-4**.

### 5B.2.2 X-ray studies

Single crystals of boron compounds **1-4** were obtained from slow evaporation of a mixture of dichloromethane and hexane and studied using single crystal x-ray crystallography (Figure **5B.2** and **5B.3**). Compounds **1**, **2** and **4** were crystallised in a monoclinic space group of  $P2_1/c$  while compound **3** was crystallised in a monoclinic space group of  $C2/c$ . The boron center in all four compounds lies in a distorted tetrahedral geometry. The B-N bond and B-C bond distances were found to be 1.632 Å, 1.607-1.622 Å for **1**; 1.64 Å, 1.617-1.623 Å for **2**; 1.654 Å, 1.602-1.608 Å for **3** and

1.640 Å, 1.620-1.623 Å for **4**, respectively which are consistent with literature reported value.<sup>48-49</sup>

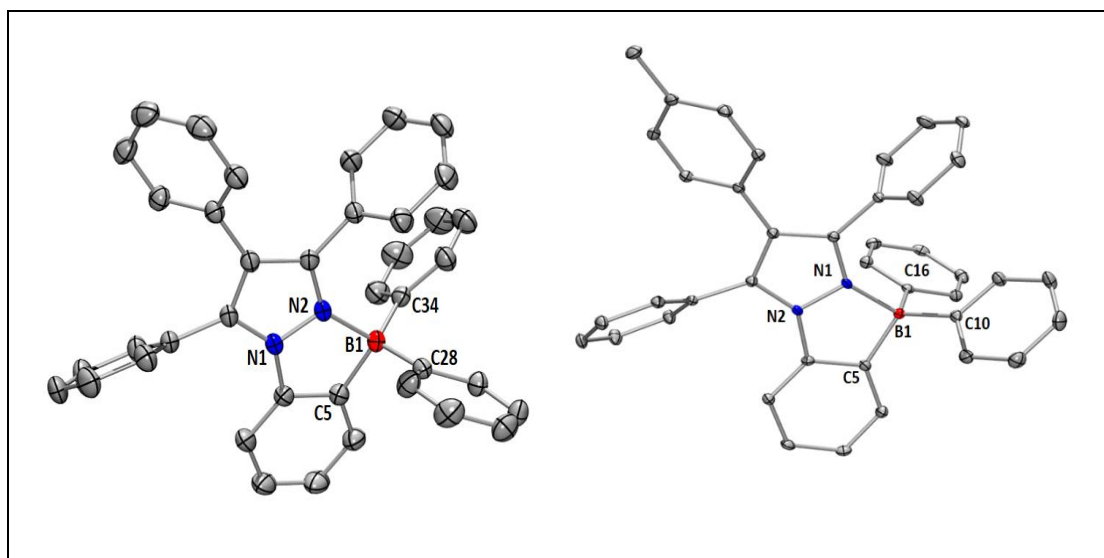


**Figure 5B.2:** Molecular structure of compound **1** (Left): Selected bond distances (Å): B1-N2: 1.633(2) , B1-C5: 1.619(2) , B1-C34: 1.607(2) , B1-C28: 1.622(2) . Bond angles ( °): C5-B1-N2: 94.7(1), C34-B1-N2: 110.1(1), C5-B1-C28: 107.65(1), C34-B1-C28: 116.1(1) and compound **2** (right): Selected bond distances (Å): B1-N1: 1.639(1) , B1-C5: 1.619(1) , B1-C10: 1.617(1) , B1-C16: 1.623(1) . Bond angles ( °): C5-B1-N1: 94.6(8), C16-B1-N1: 107.0(9), C16-B1-C10: 115.2(1), C5-B1-C10: 115.2(9).

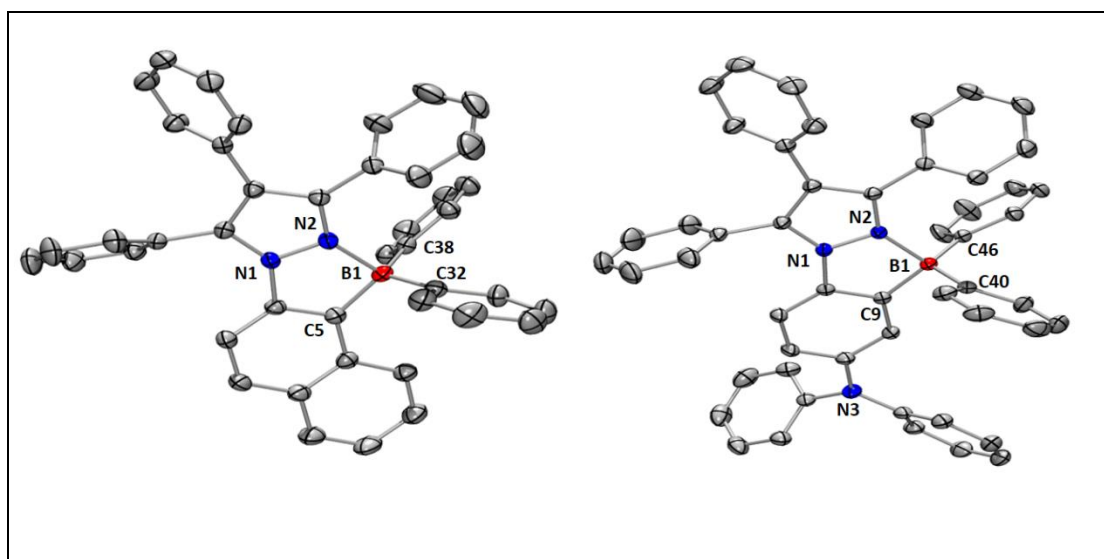
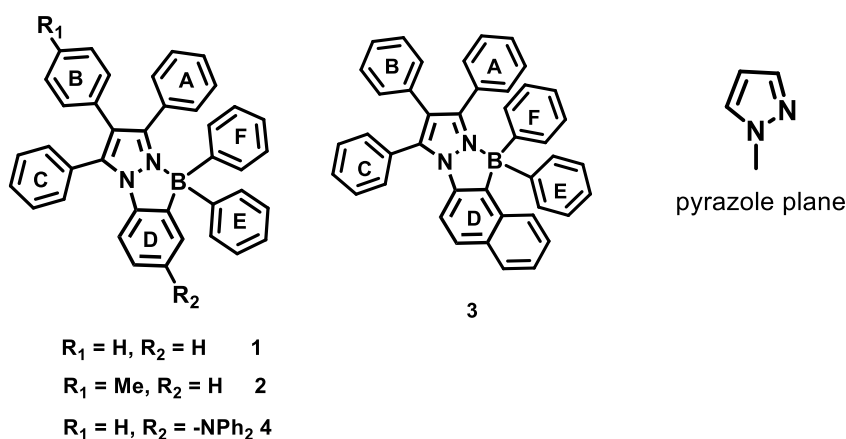


**Figure 5B.3:** Molecular structure of compound **3** (Left): Selected bond distances (Å): B1-N2: 1.654(2) , B1-C5: 1.601(3) , B1-C32: 1.605(3) , B1-C38: 1.608(3). Bond angles

( $^{\circ}$ ): C5-B1-N2: 94.5(1), C38-B1-N2: 112.1(1), C5-B1-C32: 112.1(1), C38-B1-C32: 115.2(1) and compound **4** (right): Selected bond distances ( $\text{\AA}$ ): B1-N2: 1.640(1), B1-C9: 1.620(2), B1-C40: 1.619(2), B1-C46: 1.623(2). Bond angles ( $^{\circ}$ ): C9-B1-N2: 95.1(9), C46-B1-N2: 108.8(1), C40-B1-C9: 110.1(1), C46-B1-C40: 118.1(1).

Table **5B.1** Comparison of deviation of boron from  $\text{C}_2\text{N}_2\text{B}$  plane ( $\text{\AA}$ ) and interplanar angles (degree) for compound **1-4**.



Compound	1	2	3	4
Deviation of boron (B) from $\text{C}_2\text{N}_2\text{B}$ plane ( $\text{\AA}$ )	0.044	0.089	0.05	0.038
Pyrazole // Plane A	70.6(2)	75.2(8)	63.2(2)	53.1(1)
Pyrazole // Plane B	41.8(2)	41.3(7)	52.1(3)	41.2(6)
Pyrazole // Plane C	66.9(2)	61.6(7)	59.3(2)	85.5 (8)
Pyrazole // Plane D	7.7(2)	7.1(8)	13.2(2)	7.2 (9)
Pyrazole // Plane E	86.7(2)	63.6(8)	81.2(2)	79.2(7)
Pyrazole // Plane F	79.5(2)	79.0(7)	78.7(2)	78.2 (2)

From the crystal data we observed the deviation of boron atom from the pyrazole plane ( $\text{C}_2\text{N}_2\text{B}$ ) which are ranging from 0.038  $\text{\AA}$  to 0.089  $\text{\AA}$  (Table **5B.1**). The interplanar angle between the pyrazole plane and plane A is 70.60  $^{\circ}$  (for compound **1**), 75.24  $^{\circ}$  (for

compound **2**), 63.24 ° (for compound **3**) and 53.21 ° (for compound **4**). Similarly the interplanar angles between the pyrazole and other planes are listed in the table **5B.1**. The phenyl rings attached to the pyrazole are surrounded in a nonplanar propellar shape arrangement. The propellar shape forced by the phenyl groups restricts these molecules to stack in a face to face fashion. Molecular packing of these compounds reveal several C-H $\cdots$  $\pi$  interactions with distances in the range of 2.778 Å to 2.947 Å, which assists in enhancing the molecular rigidity and limits the conformational freedom (Figure **5B.4** - **5B.7**) thus helps to get better turn on emission in the aggregate state, which will be discussed in the following section.

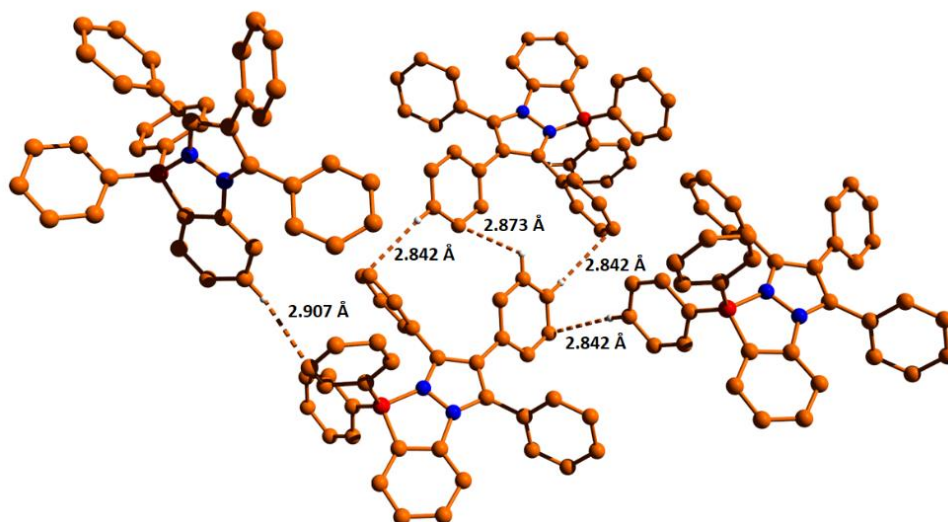


**Figure 5B.4:** Intermolecular interaction in compound **1** (C-H $\cdots$  $\pi$  : 2.842 Å to 2.907 Å).

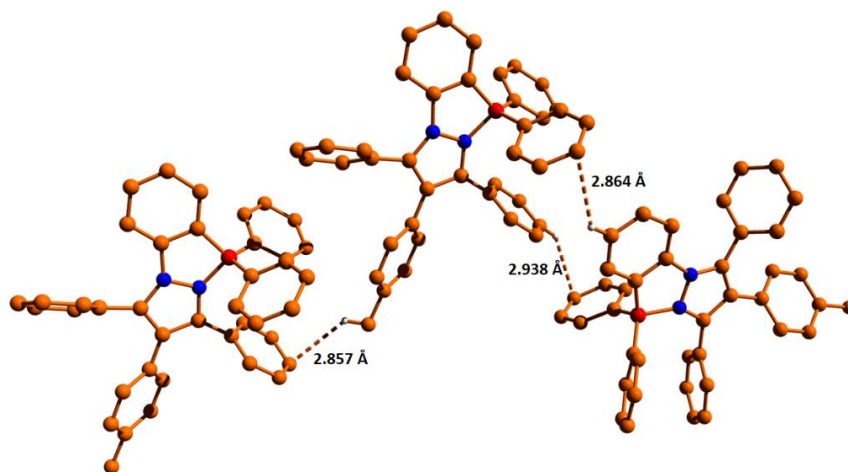


**Figure 5B.5:** Intermolecular interaction in compound **2** (C-H... $\pi$  : 2.857 Å to 2.947 Å).

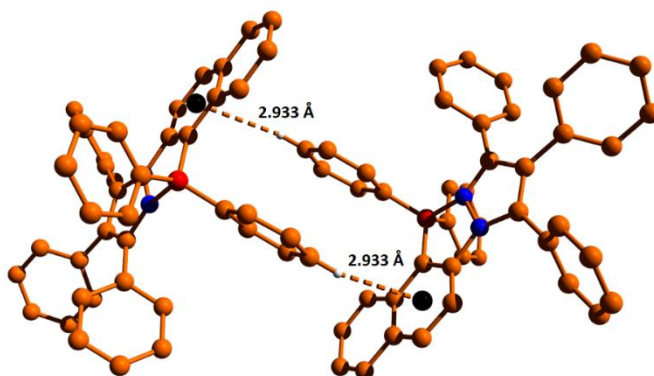


**Figure 5B.6:** Intermolecular interaction in compound **3** (C-H... $\pi$  : 2.933 Å).

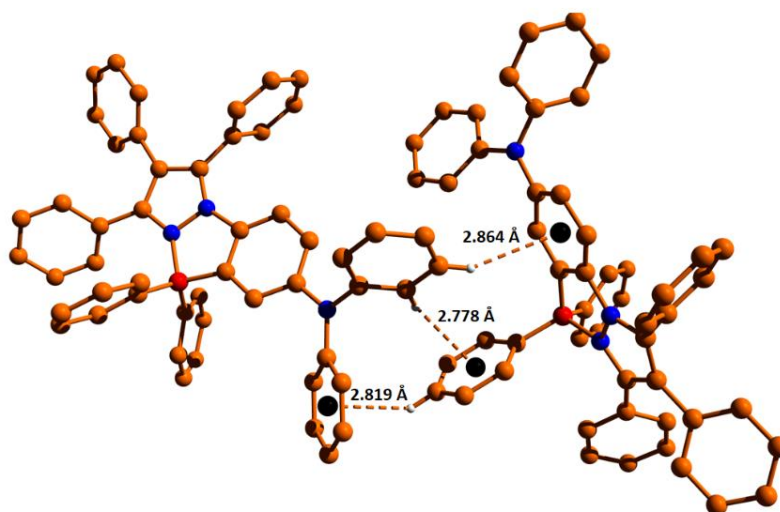


**Figure 5B.7** Intermolecular interaction in compound **4** (C-H... $\pi$  : 2.778 Å to 2.864 Å).

**Table 5B.2:** Crystal data and structure refinement parameters for compounds **1** and **2**.

	Compound <b>1</b>	Compound <b>2</b>
Empirical formula	C <sub>156</sub> H <sub>116</sub> B <sub>4</sub> N <sub>8</sub>	C <sub>40</sub> H <sub>31</sub> BN <sub>2</sub>
MW	2145.80	550.48
T, K	297 (3)	293 (2)
Wavelength, Å	0.71073	1.54184
Crystal system	monoclinic	monoclinic
Space group	P2 <sub>1</sub> /c	P2 <sub>1</sub> /n
a, Å	9.5738(5)	11.20170(10)
b, Å	26.0567(13)	16.8175(2)
c, Å	12.1791(7)	15.7113(2)
α, deg	90	90
β, deg	103.045(6)	94.9040(10)
γ, deg	90	90
V, Å <sup>3</sup>	2959.8(3)	2948.93(6)
Z	1	4
ρ calc, gcm <sup>-3</sup>	1.204	1.240
μ, mm <sup>-1</sup>	0.069	0.543
F(000)	1128	1160
2θ range, deg	6.79-52.742	7.716-150.65
limiting indices	-11 ≤ h ≤ 11	-14 ≤ h ≤ 13
	-32 ≤ k ≤ 28	-20 ≤ k ≤ 18
	-15 ≤ l ≤ 15	-19 ≤ l ≤ 19
no. of reflns collected	26375	23143
no. of indepe reflns	6017[Rint=0.1514]	5963[Rint=0.0341]
refinement method	Full matrix least square on F <sup>2</sup>	Full matrix least square on F <sup>2</sup>
No. of datas/restraints/params	6017/0/379	5963/0/390
Goodness-of-fit on F <sup>2</sup>	1.054	1.061
final R indices [I ≥ 2σ(I)]	R <sub>1</sub> =0.0810	R <sub>1</sub> =0.0406
	wR <sub>2</sub> =0.1989	wR <sub>2</sub> =0.0996
R indices (all data)	R <sub>1</sub> =0.0945	R <sub>1</sub> =0.0421
	wR <sub>2</sub> =0.2150	wR <sub>2</sub> =0.1006
peakmax/holemin (e Å <sup>-3</sup> )	0.38/-0.34	0.37/-0.19

**Table 5B.3:** Crystal data and structure refinement parameters for compounds **3** and **4**.

	Compound <b>3</b>	Compound <b>4</b>
Empirical formula	C <sub>43</sub> H <sub>31</sub> BN <sub>2</sub>	C <sub>51</sub> H <sub>38</sub> BN <sub>3</sub>
MW	586.51	703.65
T, K	293(2)	283(17)
Wavelength, Å	0.71073	1.54184
Crystal system	monoclinic	monoclinic
Space group	C2/c	P2 <sub>1</sub> /c

a, Å	32.479(5)	13.7883(2)
b, Å	9.0655(15)	12.0690(10)
c, Å	21.845(3)	23.6292(3)
$\alpha$ , deg	90	90
$\beta$ , deg	102.660(16)	104.9760(10)
$\gamma$ , deg	90	90
V, Å <sup>3</sup>	6275.7(17)	3798.60(8)
Z	8	4
$\rho$ calc, gcm <sup>-3</sup>	1.241	1.230
$\mu$ , mm <sup>-1</sup>	0.071	0.544
F(000)	2464	1480
2 $\theta$ range, deg	7.05-52.736	6.636-149.008
limiting indices	$-40 \leq h \leq 40$	$-17 \leq h \leq 17$
	$-11 \leq k \leq 11$	$-15 \leq k \leq 13$
	$-27 \leq l \leq 26$	$-29 \leq l \leq 29$
no. of reflns collected	35404	29382
no. of indepe reflns	6409[Rint=0.1172]	7669[Rint=0.0302]
refinement method	Full matrix least square on F <sup>2</sup>	Full matrix least square on F <sup>2</sup>
No. of datas/restraints/params	6409/0/415	7669/0/496
Goodness-of-fit on F <sup>2</sup>	0.998	1.049
final R indices [ $I \geq 2\sigma(I)$ ]	R <sub>1</sub> =0.0564	R <sub>1</sub> =0.0514
	wR <sub>2</sub> =0.1152	wR <sub>2</sub> =0.1358
R indices (all data)	R <sub>1</sub> =0.1221	R <sub>1</sub> =0.0542
	wR <sub>2</sub> =0.1375	wR <sub>2</sub> =0.1380
peakmax/holemin (e Å <sup>-3</sup> )	0.16/-0.21	0.37/-0.30

### 5B.2.3 Photophysical properties

The photophysical properties of compounds **1-4** were investigated in toluene, tetrahydrofuran, dichloromethane, acetonitrile, dimethylformamide and in solid state (Table **5B.3**). The absorption and emission spectra of all the boron compounds in THF solution showed absorption maxima between 305 to 362 nm. Upon excitation at the longer wavelength maxima, the emission maxima of these boron complexes were tuned from 413 nm to 523 nm (Figure **5B.8**).

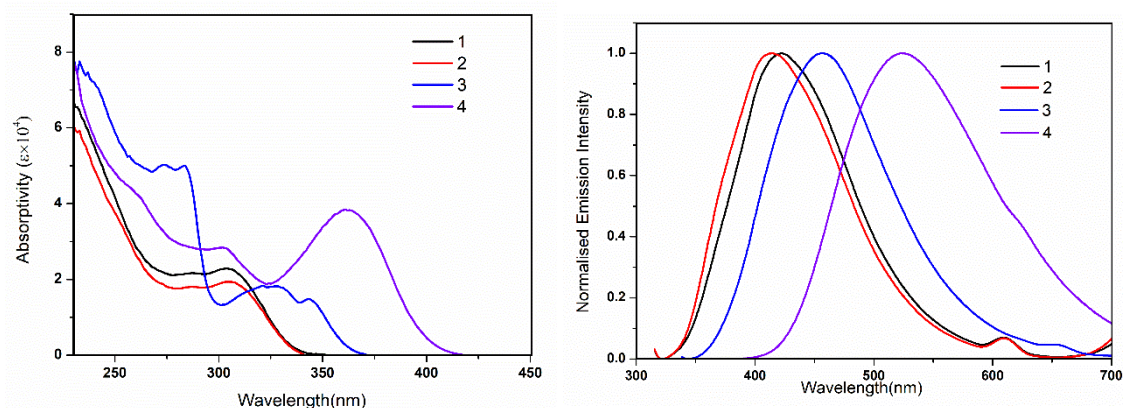


**Figure 5B.8:** (Left) Absorption spectra of compounds **1-4** in 10<sup>-5</sup> M THF. (Right) Normalised emission spectra of compounds **1-4** in 10<sup>-5</sup> M THF.

Compounds **3** and **4** showed red shifted emission compared to compounds **1** and **2**. The emission spectra of compounds **1-3** did not alter with solvent polarity, which indicates that the stabilisation of excited states with solvent molecules is poor in these compounds. However compound **4** is more red shifted compared to other complexes due to intramolecular charge transfer from NPh<sub>2</sub> group. This was further supported by the positive solvatochromism with varying solvent polarity from toluene to acetonitrile (Figure 5B.9).

**Table 5B.4:** Photophysical data of compounds **1-4**

Compound	Solvent	$\lambda_{\text{max}}$ (nm)	$\epsilon_{\text{max}}$ (M <sup>-1</sup> cm <sup>-1</sup> × 10 <sup>4</sup> )	$\lambda_{\text{em}}$ (nm)	$\Phi_{\text{F}}$	Stokes Shift (nm)	$\tau$ (ns)
<b>1</b>	Toluene	305	3.71	423	0.07	118	
	THF	305	2.27	422	0.07	117	0.76
	CH <sub>2</sub> Cl <sub>2</sub>	305	1.82	420	0.12	115	
	CH <sub>3</sub> CN	300	2.50	415	0.06	115	
	DMF	302	3.44	417	0.10	115	
	Solid			377	0.45		
<b>2</b>	Toluene	306	1.81	417	0.10	111	
	THF	305	1.93	413	0.11	108	0.76
	CH <sub>2</sub> Cl <sub>2</sub>	305	1.90	410	0.08	105	



	CH <sub>3</sub> CN	301	2.04	408	0.09	107	
	DMF	301	1.30	405	0.10	104	
	Solid			377	0.24		
<b>3</b>	Toluene	328	1.84	454	0.27	126	
	THF	328	1.82	456	0.20	128	2.37
	CH <sub>2</sub> Cl <sub>2</sub>	328	1.52	452	0.29	124	
	CH <sub>3</sub> CN	323	1.66	450	0.24	127	
	DMF	325	2.00	452	0.25	127	
	Solid			435	0.08		
<b>4</b>	Toluene	368	2.49	506	0.53	138	3.92
	THF	362	3.84	523	0.23	161	2.77
	CH <sub>2</sub> Cl <sub>2</sub>	357	3.44	522	0.33	155	3.39
	CH <sub>3</sub> CN	353	2.90	543	0.09	190	1.69
	DMF	359	2.94	542	0.11	183	1.70
	Solid			480	0.41		

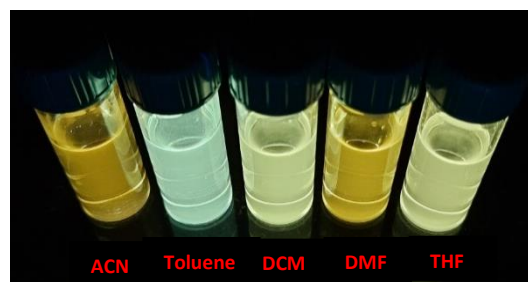
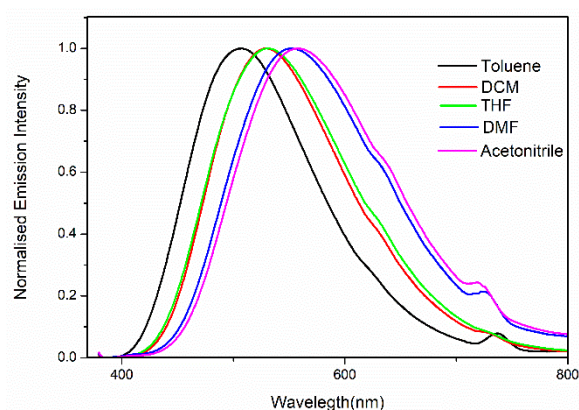


**Figure 5B.9:** (Left) Solvatochromic studies of compound **4**. (Right) Photograph of compound **4** in different solvents under handheld UV lamp irradiated at 365 nm.

The large Stokes shift and high fluorescence quantum yield (0.53 in toluene) in compound **4** is due to intramolecular charge transfer emission process. The blue shifted emission in nonpolar or less polar solvent is due to high energy locally excited (LE) states and red shifted emission is due to twisted intramolecular charge transfer (TICT) states.<sup>50</sup>

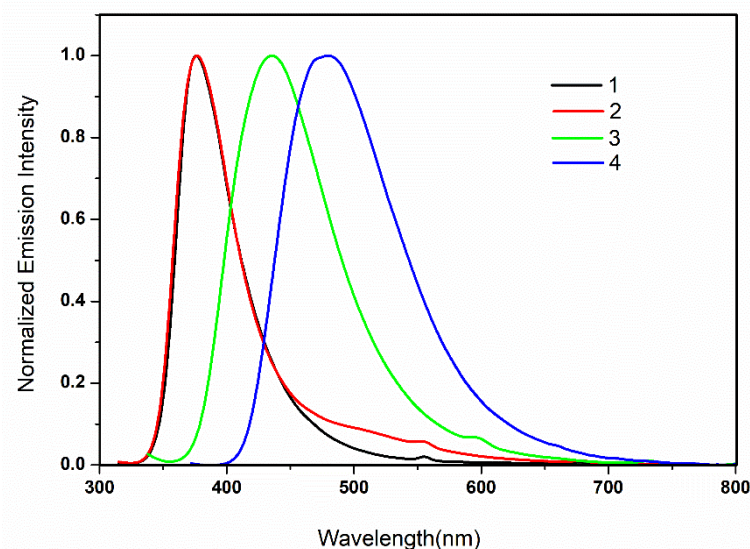


**Figure 5B.10:** Normalised emission spectra of compounds **1-4** in solid state.

Compounds **1-4** showed blue shifted emission in the solid state compared to their solution state (Figure **5B.10**) due to high energy LE states.<sup>50</sup> However, solid state fluorescence quantum yields are high due to restriction of intramolecular rotation and close packing in the solid state (Table **5B.1**) as discussed in the previous section.

#### 5B.2.4 AIEE phenomenon

Owing to the propeller type arrangement of phenyls around the pyrazole moiety it is expected that these molecules should exhibit AIEE phenomenon. To verify this, we studied the emission behaviour of compounds **1-4** in the aggregate states (Figure **5B.11-5B.16**). Compounds **1-4** are weakly fluorescent in tetrahydrofuran solutions and the quantum yields observed are (0.07)**1**, (0.11)**2**, (0.20) **3** and (0.23)**4**. The emission intensity enhances with gradual addition of water, keeping the concentration and measurement conditions the same.

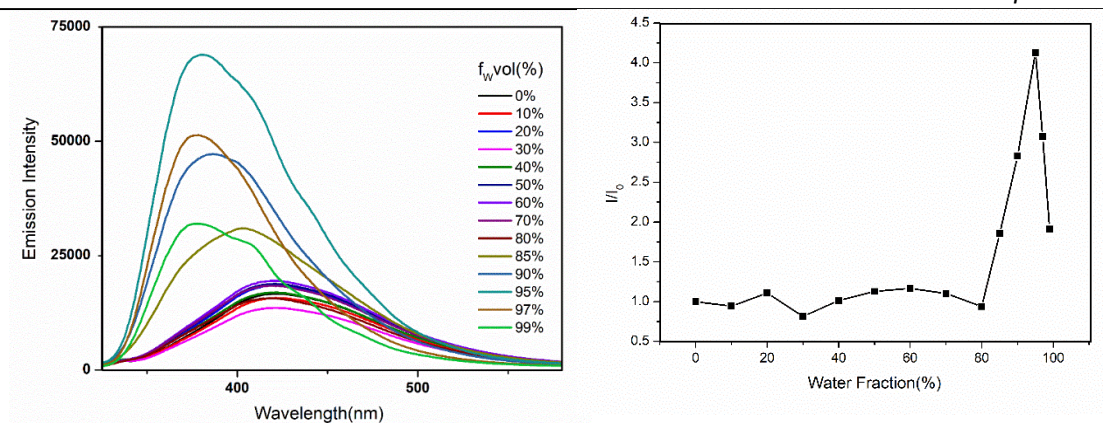


**Figure 5B.11:** (Left) Emission spectra of compound **1** (excited at 305nm) in THF:H<sub>2</sub>O mixture. (Right) Relative intensity vs. water fraction of compound **1** in THF:H<sub>2</sub>O mixture.

The observed enhancement in emission is due to the formation of nanoaggregates. As shown in figure **5B.11-5B.15**, the photoluminescence intensity and intensity ratio showed negligible changes until the addition of 70% water by keeping the volume and concentration the same. However there is an abrupt increase in intensity was observed with further increase of water fraction. After 70% of water fraction the mixtures start forming aggregates which is responsible for the AIEE phenomenon. The formation of the aggregates was analysed using dynamic light scattering (DLS). From the DLS the particle size was found to be 122 nm (for compound **1**), 91 nm (for compound **2**), 122 nm (for compound **3**), and 142 nm (for compound **4**).

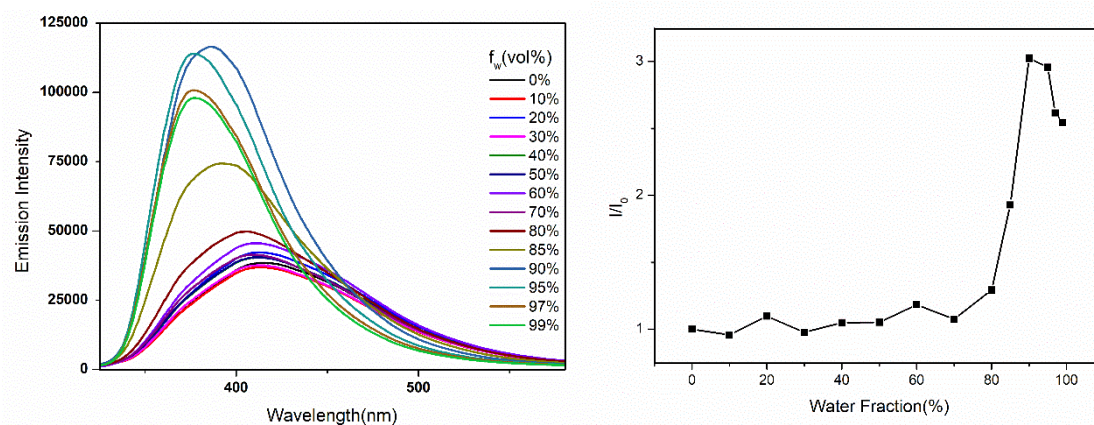


**Figure 5B.12:** (Left) Emission spectra of compound **2** (excited at 305nm) in THF:H<sub>2</sub>O mixture.(Right) Relative intensity vs. water fraction of compound **2** in THF:H<sub>2</sub>O mixture.

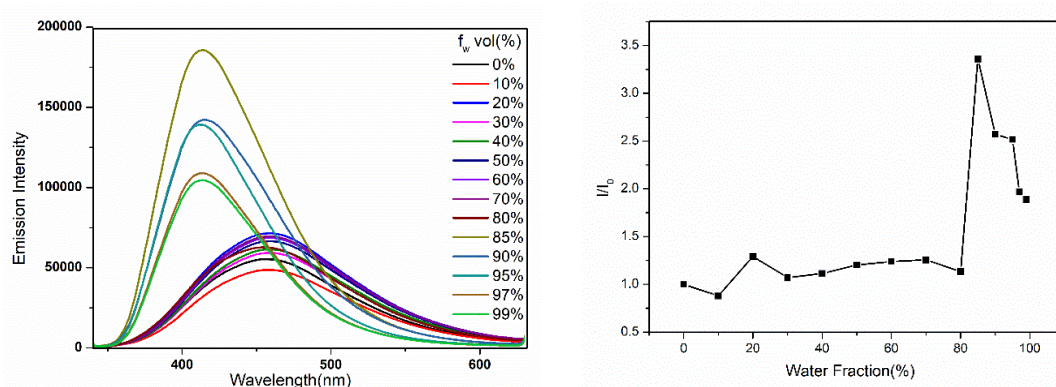


**Figure 5B.13** (Left) Emission spectra of compound **3** (excited at 328 nm) in THF:H<sub>2</sub>O mixture.(Right) Relative intensity vs. water fraction of compound **3** in THF:H<sub>2</sub>O mixture.

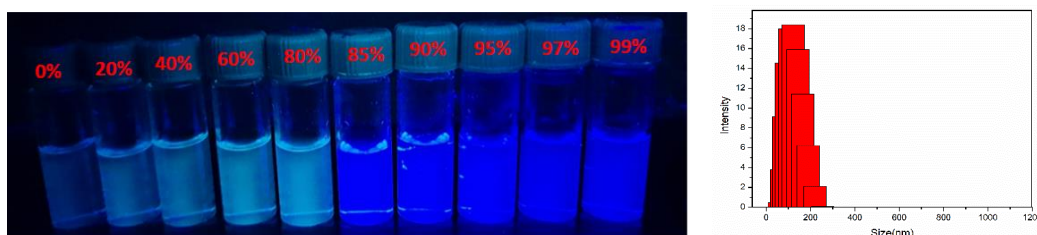


**Figure 5B.14:** (Left) Photograph of compound **3** in THF:H<sub>2</sub>O mixture under a handheld UV lamp at 365 nm. (Right) Particle size distribution graph of compound **3** at H<sub>2</sub>O :THF (85:15).

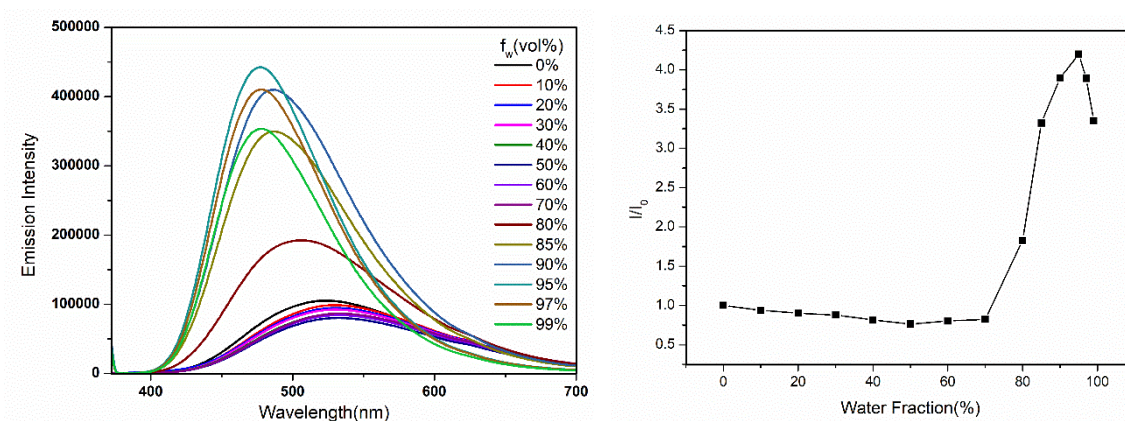




**Figure 5B.15:** (Left) Emission spectra of compound **4** (excited at 362 nm) in THF:H<sub>2</sub>O mixture. (Right) Relative intensity vs. water fraction of compound **4** in THF:H<sub>2</sub>O mixture.

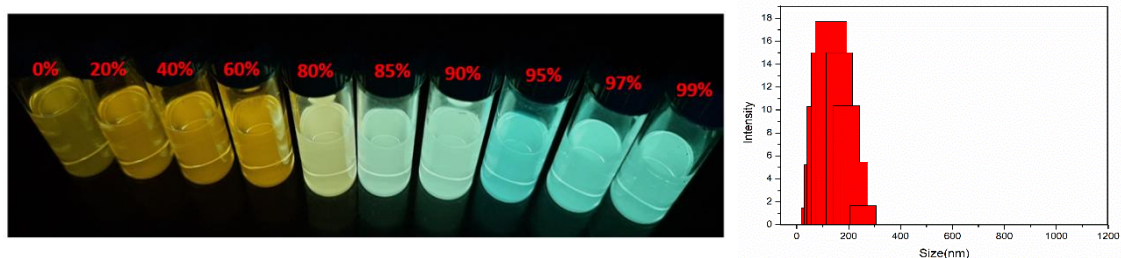


**Figure 5B.16** (Left) Photograph of compound **4** in THF:H<sub>2</sub>O mixture under a hand held UV lamp. (Right) Particle size distribution graph of compound **4** at H<sub>2</sub>O: THF (95:5).

To understand the AIEE phenomenon, the emission properties of compounds **1-4** were investigated at different temperatures (Figure **5B.17** and **5B.18**). The photoluminescence intensity decreased gradually with increase in temperature. Molecular rotations will be lower at low temperature due to radiative decay of singlet excited states and increase with increase in temperature. At low temperature, restriction of intramolecular rotation phenomenon plays a vital role, which helps in increasing emission intensity.

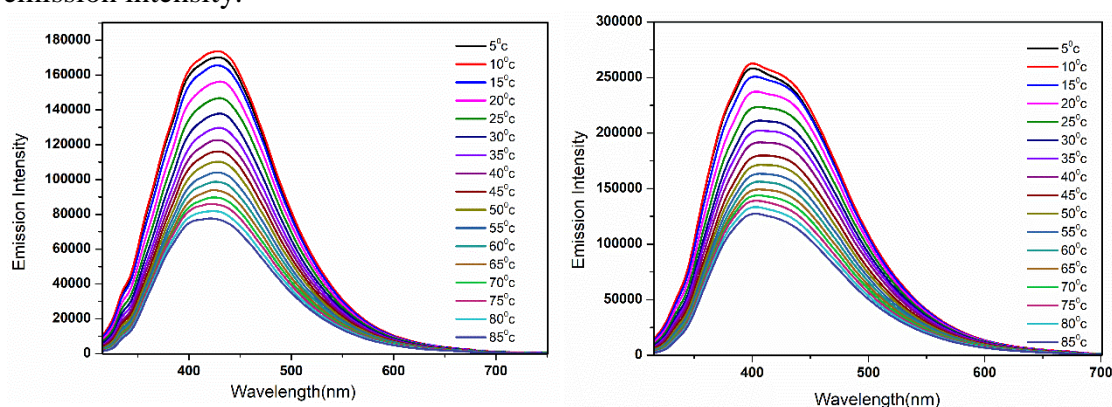


**Figure 5B.17:** Temperature dependent emission spectra of compound **1** (Left) and **2** (Right) in THF( $10^{-5}$  M).

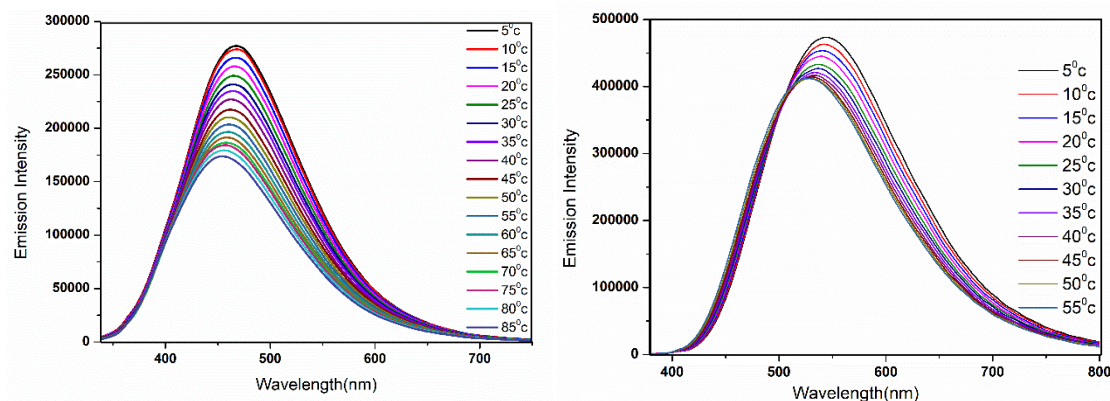


**Figure 5B.18:** Temperature dependent emission spectra of compound **3** (Left) and **4** (Right) in THF( $10^{-5}$  M).

To support the RIR mechanism, we have investigated PL properties of compounds **1-4** by blending glycerol with methanol (Figure 5B.19 and 5B.20). The emission intensity increased with increase of glycerol fraction, when the compounds PL are recorded in mixed solvents of glycerol and methanol. The PL intensity marginally increased from 0 to 50%, however the emission becomes stronger after 50%. These experiments further supports that the restricted intramolecular rotation plays a vital role for enhanced emission in the aggregate state.

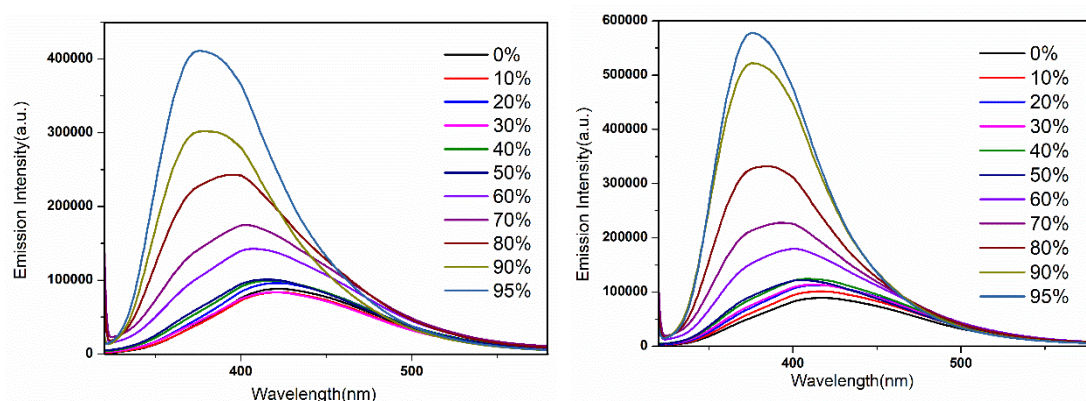


**Figure 5B.19:** Emission spectra of compound **1** (Left) and **2** (Right) in methanol/glycerol mixture with increasing glycerol fraction (0 to 95%).

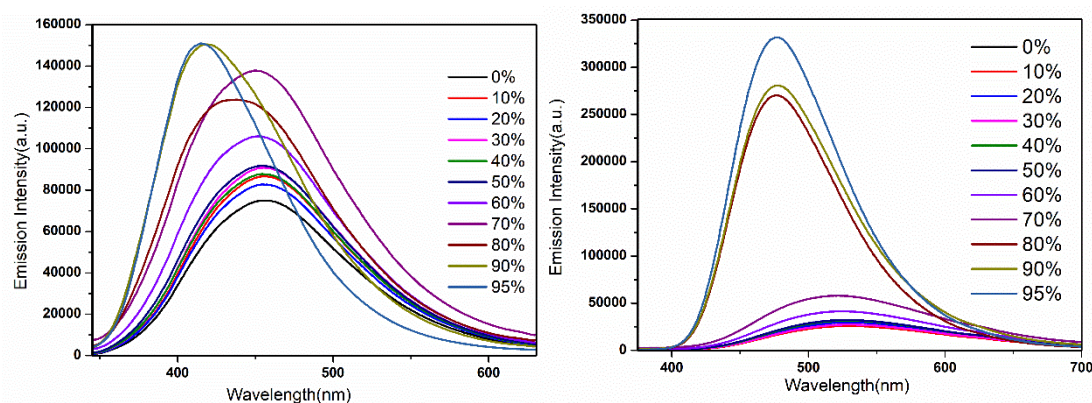


**Figure 5B.20:** Emission spectra of compound **3** (Left) and **4** (Right) in methanol/glycerol mixture with increasing glycerol fraction (0 to 95%).

### 5B.2.5 Thermal studies

Thermal properties of compounds **1-4** were studied by thermogravimetric analysis under nitrogen atmosphere at a heating rate of  $10\text{ }^{\circ}\text{C min}^{-1}$ . As shown in the figure **5B.21** the decomposition temperature (5% weight loss) for **1**, **2**, **3** and **4** was  $281\text{ }^{\circ}\text{C}$ ,  $210\text{ }^{\circ}\text{C}$ ,  $209\text{ }^{\circ}\text{C}$  and  $331\text{ }^{\circ}\text{C}$  respectively, which suggest that they are thermally stable.

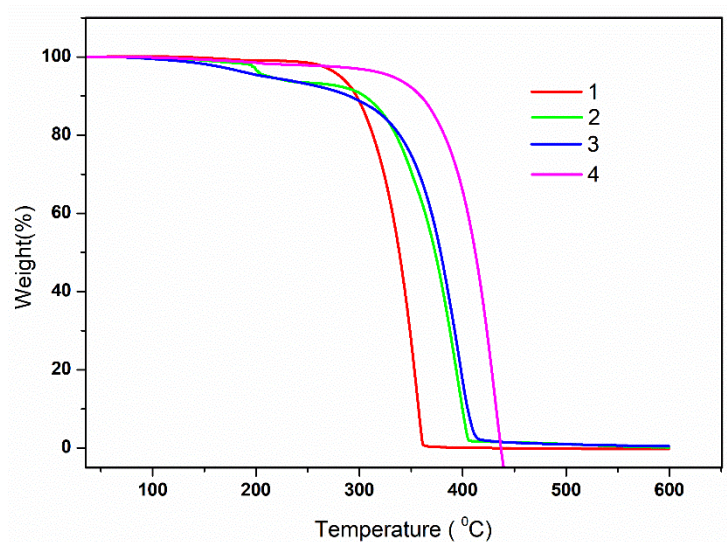


**Figure 5B.21:** TGA curves of compounds **1-4** under nitrogen at a heating rate of  $10\text{ }^{\circ}\text{C min}^{-1}$ .

### 5B.2.5 Electrochemical properties

The electrochemical properties of compounds **1-4** were studied in 0.1 M dimethoxyethane(DME) solution using  $\text{Bu}_4\text{NPF}_6$  as the electrolyte (Figure 5B.22). Compounds **1-4** show an irreversible reduction peak at -2.82 V (for **1**), -2.83 V (for **2**), -2.81 V (for **3**) and -2.77 V (for **4**). The observed reduction potential of compounds **1-4** are much more negative than the reported  $\text{BPh}_2$  complexes.<sup>51-53</sup> Compound **4** exhibits one reversible oxidation peak at 0.43 V, which is due to the presence of electron donating  $\text{NPh}_2$  group.

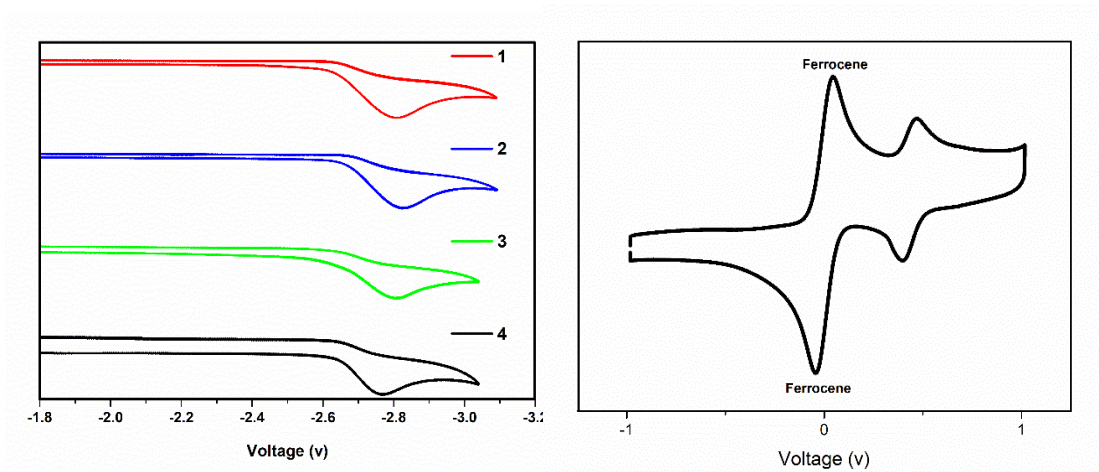


**Figure 5B.22:** (Left) Cyclic voltammograms of compounds **1-4** (vs. ferrocene/ferrocenium) with 0.1 M  $\text{Bu}_4\text{NPF}_6$  in DME as the supporting electrolyte (scan rate  $100 \text{ mV s}^{-1}$ ). (Right) Plot depicting oxidation in compound **4**.

### 5B.3 Conclusions

We have synthesized a series of boron doped tetraaryl pyrazoles and characterised with different technique. The AIEE phenomenon in these compounds have been studied in detail. From the crystal structure analysis it was realised the presence of  $\text{C-H} \cdots \pi$  interaction which are responsible for the AIEE phenomenon observed in compounds **1-4**. The interesting electrochemical and photophysical properties suggests that these compounds have the potential to use them as emitters in the fabrication of OLEDs.



---

## 5B.4 Experimental section

### 5B.4.1 General information

All reagents and starting materials were purchased from Sigma-Aldrich, Alfa-Aesar and Spectrochem chemical companies; and used as received unless otherwise noted. Chlorinated solvents, acetonitrile, and DMF were distilled from  $\text{CaH}_2$ . THF and toluene were distilled from Na/benzophenone prior to use. All 400 MHz  $^1\text{H}$ , 100 MHz  $^{13}\text{C}$ , NMR spectra were recorded on a Bruker ARX 400 spectrometer operating at 400 MHz. All  $^1\text{H}$  and  $^{13}\text{C}$  NMR spectra were referenced internally to solvent signals. All NMR spectra were recorded at ambient temperature. ESI mass spectra were recorded on Bruker, micrOTOF-QII mass spectrometer. The absorbance spectra were recorded on a JASCO V-730 UV-Visible spectrometer. The fluorescence spectra were recorded using Edinburgh FS5 spectrofluorometer. Absolute fluorescence quantum yields of compounds **1-4** were measured by integrating sphere method using Edinburgh FS5 spectrofluorometer. The fluorescence spectra are corrected for the instrumental response. Cyclic voltammetry measurements were performed with a conventional three electrode cell using an electrochemical workstation (CH Instrument, Model: 1100A). The three-electrode system consisted of a Glassy carbon working electrode, a Pt wire as the secondary electrode, and a Ag wire as the reference electrode. The voltammograms were recorded with ca.  $1.0 \times 10^{-3}$  M solution in dimethoxyethane containing  $\text{Bu}_4\text{NPF}_6$  (0.1 M) as the supporting electrolyte. The scans were referenced after the addition of a small amount of ferrocene as the internal standard. Single-crystal X-ray diffraction data were collected on a Bruker APEXII diffractometer using Mo- $\text{K}\alpha$  radiation (0.71073 Å) and Rigaku Oxford X-ray diffractometer Cu- $\text{K}\alpha$  (1.54184 Å). SADABS absorption corrections were applied. The structures were solved and refined with SHELX suite of programs. All non-hydrogen atoms were refined with anisotropic

displacement coefficients. The H atoms were placed at calculated positions and were refined as riding atoms.

### 5B.4.2 Synthetic procedures and spectral characterisations

#### General procedure for the synthesis of compounds 1-4

A three-neck round-bottom flask with a dropping funnel was degassed and after purging with vacuum–nitrogen cycles, dichloromethane solution of compounds **1a** – **4a** were added. *N,N*-diisopropylethylamine (*i*-Pr<sub>2</sub>NEt) was added to this solution at 0 °C. After 10 minute, BBr<sub>3</sub> (1.0 M in dichloromethane) was added dropwise at 0 °C and the reaction mixture was heated to room temperature. The reaction mixture was stirred at room temperature for 24 h, a saturated potassium carbonate aqueous solution was added and this mixture was extracted with dichloromethane. The organic layers were washed with water, dried over sodium sulfate and concentrated using a rotary evaporator to give the dibromoboron compound. This crude dibromoboron product was charged in a round-bottom flask and after purging with vacuum–nitrogen cycles, tetrahydrofuran was added. To this stirred solution was added PhMgBr (1.0 M in THF) at room temperature and reaction mixture was refluxed for 24h. The reaction was quenched with water and extracted with ethyl acetate. The extracted organic phase was washed with aqueous sodium carbonate, brine and dried over anhydrous sodium sulphate. The crude product was finally purified by silica gel column chromatography (*n*-hexane/dichloromethane).

##### 5B.4.2.1 Synthesis of compound 1

The quantities involved are as follows: compound **1a** (0.80 g, 2.14 mmol), *N,N*-diisopropylethylamine (0.370 mL, 2.14 mmol), BBr<sub>3</sub> (1.0 M in CH<sub>2</sub>Cl<sub>2</sub>, 6.44 mL, 6.44 mmol), and PhMgBr (1.0 M in THF, 8.56 mL, 8.56 mmol). Yield: 0.69 g (60 %). Mp:

190 °C.  $^1\text{H}$  NMR (400 MHz,  $\text{CDCl}_3$ )  $\delta$  7.63 – 7.52 (m, 6H), 7.25 – 7.00 (m, 17H), 6.99 (t,  $J$  = 7.8 Hz, 1H), 6.94 – 6.91 (m, 2H), 6.86 – 6.84 (m, 2H), 6.62 (d,  $J$  = 8.1 Hz, 1H).  $^{13}\text{C}$  NMR (101 MHz,  $\text{CDCl}_3$ )  $\delta$  112.26, 124.76, 125.52, 125.58, 127.02, 127.23, 127.28, 127.83, 127.86, 128.13, 128.38, 129.05, 129.28, 129.96, 130.21, 130.41, 130.62, 130.92, 131.58, 134.03, 137.30, 138.75, 146.98.  $^{11}\text{B}$  NMR (128 MHz,  $\text{CDCl}_3$ )  $\delta$  = 1.20 ppm. ESI-MS: calcd for  $\text{C}_{39}\text{H}_{30}\text{BN}_2$  ( $[\text{M}+\text{H}]^+$ ): 537.2503, observed : 537.2492. IR (KBr):  $\nu(\text{cm}^{-1})$  = 3064(m), 3000(m), 1459(s), 1450(m), 1378(s), 1027(m), 780(m), 697(s).

#### 5B.4.2.2 Synthesis of compound 2

The quantities involved are as follows: compound **2a** (1.20 g, 3.10 mmol), *N,N*-diisopropylethylamine (0.537 mL, 3.10 mmol),  $\text{BBr}_3$  (1.0 M in  $\text{CH}_2\text{Cl}_2$ , 9.31 mL, 9.31 mmol), and  $\text{PhMgBr}$  (1.0 M in THF, 12.4 mL, 12.4 mmol). Yield: 0.8 g (47 %). Mp: 190 °C.  $^1\text{H}$  NMR (400 MHz,  $\text{CDCl}_3$ )  $\delta$  = 7.55 (m, 5H), 7.49 (d,  $J$ =8.1, 1H), 7.23-7.14(m,12H),7.06(t,  $J$ =7.8, 2H) 6.96 (t,  $J$ =7.8, 1H), 6.88 (d,  $J$ =8.1, 2H), 6.82 (d,  $J$ =8.1, 2H), 6.77 (d,  $J$ = 8.1, 2H), 6.57 (d,  $J$ = 8.1, 1H), 2.22(s, 3H).  $^{13}\text{C}$  NMR (101 MHz,  $\text{CDCl}_3$ )  $\delta$  21.14, 112.19, 124.71, 125.46, 125.52, 126.88, 126.98, 127.18, 127.81, 127.97, 128.50, 128.87, 128.95, 129.24, 129.98, 130.32, 130.62, 130.91, 131.53, 134.01, 136.90, 137.15, 138.76, 146.87.  $^{11}\text{B}$  NMR (128 MHz,  $\text{CDCl}_3$ )  $\delta$ = 1.90 ppm. ESI-MS: calculated for  $\text{C}_{40}\text{H}_{32}\text{BN}_2$  ( $[\text{M}+\text{H}]^+$ ): 551.2660, observed : 551.2644. IR (KBr):  $\nu(\text{cm}^{-1})$  = 3062(m), 1515(m), 1450(s), 1377(m), 1023(m), 824(m), 762(m), 694(s).

#### 5B.4.2.3 Synthesis of compound 3

The quantities involved are as follows: compound **3a** (0.5 g, 1.18 mmol), *N,N*-diisopropylethylamine (0.204 mL, 1.18 mmol),  $\text{BBr}_3$  (1.0 M in  $\text{CH}_2\text{Cl}_2$ , 3.54 mL, 3.54

mmol), and PhMgBr (1.0 M in THF, 4.72 mL, 4.72 mmol). Yield: 0.45 g (65 %). Mp: 243 °C.  $^1\text{H}$  NMR (400 MHz,  $\text{CDCl}_3$ )  $\delta$  = 7.77 (dd,  $J$ =12, 8.1, 2H), 7.66 – 7.50 (m, 6H), 7.32 (q,  $J$ =8.0, 2H), 7.22 (t,  $J$ =7.6, 1H), 7.11 (m, 16H), 6.86 (dd,  $J$ =13.1, 8.1, 3H), 6.79 (d,  $J$ =7.7, 2H).  $^{13}\text{C}$  NMR (101 MHz,  $\text{CDCl}_3$ )  $\delta$  112.04, 124.57, 125.52, 125.61, 126.08, 127.04, 127.11, 127.39, 127.95, 128.07, 128.16, 128.70, 129.08, 129.26, 129.58, 129.97, 130.17, 130.39, 130.78, 130.86, 132.49, 134.75, 134.95, 135.48, 136.77, 146.57.  $^{11}\text{B}$  NMR (128 MHz,  $\text{CDCl}_3$ )  $\delta$  = 3.12 ppm. ESI-MS: calculated for  $\text{C}_{43}\text{H}_{32}\text{BN}_2$  ( $[\text{M}+\text{H}]^+$ ): 587.2660, observed : 587.2657. IR (KBr):  $\nu(\text{cm}^{-1})$  = 3064(m), 2923(m), 1508(m), 1376(m), 1025(m), 806(m), 701(s).

#### 5B.4.2.4 Synthesis of compound 4

The quantities involved are as follows: compound **4a** (0.545 g, 1.009 mmol), *N,N*-diisopropylethylamine (0.257 mL, 1.009 mmol),  $\text{BBr}_3$  (1.0 M in  $\text{CH}_2\text{Cl}_2$ , 3.029 mL, 3.029 mmol), and PhMgBr (1.0 M in THF, 4.3 mL, 4.03 mmol). Yield: 0.42g (60 %). Mp: 220 °C.  $^1\text{H}$  NMR (400 MHz,  $\text{CDCl}_3$ )  $\delta$  = 7.52 (q,  $J$ =6.2, 5.3, 4H), 7.29 (d,  $J$ =2.4, 1H), 7.23 – 6.99 (m, 25H), 6.94 (t,  $J$ =7.2, 2H), 6.91 – 6.85 (m, 2H), 6.79 (d,  $J$ =7.5, 2H), 6.59 (dd,  $J$ =8.7, 2.5, 1H), 6.40 (d,  $J$ =8.7, 1H).  $^{13}\text{C}$  NMR (101 MHz,  $\text{CDCl}_3$ )  $\delta$  112.93, 120.92, 122.70, 122.73, 124.35, 125.55, 125.57, 126.61, 127.04, 127.06, 127.24, 127.92, 127.94, 128.19, 128.21, 128.51, 129.06, 129.15, 129.17, 129.32, 130.15, 130.25, 130.42, 130.71, 131.05, 133.92, 134.12, 134.14, 136.68, 146.77, 147.03, 147.87, 149.74.  $^{11}\text{B}$  NMR (128 MHz,  $\text{CDCl}_3$ )  $\delta$  = 2.58 ppm. ESI-MS: calculated for  $\text{C}_{51}\text{H}_{39}\text{BN}_3$  ( $[\text{M}+\text{H}]^+$ ): 704.3240, observed : 704.3213. IR (KBr):  $\nu(\text{cm}^{-1})$  = 3035(m), 1580(m), 1492(m), 1281(m), 1027(m), 752(m), 695(s).

#### 5B.5 References

1. Lu, Z.; Jiang, Q.; Zhu, W.; Xie, M. ; Hou, Y. ; Chen, X.; Wang, Z.; Zou, D. ; Tsutsui, T. *Synth. Met.* **2000**, *111–112*, 425.
2. He, Z. ; Milburn, G. H.W. ; Baldwin, K. J.; Smith, D. A.; Danel, A. ; Tomasik, P. J. *Lumin.* **2000**, *86*,1.
3. Tao, Y. T.; Balasubramaniam, E.; Danel, A. ; Tomasik, P. *Appl. Phys. Lett.* **2000**, *77*, 933–935.
4. Akasaki, I. *Angew. Chem. Int. Ed.* **2015**, *54*, 7750–7763.
5. Amano, H. *Angew. Chem. Int. Ed.* **2015**, *54*, 7764–7769.
6. Nakamura, S. *Angew. Chem. Int. Ed.* **2015**, *54*, 7770–7788.
7. Friend, R. H. ; Gymer, R. W.; Holmes, A. B.; Burroughes, J. H.; Marks, R. N. ; Taliani, C.; Bradley, D. C. C. ; Dos Santos, D. A.; Bredas, J. L.; Lodglund, M.; Salaneck, W. R. *Nature* **1999**, *397*, 121–128.
8. Baldo, M. A.; O'Brien, D. F. ; You, Y.; Shoustikov, A.; Sibley, S.; Thompson, M. E.; Forrest, S. R. *Nature* **1998**, *395*, 151–154.
9. Braun, C. A.; Zomerman, D.; Aguiar, I. ; Qi, Y.; Delgado, W. T.; Ferguson, M. J.; McDonald, R.; Souza, G. L. C.; He, G. ; Brown, A. ; Rivard, E. *Faraday Discuss.* **2017**, *196*, 255-268.
10. Birks, J. B. *Photophysics of Aromatic Molecules*, Wiley, London, 1970.
11. Yuan, W. Z. ; Lu, P. ; Chen, S.; Lam, J. W. Y.; Wang, Z.; Liu, Y.; Kwok, H. S.; Ma, Y.; Tang, B. Z. *Adv. Mater.* **2010**, *22*, 2159–2163.
12. Luo, J. ; Xie, Z.; Lam, J. W. Y. ; Cheng, L.; Chen, H.; Qiu, C. ; Kwok, H. S.; Zhan, X.; Liu, Y.; Zhu, D. ; Tang, B. Z. *Chem. Commun.* **2001**, 1740.
13. An, B.-K.; Kwon, S.-K.; Jung, S.-D.; S. Y. Park, *J. Am. Chem. Soc.* **2002**, *124*, 14410.

- 
14. Chen, L.; Jiang, Y. ; Nie, H.; Lu, P.; Sung, H. H. Y.; Williams, I. D.; Kwok, H. S.; Huang, F.; Qin, A.; Zhao, Z. ; Tang, B. Z. *Adv. Funct. Mater.* **2014**, *24*, 3621.
15. Chen, L.; Lin, G. ; Peng, H.; Ding, S.; Luo, W.; Hu, R. ; Chen, S.; Huang, F.; Qin, A. ; Zhao, Z. ; Tang, B. Z. *Mater. Chem. Front.* **2017**, *1*, 176-180.
16. Chen, L.; Jiang, Y.; Nie, H.; Hu, R.; Kwok, H. S.; Huang, F.; Qin, A.; Zhao, Z.; Tang, B. Z. *ACS Appl. Mater. Interfaces* **2014**, *6*, 17215–17225.
17. Furue , R.; Nishimoto , T.; Park, I. S. ; Lee, J.; Yasuda, T. *Angew. Chem. Int. Ed.* **2016**, *55*, 7171 –7175.
18. Liu, H.; Fan, J.; Guo, J.; Zeng, J.; Qiu, F.; Zhao, Z. ; Tang, B. Z. *Adv. Optical Mater.* **2020**, 2001027.
19. Ding, D.; Li, K.; Liu, B. ; Tang, B. Z. *Acc. Chem. Res.* **2013**, *46*, 2441.
20. Hu, R.; Leung, N. L. C.; Tang, B. Z. *Chem. Soc. Rev.* **2014**, *43*, 4494.
21. Zhang, X.; Zhang, X.; Tao, L.; Chi, Z.; Xu, J.; Wei, Y. *J. Mater.Chem. B* **2014**, *2*, 4398.
22. Chi, Z.; Zhang, X.; Xu, B.; Zhou, X.; Ma, C.; Zhang, Y.; Liu, S.; Xu, J. *Chem. Soc. Rev.* **2012**, *41*, 3878.
23. Mukundam, V.; Dhanunjayarao, K.; Mamidala, R.; Venkatasubbaiah, K. *J. Mater. Chem. C* **2016**, *4*, 3523.
24. Mukundam, V.; Kumar, A.; Dhanunjayarao, K.; Ravi, A.; Peruncheralathan, S.; Venkatasubbaiah, K. *Polym. Chem.* **2015**, *6*, 7764.
25. Katritzky, A. R.; Ramsden, C. A.; Scriven, E. F. V.; Taylor, R. J. K. in *Comprehensive Heterocyclic Chemistry III*, Elsevier, Oxford, 2008, p. 1
26. Fustero, S., Simón-Fuentes, A. ; Sanz-Cervera, J. F. *Org. Prep. Proced. Int.* **2009**, *41*, 253.
-

- 
27. Fustero, S.; Sánchez-Roselló, M.; Barrio, P.; Simón-Fuentes, A. *Chem. Rev.* **2011**, *111*, 6984.
28. Elguero, J. ; A. R. K.W. Rees, in *Comprehensive Heterocyclic Chemistry*, Pergamon, Oxford, 1984, p. 167.
29. Kost, A. N. ; Grandberg, I. I.; Boulton, A. R. K. a. A. J. in *Adv. Heterocycl. Chem.* Academic Press, 1966, p. 347.
30. Elguero, J. ; Scriven, A. R. K. W. R. F. V. in *Comprehensive Heterocyclic Chemistry II*, Pergamon, Oxford, 1996, p. 1.
31. Harb, A. F. A.; Abbas, H. H. ; Mostafa, F. H. *J. Iran. Chem. Soc.* **2005**, *2*, 115–123.
32. Harb, A. F. A.; Abbas, H. H. ; Mostafa, F. H. *Chem. Pap.* **2005**, *59*, 187–195.
33. Chandrasekhar, V. ; Deria, P.; Krishnan, V.; Athimoolam, A.; Singh, S.; Madhavaiah, C.; Srivatsan, S. G. ; Verma, S. *Bioorg. Med. Chem. Lett.* **2004**, *14*, 1559.
34. Chandrasekhar, V.; Athimoolam, A.; Krishnan, V.; Azhakar, R.; Madhavaiah, C. ; Verma, S. *Eur. J. Inorg. Chem.* **2005**, *2005*, 1482.
35. Chandrasekhar, V.; Athimoolam, A.; Srivatsan, S. G.; Sundaram, P. S.; Verma, S.; Steiner, A.; Zacchini, S. ; Butcher, R. *Inorg. Chem.* **2002**, *41*, 5162.
36. Maeda, H.; Ito, Y.; Kusunose, Y.; Nakanishi, T. *Chem. Commun.* **2007**, 1136.
37. Gemming, S.; Schreiber, M.; Thiel, W. ; Heine, T.; Seifert, G.; Avelino de Abreu, H.; Anderson Duarte, H. *J. Lumin.* **2004**, *108*, 143.
38. Chandrasekhar, V.; Azhakar, R.; Krishnan, V.; Athimoolam, A. ; Pandian, B. M. *J. Am. Chem. Soc.* **2006**, *128*, 6802.
39. Lu, Z.; Jiang, Q.; Zhu, W.; Xie, M.; Hou, Y.; Chen, X.; Wang, Z.; Zou, D. ; Tsutsui, T. *Synth. Met.* **2000**, *111–112*, 425.
40. He, Z.; Milburn, G. H.W.; Baldwin, K. J.; Smith, D. A.; Danel, A.; Tomasik, P. *J. Lumin.* **2000**, *86*,1.
-

- 
41. Tao, Y. T.; Balasubramaniam, E.; Danel, A.; Tomasik, P. *Appl. Phys. Lett.* **2000**, 77, 933–935.
42. Huisgen, R.; Seidel, M.; Wallbillich, G.; Knupfer, H. *Tetrahedron* **1962**, 17,3.
43. Komatsu, M.; Yoshida, Y.; Uesaka, ; Ohshira Y.; Agawa, T. *J. Org. Chem.* **1984**, 49, 1300.
44. Duncan, D. C.; Trumbo, T. A.; Almquist, C. D.; Lentz, T. A.; Beam, C. F. *J. Heterocycl. Chem.* **1987**, 24, 555.
45. Romashin, Y. N.; Liu, M. T. H.; Nijjara, S. S.; Attanasib, O. A. *Chem. Commun.* **2000**, 114.
46. Mukherjee, S.; Salini, P. S.; Srinivasan, A. ; Peruncheralathan, S. *Chem. Commun.* **2015**, 51, 17148.
47. Ishida, N.; Moriya, T.; Goya, T.; Murakami, M. *J. Org. Chem.* **2010**, 75, 8709.
48. Dhanunjayarao, K.; Sa, S.; Nayak, P.; Ponniah S. J.; Venkatasubbaiah, K. *Organometallics* **2019**, 38, 870.
49. Dhanunjayarao, K.; Sa, S.; Aradhyula, B. P. R.; Venkatasubbaiah, K. *Tetrahedron* **2018**, 74, 5819.
50. Kundu, A.; Karthikeyan, S.; Sagara, Y.; Moon, D.; Anthony, S. P. *ACS Omega*, **2019**, 4, 5147.
51. Crossley, D. L.; Vitorica-Yrezabal, I.; Humphries, M. J.; Turner, M. L.; Ingleson, M. J. *Chem. Eur. J.* **2016**, 22, 12439.
52. Liu, K. ; Lalancette, R. A.; Jäkle, F. *J. Am. Chem. Soc.* **2017**, 139, 18170.
53. Liu, K.; Lalancette, R. A.; Jäkle, F. *J. Am. Chem. Soc.* **2019**, 141, 7453.
54. Rao, Y. L ; Wang, S. *Inorg. Chem.* **2011**, 50, 12263.
55. Li, D.; Zhang, H.; Wang, Y. *Chem. Soc. Rev.* **2013**, 42, 8416.
-



- 
56. Frath, D.; Massue, J. ; Ulrich, G. ; Ziessel, R. *Angew. Chem., Int. Ed.* **2014**, *53*, 2290.
57. Haque, A.; Al-Balushi, R. A.; Raithby, P. R.; Khan, M. S. *Molecules* **2020**, *25*, 2645.
58. Wakamiya, A.; Taniguchi, T. ; Yamaguchi, S. *Angew. Chem. Int. Ed.* **2006**, *45*, 3170.
59. Dou, C.; Ding, Z.; Zhang, Z.; Xie, Z.; Liu, J.; Wang, L. *Angew. Chem. Int. Ed.* **2015**, *54*, 3648.
60. Crossley, D. L.; Cade, I. A.; Clark, E. R.; Escande, A.; Humphries, M. J.; King, S. M. ; Vitorica-Yrezabal, I.; Ingleson, M. J. ; Turner, M. L. *Chem. Sci.* **2015**, *6*, 5144.
61. Dou, C.; Long, X.; Ding, Z.; Xie, Z.; Liu, J.; Wang, L. *Angew. Chem. Int. Ed.* **2016**, *55*, 1436.
62. Shimogawa, H.; Endo, M.; Taniguchi, T.; Nakaike, Y.; Kawaraya, M.; Segawa, H.; Murata, Y.; Wakamiya, A. *Bull. Chem. Soc. Jpn.* **2017**, *90*, 441.
63. Vanga , M.; Lalancette, R. A.; Jäkle, F. *Chem. Eur. J.* **2019**, *25*, 1 0133 .
64. Mukundam, V.; Sa, S.; Kumari , A.; Das, R.; Venkatasubbaiah, K. *J. Mater. Chem. C* **2019**, *7*, 12725.
65. Mukundam, V.; Sa, S.; Kumari, A.; Murali, A. C.; Nayak, P.; Das, R.; Venkatasubbaiah, K. *Dalton Trans.* **2020**, *49*, 7737.
66. Matsuo, K. ; Yasuda, T. *Chem. Commun.* **2017**, *53*, 8723.



## CHAPTER 6

### Synthesis of pyrazole anchored three-coordinated organoboranes and their application in the detection of picric acid

<b>6.1 Introduction</b>	209
<b>6.2 Results and discussion</b>	210
<b>6.2.1</b> Synthesis and characterisation	210
<b>6.2.2</b> X-ray studies	211
<b>6.2.3</b> Photophysical properties	214
<b>6.2.4</b> Electrochemical properties	215
<b>6.2.5</b> Theoretical calculations	216
<b>6.2.6</b> Picric acid sensing	218
<b>6.2.7</b> Nonlinear optical properties	225
<b>6.3 Conclusions</b>	232
<b>6.4 Experimental section</b>	232
<b>6.4.1</b> General information	232
<b>6.4.2</b> Synthetic procedures and spectral characterisations	233
<b>6.5 References</b>	236



## 6.1 Introduction

Three-coordinated organoboranes are an important class of compounds which possess an empty p-orbital through which they can establish interaction with an organic  $\pi$ -system and consequently could serve as a  $\pi$ -acceptor. Furthermore, the empty p-orbital of boron extends the  $\pi$ -conjugation in organic systems, which leads to unique absorption and emission properties. These unusual properties which are facilitated by interactions with boron compounds have been exploited in many opto-electronic applications.<sup>1-23</sup> For instance, Marder, Lambert, Fang, Mullen, Jäkle and Perry have carried out extensive studies of such chromophores in the context of non-linear optics.<sup>24-33</sup> Shirota and others have demonstrated the use of tricoordinated boranes for realizing electron transport as well as efficient emitters.<sup>34</sup> Wang, Yamaguchi, Tamao and others have shown that tri-coordinated boron compounds could be employed for realizing effective fluorescent and colorimetric sensors for the detection of fluoride anion.<sup>35-40</sup>

The recognition and sensing of nitro-explosives has attracted substantial attention owing to ever-increasing usage in terrorism related activities. Among the nitro explosives, 2,4,6-trinitrophenol (picric acid, PA) has shown superior explosive capabilities as compared to its counterpart trinitrotoluene (TNT).<sup>41-45</sup> Furthermore, picric acid can create severe health problems such as skin irritation, skin allergies, nausea and damage to respiratory organs.<sup>46,47</sup> Hence, selective, reliable and convenient detection of picric acid is in high demand. Even though various fluorescent sensors, such as polymers, nanoparticles, mesoporous and metal organic frameworks have been reported for the detection of nitro-aromatic explosives, most of these investigations were directed towards the detection of TNT and discernibly weaker importance was given to the more powerful explosive picric acid.<sup>48-58</sup> Although ample reports exist for

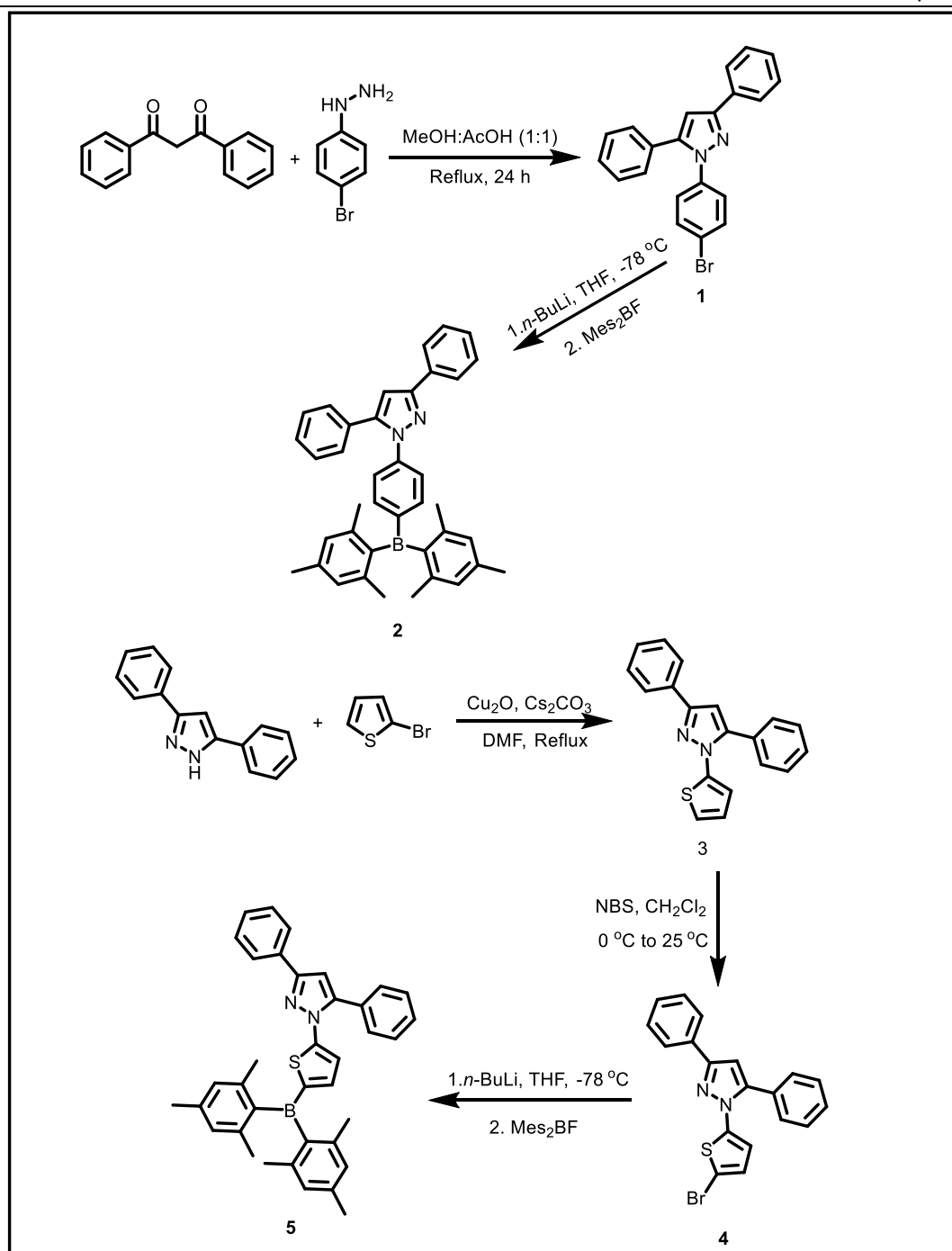
the detection of picric acid, owing to similar electron affinities of poly nitro-aromatics, the augmentation of an effective and reliable sensor for picric acid with high selectivity is still a challenging task. We propose a very efficient and selective sensor based on tri-coordinated boron. To the best of our knowledge this is the first example of the use of tri-coordinated borane based fluorophores for the selective detection of picric acid.

Tri-coordinated boron has been chosen as the fluorophore unit because of its widely studied properties as discussed *vide supra*. A pyrazole unit at the para position of the phenyl ring or 5-position of thiophene was placed to act as an H-bond accepting site. We anticipate that the lone pair on the pyrazole nitrogen will help in forming H-bonding with picric acid through N $\cdots$ H–O interaction and consequently it would help to detect the picric acid selectively.

## 6.2 Results and discussion

### 6.2.1 Synthesis and characterisation

The starting material 1-(4-bromophenyl)-3,5-diphenyl-1H-pyrazole (**1**) was prepared by following the literature reported procedure<sup>59</sup> and compound **3** was synthesized by Cu<sub>2</sub>O catalysed Ullmann-type coupling reaction of 3,5-diphenyl pyrazole and 2-bromothiophene followed by bromination using N-bromosuccinimide. Compound **1** or **4** was reacted with *n*-butyllithium, then quenched with dimesitylboron fluoride, which yields the desired triaryl borane-pyrazole compounds **2** and **5** in 73 and 55% respectively (Scheme 6.1). The formation of compounds **2** and **5** were confirmed using <sup>1</sup>H, <sup>13</sup>C and <sup>11</sup>B NMR spectroscopy.



**Scheme 6.1:** Synthetic route to compound **2** and **5**.

### 6.2.2 X-ray studies

Compounds **2** and **5** were further characterized using single crystal X-ray diffraction crystallography (Fig. 6.1 & Table 6.1). Compounds **2** and **5** crystallize in the monoclinic *P2<sub>1</sub>/n* and *P2<sub>1</sub>/c* space groups respectively. The boron centre adopts a

trigonal planar geometry ( $\angle_{\text{C-B-C}} = 359.9^\circ$  for **2** &  $360.0^\circ$  for **5**) as shown in Fig. 6.1.

The boron–carbon bond distances ( $1.572(2)$ – $1.583(2)$  Å for **2** and  $1.538(3)$ – $1.579(3)$  Å for **5**) are comparable to the literature reported analogues tri-coordinated boron compounds.

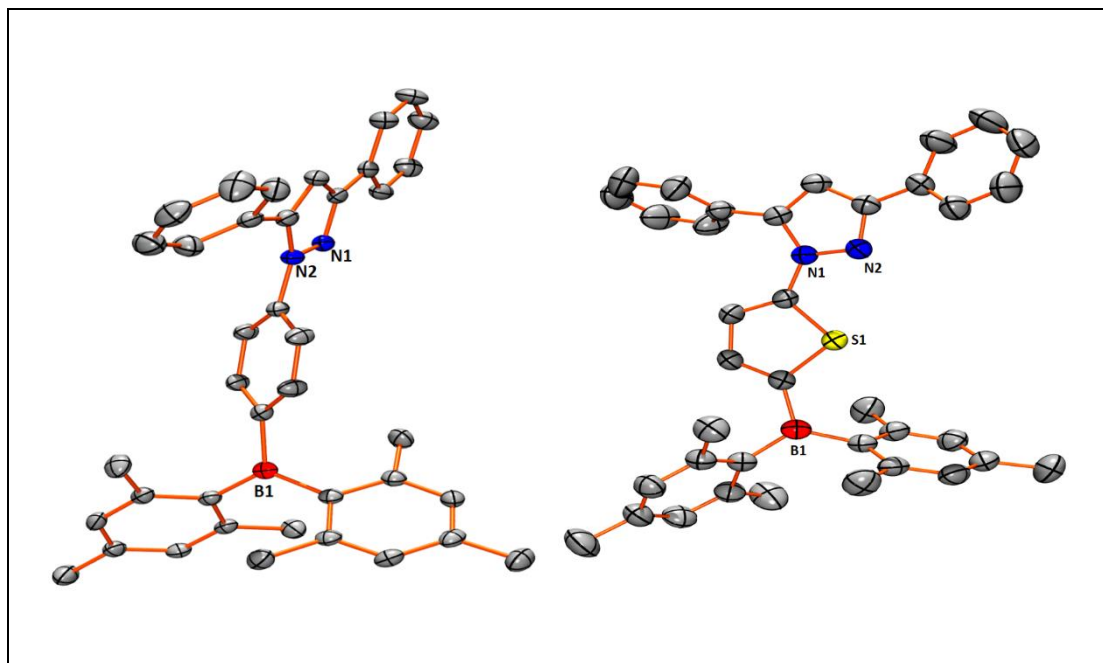


**Figure 6.1:** Molecular structure of compound **2** (Left) and **5** (Right).

**Table 6.1:** Crystal data and structure refinement parameters for compound **2** and **5**.

Crystal Parameters	Compound <b>2</b>	Compound <b>5</b>
Empirical formula	$\text{C}_{15}\text{H}_{38}\text{N}_{15}\text{B}_{15}$	$\text{C}_{40}\text{H}_{38}\text{BS}_{0.25}\text{N}_{0.25}$
$M_r$	544.57	541.03
$T$ [K]	100	296.15
Wavelength, Å	0.71073 Å	0.71073 Å
Crystal system	Monoclinic	Monoclinic
Space group	$P2_1/n$	$P2_1/c$
$a$ [Å]	8.2587(4)	13.5234(3)
$b$ [Å]	30.5396(17)	11.1663(3)
$c$ [Å]	11.9793(7)	20.6115(5)



$\alpha$ [°]	90	90
$\beta$ [°]	91.502(3)	93.494(2)
$\delta$ [°]	90	90
$V$ [Å <sup>3</sup> ]	3020.3(3)	3106.68(13)
$Z$	4	4
$\rho_{\text{calc}}$ [g cm <sup>-3</sup> ]	1.1975	1.157
$\mu$ (MoK $\alpha$ ) [mm <sup>-1</sup> ]	0.069	0.081
$F(000)$	1160.4	1155.0
$\theta$ range [°]	6.8 – 63.1	3.96 – 55.868
limiting indices	-11 ≤ h ≤ 11 -42 ≤ k ≤ 44 -16 ≤ l ≤ 17	-17 ≤ h ≤ 17 -14 ≤ k ≤ 13 -27 ≤ l ≤ 27
reflns collected	37064	26106
independent reflns	9918 [ $R(\text{int}) = 0.0940$ ]	7413 [ $R(\text{int}) = 0.0385$ ]
absorption correction	Semi-empirical from equivalents	Semi-empirical from equivalents
refinement method	Full-matrix least square on $F^2$	Full-matrix least square on $F^2$
data / restraints / parameters	9918/0/385	7413/0/376
Goodness-of-fit on $F^2$	0.986	1.029
final R indices [ $I > 2\sigma(I)$ ] <sup>[a]</sup>	$R_I = 0.0642$ $wR_2 = 0.1485$	$R_I = 0.0474$ $wR_2 = 0.1215$
R indices (all data) <sup>[a]</sup>	$R_I = 0.1139$ $wR_2 = 0.1714$	$R_I = 0.0760$ $wR_2 = 0.1380$
peak <sub>max</sub> /hole <sub>min</sub> [e Å <sup>-3</sup> ]	0.53 and -0.48	0.26 and -0.24

<sup>[a]</sup>  $R_I = \sum ||F_o| - |F_c|| / \sum |F_o|$ ;  $wR_2 = \{\sum [w(F_o^2 - F_c^2)^2] / \sum [w(F_o^2)^2]\}^{1/2}$ .

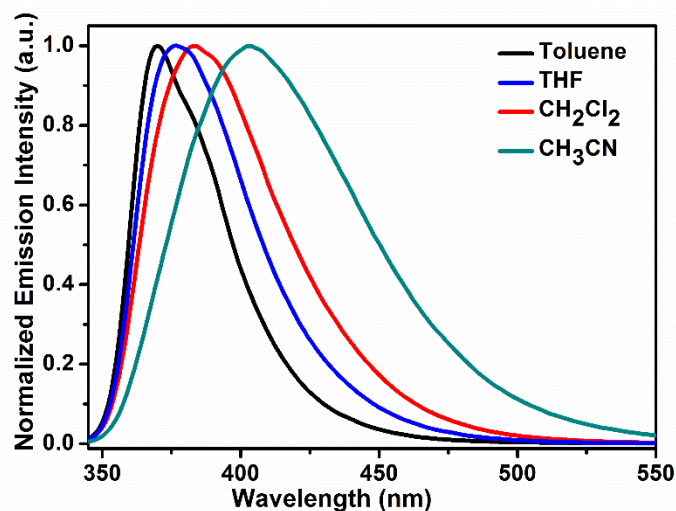
### 6.2.3 Photophysical properties

The optical properties of compound **2** and **5** were investigated by UV-Visible absorption and emission spectra in four different solvents of varying polarity. The resulting data are summarized in table 6.2. The absorption spectra of compound **2** shows a weak solvatochromism, however the emission spectra exhibits strong solvatochromism (Figure 6.2). The emission maxima shifted from  $\lambda_{em} = 370$  nm (toluene) to  $\lambda_{em} = 403$  nm ( $\text{CH}_3\text{CN}$ ), and the Stokes shift increases from  $2913\text{ cm}^{-1}$  to  $5673\text{ cm}^{-1}$  with increasing solvent polarity which indicates the presence of different charge distribution in the excited state in polar solvents compared to the ground state. The emission spectra of compound **5** did not show any solvatochromism, however, its absorption spectra showed weak solvatochromism. The absorption and emission maxima of compound **5** (358 nm & 415 nm in  $\text{CH}_3\text{CN}$ ) exhibits a slight red shift in comparison with compound **2** (328 nm & 403 nm in  $\text{CH}_3\text{CN}$ ) which is attributed due to electron donating nature of thiophene (Fig. 6.3). The quantum yield for compounds **2** & **5** are 0.23 & 0.15 (in THF) respectively (Table 6.2) which are comparable with other reported pyrazole based systems.<sup>58</sup>

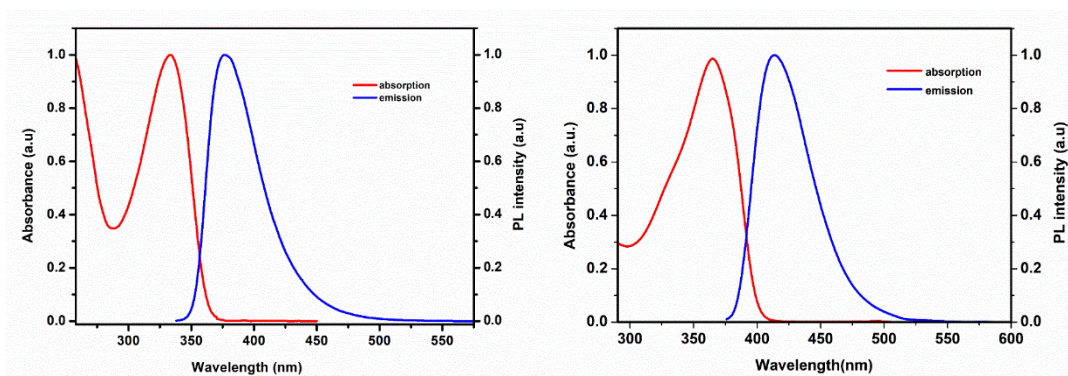
**Table 6.2:** Photophysical data of compound **2** and **5**.

Compound	solvent	$\lambda_{abs}^a$ (nm)	$\epsilon_{max}$ ( $\text{M}^{-1}\text{ cm}^{-1} \times 10^3$ )	$\lambda_{em}^{a,b}$ (nm)	$\Phi_f^c$
<b>2</b>	Toluene	334	33.19	370	0.35
	THF	333	36.55	377	0.23
	$\text{CH}_2\text{Cl}_2$	331	30.00	383	0.14
	$\text{CH}_3\text{CN}$	328	30.88	403	0.12
<b>5</b>	Toluene	368	25.00	411	0.17
	THF	366	33.74	413	0.15
	$\text{CH}_2\text{Cl}_2$	361	27.61	413	0.14
	$\text{CH}_3\text{CN}$	358	29.61	415	0.12

<sup>a</sup>Absorption maximum (concentrations in solutions were  $10^{-5}$  M). <sup>b</sup>Excited at absorption maximum. <sup>c</sup>Absolute fluorescence quantum yields were measured by integrating sphere method.



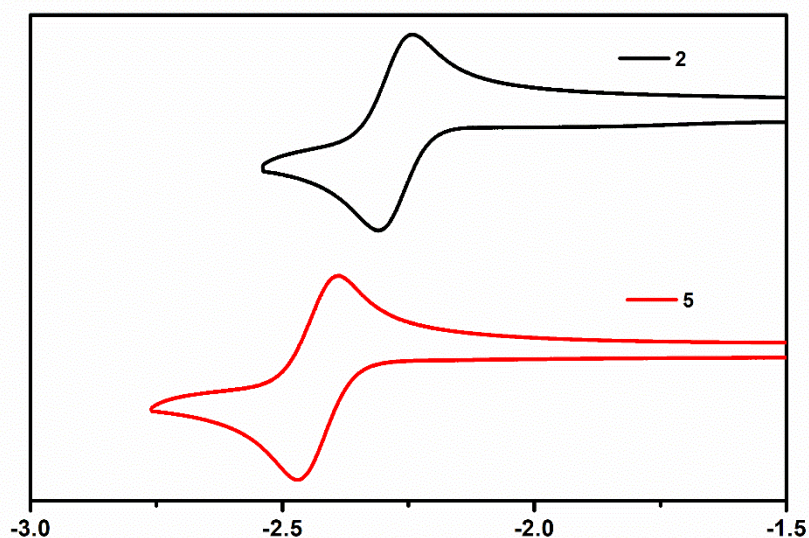
**Figure 6.2:** Normalised emission spectra of compound **2** with increasing solvent polarity.



**Figure 6.3:** Normalized UV-Vis absorption and fluorescence spectra of compounds **2** (left) and **5** (right) in  $10^{-5}$  M acetonitrile.

#### 6.2.4 Electrochemical properties

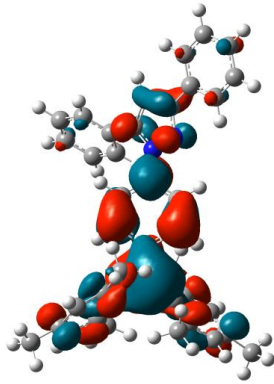
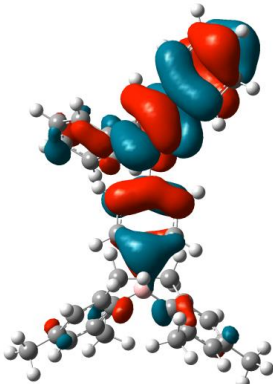
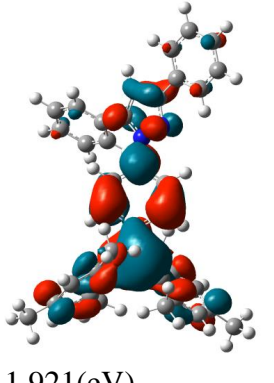
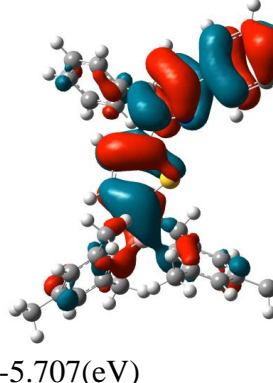
The electrochemical properties of compound **2** and **5** were studied in 0.1M dimethylformamide (DMF) solution using  $\text{Bu}_4\text{NPF}_6$  as the electrolyte. Cyclic voltammetry studies showed a reversible reduction wave for both **2** and **5** (Fig. 6.4). Compound **5** ( $E_{1/2} = -2.42$  V) showed more negative potential than compound **2** ( $E_{1/2} = -2.27$  V).



**Figure 6.4:** Cyclic voltammograms of compound **2** & **5** (vs. Ferrocene/Ferrocenium) with 0.1 M  $n\text{Bu}_4\text{NPF}_6$  in DMF as the supporting electrolyte (scan rate 100 mV/s).

### 6.2.5 Theoretical calculations

To better understand the photophysical properties of compounds **2** and **5**, theoretical calculations were performed by Gaussian09 program using 6-31G(d,p) (B3LYP) as the basis set. As shown in Fig. 6.5, the HOMO of compounds **2** and **5** are dominated by the orbitals from the pyrazole, one of the phenyl ring with small dihedral angle attached to the pyrazole (the dihedral angles between the pyrazole and the phenyl rings are 46.0 & 5.0 for **2**; 50.7 & 4.3° for **5**) and the spacer ('phenyl' in case of **2** and 'thiophene' in case of **5**); whereas the LUMO gets in maximum contribution from the boron and the spacer (phenyl or thiophene) indicates that the pyrazole unit is the donor and the boron moiety acts as an acceptor. Excitation data were determined using TD-DFT (B3LYP/631g(d,p))–PCM solvation (THF))) calculations (Table 6.3).

Compound	LUMO	HOMO
<b>2</b>	 -1.822(eV)	 -5.794(eV)
<b>5</b>	 -1.921(eV)	 -5.707(eV)

**Figure 6.5:** Computed orbitals for compound **2** and **5**.

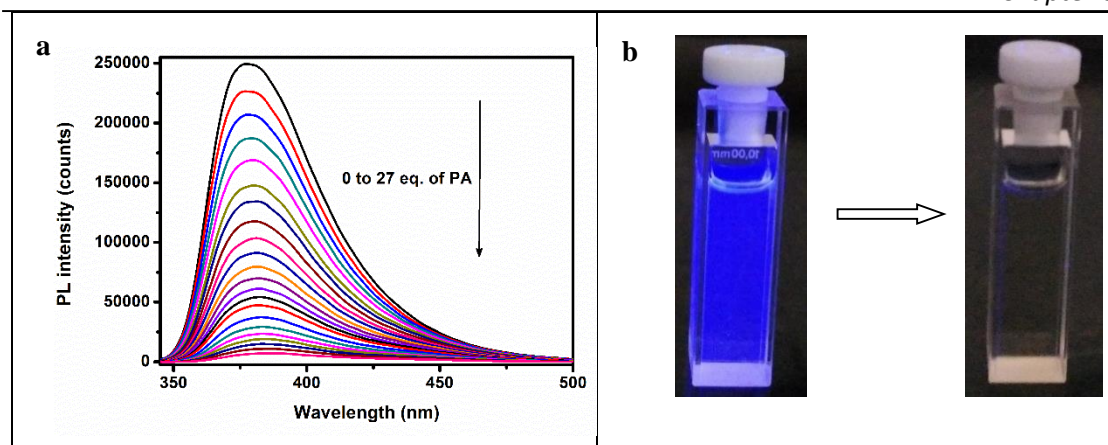
**Table 6.3:** Calculated electronic transitions for compound **2** & **5** from TD-DFT (B3LYP/631g(d,p))– PCM solvation (THF))) calculations

Compound	Transition	MO contributions	Energy gap eV (nm)	Oscillator strength/f
<b>2</b>	$S_0 \rightarrow S_1$	HOMO-2 $\rightarrow$ LUMO	3.42 (361)	0.5599
		HOMO $\rightarrow$ LUMO		
	$S_0 \rightarrow S_2$	HOMO-1 $\rightarrow$ LUMO	3.47 (357)	0.1042
	$S_0 \rightarrow S_3$	HOMO-3 $\rightarrow$ LUMO	3.37 (337)	0.0266
		HOMO-2 $\rightarrow$ LUMO		

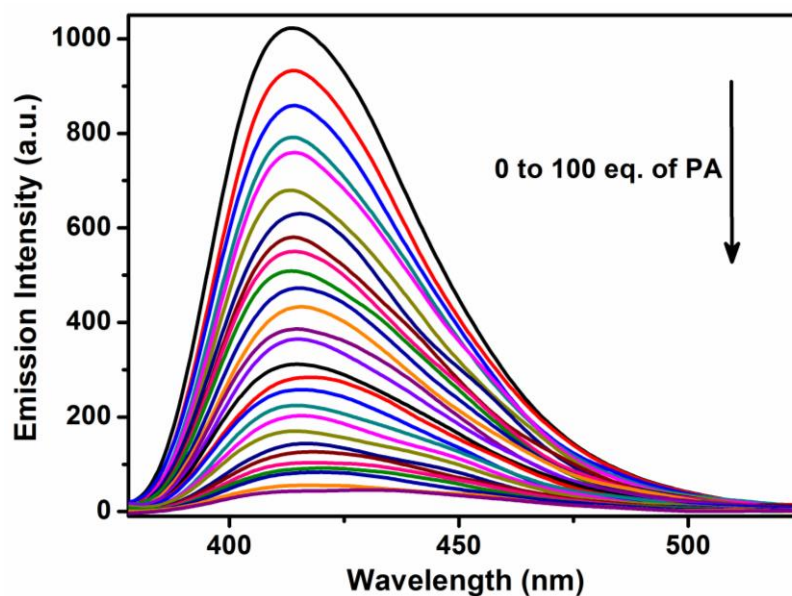
		HOMO→LUMO		
<b>5</b>	$S_0 \rightarrow S_1$	HOMO-3→LUMO	3.24 (382)	0.7038
		HOMO→LUMO		
	$S_0 \rightarrow S_2$	HOMO-1→LUMO	3.46 (358)	0.0870
	$S_0 \rightarrow S_3$	HOMO-3→LUMO	3.59 (345)	0.0084
		HOMO-2→LUMO		

### 6.2.6 Picric acid sensing

With this well-defined triarylborane anchored pyrazole in hand, we examined the application of compound **2** as a probe for picric acid detection in THF. As shown in Fig. 6.6, gradual addition of picric acid to a solution of compound **2** in THF causes substantial quenching of the emission. Addition of 14 equiv. (140  $\mu$ M) solution of picric acid quenches about 89% and 44% of emission intensity for the compounds **2** and **5** respectively (Fig. 6.6 and Fig. 6.7). It is worth noting that 90% fluorescence quenching was observed for **2** at 14 equiv. of PA and that for the **5** it was observed at 70 equiv. of PA in THF. As picric acid is freely soluble in water, determination of PA in aqueous medium is necessary. Both the compounds **2** and **5** are not soluble in water; in order to use them in aqueous environment, mixed solvent system was adopted (THF: H<sub>2</sub>O; 70 : 30) for further sensing studies. Aliquots of PA in water was added to compounds **2** and **5** in THF/H<sub>2</sub>O (70 : 30) as described *vide supra*. About ~20% emission quenching was realized for **2** & **5**, upon addition of 0.5 equiv. of picric acid in H<sub>2</sub>O. The emission further quenched to ~90% upon further addition of PA (92% quenching was observed for **2** at 7 equiv. of PA and 90% quenching was observed for **5** at 4.4 equiv. of PA) to compounds **2** and **5** respectively (Fig. 6.8).

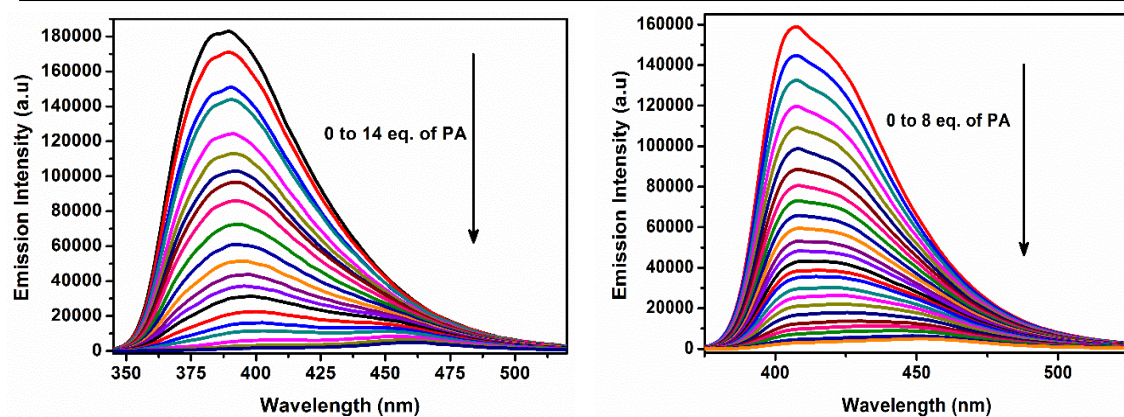


**Figure 6.6:** (a) Fluorescence quenching of compound **2** with the addition of different concentrations of PA (0, 0.25, 0.5, 0.75, 1.0, 1.5, 2.0, 3.0, 4.0, 5.0, 6.0, 7.0, 8.0, 9.0, 10.0, 12.0, 14.0, 16.0, 18.0, 23.0, and 27.0 equiv. of PA) in THF ( $10^{-5}$  M; excited at 333 nm). (b) Color change under a UV lamp before (left) and after (right) the addition of PA.



**Figure 6.7:** Fluorescence quenching of compound **5** with the addition of different concentrations of PA (0, 2, 4, 6, 8, 10, 12, 14, 16, 18, 20, 23, 26, 29, 33, 37, 41, 45, 50, 55, 60, 65, 70, 75, 80, 90, and 100 equiv of PA) in THF ( $10^{-5}$  M; excited at 366 nm).

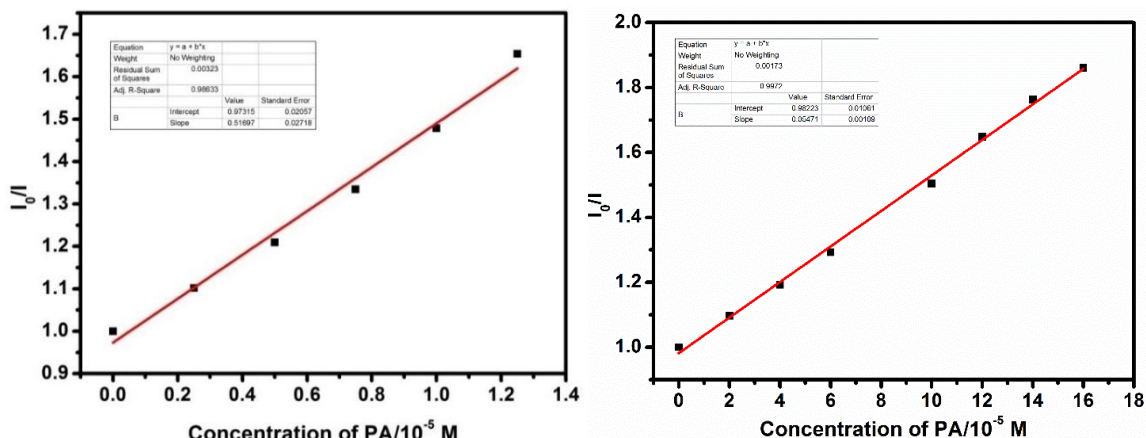




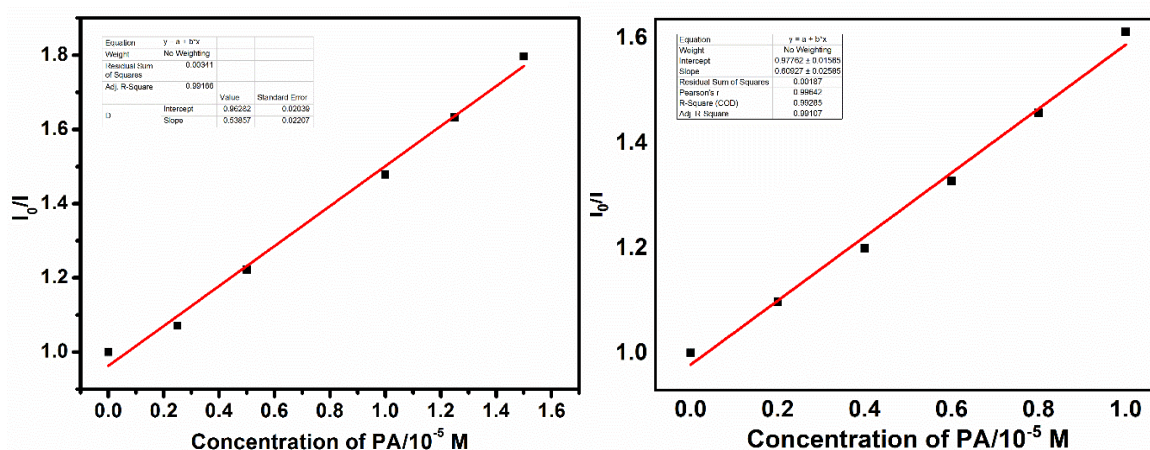
**Figure 6.8:** (Left) Fluorescence quenching of compound **2** ( $10^{-5}$  M, excited at 333 nm) in a mixed solvent of THF: H<sub>2</sub>O (70 : 30) with different concentrations of PA (0, 0.25, 0.5, 0.75, 1.0, 1.25, 1.50, 1.75, 2.0, 2.5, 3.0, 3.5, 4.0, 4.5, 5.0, 6.0, 7.0, 10.0, 12.0, and 14.0 equiv. of PA). (Right) Fluorescence quenching of compound **5** ( $10^{-5}$  M, excited at 366 nm) in a mixed solvent of THF: H<sub>2</sub>O (70 : 30) with different concentrations of PA (0, 0.2, 0.4, 0.6, 0.8, 1.0, 1.2, 1.4, 1.6, 1.8, 2.0, 2.2, 2.4, 2.6, 2.8, 3.0, 3.3, 3.6, 4.0, 4.4, 5.0, 5.5, 6.0, 7.0 and 8.0 equiv. of PA).

We further studied the fluorescence quenching of compounds **2** and **5** using Stern–Volmer plot. At lower concentration of picric acid, the quenching constant was calculated using Stern–Volmer plot and was found to be  $5.2 \times 10^4 \text{ M}^{-1}$  and  $0.5 \times 10^4 \text{ M}^{-1}$  for compounds **2** and **5** in THF (Fig. 6.9) respectively which confirms the high sensitivity of both the compounds towards picric acid in THF, whereas quenching constant is  $5.4 \times 10^4 \text{ M}^{-1}$  for **2** in THF : H<sub>2</sub>O (70 : 30) and  $6.1 \times 10^4 \text{ M}^{-1}$  for **5** in THF : H<sub>2</sub>O (70 : 30) (Fig. 6.10).



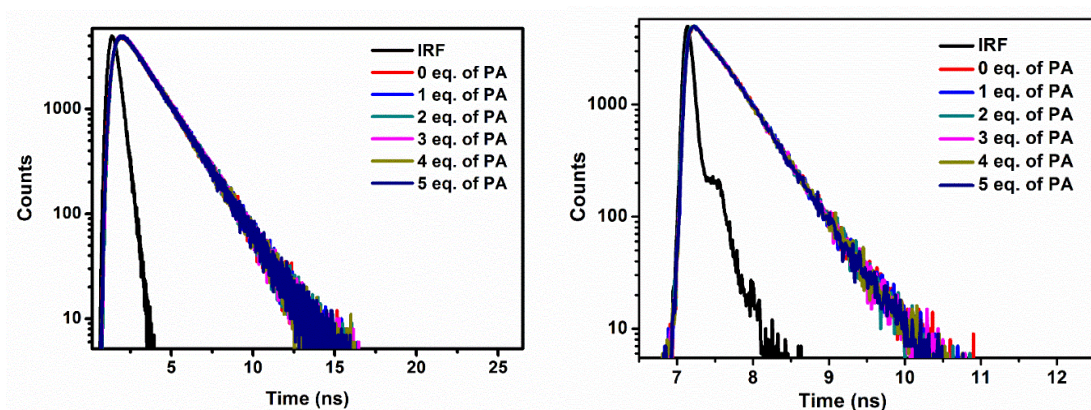


**Figure 6.9:** Stern-Volmer plot of compound **2** (left) and **5** (Right) in  $10^{-5}$  M with addition of different concentration of PA in THF.



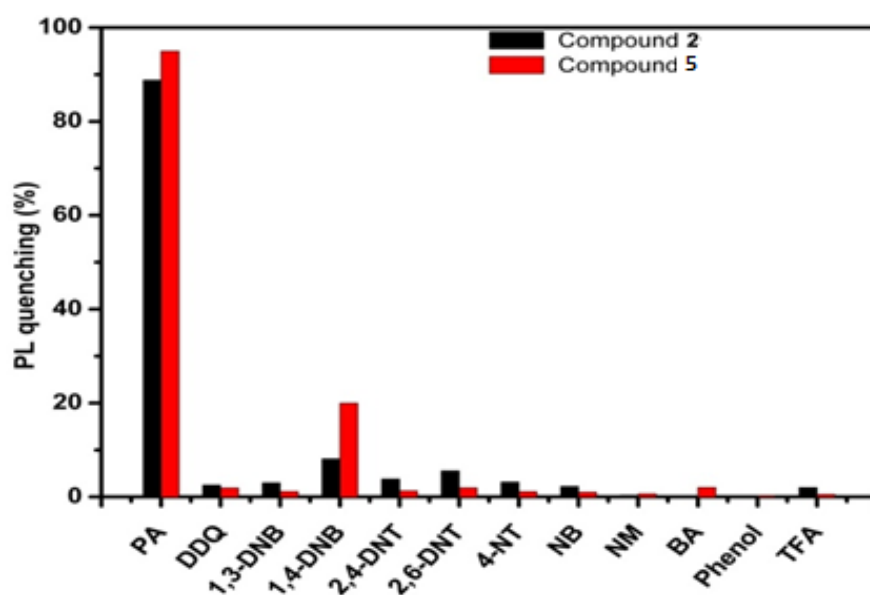
**Figure 6.10:** Stern-Volmer plot of compound **2** (left) and **5** (Right) in  $10^{-5}$  M with addition of different concentration of PA in THF: H<sub>2</sub>O (70:30) mixture.

Time resolved fluorescence measurements were carried out to realize the origin of the quenching process. As shown in the figure **6.11** the fluorescence life time of **2** and **5** is invariant in the presence of picric acid, which suggests that the mechanism of quenching is static.



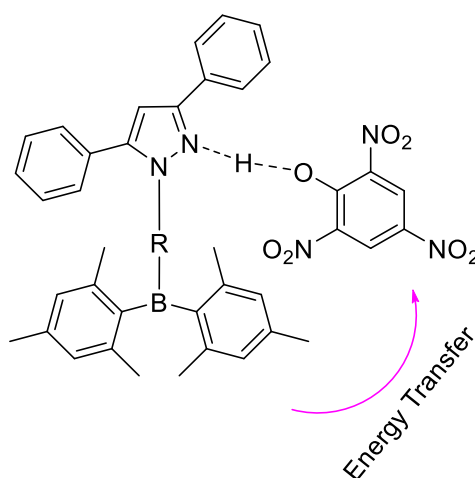
**Figure 6.11:** (Left) Fluorescence lifetime decay of compound **2** after the addition of 0, 1, 2, 3, 4 and 5 equiv. of PA in  $10^{-5}$  M THF. (Right) Fluorescence lifetime decay of compound **5** after the addition of 0, 1, 2, 3, 4 and 5 equiv. of PA in  $10^{-5}$  M THF.

In order to judge the selectivity of compounds **2** & **5**, fluorescence response of the probes with different nitroaromatics (Figure 6.12) and other analytes such as 1,3-dinitrobenzene (1,3-DNB), 1,4-dinitrobenzene (1,4-DNB), 2,4-dinitrotoluene (2,4-DNT), 2,6-dinitrotoluene (2,6-DNT), 4-nitrotoluene (4-NT), nitrobenzene (NB), DDQ, nitromethane (NM), benzoic acid (BA), phenol and trifluoroacetic acid (TFA) were studied.



**Figure 6.12:** Fluorescence quenching efficiencies of compounds **2** and **5** in THF : H<sub>2</sub>O (70 : 30) ( $10^{-5}$  M; excited at 333 nm) toward different nitroaromatics and other analytes (6 equiv.) like picric acid (PA), 1,3-dinitrobenzene (1,3-DNB), 1,4-dinitrobenzene (1,4-DNB), 2,4-dinitrotoluene (2,4-DNT), 2,6-dinitrotoluene (2,6-DNT), 4-nitrotoluene (4-NT), nitrobenzene (NB), DDQ, nitromethane (NM), benzoic acid (BA), phenol and trifluoroacetic acid (TFA).

Among the different nitroaromatics and analytes tested, picric acid results in 90% quenching of emission of the probes (**2** & **5**), however the emission (**2** & **5**) quenching by other analytes was negligible. The selective emission response towards picric acid indicates that there is an interaction between compound **2** or **5** and picric acid. In general, pyrazoles are prone to form hydrogen bonding with themselves through N–H···N intermolecular hydrogen bonding and with other molecules through intramolecular hydrogen bonding ( $N\cdots H-X$ ; X may be O or N). We propose that  $N\cdots H-O$  interaction between compound **2** or **5** and picric acid resulted in selective fluorescence quenching (Fig. 6.13). Compounds **2** & **5** showed a much better or comparable detection limits compared to other fluorescent probes reported in the literature (Table 6.4 and table 6.5).

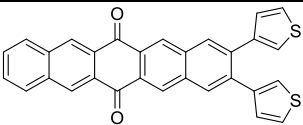
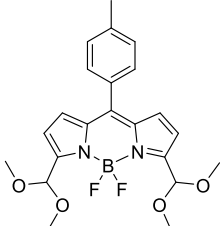
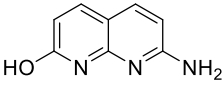
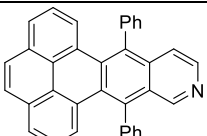


**Figure 6.13:** Proposed quenching mechanism

**Table 6.4:** Limit of detection (LOD) data for compound **2** and **5**

Probe	Detection Medium	Detection Limit
Compound <b>2</b>	THF:H <sub>2</sub> O(70:30)	$1.63 \times 10^{-7} \text{M}$
Compound <b>5</b>	THF:H <sub>2</sub> O(70:30)	$1.95 \times 10^{-7} \text{M}$
Compound <b>2</b>	THF	$1.28 \times 10^{-7} \text{M}$
Compound <b>5</b>	THF	$3.06 \times 10^{-4} \text{M}$

**Table 6.5:** Limit of detection (LOD) data for recently reported probes for picric acid

Probe	Detection Medium	Detection Limit(M)	References
	THF	$1 \times 10^{-6}$	65
	CH <sub>3</sub> CN:H <sub>2</sub> O (9:1)	$7.27 \times 10^{-7}$	66
	H <sub>2</sub> O:CH <sub>3</sub> OH (8:2)	$4.3 \times 10^{-6}$	67
	CH <sub>3</sub> CN	$2.42 \times 10^{-6}$	68

To get deeper insight into the quenching mechanism, we carried out <sup>1</sup>H NMR studies of compound **2** in DMSO-*d*<sub>6</sub>. In the presence of picric acid, a slight shift of all the protons corresponding to compound **2** was observed, which confirm that the proposed mechanism involves the electrostatic interaction (N $\cdots$ H–O) between compound **2** and picric acid (Figure 6.14).

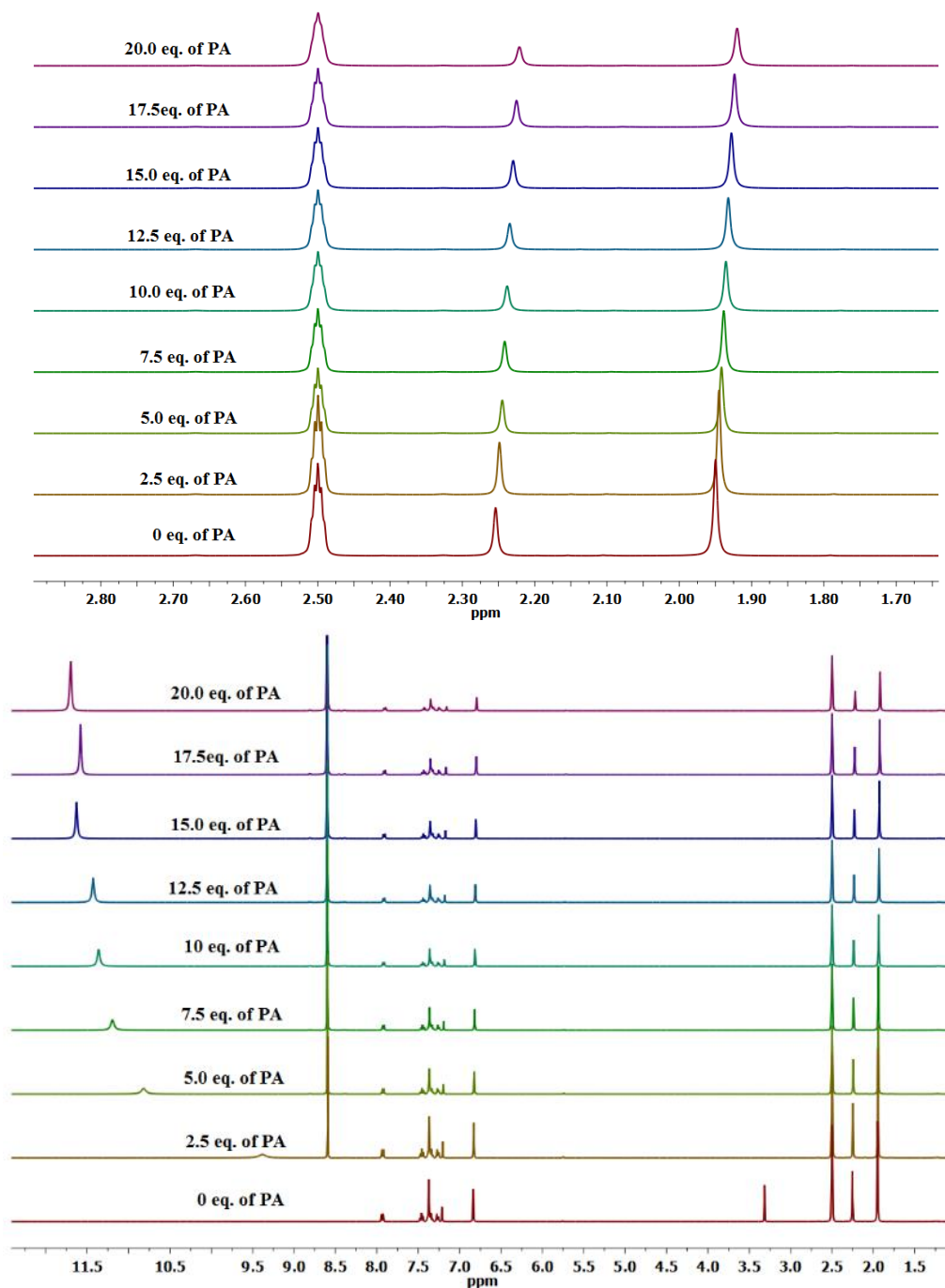


**Figure 6.14:**  $^1\text{H}$  NMR titration of compound **2** upon the addition of 0, 2.5, 5.0, 7.5, 10.0, 12.5, 15.0, 17.5 and 20.0 equiv. of PA in  $\text{DMSO-}d_6$ .

### 6.2.7 Nonlinear optical properties

Griesbeck *et al.* showed that three-coordinated boron compounds possess small dipole moment in ground state and large dipole moment in first excited singlet state. In

addition, they have tendency to show intense intramolecular charge transfer transitions when attached with a suitable electron enrich chromophore which can greatly enhance the probability of nonlinear absorption.<sup>26</sup> In order to investigate the nonlinear optical behaviour and subsequently, determine the nonlinear absorption coefficient ( $\beta$ ) and nonlinear refractive index ( $n_2$ ), we used the single beam Z-scan technique.<sup>60</sup> The details about the experimental setup could be found elsewhere.<sup>61</sup> In order to measure  $n_2$  and  $\beta$ , we irradiated the solution (concentration: 0.04 mM in dichloromethane) to an intense laser beam from Yb-doped ultrashort pulse ( $\Delta\tau = 370$  fs) fiber laser (Model: Cazadero, M/S Calmar Inc., USA) at wavelength of  $\lambda = 515$  nm and at 1 kHz repetition rate. The solution was contained in a 1.0 mm thick optical cell which was translated across the focal point of the focused Gaussian laser beam along the beam propagation direction. In closed-aperture (CA) Z-scan, the optical power of transmitted beam from the sample is recorded through a finite-size circular aperture which is placed in the far field. For an open aperture (OA) Z-scan, the entire laser beam transmitted through the sample is measured. Figure 6.15 shows the normalized transmittance of CA and OA in the Z-scan experiment for compounds **2** and **5**.

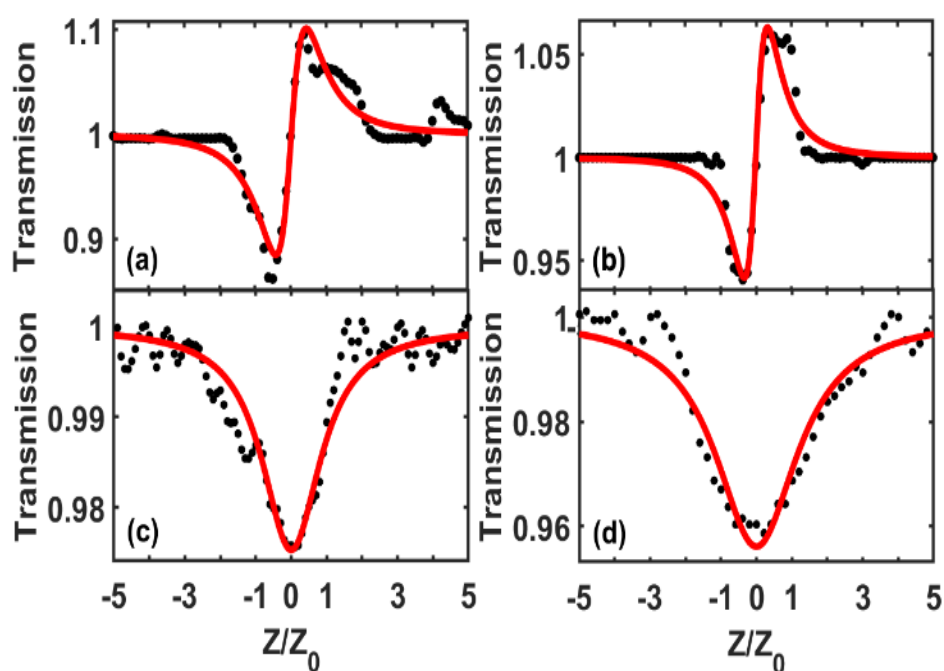


**Figure 6.15:** Normalized Z-scan (a and b) CA transmittance. (c and d) OA transmittance of **2** and **5** respectively in dichloromethane.

The measured normalised z-dependent transmission is represented by black dots. It is to be noted that the laser intensity ( $I$ ) is relatively small and uniform in the regions which are far from the focal point. This leads to a negligible nonlinear optical absorption ( $NLA = \beta I$ ) in this region and consequently, the actual transmission is normalised with respect to this value of transmission (far from focal point). Near the focal point, the nonlinear optical effects are more pronounced, which results in significant alteration in transmission.

It is to note that the CA normalized transmission in figure **6.15** (a) and (b) exhibits a familiar valley–peak behaviour which indicates a self-focusing behaviour in both the compounds **2** and **5**. Alternately, the variation of normalized transmittance results in a positive value of  $n_2$ , thereby depicting a strong electrostrictive effect. According to this, both the compounds exhibit a tendency to have a higher density in regions where the laser intensity is high and consequently, such compounds are expected to offer resistance to thermal lensing effect. In order to estimate the values of  $n_2$ , the experimental measurements have been fitted with the mathematical relation given by,<sup>62</sup>

$$T(z, \Delta\phi_0) = 1 - \frac{4\Delta\phi_0 x}{(x^2+9)(x^2+1)} - \frac{2(x^2+3)\Delta\Psi_0}{(x^2+9)(x^2+1)} \dots (1)$$

where  $T$  represents the normalized transmittance,  $x = z/z_0$ ,  $z_0$  being rayleigh range.  $\Delta\phi_0$  is the on-axis phase-shift. The value of  $n_2$  can be estimated by the relation  $\Delta\phi_0 = kn_2I_0L_{\text{eff}}$ ,  $k = 2\pi/\lambda$  is the wave vector and  $\lambda$  is the pump wavelength,  $\Delta\Psi_0 = \beta I_0L_{\text{eff}}/2$  is the phase change due to nonlinear absorption. It is worthwhile to point out that NLA has been included in Eq. (1) so as to account for any kind of asymmetric behaviour. Figures **6.15** (c, d) shows the normalized transmission for the OA Z-scan measurement. There is an apparent transmission drop at the focus

( $z = 0$ ) for the compounds **2** and **5**. Transmission drop near the focus is essentially a consequence of two-photon absorption (TPA) or multi-photon absorption (MPA) which is characterized by a positive value of  $\beta$ . In absence of other nonlinear optical effects or parasitic effects, the normalized transmission is symmetric with respect to the focus ( $z = 0$ ), where it has a minimum transmission.

The absorption coefficient ( $\beta$ ) can be estimated from the OA normalized transmission as <sup>60</sup>,

$$T(z, S = 1) = 1 - \frac{\beta I_0 L_{eff}}{2^2(1+x^2)} \quad \dots (2)$$

where  $x = z/z_0$ ,  $I_0$  is the on-axis peak irradiance at focus ( $z = 0$ ),  $L_{eff}$  is the effective sample length. The results are summarized in table **6.6** for compounds **2** and **5** along with the two-photon absorption cross-section (TPAC) in GM units (1 GM= $10^{-50}$  cm<sup>4</sup> s/photon).

**Table 6.6:** Optical nonlinear coefficients of **2** and **5** at 1kHz repetition rates

Compound	$n_2$ (x $10^{-16}$ cm <sup>2</sup> W <sup>-1</sup> )	$\beta$ (x $10^{-12}$ cm W <sup>-1</sup> )	TPAC (GM)
<b>2</b> (w/o picric acid)	2.3	2.0	7
<b>5</b> (w/o picric acid)	1.14	4.0	13
Picric acid	-	6.59	23
<b>2</b> (with 7% picric acid)	1.73	10.9	38
<b>5</b> (with 14% picric acid)	1.9	4.8	17
<b>5</b> (with 40% picric acid)	-	25.1	66



Recently, there have been a concerted effort to identify and ascertain a plausible mechanism behind the high nonlinearity in PA coordinated crystals. However, such investigations have rarely been carried out in the context of PA in solutions where the flexibility in realizing  $\pi$ -conjugations are significantly higher. It has been pointed out by Karthikeyan et al. that  $\text{NO}_2$  and OH groups in PA are discernibly easy to polarise. Consequently, PA interact with nearby species through rapid charge delocalization.<sup>63</sup> It is worthwhile to note that the presence of three electron withdrawing  $\text{NO}_2$  groups in PA makes it a good  $\pi$ -acceptor for neutral carrier donor molecule. However,  $\text{NO}_2$  group present at the para-position exhibits maximum charge delocalization which gives rise to the possibility of a longer conjugation length when interacts with electron-donating species. Thus, detection of PA through enhancing the nonlinear optical interactions could be plausible option. In order to investigate this aspect, we measured the nonlinear optical coefficients for pure PA solution which resulted in  $\beta = 6.59 \times 10^{-12} \text{ cm W}^{-1}$ . This value is higher than the compounds **2** and **5** which could be attributed to the presence of phenolic (OH) group. This favours the formation of hydrogen-bonding interactions, which leads to increased molecular hyperpolarizability.<sup>64</sup> In our work, we observed the fluorescence quenching on addition of PA to the pyrazole anchored boron fluorophore which encouraged us to have a further investigation of how does it affect the nonlinearity of these compounds. Since, PA is explosive in nature, we have added limited concentrations (7.0 equiv. and 14.0 equiv. to the compounds **2** and **5** respectively). This concentration quenches the fluorescence of each solution by approximately 40%. The normalized CA and OA transmittance of compounds **2** and **5** after adding PA is shown below.

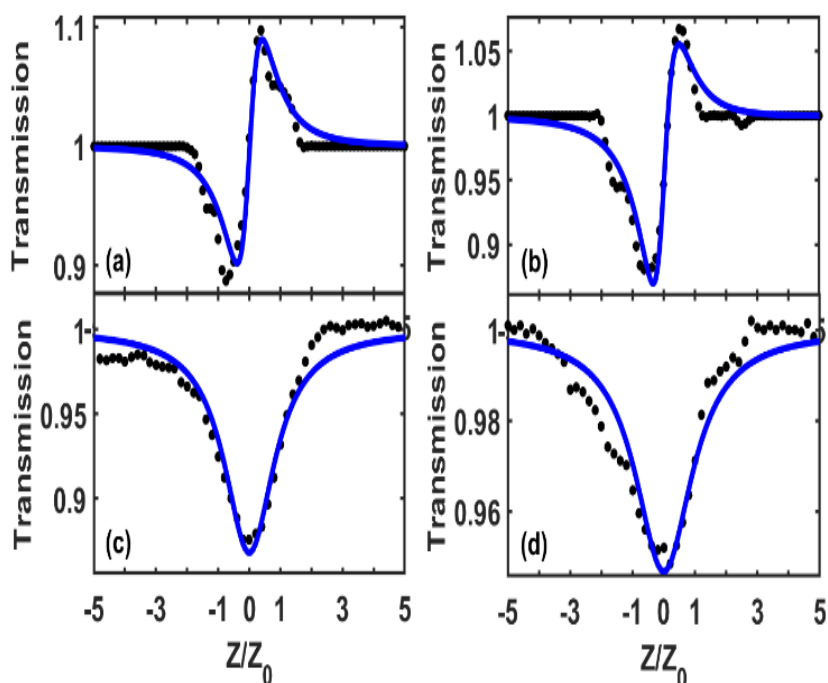


**Figure 6.16:** Normalized Z-scan (a and b) CA transmittance. (c and d) OA transmittance after adding 7.0 equiv. and 14.0 equiv. PA in compounds **2** and **5** respectively. Solvent: dichloromethane.

It is evident from the figure **6.16** (a) and (b) above, that the addition of PA does not change the behaviour of the CA transmittance and hence, it does change the sign of  $n_2$  for **2** as well as **5**. From table **6.6**, it could be observed that there is a marginal change in the value of  $n_2$  with the addition of 7.0 equiv. of PA in **2** and **5** which indicates that the optical phase changes are insignificant. On the other hand, we observed a significant change in the value of  $\beta$  in case of **2**. For 7.0 equiv. PA addition to **2**, we observed more than fivefold increase in the value of  $\beta$ . This change can be attributed to the significant alteration in  $\pi$ -conjugation of the compound due to the association of OH from PA to the lone pair of electrons at nitrogen in pyrazole. In case of **5**, however, there is small change in the value of  $\beta$  after addition of 14.0 equiv. of PA. Further,  $\beta$  increases significantly with increase in PA concentration. In fact, we observed that  $\beta =$

$25.1 \times 10^{-12} \text{ cm W}^{-1}$  when 40.0 equiv. PA is added to **5**. At low PA concentration, the probability of the formation of **5**-PA is appreciably small, however, at high PA concentration the equilibrium shifts to form **5**-PA *via* intermolecular hydrogen bond, which, in turn results in a gradual increase in the effective conjugation length. For a comparison, we have listed the values of  $n_2$  and  $\beta$  for some similar organic compounds in table 6.7. The comparison reveals that **2** and **5** possesses appreciable third order nonlinear response which scales up higher with the addition of picric acid. Table 6.6 also presents a few measurements which were carried out using continuous-wave (CW) laser which yields exceptionally high values of NLO coefficients due to large thermo-optic manifestations.

**Table 6.7:** Comparison of optical nonlinearity coefficients of similar molecules

Compound	Laser Parameters	$n_2 \text{ (cm}^2\text{W}^{-1}\text{)}$	$\beta \text{ (cm W}^{-1}\text{)}$	TPAC (GM)	Reference
BPI* (crystal)	He-Ne Laser	$-4.27 \times 10^{-8}$	$3.37 \times 10^{-3}$		69
PP* (crystal)	532nm, CW Nd-Yag	$-7.35 \times 10^{-8}$	$-0.10 \times 10^{-4}$		64
45-1	735 nm	-	-	22	19
N2TFABD P*	1200nm, 45fs, 1kHz	-	-	9	70
N2TFABD P*	1200nm, 45fs, 1kHz	-	-	9	70
3TFABDP *	1200nm, 45fs, 1kHz	-	-	8	70
TVBVT*	800nm, 100fs, 82MHz	$-9.72 \times 10^{-10}$	-	-	71
HEAP*	He-Ne	$-9.2 \times 10^{-5}$	14.0		72

Therefore, NLO measurements and material stability of compounds **2** and **5** suggest that they are potential candidates for optical switching and limiting applications. To probe the effect of triarylborane linkage with triaryl pyrazole, we synthesized triaryl

pyrazole<sup>59</sup> and studied its photophysical properties. Although, the quenching phenomenon was similar to that of **2**, the observed absolute quantum yield was lower than that of **2**, which is the advantage of linking triaryl pyrazole with triarylborane.

### 6.3 Conclusions

In summary, 3,5-diphenylpyrazole anchored tri-coordinated boron compounds have been synthesized. The fluorescence studies revealed that compounds **2** and **5** are highly selective and sensitive for the detection of picric acid. The presence of 3,5-diphenyl pyrazole moiety endowed our design to have the potential to discriminate picric acid over other analytes. Subsequently, we measured the NLO properties (namely  $n_2$  and  $\beta$ ) for the compounds **2** and **5** which revealed a direct dependence on addition of concentration of PA to the solution. The addition of PA essentially provides a plausible route to enhance the effective conjugation length of the compounds thereby, larger values of nonlinear optical coefficients. In future, it would be worthwhile to investigate and corroborate the precise impact of quenching of linear absorption due to PA addition on the nonlinear absorption. The results presented here hold a great capability for development of new selective chemosensors based on tri-coordinated boron system.

### 6.4 Experimental section

#### 6.4.1 General information

All reagents and starting materials were purchased from Sigma-Aldrich, Alfa-Aesar and Spectrochem chemical companies and used as received unless otherwise noted. Chlorinated solvents acetonitrile, and DMF were distilled from CaH<sub>2</sub>. THF and toluene were distilled from Na/benzophenone prior to use. All 400 MHz <sup>1</sup>H, 100 MHz <sup>13</sup>C, NMR spectra were recorded on a Bruker ARX 400 spectrometer operating at 400 MHz. All <sup>1</sup>H and <sup>13</sup>C NMR spectra were referenced internally to solvent signals. All NMR spectra were recorded at ambient temperature. ESI mass spectra were recorded on

Bruker, micrOTOF-QII mass spectrometer. The absorbance spectra were recorded on a JASCO V-730 UV-Visible spectrometer. The fluorescence spectra were recorded using Edinburgh FS5 spectrofluorometer. Absolute fluorescence quantum yields of compounds 2 and 5 were measured by integrating sphere method using Edinburgh FS5 spectrofluorometer. The fluorescence spectra are corrected for the instrumental response. Cyclic voltammetry measurements were performed with a conventional three electrode cell using an electrochemical workstation (CH Instrument, Model: 1100A). The three-electrode system consisted of a Glassy carbon working electrode, a Pt wire as the secondary electrode, and a Ag wire as the reference electrode. The voltammograms were recorded with ca.  $1.0 \times 10^{-3}$  M solution in DMF containing  $\text{Bu}_4\text{NPF}_6$  (0.1 M) as the supporting electrolyte. The scans were referenced after the addition of a small amount of ferrocene as the internal standard. Single-crystal X-ray diffraction data were collected on a Bruker APEXII diffractometer using Mo-K $\alpha$  radiation (0.71073 Å). SADABS absorption corrections were applied. The structures were solved and refined with SHELX suite of programs. All non-hydrogen atoms were refined with anisotropic displacement coefficients. The H atoms were placed at calculated positions and were refined as riding atoms. The structures were optimized using 6-31G(d,p) (B3LYP) as the basis set. Frequency calculations confirmed the optimized structures to be local minimum structures. Excitation data were determined using TD-DFT (B3LYP/631g(d,p))–calculations.

## 6.4.2 Synthetic procedures and spectral characterisations

### 6.4.2.1 Synthesis of compound 1

To a solution of 4-bromo phenylhydrazine (5.48 g, 29.30 mmol) and 1,3-diphenylpropane-1,3-dione (5.00 g, 22.30 mmol) in methanol (80 mL) was added AcOH (80 mL). The reaction mixture was heated to reflux for 24 h. After cooling

to RT, the mixture was poured into water and extracted with  $\text{CH}_2\text{Cl}_2$ . The combined extracts were washed with saturated sodium carbonate solution followed by brine and dried over anhydrous  $\text{Na}_2\text{SO}_4$ . Solvent was removed under reduced pressure and the residue was purified by silica gel column chromatography using ethyl acetate and *n*-hexane as eluent. Yield: 6.28 g, (75%). mp: 280 °C.  $^1\text{H}$  NMR (400 MHz,  $\text{CDCl}_3$ ):  $\delta$  = 7.99 (d,  $J$  = 7.5 Hz, 2H), 7.51 – 7.47 (m, 4H), 7.43 – 7.28 (m, 8H), 6.86 (s, 1H).  $^{13}\text{C}$  NMR (100 MHz,  $\text{CDCl}_3$ ):  $\delta$  = 152.27, 144.36, 139.14, 132.83, 131.98, 130.30, 128.76, 128.72, 128.66, 128.55, 128.18, 126.54, 125.83, 120.92, 105.70. HR-MS (ESI): calcd. for  $\text{C}_{21}\text{H}_{15}\text{Br}_1\text{N}_2$  ( $[\text{M} + \text{H}]^+$ ) : 375.0491, found : 375.0464.

#### 6.4.2.2 Synthesis of compound 2

Compound 1 (4.41 g, 11.75 mmol) was dissolved in anhydrous THF (150 mL) under nitrogen atmosphere and the resulting solution was cooled to -78 °C with stirring. Then, *n*-Butyllithium (8.1 mL, 12.93 mmol, 1.6M solution in hexane) was slowly added to the stirred solution over 20 min. After 1h, a solution of dimesitylfluoroborane (3.47 g, 12.93 mmol) in 35 mL of dry THF was added over 10 min. The reaction mixture was allowed to warm to room temperature and stirred for 24h. After 24h, water was added to the reaction mixture and extracted with ethyl acetate. The combined extracts were washed with brine and dried over anhydrous  $\text{Na}_2\text{SO}_4$ . Solvent was removed under reduced pressure and the obtained residue was purified by silica gel column chromatography using ethyl acetate and *n*-hexane as eluent. Yield: 4.67 g, (73%). mp: 192 °C.  $^1\text{H}$  NMR (400 MHz,  $\text{CDCl}_3$ ):  $\delta$  = 8.02 (d,  $J$  = 7.5 Hz, 2H), 7.59 (d,  $J$  = 8.1 Hz, 2H), 7.50 (t,  $J$  = 7.5 Hz, 2H), 7.45 – 7.35 (m, 8H), 6.91 (s, 5H), 2.38 (s, 6H), 2.11 (s, 12H).  $^{13}\text{C}$  NMR (100 MHz,  $\text{CDCl}_3$ ):  $\delta$  = 152.43, 144.86, 144.70, 142.79, 141.61, 140.87,

138.91, 137.13, 133.00, 130.66, 128.89, 128.75, 128.53, 128.49, 128.36, 128.21, 125.96, 124.64, 105.75, 23.55, 21.31. HR-MS (ESI): calcd. for  $C_{39}H_{37}B_1N_2$  ( $[M+H]^+$ ): 545.3129, found : 545.3138.

#### 6.4.2.2 Synthesis of compound 3

To a mixture of 3,5-diphenyl-1H-pyrazole, (6.00 g, 27.24 mmol), 2-bromo thiophene (3.91 mL, 40.86 mmol),  $Cu_2O$  (389 mg, 2.724 mmol),  $Cs_2CO_3$  (9.76 g, 29.96 mmol) was added degassed dry DMF under nitrogen atmosphere. The reaction mixture was heated at reflux for 48 h. After cooling to room temperature, 200 mL of  $H_2O$  and 200 mL of  $CH_2Cl_2$  were added, and the phases were separated. The aqueous phase was extracted with ( $3 \times 75$  mL) of  $CH_2Cl_2$  and the combined organic phases were dried over  $Na_2SO_4$ , and the solvent was removed under reduced pressure. The obtained residue was purified by silica gel column chromatography using ethyl acetate and *n*-hexane as eluent. Yield: 3.95 g, (48%). mp: 132 °C.  $^1H$  NMR (400 MHz,  $CDCl_3$ ):  $\delta$  = 7.93 (d,  $J$  = 8 Hz, 2H), 7.47 – 7.35 (m, 8H), 7.14 (d,  $J$  = 8 Hz, 1H), 6.87 – 6.84 (m, 1H), 6.81 (s, 1H), 6.75 (d,  $J$  = 4 Hz, 1H).  $^{13}C$  NMR (100 MHz,  $CDCl_3$ ):  $\delta$  = 152.45, 145.75, 142.22, 132.70, 130.10, 128.98, 128.88, 128.78, 128.60, 128.37, 126.04, 125.65, 123.05, 121.75, 105.39. HR-MS (ESI): calcd. for  $C_{19}H_{14}N_2S$  ( $[M+H]^+$ ): 303.0950, found : 303.0945.

#### 6.4.2.3 Synthesis of compound 4

Compound **3** (3.50 g, 11.57 mmol) was dissolved in 80 mL and *N*-bromosuccinimide (2.26 g, 12.70 mmol) was added. Then the reaction mixture was stirred for 24 h in dark condition. To this mixture, 100 mL of  $H_2O$  and 70 mL of  $CH_2Cl_2$  were added to the mixture and the organic phase was collected and the aqueous phase extracted with ( $2 \times 50$  mL) of  $CH_2Cl_2$ . The combined organic phases were dried over  $Na_2SO_4$ , and solvent was removed under reduced

pressure. The obtained residue was purified by silica gel column chromatography using ethyl acetate and *n*-hexane as eluent. Yield: 3.96 g, (90%). mp: 138 °C.  $^1\text{H}$  NMR (400 MHz,  $\text{CDCl}_3$ ):  $\delta$  = 7.92 (d,  $J$  = 7.1 Hz, 2H), 7.48 – 7.36 (m, 8H), 6.82 (d,  $J$  = 4.0 Hz, 1H), 6.78 (s, 1H), 6.44 (d,  $J$  = 4.0 Hz, 1H).  $^{13}\text{C}$  NMR (100 MHz,  $\text{CDCl}_3$ ):  $\delta$  = 152.77, 145.54, 142.64, 132.44, 129.77, 129.19, 129.07, 128.85, 128.79, 128.57, 128.43, 126.05, 121.29, 109.77, 105.77. HR-MS (ESI): calcd. for  $\text{C}_{19}\text{H}_{13}\text{N}_2\text{SBr}([\text{M} + \text{H}]^+)$ : 381.0056, found: 381.0052.

#### 6.4.2.4 Synthesis of compound 5

Compound **5** was prepared by following a procedure similar to that used for compound **2**. The quantities involved are as follows: Compound **4** (3.00 g, 7.87 mmol), *n*-butyllithium (5.41 mL, 8.66 mmol, 1.6M solution in hexane), dimesitylfluoroborane (2.32 g, 8.66 mmol). Yield: 2.38 g, (55%). mp: 192 °C.  $^1\text{H}$  NMR (400 MHz,  $\text{CDCl}_3$ ):  $\delta$  =  $^1\text{H}$  NMR (400 MHz,  $\text{CDCl}_3$ )  $\delta$  = 7.91 (d,  $J$  = 7.2, 8.0 Hz, 2H), 7.46 – 7.34 (m, 8H), 7.18 (d,  $J$  = 4 Hz, 1H), 6.82 (s, 4H), 6.78 (s, 1H), 6.75 (d,  $J$  = 3.9 Hz, 1H), 2.31 (s, 6H), 2.14 (s, 12H).  $^{13}\text{C}$  NMR (100 MHz,  $\text{CDCl}_3$ ):  $\delta$  = 153.87, 152.87, 145.33, 140.94, 139.71, 138.71, 132.45, 130.16, 129.31, 129.19, 128.80, 128.70, 128.54, 128.30, 126.12, 121.80, 106.53, 23.58, 21.33. HR-MS (ESI): calcd. for  $\text{C}_{37}\text{H}_{35}\text{N}_2\text{SB}([\text{M} + \text{H}]^+)$ : 551.2693, found: 551.2701.

## 6.5 References

1. Jäkle, F. *Chem. Rev.*, **2010**, *110*, 3985.
2. Elbing, M.; Bazan, G. C. *Angew. Chem., Int. Ed.*, **2008**, *47*, 834.
3. Gabbai, F. P. *Angew. Chem., Int. Ed.*, **2012**, *51*, 6316.
4. Li, S. Y.; Sun, Z. B.; Zhao, C. H. *Inorg. Chem.*, **2017**, *56*, 8705.
5. Mellerup, S. K. ; Wang, S. *Trends Chem.*, **2019**, *1*, 77.



- 
6. Grotthuss, E.; John, A.; Kaese, T. ; Wagner, M. *Asian J. Org. Chem.*, **2018**, 7, 37.
  7. Kirschner, S.; Mewes, J.-M.; Bolte, M.; Lerner, H.-W.; Dreuw A.; Wagner, M. *Chem. Eur. J.*, **2017**, 23, 5104.
  8. John, A.; Bolte, M.; Lerner, H. W.; Wagner, M. *Angew. Chem., Int. Ed.*, **2017**, 56, 5588.
  9. Mercier, L. G.; Piers, W. E.; Parvez, M. *Angew. Chem., Int. Ed.*, **2009**, 48, 6108.
  10. Hu, K. ; Zhang, Z.; Burke, J.; Qin, Y. *J. Am. Chem. Soc.*, **2017**, 139, 11004.
  11. Yoshii, R.; Hirose, A.; Tanaka K.; Chujo, Y. *J. Am. Chem. Soc.*, **2014**, 136, 18131.
  12. Kushida, T.; Shuto, A.; Yoshio, M.; Kato, T.; Yamaguchi, S. *Angew. Chem., Int. Ed.*, **2015**, 54, 6922.
  13. Escande, A.; Ingleson, M. J. *Chem. Commun.*, **2015**, 51, 6257.
  14. Wang, X. Y.; Wang, J. Y.; Pei, J. *Chem. – Eur. J.*, **2015**, 21, 3528.
  15. Møllerup, S. K.; Wang, S. *Chem. Soc. Rev.*, **2019**, 48, 3537.
  16. Pandey, U. P.; Thilagar, P. *Adv. Opt. Mater.*, **2020**, 1902145.
  17. Riensch, N. A.; Fritze, L.; Schindler, T.; Kremer, M.; Helten, H. *Dalton Trans.*, **2018**, 47, 10399.
  18. Lin, H.; Patel, S.; Jäkle, F. *Macromolecules*, **2020**, 53, 10601.
  19. Ji, L.; Griesbeck, S.; Marder, T. B. *Chem. Sci.*, **2017**, 8, 846.
  20. Pagidi, S.; Kalluvettukuzhy, N. K.; Thilagar, P. *Inorg. Chem.*, **2020**, 59, 3142.
  21. Yuan, K.; Kahan, R. J.; Si, C.; Williams, A.; Kirschner, S.; Uzelac, M. ; Zysman-Colman, E.; Ingleson, M. *Chem. Sci.*, **2020**, 11, 3258.
  22. Mishiba, K.; Tanaka, Y.; Akita, M. *Chem. – Eur. J.*, **2021**, 27, 1.
  23. Ji, L.; Krummenacher, I.; Friedrich, A.; Lorbach, A.; Haehnel, M.; Edkins, K.; Braunschweig, H.; Marder, T. B. *J. Org. Chem.*, **2018**, 83, 3599.

- 
24. Yuan, Z.; Entwistle, C. D.; Collings, J. C.; Albesa-Jové, D.; Batsanov, A. S.; Howard, J. A. K.; Taylor, N. J.; Kaiser, H. M.; Kaufmann, D. E.; Poon, S.-Y.; Wong, W.-Y.; Jardin, C.; Fathallah, S.; Boucekkine, A.; Halet, J.-F.; Marder, T. B. *Chem. – Eur. J.*, **2006**, *12*, 2758.
25. Collings, J. C.; Poon, S.-Y.; Droumaguet, C. L.; Charlot, M.; Katan, C.; Palsson, L.-O.; Beeby, A.; Mosely, J. A.; Kaiser, H. M.; Kaufmann, D.; Wong, W.-Y.; Blanchard-Desce, M.; Marder, T. B. *Chem. – Eur. J.*, **2009**, *15*, 198.
26. Griesbeck, S.; Michail, E.; Rauch, F.; Ogasawara, H.; Wang, C.; Sato, Y.; Edkins, R. M.; Zhang, Z.; Taki, M.; Lambert, C.; Yamaguchi, S.; Marder, T. B. *Chem. – Eur. J.*, **2019**, *25*, 13164.
27. Griesbeck, S.; Michail, E.; Wang, C.; Ogasawara, H.; Lorenzen, S.; Gerstner, L.; Zang, T.; Nitsch, J.; Sato, Y.; Taki, M.; Lambert, C.; Yamaguchi, S.; Marder, T. B. *Chem. Sci.*, **2019**, *10*, 5405.
28. Stahl, R.; Lambert, C.; Kaiser, C.; Wortmann, R.; Jakober, R. *Chem. – Eur. J.*, **2006**, *12*, 2358.
29. Reitzenstein, D.; Lambert, C. *Macromolecules*, **2009**, *42*, 773.
30. Liu, Z.-Q.; Fang, Q.; Cao, D.-X.; Wang, D.; Xu, G.-B. *Org. Lett.*, **2004**, *6*, 2933.
31. Proń, A.; Baumgarten M.; Mullen, K. *Org. Lett.*, **2010**, *12*, 4236.
32. Chen, P.; Marshall, A. S.; Chi, S.-H.; Yin, X.; Perry J. W.; Jäkle, F. *Chem. – Eur. J.*, **2015**, *21*, 18237.
33. Zhang, F.; Noda, T.; Kageyama, H.; Shirota, Y. *Proc. SPIE*, **2009**, 7213(1–5), 721302.
34. Yamaguchi, S.; Akiyama S.; Tamao, K. *J. Am. Chem. Soc.*, **2001**, *123*, 11372.
35. Parab, K.; Venkatasubbaiah, K.; Jäkle, F.; *J. Am. Chem. Soc.*, **2006**, *128*, 12879.
36. Møllerup, S. K.; Rao, Y.-L.; Amarne, H.; Wang, S. *Org. Lett.*, **2016**, *18*, 4436.
-

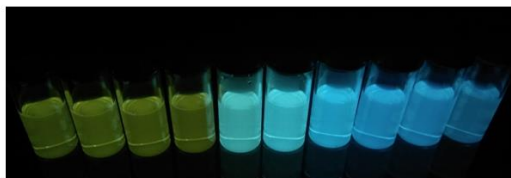
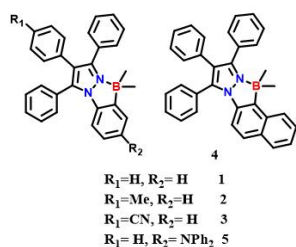
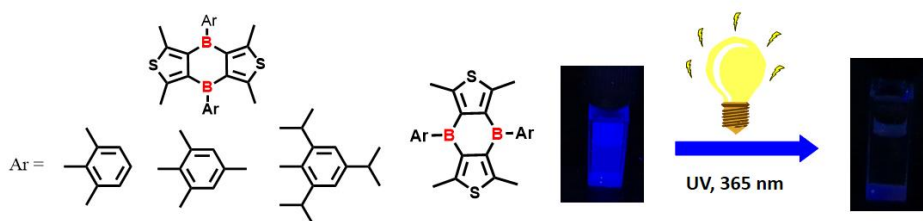
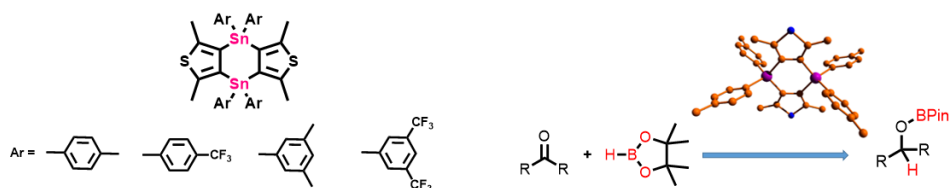
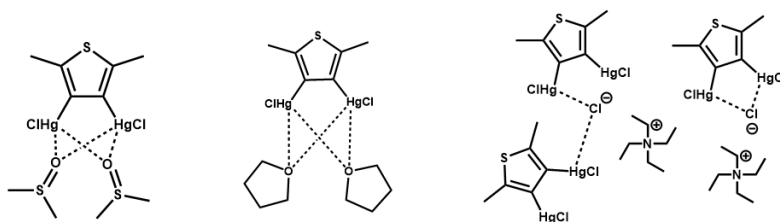
- 
37. Brazeau, A. L.; Yuan, K.; Ko, S.-B.; Wyman, I.; Wang, S. *ACS Omega*, **2017**, 2, 8625.
38. Swamy, C. A.; Mukherjee, P. S.; Thilagar, P. *Inorg. Chem.*, **2014**, 53, 4813.
39. Lee, H.; Jana, S.; Kim, J.; Lee, S. U.; Lee, M. H. *Inorg. Chem.*, **2020**, 59, 1414.
40. Caygill, J. S.; Davi, F.; Higson, S. P. J. *Talanta*, **2012**, 88, 14.
41. Salinas, Y.; Martinez-Manez, R.; Marcos, M. D.; Sancenon, F.; Costero, A. M.; Parra M.; Gil, S. *Chem. Soc. Rev.*, **2012**, 41, 1261.
42. Germain, M. E.; Knapp, M. J. *Chem. Soc. Rev.*, **2009**, 38, 2543.
43. Sohn, H.; Calhoun, R. M.; Sailor, M. J.; Trogler, W. C. *Angew. Chem., Int. Ed.*, **2001**, 40, 2104.
44. Akhavan, J. *The Chemistry of Explosives*, The Royal Society of Chemistry, London, 2nd edn, **2004**.
45. Ashbrook, P. C.; Houts, T. A. *Chem. Health Saf.*, **2003**, 10, 27.
46. Wollin, K. M.; Dieter, H. H. *Arch. Environ. Contam. Toxicol.*, **2005**, 49, 18.
47. Hengchang, M.; Zhongwei, Z.; Yuanyuan, J.; Lajia, Z.; Chunxuan, ; Haiying, C.; Zengming, Y.; Zhiwang, Y.; Ziqiang, L. *RSC Adv.*, **2015**, 5, 87157.
48. Areti, S.; Bandaru, S.; Kandi R.; Rao, C. P. *ACS Omega*, **2019**, 4, 1167..
49. Lin, Q.; Guan, X.-W. ; Fan, Y.-Q.; Wang, J.; Liu, L.; Liu, J.; Yao, H. ; Zhang, Y.-M.; Wei, T.-B. *New J. Chem.*, **2019**, 43, 2030.
50. Madhu, S.; Bandela, A.; Ravikanth, M. *RSC Adv.*, **2014**, 4, 7120.
51. Sohn, H. ; Sailor, M. J.; Magde, D.; Trogler, W. C. *J. Am. Chem. Soc.*, **2003**, 125, 3821.
52. Liu, J. ; Zhong, Y. ; Lu, P. ; Hong, Y.; Lam, J. W. Y. ; Faisal, M.; Yu, Y.; Wong, K. S; Tang, B. Z. *Polym. Chem.*, **2010**, 1, 426.
53. Shanmugaraju, S.; Mukherjee, P.S. *Chem. Commun.*, **2015**, 51, 16014.
-

- 
54. Tanwar, A. S.; Hussain, S. ; Malik, A. H. ; Afroz, M. A.; Iyer, P. K. *ACS Sens.*, **2016**, *1*, 1070.
56. Dhanunjayarao, K.; Mukundam, V.; Venkatasubbaiah, K. *Inorg. Chem.*, **2016**, *55*, 11153.
57. Mukundam, V.; Kumar, A.; Dhanunjayarao, K.; Ravi, A.; Peruncheralathan, S.; Venkatasubbaiah, K. *Polym. Chem.*, **2015**, *6*, 7764.
58. Mukundam, V.; Dhanunjayarao, K. ; Mamidala, R.; Venkatasubbaiah, K. *J. Mater. Chem. C*, **2016**, *4*, 3523.
59. Mukundam, V. Sa, S. ; Kumari, A., Das, R, Venkatasubbaiah, K., *J. Mater. Chem. C*, **2019**, *7*, 12725.
60. Bahae, M. S.; Said, A. A.; Wei, T. H.; Hagan, D. J.; Stryland, E. W. V. *IEEE J. Quantum Electron.*, **1990**, *26*, 760.
61. Mukundam, V. ; Sa, S.; Kumari, A. ; Murali, A. C. ; Nayak, P. ; Das, R.; Venkatasubbaiah, K. *Dalton Trans.*, **2020**, *49*, 7737.
62. Yin, M.; Li, H.; Tang, S. H.; Ji, W. *Appl. Phys. B*, **2000**, *70*, 587.
63. Karthikeyan, K. V.; Anandhi, S.; Ramkumar, V.; Shyju, T. S.; Jaisankar, S. N.; Suriakarthick, R. *Mater. Res. Express*, **2019**, *6*, 075105.
64. Manonmani, M.; Balakrishnan, C.; Ahamed, S. R.; Vinitha, G.; Meenakshisundaram, S. P.; Sockalingam, R. M. *J. Mol. Struct.*, **2019**, *1190*, 1.
65. Bhalla, V.; Gupta, A.; Kumar, M., *Org. Lett.* **2012**, *14*, 3112.
66. Madhu, S.; Bandela, A.; Ravikanth, M., *RSC Adv.* **2014**, *4*, 7120.
67. Chahal, M. K.; Sankar, M. *Anal. Methods* **2015**, *7*, 10272.
68. Yu, X.; Wan, J.; Chen, S.; Li, M.; Gao, J.; Yang, L.; Wang, H.; Chen, D.; Pan, Z.; Li, J. *Talanta*, **2017**, *174*, 462.
69. Amudha, M.; Madhavan, J.; Praveen Kumar, P. *J. Opt.* **2017**, *46*, 382.
-

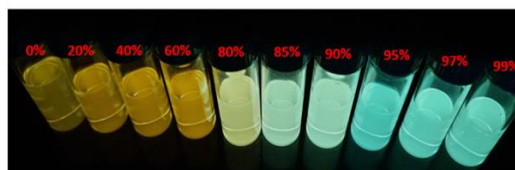
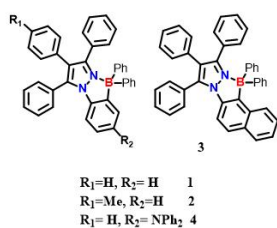
- 
70. Yılmaz, H.; Küçüköz, B.; Sevinç, G.; Tekin, S.; Yaglioglu, H. G.; Hayvalı, M.; Elmali, A. *Dyes Pig.* **2013**, *99*, 979.
71. Ju, C.; Zhou, Y.; Semin, S.; Yang, G.; Tinnemans, P.; Duan, Y.; Feng, Y.; Rasing, T.; Xu, J. *Dyes Pig.* **2019**, *162*, 776.
72. Sudharsana, N.; Keerthana, B.; Nagalakshmi, R.; Krishnakumar, V.; Guru Prasad, L. *Mater. Chem. Phys.* **2012**, *134*, 736.



# Summary



Aggregation Induced Emission Enhancement



Aggregation Induced Emission Enhancement

